Reinforced Concrete Shear Walls with Welded Wire Grids as Boundary Element Transverse Reinforcement

By Mansour Navidpour

A Thesis Submitted to
the Faculty of Graduate Studies and Research
in Partial Fulfilment of the Requirements
For the Degree of
Doctorate of Philosophy
in Civil Engineering

Department of Civil Engineering
University of Ottawa
Ottawa, Canada
May 2018

Supervisor: Dr. Murat Saatcioglu

Abstract

Reinforced concrete shear walls as seismic force resisting systems may experience inelastic deformations if subjected to strong seismic excitations. These walls are designed to provide strength, stiffness, energy dissipation capacity and lateral drift control for seismic resistance. Shear wall deformability is largely dependent on adequate confinement of core concrete in boundary elements, prevention of longitudinal bar buckling, as well as proper design and detailing of the web section.

Conventional transverse reinforcement placed in shear wall boundary elements consists of hoops, overlapping hoops and crossties, based on the geometry and number of longitudinal bars used. The confinement steel requirement of current building codes (ACI 318 or CSA A23.3) often results in congestion of steel cage due to the high transverse reinforcement ratio required. Placing multiple hoops with 135-degree bends combined with crossties to satisfy the code confinement requirements can create concrete placement and construction problems. In addition, the required time to assemble conventional steel cages with multiple individual ties per spacing can be time consuming, potentially impacting the overall cost and duration of construction.

Welded Wire Reinforcement (WWR) is available in the construction industry as concrete reinforcement in the form of welded wire fabric (WWF) manufactured from relatively small diameter wires in comparison to the bar sizes typically used in structural applications. As an alternative to using conventional transverse hoops, prefabricated WWR grids can be used to provide required transverse reinforcement in boundary elements. WWR grids are manufactured using robots to weld cut steel pieces accurately before they are shipped to the job site, resulting in better construction quality and reduced construction time. However, research on the use of WWR is limited in the literature. Further experimental and analytical research is needed to establish design requirements for such reinforcement, especially when used in earthquake resistant construction with requirements for ductile response.

The current research project, involved three main phases; i) tests of 3 large-scale reinforced concrete shear walls with WWR grids used as boundary element transverse reinforcement, ii) material tests of grid samples, including those cast in concrete, iii) non-linear finite element analysis. The wall tests were conducted under slowly-applied lateral deformation reversals to investigate their strength and ductility for suitability as seismic resistant structural elements. Material tests were conducted to have a better understanding of WWR behavior, especially their weld capacity. Analytical research was undertaken to expand the experimental findings on shear wall behavior, as well as to conduct parametric investigation to understand the impact of changes in grid strength and ductility.

The results indicated that WWR grids can be used as boundary element transverse reinforcement in earthquake resistant shear wall. However, strength and ductility of grids should be established carefully prior to such application. Design strength of WWR grids should be established through burst tests to ensure ductile yielding of wire reinforcement prior to premature weld failure. Those grids that exhibit weld failures may be used with reduced design strength to permit the development of sufficient inelastic deformability in flexure-dominant shear walls.

Table of Contents

List of Figures

List of Tables

Chapter 1

Introduction

1.1 General

Within the last four decades, the efforts of engineering community have resulted in significant progress in creating guidelines and design procedures for design and construction of earthquake resistant structures. One of the recommended approaches for building structures involves using shear walls as lateral force resisting systems. A properly designed shear wall is expected to withstand earthquake forces without significant damage, while maintaining overall structural integrity, stability, strength and drift control. Under strong earthquakes, plastic hinges may form in wall critical regions, facilitating dissipation of energy, while ensuring ductile behaviour. The plastic hinges are typically formed at the base of the structure where the highest force demand is present.

Current design codes promote ductile flexural mode of behaviour while ensuring suppression of brittle failures. A multi-storey shear wall subjected to lateral seismic forces develop internal force couples in flexure critical regions. One end of the wall is subjected to a tensile force and the opposite end develops a compressive force. These two coupling forces are linked through the wall web, which should have sufficient shear capacity to prevent premature shear failure. Tensile forces in the end zones (or boundary elements) are resisted by the longitudinal steel reinforcement, given that the re-bars can develop their full capacity having sufficient lap length with the starter bars. The compressive forces are resisted by a combination of concrete and longitudinal steel bars, similar to a column. In order to achieve the design capacity of this column-like element, sufficient transverse reinforcements should be placed at proper spacing to prevent longitudinal bars from buckling, while also providing confinement to the core

concrete. The performance of transverse reinforcement is dependent on the volumetric ratio, strength and spacing of transverse reinforcement, as well as the distribution of longitudinal reinforcement, arrangement of transverse reinforcement, concrete strength and sectional geometry. A proper combination of these key design parameters results in desired behaviour with confined core concrete and associated ductile behaviour.

Conventional ties used in shear wall boundary elements are built from normal strength steel bars bent into hoops or overlapping hoops with 90 or 135 degree bends, and crossties with 90, 135 or 180 degree bends. Minimum bend lengths are specified by design codes to ensure that these bends can develop sufficient anchorage into the core concrete. The use of closely spaced hoops, overlapping hoops and crossties often results in the congestion of cages, hindering concrete placement and causing challenges during construction. The time required for steel cage assembly and the extra effort required during concrete placement in congested areas could potentially impact the construction schedule and the cost of construction.

An alternative to conventional tie reinforcement is prefabricated grids with potentially superior performance, easy cage assembly and speed of construction. Fiber Reinforcing Plastic (FRP) grids as well Welded Wire Reinforcement (WWR) grids have been considered in the past as two potential alternatives, with the latter having the advantage of ductile behaviour of steel. While limited research has been conducted on the use of grids as transverse reinforcement, mostly for columns, additional research is needed to further investigate the use of WWR grids as transverse reinforcement in shear wall boundary elements. In the past, WWR was assigned various names, such as welded wire fabric (WWF) and welded wire mesh, ASTM harmonized the names as welded wire reinforcement (WWR) (ASTM A1064-12 – Note 1).

When high strength reinforcing steel is used to produce conventional hoops and crossties, they tend to show more brittle failure and they are harder to bend. They also have higher residual stresses at bent corners. The use of WWR grids overcomes the problems associated with producing both normal-strength and high-strength steel hoops and crossties.

1.2 Objective

The primary objective of this research project is to assess the performance of WWR as transverse reinforcement in shear wall boundary elements, with an emphasis on nonlinear behavior and seismic performance. The objective also includes the development of a design procedure for WWR in earthquake resistant shear walls through combined experimental and

analytical research, as well as the development of a methodology for quality assurance of WWR as a structural material.

ACI 318-14, which was published while this research study was underway, added a new restriction in Clause 20.2.2.4, as sub-note [2] to Table 20.2.2.4a. Accordingly, WWR as defined in "*ASTM A1064 and A1022 is not permitted in special seismic systems where the weld is required to resist the stresses in response to confinement, lateral support of longitudinal bars, shear, or other actions*". This current research aims to provide additional information and experimental evidence on the performance of WWR grids for such applications.

1.3 Scope

The scope comprises of experimental work, computer modelling and analytical research, as well as the development of a design procedure and recommendations for material testing. The following shows the itemized breakdown of the scope:

- Review of previous research and development on earthquake resistant reinforced concrete shear walls. The review emphasizes research on large scale shear wall tests with different sectional geometries. The behavior of these walls under monotonic and reverse cyclic loading is studied.
- Material tests to establish the properties of materials used in the research project: concrete, reinforcing steel bars, welded wire reinforcement (WWR) and prestressing tendons.
- WWR grid tests either as individual elements or embedded in concrete and forming small-scale test specimens. The tests in this category include the following:
    - Material testing to establish the shear capacity of WWR joints as per ASTM 1064 – 12.
    - Material testing to establish the capacity of WWR grids under direct shear applied parallel to the longitudinal side of grids, as well as along the grid diagonal.
    - Tests of WWR grids embedded in concrete under direct shear, applied parallel to the longitudinal side of grids, as well as along the grid diagonal.
    - Tests of small scale columns under concentric and eccentric axial loads to assess grid resistance to bar buckling.

- Designing, building and testing of three large-scale shear walls to investigate the behavior of WWR grids as boundary element ties. The three shear walls consist of:
    - Shear wall No. 1: Rectangular shear wall built using 52 MPa concrete with a wall aspect ratio of $\frac{\ell_w}{h_w} = 1.55$. The wall is designed to have nominal shear capacity approximately equal to the shear force corresponding to nominal moment resistance.
    - Shear wall No. 2: Rectangular shear wall built using 82 MPa concrete with a wall aspect ratio of $\frac{\ell_w}{h_w} = 1.94$. The wall is designed and detailed to preform predominantly in the flexure mode as per ACI 318-2011.
    - Shear wall No. 3: Barbell shaped shear wall built using 83 MPa concrete with a wall aspect ratio of $\frac{\ell_w}{h_w} = 3.00$. The wall is designed and detailed to perform predominantly in the flexure mode as per ACI 318-2011.
- Analytical modelling and non-linear analysis of walls tested in the experimental program to verify the results and to validate the analytical models.
- Analytical parametric study to assess the effects of grid parameters on wall performance.
- Development of a design procedure for earthquake-resistant shear walls with boundary elements reinforced with WWR as transverse reinforcement.
- Development of recommendations for standard material tests of WWR for quality assurance in seismic structural applications.

Chapter 2

Literature Review

2.1 Shear Wall Design History

Shear walls have been used successfully in the past for providing required stiffness and strength against lateral forces due to earthquakes and winds. In 1970's, a series of research projects were conducted to better understand inelastic performance of shear walls under seismic loads and to quantify the effects of reinforcement detailing for improved ductility. The Uniform Building Code (UBC-70) in the US, followed by ACI 318-71 were the first codes in the United States with provisions for design of earthquake-resistant shear walls. In these codes, the shear walls were simply treated as deep, relatively thin, vertical cantilever reinforced concrete beams, designed for a combination of gravity and lateral forces. A graphical representation of nominal shear resistance for shear walls in the UBC-70 is shown in Figure. 2.1.

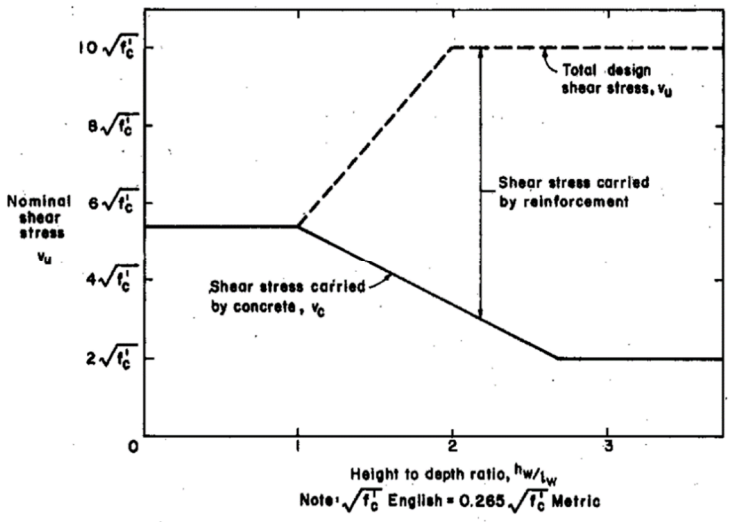

Figure 2.1 Graphical representation of the shear wall design provisions in UBC-70

The total design shear strength for the walls was determined based on the geometrical aspect ratio of the wall. For walls with an aspect ratio of less than 1.0 (height to length), the UBC-70 assumed that the total shear stress was resisted by concrete only, whereas for walls with higher aspect ratios, the total shear stress was resisted by a combination of concrete and horizontal shear reinforcement. The concrete shear stress capacity contribution decreased linearly between walls with an aspect ratio of 1.0 to 2.7 and assumed to remain constant thereafter. The UBC-70 design methodology treated shear walls as deep beams which is not an entirely correct representation of structural behaviour since the failure modes in shear walls are different than those for deep beams. Furthermore, deep beams are typically not subjected to high axial compression or tension forces like walls.

Additional research (Crist 1967, Leonhardt and Walther 1966, Cardenas and Magura 1972 and Cardenas et. al. 1973) provided a better understanding of shear wall behavior, the results of which have been incorporated in ACI 318-71. The shear stress capacity of rectangular shear walls with minimum shear reinforcement ratio of 0.0025 as per ACI 318-71 is shown in Figure 2.2. This diagram is generated as a function of moment to shear ratio and shows minimum shear strength of $4.1\sqrt{f'_c}$ (MPa) for what was considered to be high-rise walls, and $5.4\sqrt{f'_c}$ (MPa) for low-rise walls. The ultimate total design shear capacity was limited to $10\sqrt{f'_c}$ (MPa), which represented the concrete compression failure in wall "struts".

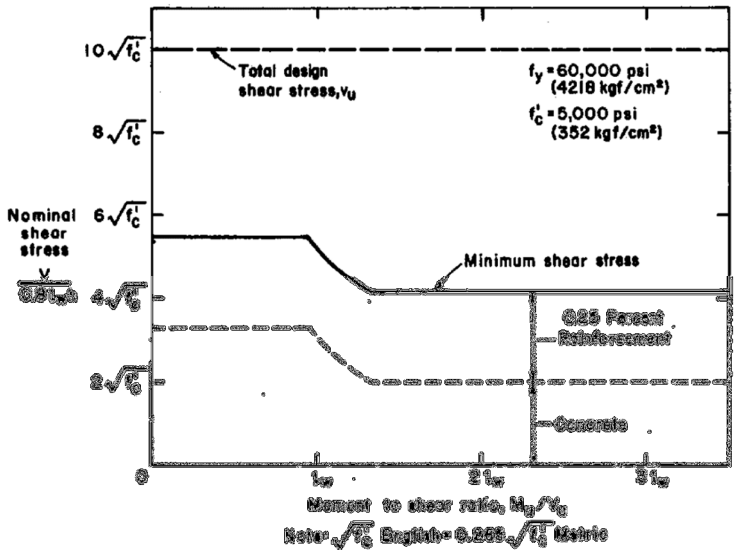

Figure 2.2 Minimum shear strength of rectangular shear walls per ACI 318-71

Portland Cement Association (PCA) tested thirteen (13) rectangular shear walls: six (6) specimens representing high-rise buildings and seven (7) specimens representing low-rise buildings (Cardenas 1973). The high-rise shear wall specimens were subjected to a combination of axial compression and lateral loads, and were designed to represent the lower portion of a shear wall in a frame-shear wall interactive structural system. During the test program, 50% of the load was applied as a point load at the point of contra-flexure and the remaining 50% was applied as a uniformly distributed load between the point of contra-flexure and the support at the base of the wall. The walls were tested under monotonic static loading. The low-rise shear wall specimens were subjected to a single static lateral force at the top of the wall and no axial compression was applied. Only one of the samples (SW-13) was subjected to ten cycles of load reversals and the remaining walls were tested under monotonic loading. The shear wall dimensions and material properties are presented in Table 2.1. The test results are shown in Table 2.2.

Table 2.1 Dimensions and Material Properties of Test Specimens (Cardenas 1973)

Mark	Height h_w ft	Concrete		Reinforcement				Axial Stress $\frac{N_u}{l_w h}$ psi
		Compressive Strength f'_c psi	Tensile Splitting Strength f'_{sp} psi	Vertical		Horizontal		
				Ratio ρ_v*	Yield Stress f_y psi	Ratio ρ_h	Yield Stress f_y psi	
SW-1	21.0	7420	660	0.0027	60,200	0.0027	61,300	415
SW-2	21.0	6880	650	0.0100	65,400	0.0027	61,000	430
SW-3	21.0	6780	615	0.0300	66,000	0.0027	60,000	420
SW-4	12.0	6740	585	0.0300	60,000	0.0027	60,000	430
SW-5	12.0	5900	565	0.0230†	60,000	0.0027	60,000	425
SW-6	21.0	5950	590	0.0230†	63,000	0.0027	70,000	430
SW-7	6.25	6240	630	0.0230†	65,000	0.0027	60,000	None
SW-8	6.25	6160	565	0.0300	65,000	0.0027	67,500	None
SW-9	6.25	6240	630	0.0300	65,000	0.0100	60,000	None
SW-10	6.25	5850	565	0.0165‡	65,000	None	None	None
SW-11	6.25	5540	535	0.0230‡	65,000	0.0075	65,000	None
SW-12	6.25	5570	530	0.0230‡	65,000	0.0100	65,000	None
SW-13	6.25	6300	630	0.0300	64,500	0.0100	66,000	None

* $\rho_v = \frac{A_s}{l_w h}$, where A_s = total area of vertical reinforcement, $l_w = 75\ in.$ and $h = 3\ in.$

† One-third of total vertical reinforcement concentrated within a distance $l_w/10$ from either extremity of cross section (amount of reinforcement in interior region $\rho_{vw} = 0.01$).

‡ One-half of total vertical reinforcement concentrated within a distance $l_w/10$ from either extremety of cross section $\rho_{vw} = 0$).

Table 2.2 Test Results (Cardenas 1973)

Mark	Calculated Parameters		Flexural Strength		Shear Strength			$\frac{Measured}{Calculated}$		Observed Mode of Failure
					Measured		Calculated †			
	Moment to shear ratio M_u/V_u at $l_w/2$ from base	Ratio d/l_w, at ultimate	Measured moment, M_u, at base kip-ft	Calculated * moment, M_u, at base kip-ft	Shear, V_u, at $l_w/2$ kips	$\frac{V_u}{hd\sqrt{f'_c}}$ ‡	$\frac{v_0 v_s}{\sqrt{f'_c}}$	Moment at the base	Shear at $l_w/2$ from base	
SW-1	$2.0l_w$	0.58	406	379	26.5	1.7	3.9	1.07	0.44	Flexure
SW-2	$2.0l_w$	0.62	675	650	41.4	2.8	4.0	1.04	0.70	Flexure
SW-3	$2.0l_w$	0.71	1073	1200	66.0	4.5	4.0	0.90	1.13	Flexure-Shear
SW-4	$1.0l_w$	0.71	1077	1139	108.6	7.4	6.6	0.95	1.12	Flexure
SW-5	$1.0l_w$	0.78	1078	1121	108.6	7.8	6.8	0.96	1.15	Flexure-Shear
SW-6	$2.0l_w$	0.78	1179	1154	72.5	5.3	4.4	1.02	1.20	Flexure
SW-7	$0.5l_w$	0.74	729	980	116.7	8.2	5.3	0.74	1.55	Shear
SW-8	$0.5l_w$	0.65	801	1009	128.1	9.1	5.6	0.79	1.63	Shear
SW-9	$0.5l_w$	0.65	954	1000	152.7	10.7	10.0	0.95	1.07	Flexure-Shear
SW-10	$0.5l_w$	0.94	429	700	68.7	4.3	3.3	0.61	1.30	Shear
SW-11	$0.5l_w$	0.94	856	1000	137.0	8.7	9.8	0.86	0.89	Shear-Anchorage
SW-12	$0.5l_w$	0.94	925	1000	148.0	9.4	10.0	0.93	0.94	Shear-Anchorage
SW-13§	$0.5l_w$	0.65	888	1000	142.1	10.0	10.0	0.89	1.00	Flexure-Shear

* based on compressive concrete limiting strain of 0.003, strain compatibility and measured material properties.
† Calculated from proposed shear strength equations.
‡ d used is $0.8l_w$ or greater.
§ SW-13 was subjected to 10 cycles of load reversals.

Table 2.2 provides a comparison between experimentally recorded capacities and code predictions. The test results from this study combined with the test results from Muto and Kokusho (1953), Ogura et. al. (1952), Benjamin and Williams (1953), Williams and Benjamin (1954), Antebi et. al. (1960) were used to verify the proposed equations in ACI 318-71. The results also showed the importance of shear wall reinforcement detailing and the distribution on flexural/shear strength, energy absorption capacity and lateral stiffness.

Research conducted by Paulay (1969, 1971) indicated that energy absorption and stiffness characteristics of walls may be significantly improved if shear reinforcement did not yield when the wall reached their flexural capacity. This was concluded based on the observation that the crack width was restrained and hence, aggregate interlock across the cracks, as well as the dowel action of the main reinforcement was maintained. Muto (1965) suggested that the wall reinforcement detailing should be divided into segments to increase shear strength to reduce the M/V ratio of the wall to make flexure as the predominant failure mode. His suggested detailing resulted in high ductility by providing shear strength in excess of flexural strength.

Cardenas and Magura (1972) conducted experimental research on six (6) large rectangular shear walls representing high-rise buildings. The walls were constructed using various amounts and distributions of vertical reinforcement, and were subjected to static axial and lateral loads, representing gravity and wind/earthquake loads respectively. The study showed the advantages of using vertical steel, concentrated at the ends of the wall, in improving ductility and energy absorption capability, as shown in Figure 2.3. The experimental work was followed by analysis aiming to predict the monotonic response of walls with varying percentages and distributions of vertical reinforcement. The analytical models indicated that the walls with concentrated reinforcement at the ends had higher ductility compared to walls with uniformly distributed reinforcement.

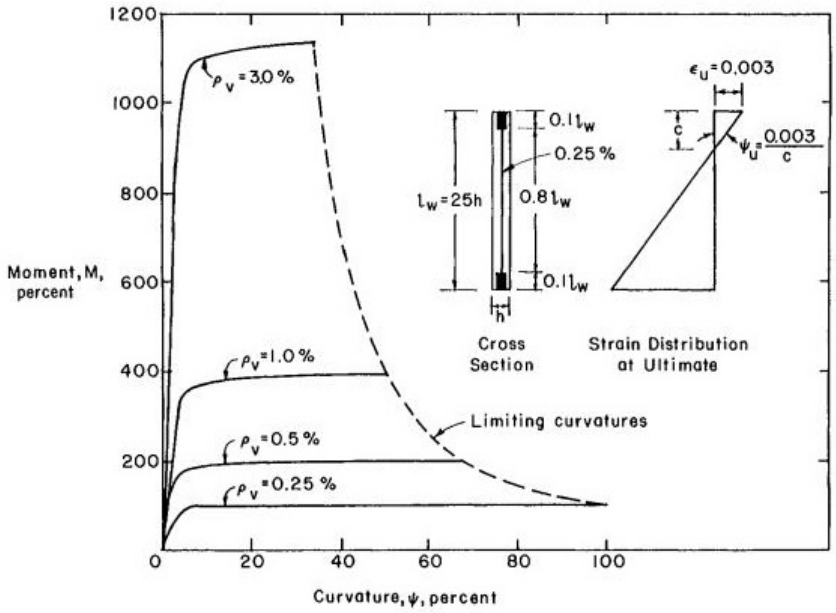

Figure 2.3 Effect of reinforcement distribution on moment curvature

(Cardenas and Magura 1972)

The previous research at PCA on low-rise shear walls, conducted in early 1970's, was expanded further by Cardenas et al. (1980). Additional large-scale walls were tested. The reinforcement detailing of the large-scale shear wall specimens is illustrated in Figure 2.4. All the walls were built with an aspect ratio of 1:1 (height to length) where the amount and distribution of horizontal and vertical reinforcement varied. The walls did not have boundary elements or any special hoop arrangements and no axial load was applied. The results of this experiment program combined with those of Barda et. al. (1977) and Fiorato et. al. (1976) were

used to develop special provision for walls in ACI 318-77. A summary of the test data of Barda (1977) and Fiorato (1976) is given in Table 2.3.

Table 2.3 Summary of Shear Wall Test Results (Barda et. al. – 1977 and Fiorato et. al. – 1976)

Specimen No.	Shape *	Reinforcement Percentage			f'_c psi	Strength $\frac{v_u}{\sqrt{f'_c}}$	
		Boundary ρ_f	Web Vertical ρ_n	Web Horizontal ρ_h		Measured psi	Calculated psi
Barda et al (1977)							
B1-1	F	1.8	0.5	0.5	4200	15.5	8.9
B2-1	F	6.4	0.5	0.5	2370	15.8	10.0
B3-2	F	4.1	0.5	0.5	3920	14.1	9.2
B4-3	F	4.1	0.5	0	2760	15.4	3.3
B5-4	F	4.1	0	0.5	4190	8.3	8.9
B6-4	F	4.1	0.25	0.5	3080	12.3	9.8
B7-5	F	4.1	0.5	0.5	3730	14.8	9.3
B8-5	F	4.1	0.5	0.5	3400	12.1	9.5
Fiorato et al (1976)							
F1	F	3.9	0.3	0.7	5580	10.5	7.8
B2	B	3.7	0.3	0.6	7780	7.2	6.0

* F = Flange, B = Barbell

Park and Paulay (1974) made significant contributions towards the development of capacity design procedure for shear walls, which led to a major progress in novel design approaches in New Zealand Standards (NZS 3101.1&.2 – 1982 and 1995). The researchers mainly focused on shear wall design and reinforcement detailing. No attempt was made to quantify or evaluate the source of lateral load, i.e. earthquake or wind loads. Ductility, energy dissipation capability, stability, longitudinal bar buckling and boundary elements of shear walls were studied extensively. For the purpose of global stability of the wall, they assumed that the floors would have sufficient diaphragm strength and evaluated the global buckling of a shear wall using the floor height as unsupported length of the wall. They assumed bending moments and horizontal shears were generated by lateral loads and axial compression due to gravity loads. They concluded that the effect of web reinforcement, both vertical and horizontal was considerable and should be included in flexural capacity evaluation.

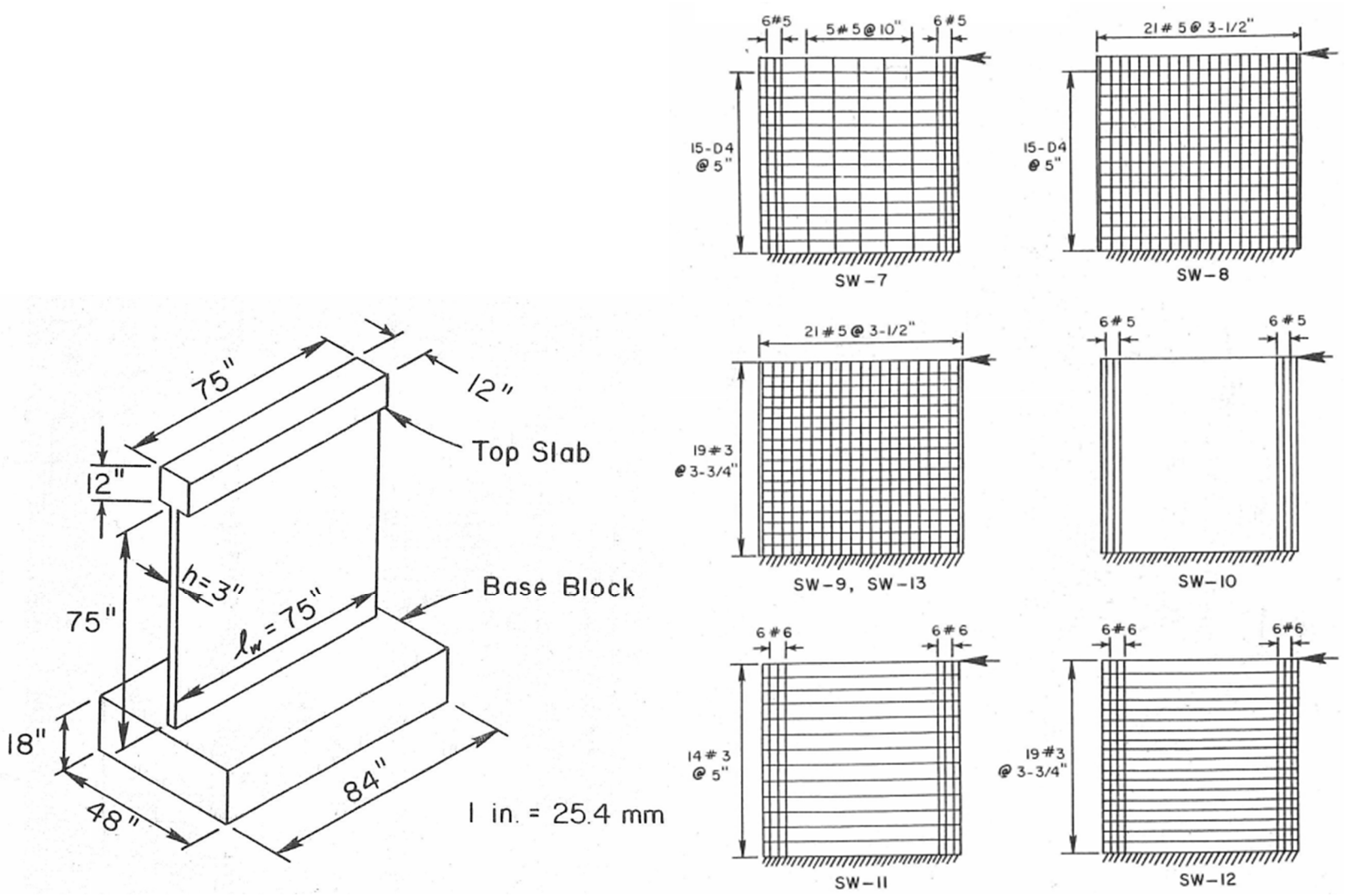

Figure 2.4 Reinforcement Layout for Low-Rise Shear Wall Specimens (Cardenas et. al. – 1980)

Park and Paulay reviewed the traditional practice of placing 0.25% uniformly distributed reinforcement in both orthogonal directions, which was the practice at the time, and realized that this methodology did not produce the most efficient design for walls. In other words, in the case of walls with uniformly distributed vertical reinforcement, the ultimate curvature and ultimate moment occurred when the longitudinal re-bars at the extreme ends of the wall experienced yield strain and the interior longitudinal bars which were not far from the neutral axis would not be efficiently utilized. This would consequently reduce the curvature ductility of shear walls. In order to improve the wall design efficiency when subjected to significant moments, they suggested placing most of the longitudinal bars at the extreme end zones since this approach would provide the longest lever arm between the coupling forces that develop in steel bars as tensile forces and in concrete at the other end in compression. The length of these zones was suggested to be approximately 10% of the total length of the wall and equal amounts of reinforcement on both ends were suggested due to the reversed nature of lateral forces. These end zones were named "*boundary elements*". It was indicated that transverse reinforcement for longitudinal bars in boundary elements should be provided to prevent the buckling of vertical bars under compressive forces, similar to axially loaded columns.

Park and Paulay also noted that in addition to providing overall reinforcement amounts and layout, special attention should be paid to the construction joints across the wall to avoid sliding shear failure. The beneficial effects of axial compression in increasing the lateral load resisting capacity of the walls should be approached cautiously since the actual axial compressive load during a seismic event could be different due to the presence of multiple shear walls in a structure (partial or full coupling of the walls).

The concept of boundary elements and related detailing requirements were subsequently introduced in ACI 318-89.

The out-of-plane instability and buckling concerns of a thin wall subjected to high compressive strains was further studied by Goodsir et al. (1983) and Goodsir (1985). During the experimental phase, they encountered out-of plane failures while experiencing inelastic deformations. The failure was explained by referring to the formation of large-scale cracks in concrete on the tension side, which lead to loss of integrity of the concrete in subsequent load cycles in the reverse direction where the same side would be subjected to compressive forces. It was suggested that the

accumulation of wide tensile cracks and application of compressive forces on such section could lead to uneven crack closure and sudden out of place movement of the compression zone. In addition, Goodsir (1982) showed that critical tie spacing requirements for columns are generally governed by confinement, buckling prevention and splicing of longitudinal bars rather than shear strength. This concern was addressed in NZC commentary on the Design of Concrete Structures (1982, 1995) and CSA A23.3 Standard (1984 and 1994) by limiting the wall thickness to unsupported wall height (i.e. height of first floor) to a minimum of 1:10. This limitation was further explained based on Eulerian buckling of struts.

2.2 Previous Research on Large Scale Shear Walls

A brief review of previous research on large-scale shear walls is presented below. The main goal of this review is to establish an understanding of the behavior of walls using conventional construction materials and use it as a comparative benchmark for the newly obtained experimental results within this research project, which utilized welded grids as boundary element tie reinforcement.

Portland Cement Association conducted a two-phase experimental study to determine the ductility, energy dissipation capability and strength of isolated cantilevered shear walls (Oesterle et al. 1976, 1979). The experimental research was followed by analytical research and was used to establish design criteria for reinforced concrete shear walls under seismic loads. The initial phase consisted of nine (9) wall tests followed by seven (7) wall tests in the second phase. The test specimens were approximately 1/3 scale, where no specific prototype walls were modelled. Two of the tests were performed on repaired wall specimens.

The experimental program included tests under monotonic and reverse cyclic loadings, and comparison of recorded flexural and shear strengths of walls under these two loading scenarios. The wall specimens also had various cross-sections (rectangular, I-shape and barbell-shape); percentages of main flexural reinforcement, horizontal shear reinforcement, and transverse hoop reinforcement; axial compression load; concrete compressive strength, and loading history. The wall specimens tested by Oesterle et al. (1976, 1979) were designed based on the requirements of ACI 318-71. The properties of test specimens and reinforcement ratios used are tabulated in Table 2.4. Wall specimen geometry is shown in Figures 2.5 to 2.17.

Table 2.4 Properties of Test Specimens (Oesterle et al. 1976, 1979)

Specimen	Shape	Axial Load psi	f'_c psi	f_y for ρ_f psi	Reinforcement (%)			
					ρ_f	ρ_h	ρ_n	ρ_s
R1		--	6490	74.2	1.47	0.31	0.25	--
R2		--	6735	65.3	4.00	0.31	0.25	2.07
B1		--	7685	65.2	1.11	0.31	0.29	--
B3		--	6860	63.5	1.11	0.31	0.29	1.28
B4 (1)		--	6530	65.3	1.11	0.31	0.29	1.28
B2		--	7775	59.5	3.67	0.63	0.29	--
B5		--	6570	64.4	3.67	0.63	0.29	1.35
B5R (2)		--	6205	--	3.67	0.63	0.29	1.35
B6		425	3165	63.9	3.67	0.63	0.29	0.81
B7		545	7155	66.4	3.67	0.63	0.29	1.35
B8		545	6085	64.9	3.67	1.38	0.29	1.35
B9 (3)		545	6395	62.3	3.67	0.63	0.29	1.35
B9R (2, 3)		450	7510	62.3	3.67	0.42	0.20	1.35
B10 (3)		545	6615	64.9	1.97	0.63	0.29	1.35
F1		--	5575	64.5	3.89	0.71	0.30	--
F2		480	6610	62.4	4.35	0.63	0.31	1.43

(1) Monotonic loading
(2) Repaired Specimen
(3) Modified reversing load history (MR Loading)
(4) 1000 psi = 1.0 ksi = 6.895 MPa

ρ_f = ratio of main flexural reinforcement area to gross concrete area of boundary element
ρ_h = ratio of horizontal shear reinforcement area to gross concrete area of a vertical section of wall web
ρ_n = ratio of vertical web reinforcement area to gross concrete area of a horizontal section of wall web
ρ_s = ratio of effective volume of confinement reinforcement to the volume of core in accordance with Eq. A.4 of ACI 318-71.

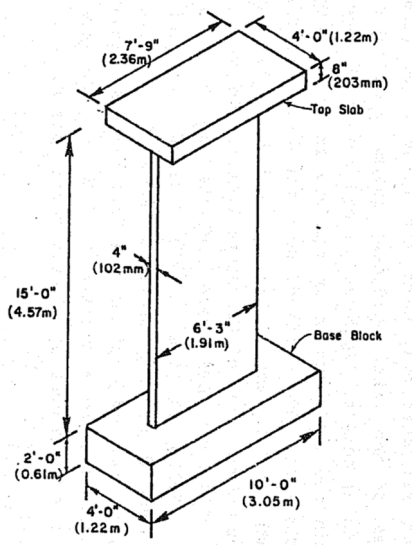

Figure 2.5 Nominal dimensions of test specimen with rectangular web-section (Oesterle et al. 1979)

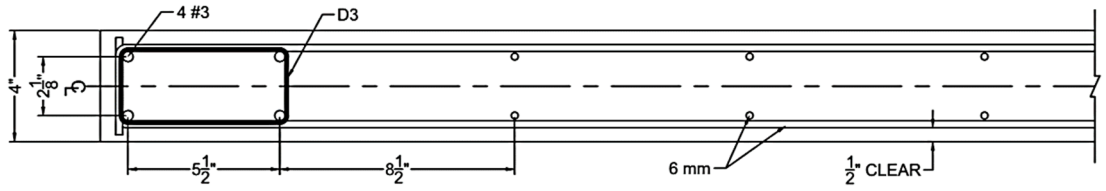

Figure 2.6 Shear Wall Specimen R1 – Cross Section (Oesterle et al. 1976)

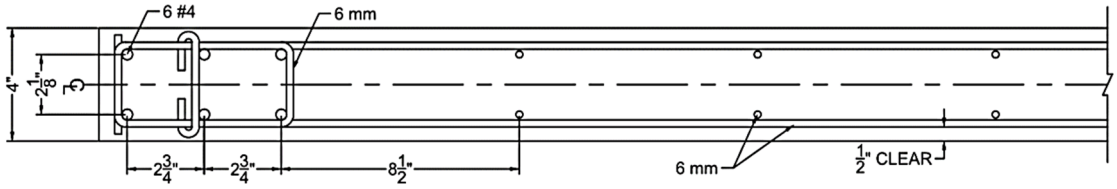

Figure 2.7 Shear Wall Specimen R2 – Cross Section (Oesterle et al. 1976)

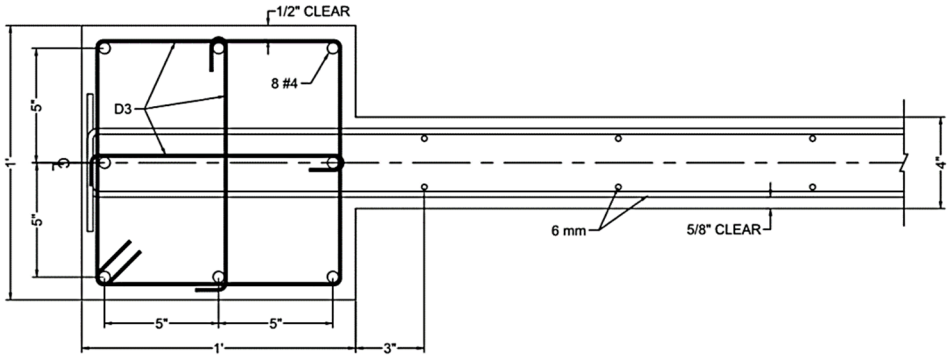

Figure 2.8 Shear Wall Specimen B1 – Cross Section (Oesterle et al. 1976)

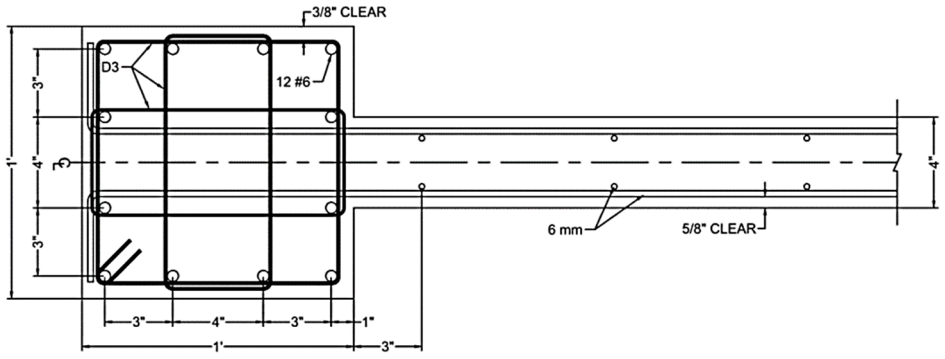

Figure 2.9 Shear Wall Specimen B2 – Cross Section (Oesterle et al. 1976)

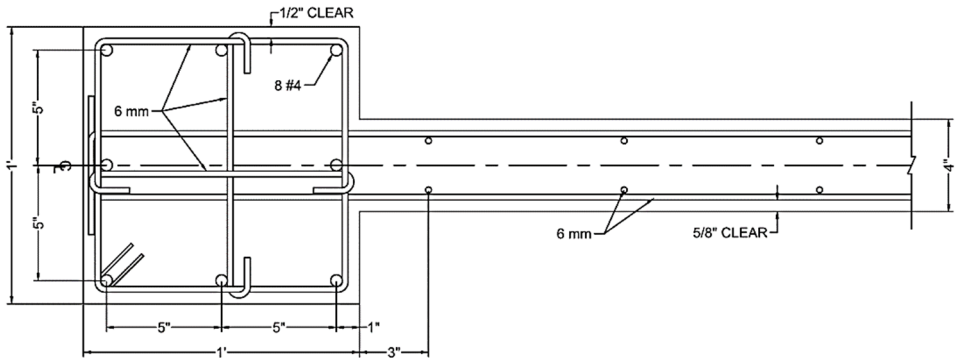

Figure 2.10 Shear Wall Specimen B3 and B4 – Cross Section (Oesterle et al. 1976)

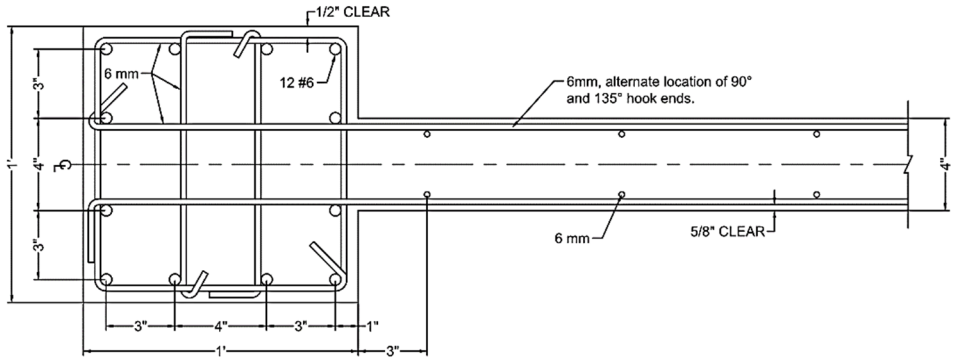

Figure 2.11 Shear Wall Specimen B5, B5R, B7 and B9 – Cross Section (Oesterle et al. 1976, 1979)

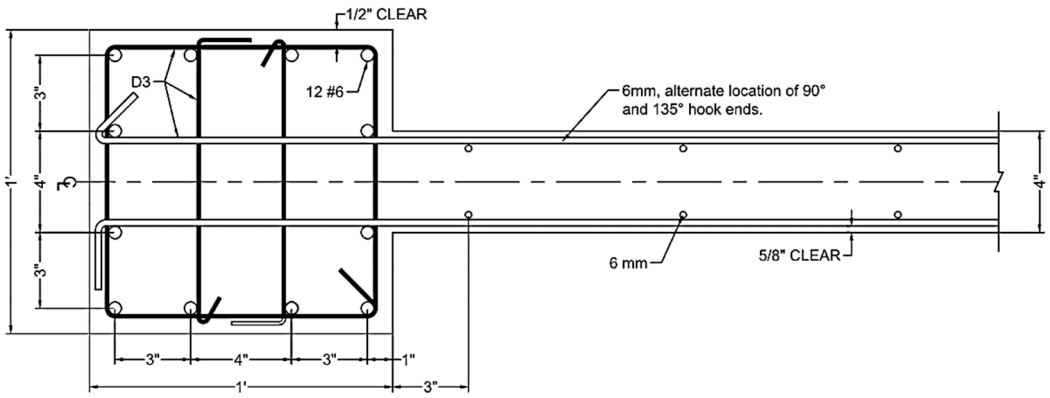

Figure 2.12 Shear Wall Specimen B6 – Cross Section (Oesterle et al. 1979)

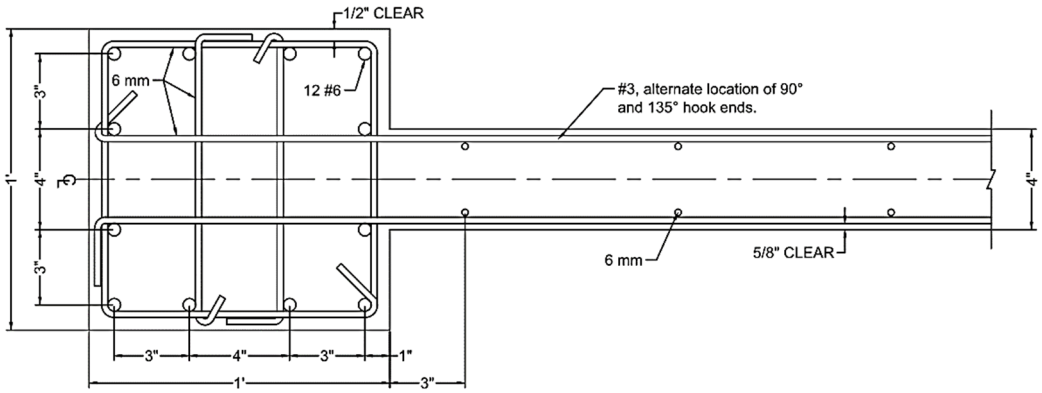

Figure 2.13 Shear Wall Specimen B8 – Cross Section (Oesterle et al. 1979)

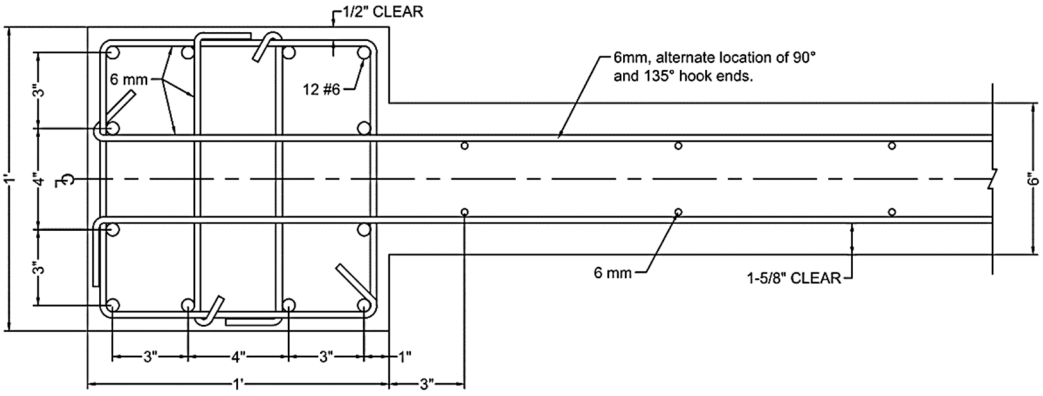

Figure 2.14 Shear Wall Specimen B9R – Cross Section (Oesterle et al. 1979)

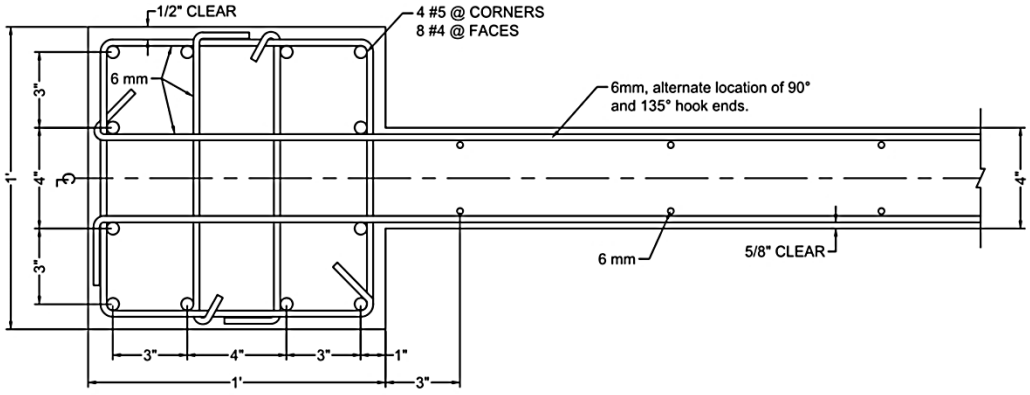

Figure 2.15 Shear Wall Specimen B10 – Cross Section (Oesterle et al. 1979)

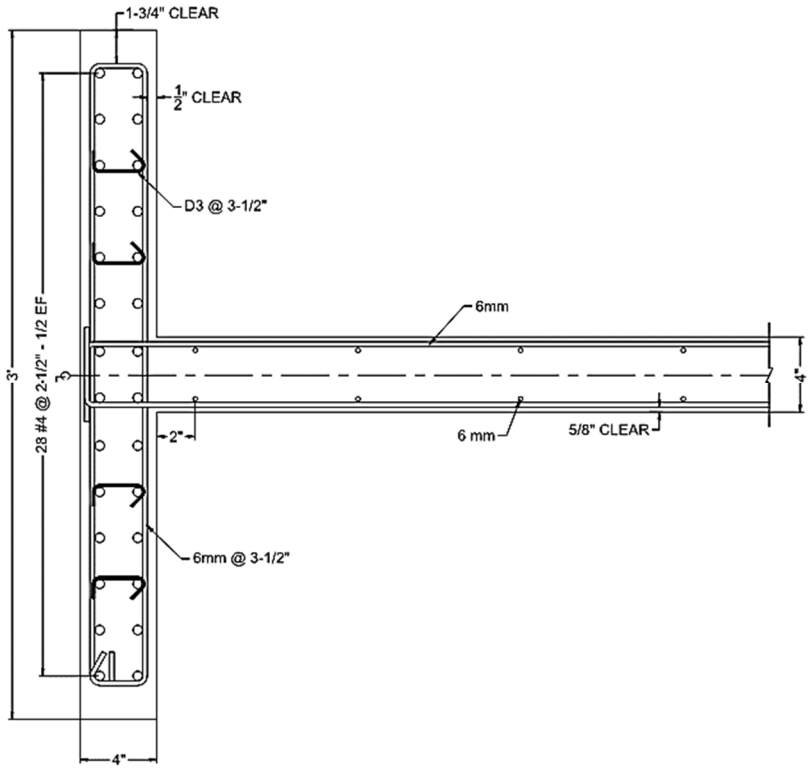

Figure 2.16 Shear Wall Specimen F1 – Cross Section (Oesterle et al. 1976)

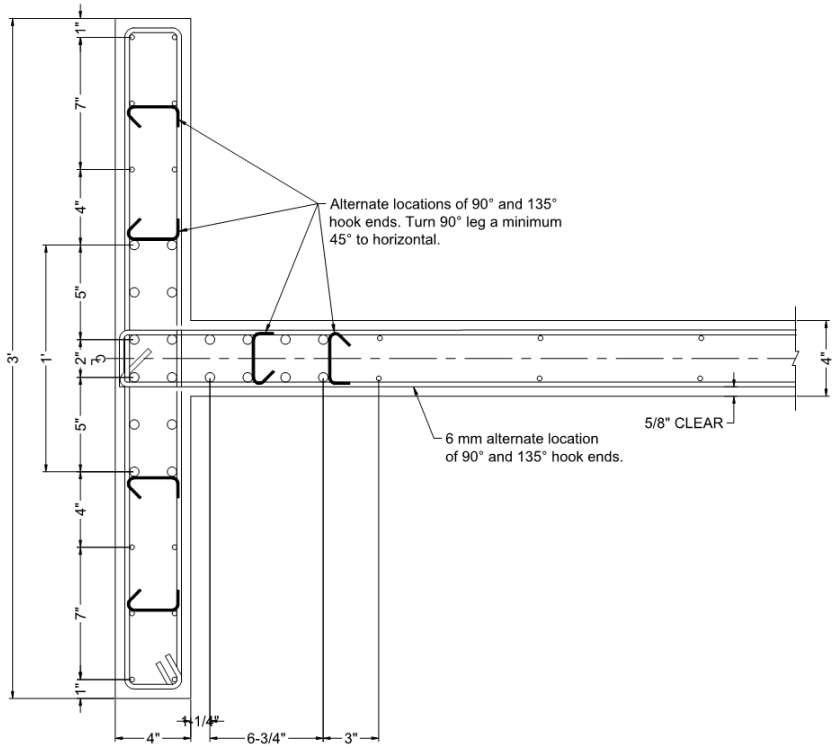

Figure 2.17 Shear Wall Specimen F2 – Cross Section (Oesterle et al. 1979)

The wall test results by Oesterle et al. (1976 and 1979) showed that the walls designed as per ACI 318-71 attained their flexural and shear design strengths; however, the code provisions underestimated the flexural capacity since it neglected strain hardening of steel reinforcement. It was concluded that this deficiency should be addressed since the seismically induced inertia forces engage the actual capacity of the wall and not the design flexural capacity. In other words, the shear demand can be significantly higher at the time wall yields and enters into the inelastic region. It should be noted that one of the rectangular walls failed prior to yielding due to out-of plane instability. The recorded and calculated strengths, as well as observed deformations for the wall specimens are tabulated in Tables 2.5 and 2.6, respectively.

It was observed that the shear capacity of the walls was limited by the crushing of web and the addition of the horizontal shear reinforcement did not increase the total shear capacity or ductility significantly. Providing transverse reinforcements (hoops) for boundary elements enhanced ductility greatly. It was noted that the confinement reinforcement was only essential in the anticipated hinging regions.

A rotational ductility of three to eight was recorded during the wall tests. The level of ductility was dependent on shear stresses, where walls with lower shear stresses (smaller than or equal to $3.0\sqrt{f'_c}$ MPa) exhibited higher ductility. The contribution of shear distortions to total lateral deformations was noted to be significant in inelastic regions. Measured strengths and ductility under reverse cyclic loading showed lower capacities than those under monotonic loading. For walls subjected to reversed cyclic loading, the loss of shear stiffness was observed and it was primarily dependent on the extent in which the wall was pushed in the previous cycle. Abrasion and concrete loss also contributed to shear strength loss. It was recommended that this variation in stiffness should be carefully considered in dynamic analysis of structural wall systems. The force-displacement graphs and the force-displacement envelopes are shown in Figures 2.18 to 2.34.

Vallenas et. al. (1979) conducted extensive experimental and analytical research on hysteretic behavior of reinforced concrete shear walls at the University of California, Berkley, California. Eight (8) reinforced concrete shear walls were built in 1/3 scale and were subjected to pseudo-static earthquake simulations. The walls were prototypes of the lower portions of seven and ten storey structures designed according to ACI 318-71. The hysteretic characteristics of the walls were investigated by quantifying strength, deformability, and energy dissipation capacities. The

researchers also further investigated the possible modes of failure. The analytical work aimed to provide a modelling technique to simulate the wall behavior under high shears when applied monotonically. It also provided a procedure for estimating total wall deformation under lateral loads by adding components due to flexure, shear and fixed end rotations.

The following variables were considered for the above mentioned experimental work: ***Wall cross sections (rectangular and framed)***: In terms of constructability, the forming of rectangular wall was simpler; however, placement of horizontal reinforcement with adequate anchorage in boundary elements was more challenging. The rectangular walls exhibited lower ductility and strength compared to the frame walls and were associated with i) introduction of significant eccentricity after crushing and spalling of concrete cover at the wall ends of rectangular walls; ii) higher steel ratio in rectangular walls and consequent reduction in overall specimen ductility compared to framed walls; iii) use of smaller diameter longitudinal bars resulting in lower buckling stresses in rectangular specimens.

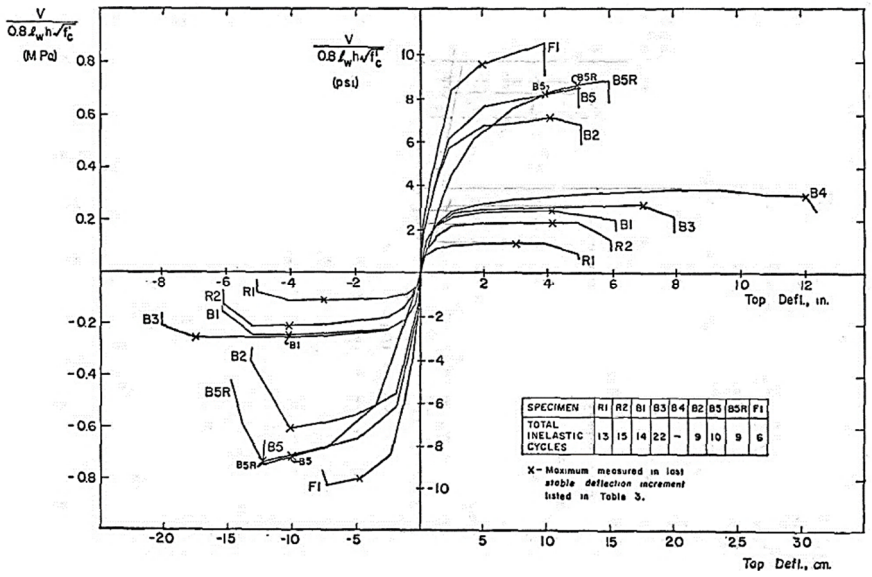

Figure 2.18 Load vs. Top Deflections Envelopes (Oesterle et al. 1976)

Table 2.5 Specimen Strengths (Oesterle et al. 1979)

Specimen	Confined Boundary Element	Axial Load psi	ACI Design				Full Yield Load					Maximum Load						Failure Mode [5]
			Flexure		Shear		Calculated [3]		Observed		$\frac{Obs.}{Clac.}$	Calculated [3]		Observed		$\frac{Obs.}{Clac.}$	$\frac{Obs.}{ACI}$ [4]	
			kips	$\sqrt{f'_c}$ [1]	kips	$\sqrt{f'_c}$	kips	$\sqrt{f'_c}$	kips	$\sqrt{f'_c}$		kips	$\sqrt{f'_c}$	kips	$\sqrt{f'_c}$			
R1	No	--	18	0.9	82 [2]	4.2	17.7	0.9	21.8	1.1	1.23	29.1	1.5	26.6	1.4	0.91	1.48	IB
R2	Yes	--	35	1.8	82 [2]	4.2	33.2	1.7	41.8	2.1	1.26	57.3	2.9	48.7	2.5	0.85	1.39	IC
B1	No	--	46	2.2	82 [2]	3.9	42.9	2.0	51.0	2.4	1.19	72.1	3.4	61.0	2.9	0.85	1.33	IB
B3	Yes	--	46	2.3	82 [2]	4.1	41.9	2.1	51.5	2.6	1.23	73.4	3.7	62.0	3.1	0.84	1.35	IB
B4	Yes	--	46	2.4	82 [2]	4.2	43.1	2.2	54.6	2.8	1.27	74.3	3.8	75.3	3.9	1.01	1.64	F
B2	No	--	129	6.1	127	6.0	115.6	5.5	128.0	6.0	1.11	170.9	8.1	152.8	7.2	0.89	1.18	WC
B5	Yes	--	129	6.6	127	6.5	123.1	6.3	138.0	7.1	1.12	213.7	11.0	171.3	8.8	0.80	1.33	WC
B5R	Yes	--	129	6.8	127	6.7	123.1	6.5	--	--	--	213.7	11.5	167.8	8.9	0.79	1.30	WC
B6	Yes	423	157	11.6	132	9.7	154.5	11.4	173.9	12.9	1.13	190.5	14.1	185.5	13.8	0.97	1.41	WC
B7	Yes	545	173	8.5	148	7.3	174.0	8.6	187.5	9.2	1.08	256.2	12.6	220.4	10.9	0.86	1.49	WC
B8	Yes	545	173	9.3	186 [6]	9.9	171.6	9.2	189.0	10.1	1.10	241.4	12.9	219.8	11.7	0.91	1.27	WC
B9	Yes	545	173	9.0	148	7.7	165.6	8.6	186.4	9.7	1.13	241.6	12.6	219.6	11.4	0.91	1.48	WC
B9R	Yes	451	173	5.6	162	5.2	165.6	5.3	--	--	--	241.6	7.7	218.7	7.0	0.91	1.35	WC
B10	Yes	575	121	6.2	148	7.6	116.1	5.9	139.7	7.2	1.20	168.0	8.7	159.0	8.2	0.95	1.32	BC
F1	No	--	145	8.1	140	7.8	148.1	8.3	150.6	8.4	1.02	242.6	13.5	187.9	10.5.	0.77	1.30	WC
F2	Yes	482	170	8.7	148	7.6	164.4	8.4	180.3	9.2	1.10	240.8	12.3	199.5	10.2	0.82	1.34	WC

[1] Lateral load in terms of nominal shear stress $v = \frac{V}{0.8 l_w b \sqrt{f'_c}}$ (psi)

[2] Shear reinforcement governed by maximum bar spacing.

[3] Calculated monotonic flexural strength from analysis based on strain compatibility using measured material properties including strain hardening of reinforcement.

[4] ACI taken as the lower of flexure or shear strength design strength with capacity reduction factor $\Phi = 1.0$.

[5] IB = "Inelastic" Bar Buckling, IC = Instability of Compression Zone, F = Flexural Bar Fracture, WC = Web Crushing, BC = Boundary Elements Crushing.

[6] Maximum $v = 10\sqrt{f'_c}$ governs, ACI Design Shear for B8 would be 256 kips = $13.7\sqrt{f'_c}$ disregarding the maximum allowable.

Table 2.6 Deformation Results (Oesterle et al. 1979)

Specimen	Top Deflection At Full Yield (in.)	Rotation at Full Yield θ_3 [2] (Rad.)	No. of Stable Inelastic Cycles	Last Stable Cycle No.	Max. Observed Top Defl. [1] (in.)	Max. Observed Rotation [1] θ_3 [2] (Rad.)	Max. Observed Shear Distort. [1] γ_3 [3] (Rad.)	Max Slip At CJI [1] (in.) [4]
R1	0.53	0.0030	13	25	- 4.06	-0.0240	-0.0130	-0.193
R2	0.85	0.0046	14	35	+ 5.25	+0.0212	-0.0300	-0.380
B1	0.70	0.0042	14	32	- 5.21	-0.0269	-0.0235	-0.258
B3	0.70	0.0090	21	39	- 7.07	+0.0276	-0.0481	+0.100 [8]
B4 [5]	0.80	0.0047	--	--	+ 12.50	+0.0630	+0.0340	+0.145
B2	1.00	0.0052	9	27	- 4.09	+0.0161	-0.0224	+0.170
B5	1.10	0.0065	10	28	+ 4.99	-0.0197	-0.0237	-0.134
B5R	2.50 [6]	0.0119 [6]	9	27	+ 4.93	+0.0204	-0.0237	+0.192
B6	1.31	0.0049	4	25	+ 3.08	-0.0136	-0.0085	-0.034
B7	1.38	0.0047	12	30	- 5.20	-0.0242	-0.0141	-0.106
B8	1.23	0.0049	12	30	+ 5.14	-0.0255	-0.01229	-0.101
B9 [7]	1.36	0.0048	1	3	- 5.43	+0.0238	-0.0137	-0.073
B9R [7]	2.99 [6]	0.0125 [6]	8	316	+ 6.88	-0.0287	-0.0197	-0.095
B10	1.17	0.0048	5	11	+ 4.99	-0.0243	-0.0112	-0.129
F1	1.00	0.0034	6	21	+ 1.99	-0.0093	-0.0080	-0.103
F2	1.13	0.0037	9	27	- 4.00	-0.0179	-0.0124	-0.062

(1) Maximum measured during last stable cycle.

(2) θ_3 = Rotation of the horizontal section approximately 74 in. (1.88m) above the base block.

(3) γ_3 = Average shear distortion in zone from base to approximately 74 in. (1.88m) above the base block.

(4) CJI = Construction Joint at the base of the wall.

(5) Monotonic Test.

(6) Measured deformation at yield load level of original specimen.

(7) Modified reversing load history.

(8) Gage failed in cycle 31 at ± 5 in. defl.

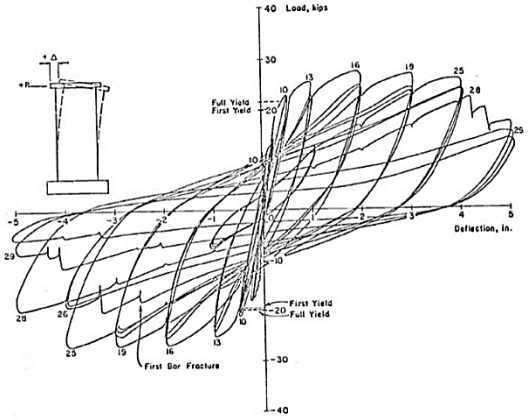

Figure 2.19 Continuous Load-Deflection Plot for Specimen R1 (Oesterle et al. 1976)

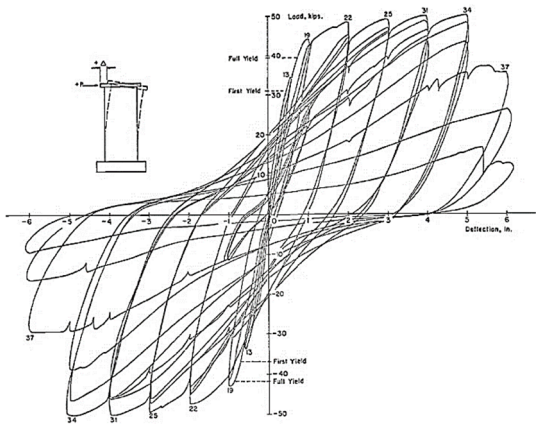

Figure 2.20 Continuous Load-Deflection Plot for Specimen R2 (Oesterle et al. 1976)

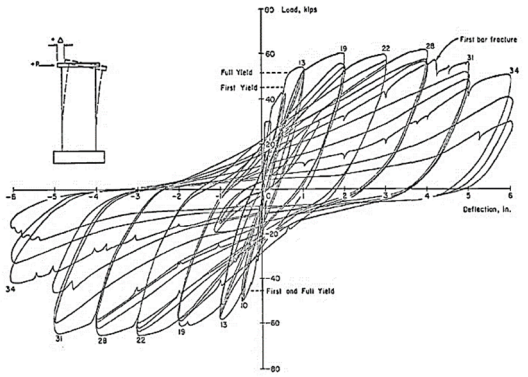

Figure 2.21 Continuous Load-Deflection Plot for Specimen B1 (Oesterle et al. 1976)

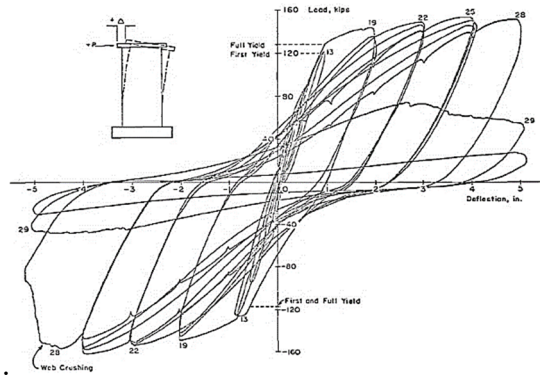

Figure 2.22 Continuous Load-Deflection Plot for Specimen B2 (Oesterle et al. 1976)

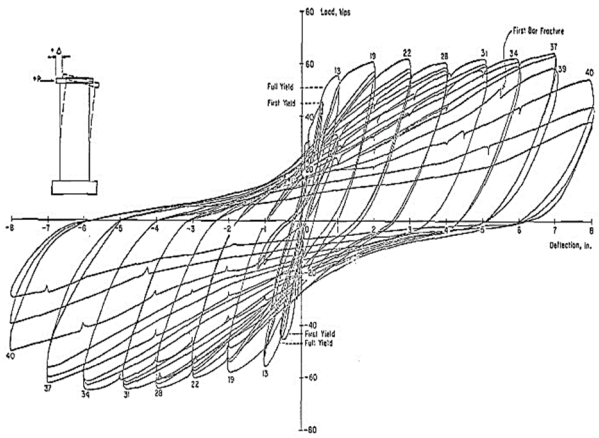

Figure 2.23 Continuous Load-Deflection Plot for Specimen B3 (Oesterle et al. 1976)

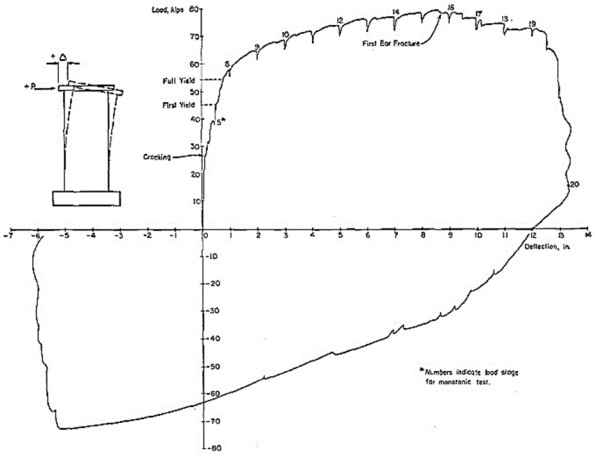

Figure 2.24 Continuous Load-Deflection Plot for Specimen B4 (Oesterle et al. 1976)

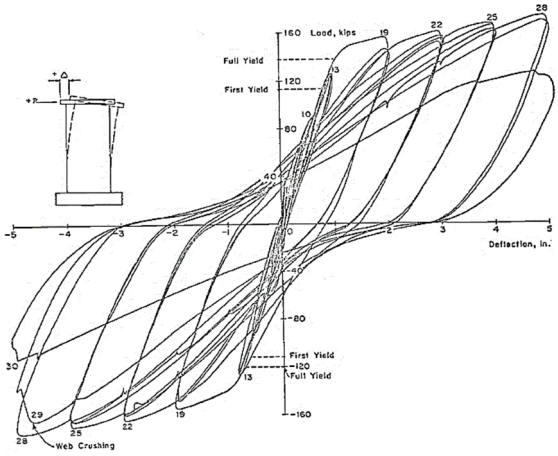

Figure 2.25 Continuous Load-Deflection Plot for Specimen B5 (Oesterle et al. 1976)

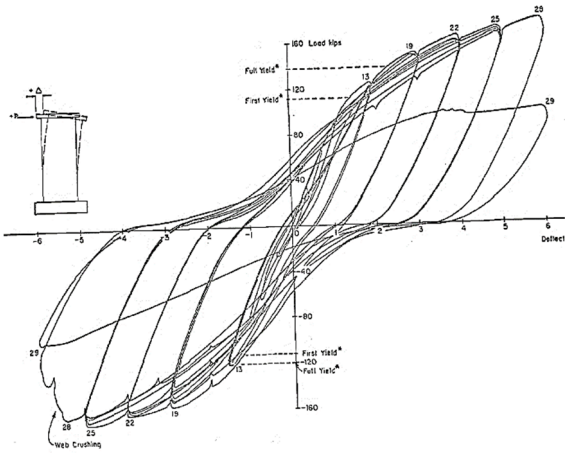

Figure 2.26 Continuous Load-Deflection Plot for Specimen B5R (Oesterle et al. 1976)

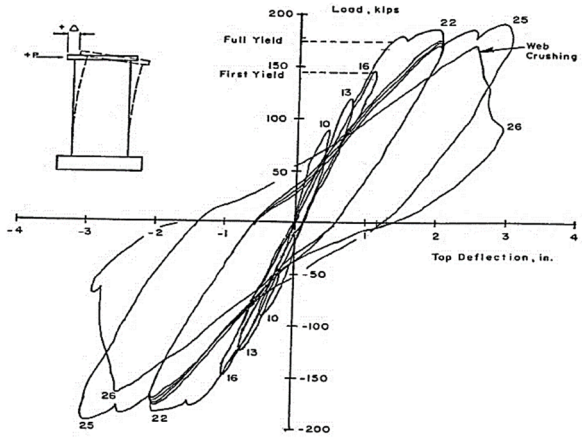

Figure 2.27 Continuous Load-Deflection Plot for Specimen B6 (Oesterle et al. 1979)

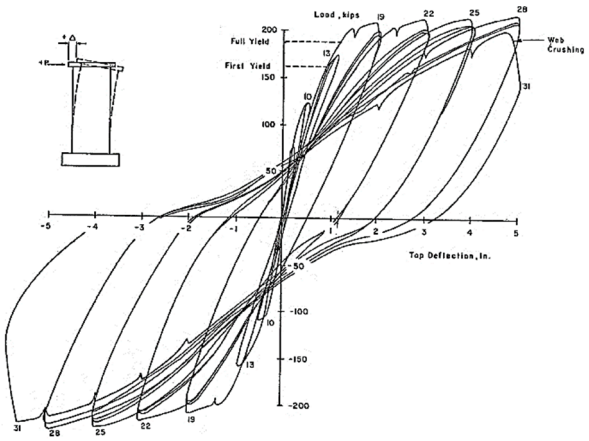

Figure 2.28 Continuous Load-Deflection Plot for Specimen B7 (Oesterle et al. 1979)

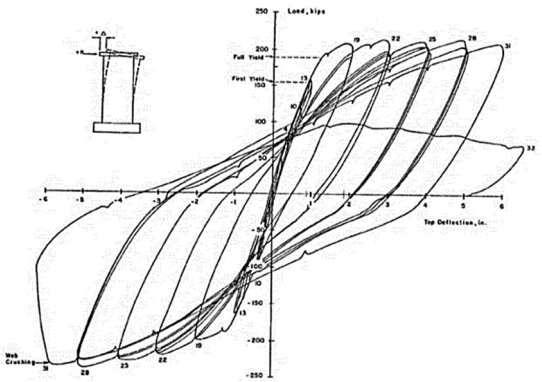

Figure 2.29 Continuous Load-Deflection Plot for Specimen B8 (Oesterle et al. 1979)

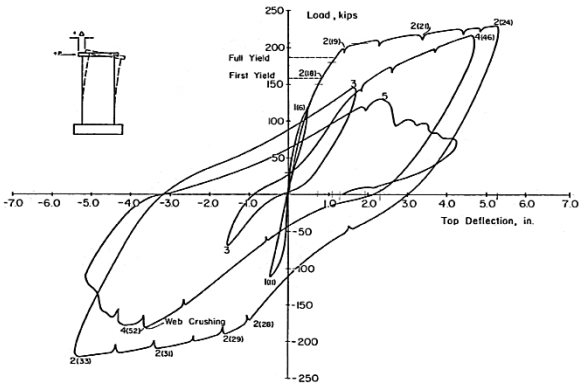

Figure 2.30 Continuous Load-Deflection Plot for Specimen B9 (Oesterle et al. 1979)

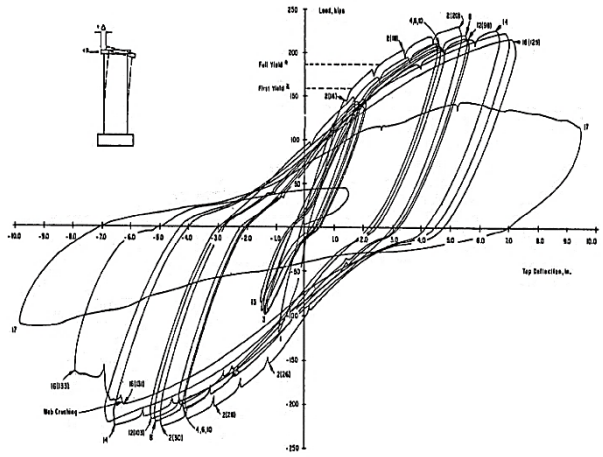

Figure 2.31 Continuous Load-Deflection Plot for Specimen B9R (Oesterle et al. 1979)

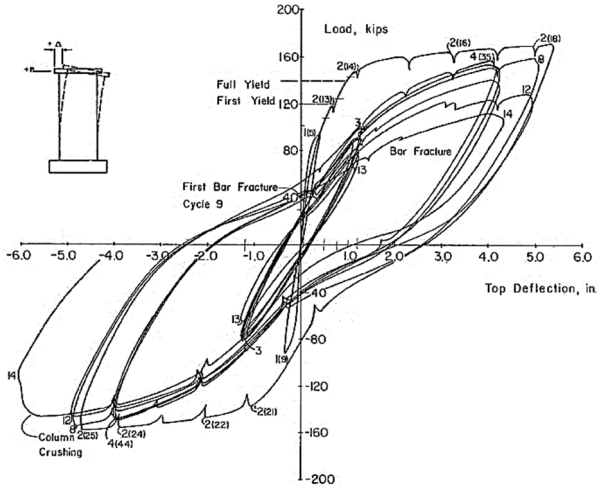

Figure 2.32 Continuous Load-Deflection Plot for Specimen B10 (Oesterle et al. 1979)

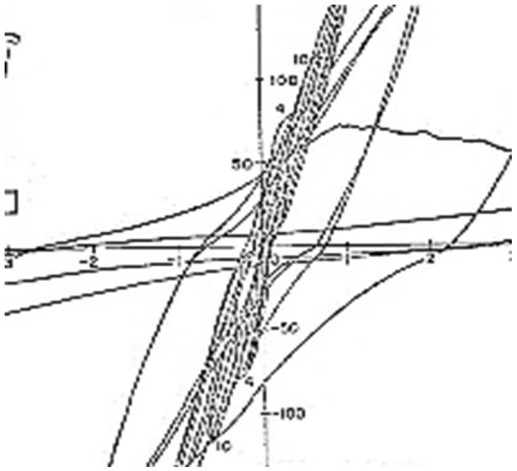

Figure 2.33 Continuous Load-Deflection Plot for Specimen F1 (Oesterle et al. 1976)

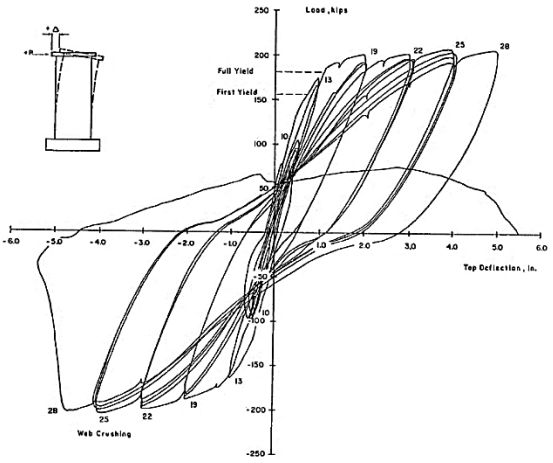

Figure 2.34 Continuous Load-Deflection Plot for Specimen F2 (Oesterle et al. 1979)

Confinement of boundary elements: the maximum achievable compressive strain in a monotonically loaded wall is limited by the buckling of longitudinal re-bars, which were directly affected by the spacing of transverse reinforcement. The spiral transverse reinforcement showed superior performance compared to rectangular hoops in controlling crack widths in boundary elements. The reduction of crack width resulted in higher stability of boundary elements under load reversals.

Loading histories: The overall deformation capacity of wall specimens subjected to reversed cyclic loading ranged between 84% to 89% of companion walls under monotonic loading. The recorded wall strength for cyclic loading was reduced to 92% - 95% compared to monotonic

loading. The contribution of shear deformations was increased for the walls subjected to load reversals. The overall energy absorption and dissipation capacities were significantly reduced for walls under load reversals, especially where large cracks had to be closed prior to partially regaining the lost stiffness (pinching).

The natural frequency and the critical damping ratio of the wall specimens were measured at several stages during the experiment. The undamaged virgin wall specimens exhibited an average critical damping ratio of 2.2%. It was observed that as the samples undergo higher load magnitudes and walls experience yielding and various levels of permanent damage, the natural frequency dropped but the damping ratio increased. This increase could be attributed to energy dissipation along the cracks. It should be noted that the actual magnitude of the natural frequency and critical damping ratios could not be quantified as a singular value since the natural frequency of the wall specimen was largely dependent on the magnitude of the applied axial load. The applied load would affect the size and distribution of cracks which affected the damping ratio. Also, the natural frequency of a single wall element was not deemed to be an appropriate representation of a building with multiple components and complex internal interactions.

The following include the topics which were considered in the analytical work of Vallenas et al. (1979):

- ***Modeling the behavior mechanism of structural walls***: the model recognized diagonal cracking under high shear conditions, which caused redistribution of stresses;
- ***the effect of residual cracks*** and temporary reduction in moment of inertia within the load reversal cycles were considered (pinching);
- ***the interaction of flexural cracks with shear cracks*** and the effect of aggregate interlock, bond capacity and dowel actions were recognized;
- ***the shear degradation*** and its influence on estimating total shear deformation was investigated.

The results of the research were used to better understand shear wall behavior in responding to seismically induced forces and how the walls absorbed and dissipated energy. The design procedures were revised to implement these understandings in design. The geometry and dimensions of the framed-wall specimens in Vallenas et. al. research is shown in Figures 2.35 to

2.38. The force-displacement recording at top of these specimens (third floor) is presented in Figures 2.39 to 2.46.

2.3 Previous Research on WWR Grids as Transverse Reinforcement

This section focuses on previous research, which implemented WWR grids as transverse reinforcement for columns or boundary elements. WWR curtains have been traditionally used as replacement for conventional re-bars or wires for flexural applications, and in some studies, they were also used as shear reinforcement for beams (Ali Mirza and MacGregor 1981, Lee et al. 1989, Lin and Perng 1998, Mansur et al. 1987 and 1991, Pincheira et al. 1989).

Razvi (1988) and Razvi and Saatcioglu (1989) conducted thirty-four (34) small scale columns to investigate concrete confinement using hoops and welded wire fabrics as transverse reinforcement. The column samples had different tie spacing, transverse reinforcement quantity, tie hooks, location and size of WWR grids. The research also focused on evaluating the performance of welded wire fabric combined with conventional hoops with 90 and 135-degree hook ties. The columns were subjected to monotonic concentric axial compression loads to failure. The columns utilizing 135-degree hooks showed superior performance compared to 90-degree hooks. The use of welded wire fabric for concrete confinement showed improvements on both strength and ductility of column specimens.

Furlong et al. (1991) studied the use of WWR as transverse reinforcement for columns. A total of eight (8) near full size column specimens were divided into four sets of twin samples, where one set was constructed using conventional reinforcement and the other using welded structural wire reinforcement. The twin samples were poured using the same concrete batch and they had identical longitudinal reinforcement ratios, as well as transverse reinforcement ratio per linear length of the columns. However, these twin columns did not have identical number or size of longitudinal bars nor did they have similar tie spacing. Also, it is noteworthy that for columns constructed using welded structural wire reinforcement, the longitudinal bars were not located at the corner of the transverse grids.

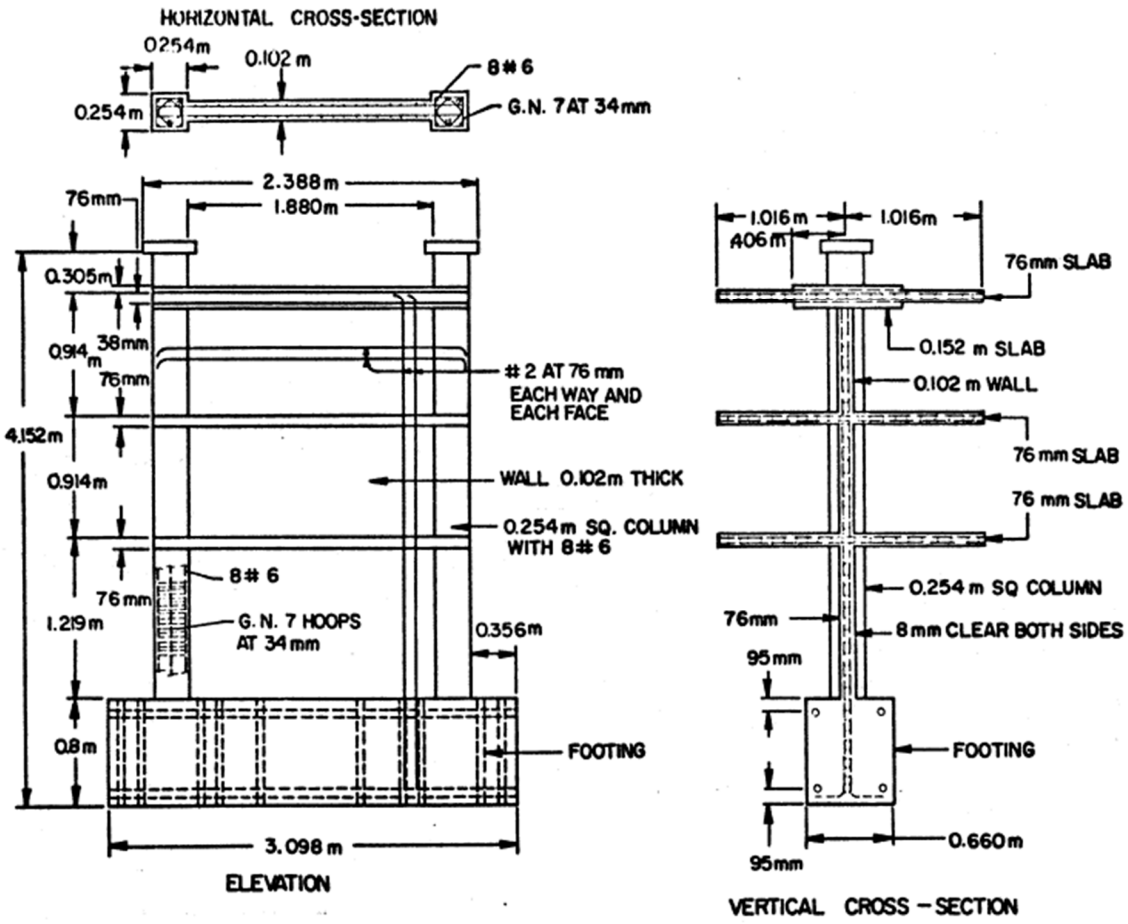

Figure 2.35 Dimensions and Details of Framed-Wall Specimens (Vallenas et. al. 1979)

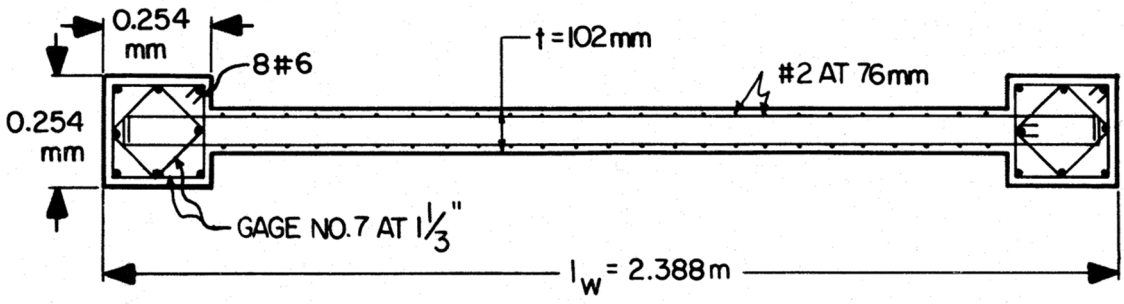

Figure 2.36 Detailed Cross-Section of Framed Wall (Vallenas et. al. 1979)

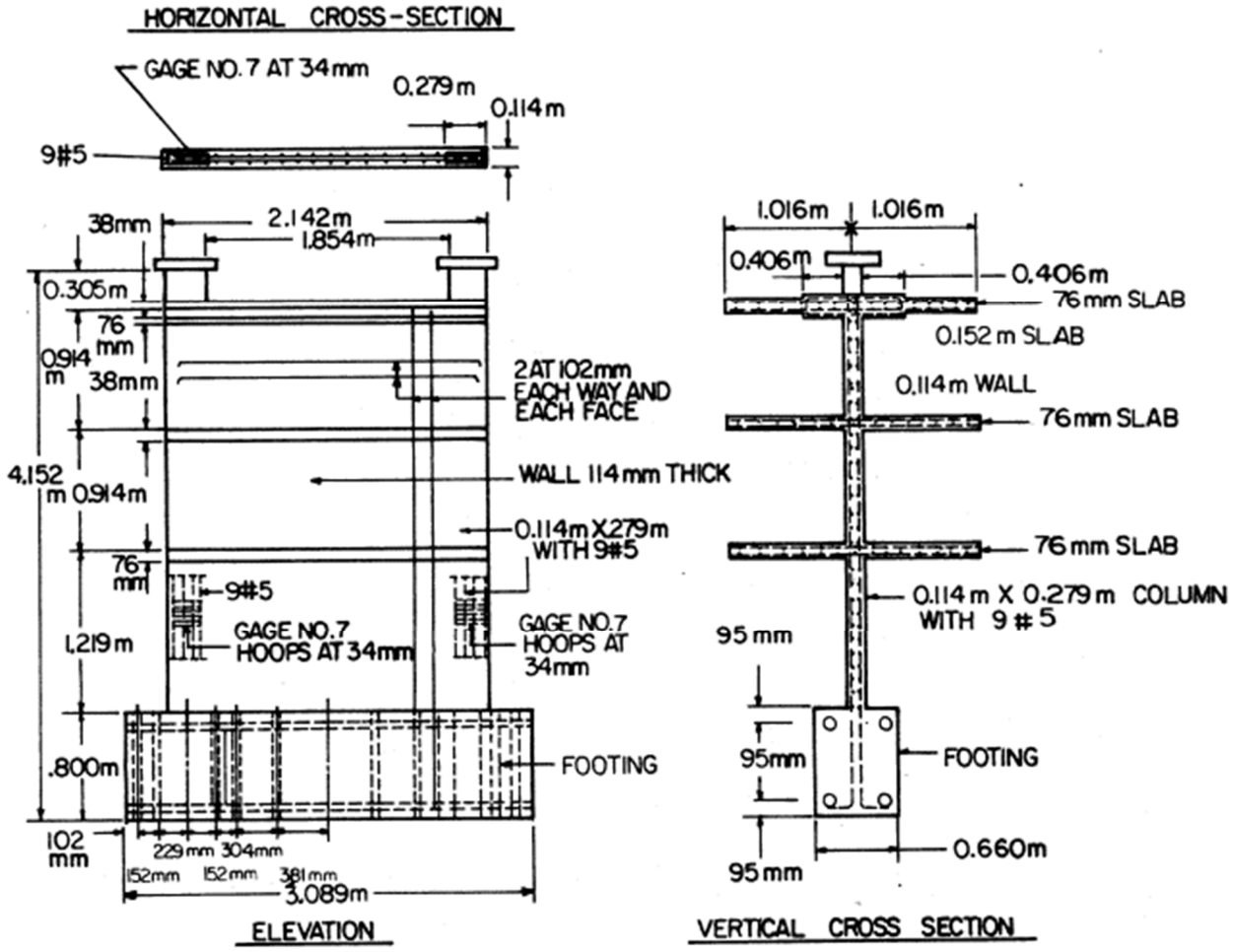

Figure 2.37 Dimensions and Details of Rectangular Specimens (Vallenas et. al. 1979)

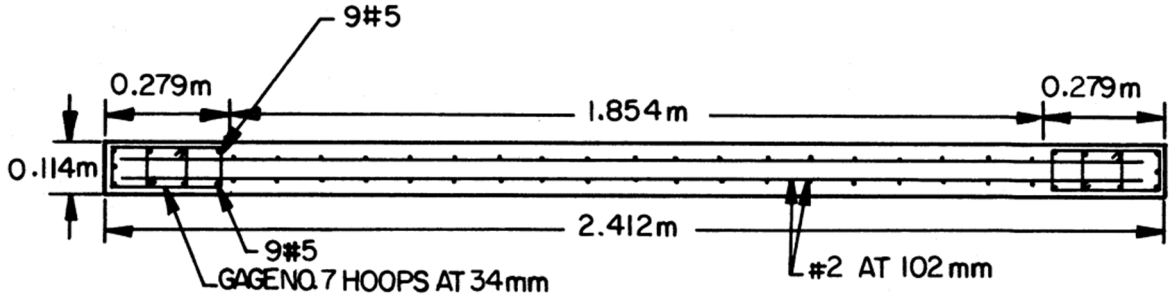

Figure 2.38 Detailed Cross-Section of Rectangular Wall (Vallenas et. al. 1979)

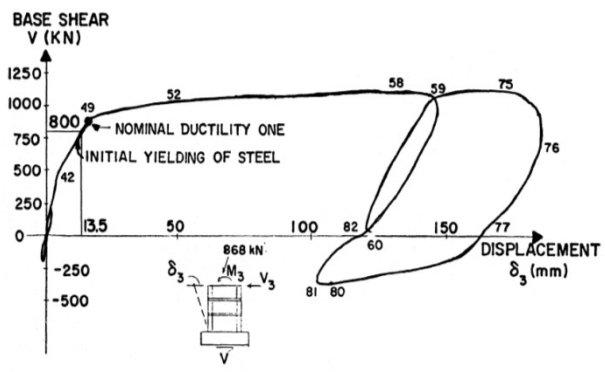

Figure 2.39 Displacement at Third Floor of Framed Wall – Monotonic Loading – Specimen 3 (Vallenas et. al. 1979)

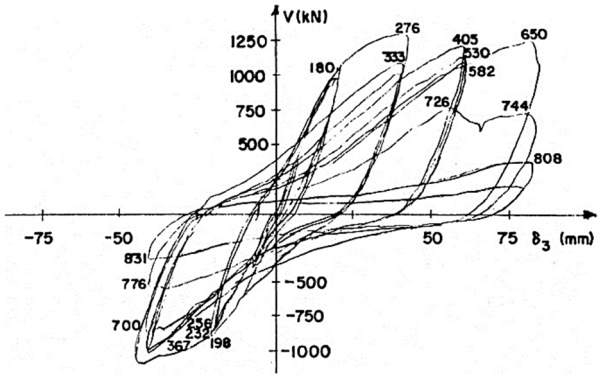

Figure 2.40 Displacement at Third Floor of Repaired Framed Wall – Cycilc Loading – Specimen 3R (Vallenas et. al. 1979)

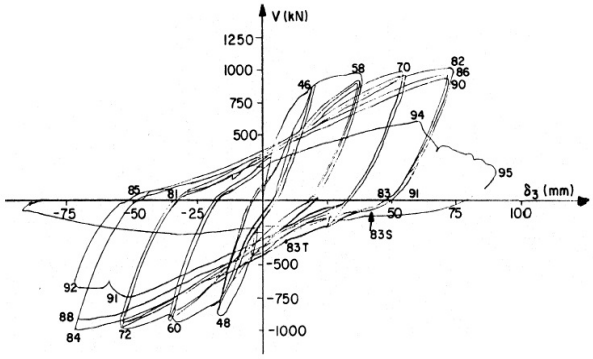

Figure 2.41 Displacement at Third Floor of Framed Wall – Cyclic Loading – Specimen 4 (Vallenas et. al. 1979)

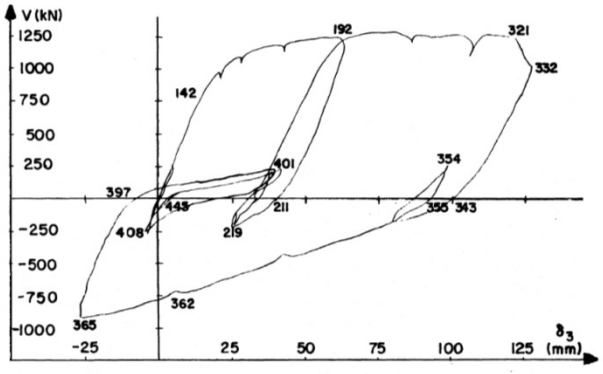

Figure 2.42 Displacement at Third Floor of Repaired Framed Wall – Monotonic Loading – 4R (Vallenas et. al. 1979)

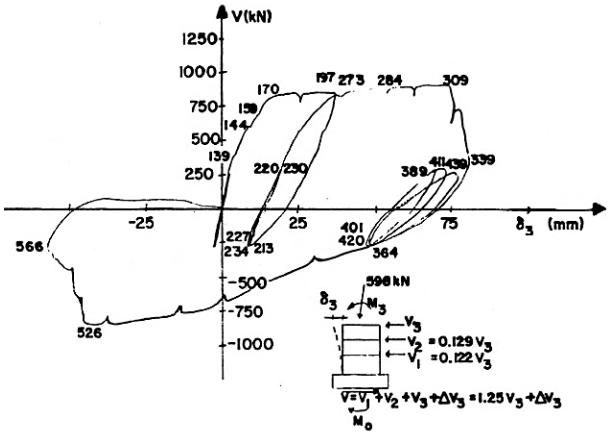

Figure 2.43 Displacement at Third Floor of Rectangular Wall Monotonic Loading – 5 (Vallenas et. al. 1979)

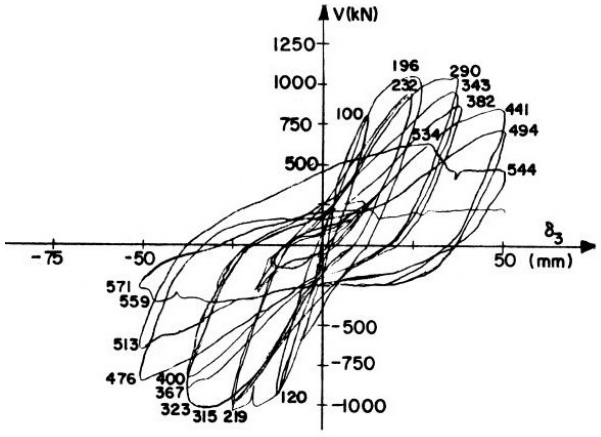

Figure 2.44 Displacement at Third Floor of Repaired Rectangular Wall – Cyclic Loading – 5R (Vallenas et. al. 1979)

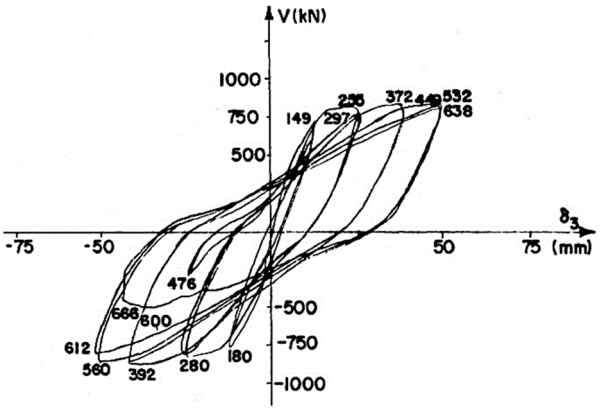

Figure 2.45 Displacement at Third Floor of Rectangular Wall – Cyclic Loading – Specimen 6 (Vallenas et. al. 1979)

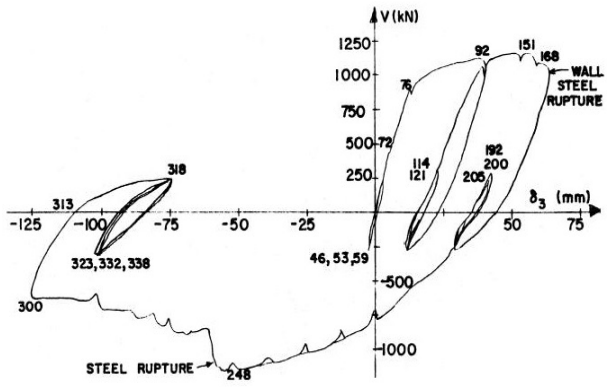

Figure 2.46 Displacement at Third Floor of Repaired Wall – Monotonic Loading – Specimen 6R (Vallenas et. al. 1979)

The welded structural wire reinforcement had a higher yield strength of 517 to 565 MPa compared to conventional reinforcement with yield strength of 400 MPa. The welded structural wire steel sheets were machine bent along each corner to form the column steel cage. The columns were then subjected to axial compression combined with an eccentricity of 1/15th of the column thickness and loaded to failure where all longitudinal bars under compression buckled as soon as the stabilizing concrete cover spalled. It was observed that conventionally reinforced columns resisted larger loads than the twin samples using welded structural wire reinforcement. Apparently, the full yield strength of the wire did not occur prior to spalling of the concrete cover and buckling of longitudinal bars. The lower overall strengths of columns with WWR were attributed to the fact that the spacing between transverse ties exceeded the maximum allowable spacing as per ACI 318-89 and also the absence of corner bars. All column samples showed an overall capacity exceeding calculated design capacity by ACI 318-89 except one, which failed at 97%. Both conventionally reinforced and WWR columns exhibited similar stiffness and capacity within the elastic range.

In 1990, Miranda et al. at University of California at Berkley conducted an experimental research on shear walls using prefabricated welded wire hoops as transverse reinforcement for boundary elements. The experiment included six (6) full size shear walls and had various transverse reinforcement ratios, sizes and spacing. The research aimed to determine practical implications of the MEDO mesh modules as transverse reinforcement to provide a better understanding of the behavior of the shear walls equipped with WWR grids before using these grids for a proposed construction of 17-storey high buildings at San Francisco State University in San Francisco,

California. The first three samples had 6.1% longitudinal reinforcement in their boundary elements whereas the second three samples had 6.0%. The volumetric ratio of transverse reinforcement varied from 0.48% to 2.0%. Using 0.48% transverse reinforcement for two of the shear walls resulted in tie spacing exceeding UBC-1988 maximum allowable limits. The wall specimens were selected to have a minimum width to length ratio of three (3). The yield strength of welded wire reinforcement ranges from 78.0 to 81.5 ksi depending on the wire size, where smaller wires showed higher yield strength. Four of the samples failed due to global buckling by reaching lateral instability. Based on the observations during the tests, the researchers indicated that theses failures could be attributed to the significant axial load on longitudinal bars prior to closure of residual cracks remaining from the previous loading cycle in the opposite direction. It was also observed the deformability of specimens using MEDO mesh modules is highly dependent on the strength of the resistance welds which join the wires in the module. In the testing program, the failure of MEDO mesh modules occurred at the resistance weld or in the heat affected zone near the resistance welds. It was recommended that since the effectiveness of these modules as transverse reinforcement is dependent on the development of the nominal yield strength of the wires, proper quality control of the manufacturing process should be maintained to a level that guarantees that the strength of the weld to be greater than the tensile strength of the wire.

In 1989 Thompson et al. studied the behavior of twelve (12) concrete column samples representing the boundary elements of shear walls incorporating MEDO modules as transverse reinforcement. The columns were loaded under monolithically increasing axial loads up to failure. The research helped to examine the hysteretic behavior of shear wall boundary elements using such type of reinforcement. The test results showed that the confinement effectiveness of the MEDO mesh modules was equal to or more effective than the confinement effectiveness of traditional deformed closed hoops in strain range of 0.00 to 0.02.

Grira and Saatcioglu (1996), Grira (1998) and Saatcioglu and Grira (1999) conducted experimental research in the Structural Laboratory at University of Ottawa using WWR grids as transverse reinforcement for columns. A total number of ten (10) full-scale 350mm x 350mm square concrete columns with longitudinal reinforcement ratios ranging from 1.96% to 3.26% were constructed and tested. The WWR grids had a center to center dimension of 292mm x 292 mm and were supplied in four (4) and nine (9) cell configurations as shown in Figure 2.47.

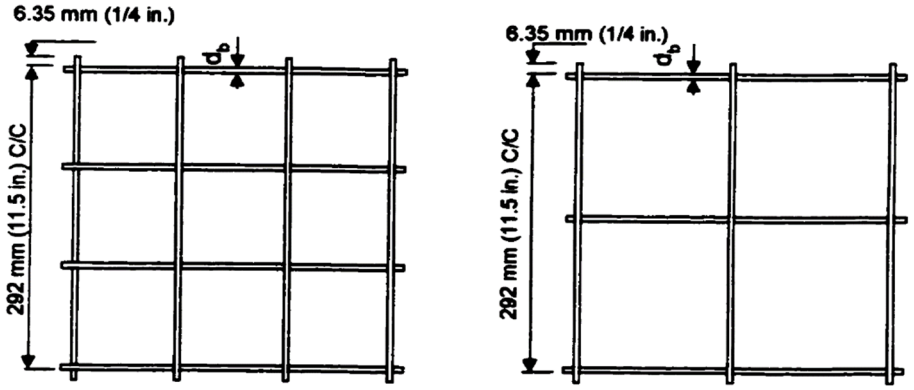

Figure 2.47 Geometric Details of Welded Wire Reinforcement Grids (Grira 1998)

The columns had volumetric transverse reinforcement ratios ranging from 1.0% to 2.66% using 6.60 mm and 9.53mm diameter wires, spaced at either 76mm or 152mm on the longitudinal bars. The ACI 318-95 code prescribed approach required a minimum transverse volumetric ratio of 1.52% to 1.55% for these columns which means five of the column specimens had less than the code prescribed transverse reinforcement amount. The wires showed yield strengths of 570 and 580 MPa for 9.53mm diameter and 6.60mm diameter wires, respectively. The columns were subjects to 20% or 40% of their nominal axial capacity, and were subjected to incrementally increasing lateral load reversals where each deformation level was repeated three times. The columns were loaded to failure where except column specimen BG-1, the specimens developed lateral drifts equal or greater than those expected in columns confined with conventional hoops and crossties of equal volumetric ratio, grade, arrangement and spacing. Column specimen BG-1 failed at 1 percent lateral deformation and had ties spaced at half the cross-sectional dimension of the column equal to only 65% of ACI 318-95 minimum required transverse reinforcement ratio. The experimental results also indicated that for the same volumetric ratio of transverse reinforcement, the columns using 9-cell grids as ties performed better than companion 4-cell grids. During the material test phase, the laboratory test results established that the strength and ductility of the steel wires forming the grids were not adversely affected by the resisting weld process. Column tests showed no grid failure prior to rupturing of the longitudinal bars in tension or buckling under compression. Two columns exhibited grid failures beyond these limiting load conditions.

It should be noted that the grids used in the research study conducted by Grira at the University of Ottawa were donated by BauMesh Company of Newport Beach who also donated the WWR grids

used in the current research study. During Grira's experimental study, the individual grids were tested and none of them showed any sign of corner weld failure and all grids failed by rupturing of the steel bars. Figures 2.48 and 2.49 illustrate an example of a tested grid and recorded force-displacement under diagonal loading (burst test). However, as reported in the upcoming chapters, testing of the new batch of grids showed failure of all grids at the weld locations, implying weaker joint capacity compared to the batch tested by Grira. This observation is further discussed at the end of the thesis where design and testing recommendations are provided.

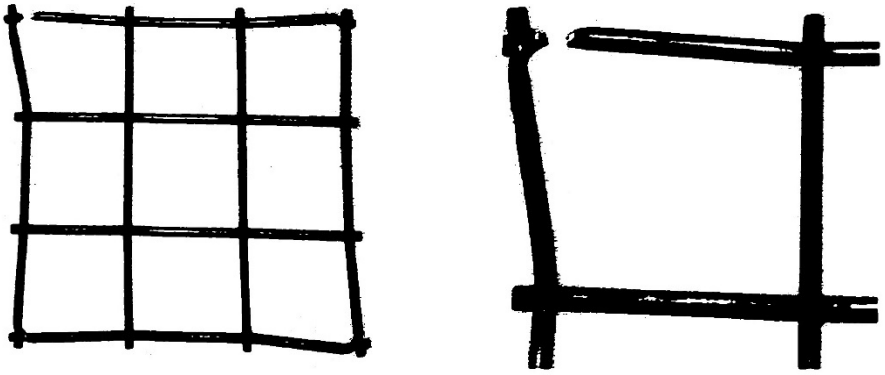

Figure 2.48 An example of failed WWR Grid under diagonal loading (Burst Test) (Grira 1998)

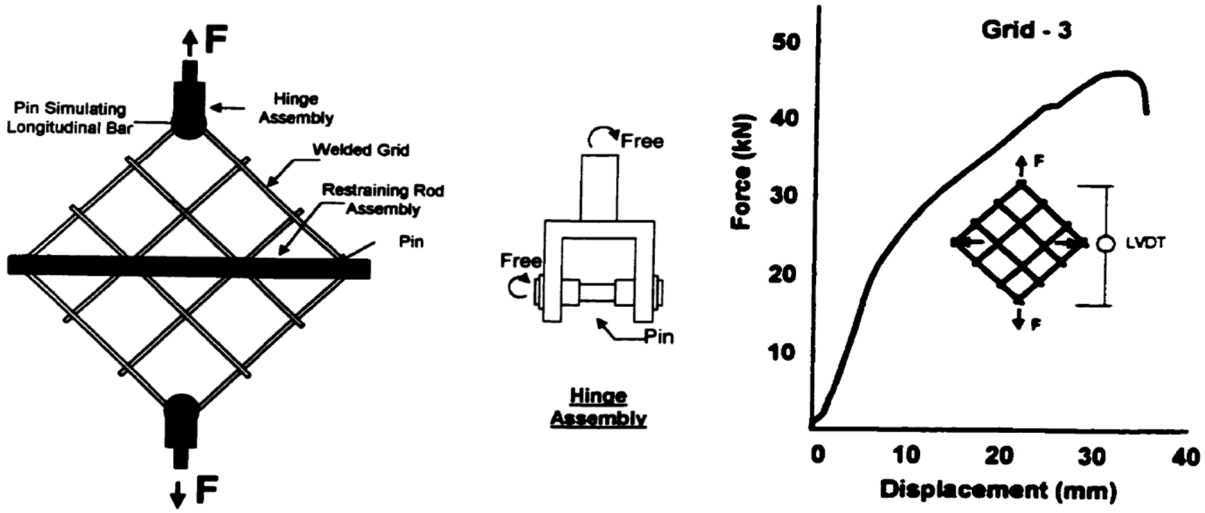

Figure 2.49 WWR Grid Burst Test (Grira 1998)

2.4 Summary of Previous WWR Grid Research and Future Needs

The previous research on WWR grids as transverse reinforcement was conducted on columns by Grira and Saatcioglu (1996, 1998, 1999) at the University of Ottawa. The research project was primarily experimental in nature and involved a large number of large-scale reinforced concrete columns tests under reverse-cyclic loading. The outcome of the research program showed ductile behavior where the grids maintained their integrity without welds failures. In almost all cases the grids failed through the rupturing of steel in tension. While this research program showed encouraging results, it did not provide sufficient information for extending these findings to other structural elements, including reinforced concrete shear wall boundary element. Furthermore, concerns over premature weld failure prompted a new limitation in the ACI 318-14 Concrete Code, disallowing the use of such grids in seismic applications. Indeed, ACI 318-14, Clause 20.2.2.4 prohibits the use of WWR grids as defined in sub-note [2] "*ASTM A1064 and A1022 is not permitted in special seismic systems where the weld is required to resist the stresses in response to confinement, lateral support of longitudinal bars, shear, or other actions*". This research aims to provide additional information and experimental evidence on the performance of WWR grids for such applications.

Chapter 3

Material Properties

3.1 General

The first step in the experimental program was to establish the characteristics of materials used in the shear wall test program. Standard cylinder tests and coupon tests were performed to establish stress-strain relationships of concrete and steel. The steel consisted of deformed reinforcement used as vertical and horizontal wall reinforcement, wires used in producing WWR, and seven wire strands used in the test setup to apply gravity loads on walls.

The properties of WWR, other than the stress-strain relationship of the wire used, is investigated in a separate test program reported in Chapter 4, with a focus on grid weld performance. This involved tests of grids, subjected to uni-directional tension in the plane of grid samples either parallel to the longitudinal grid direction or the grid diagonal. The same tests were repeated on grids embedded in concrete, forming small concrete prisms. Finally, buckling restraining action of grids was investigated through tests of small-scale reinforced concrete column under monotonic compression. The results of these small-scale grid material tests are presented in Chapter 4.

3.2 Reinforcing Steel Bars

The stress-strain relationship of conventional reinforcement used as vertical and horizontal wall reinforcement was established by performing a series of coupon tests. Representative stress-strain relationship for deformed reinforcement is shown in Figure 3.1. Initial deformations of coupons, up to approximately the onset of strain hardening, were measured using an extensometer with a 50-mm grip span. Larger deformations recorded well into the post-yield region were obtained from loading head movement of the universal loading machine. Figure 3.2 shows a typical coupon test.

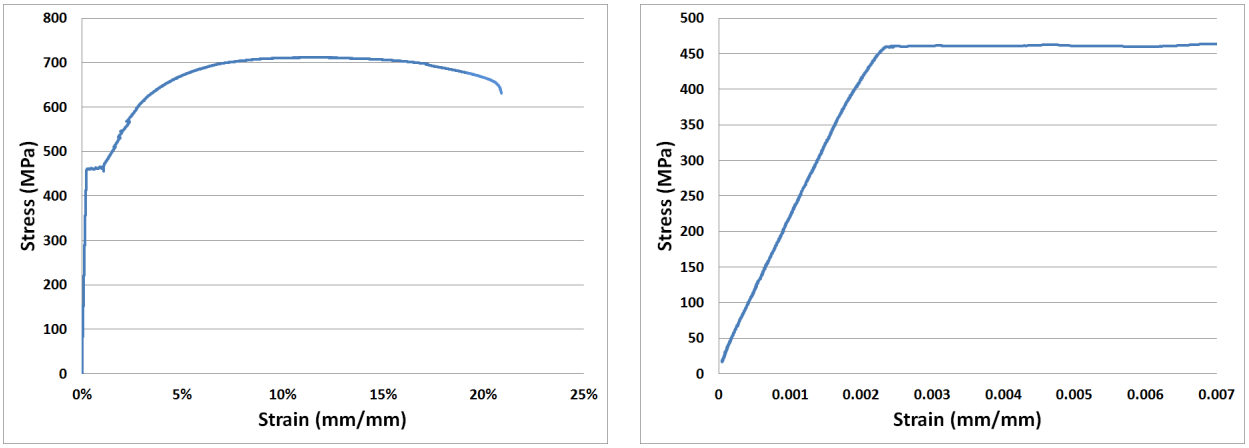

(a) (b)

Figure 3.1 Stress-Strain Relationship of Conventional Reinforcing Bars; (a) Complete Relationship up to the Bar Rupture; (b) Initial Deformations Recorded by an Extensometer

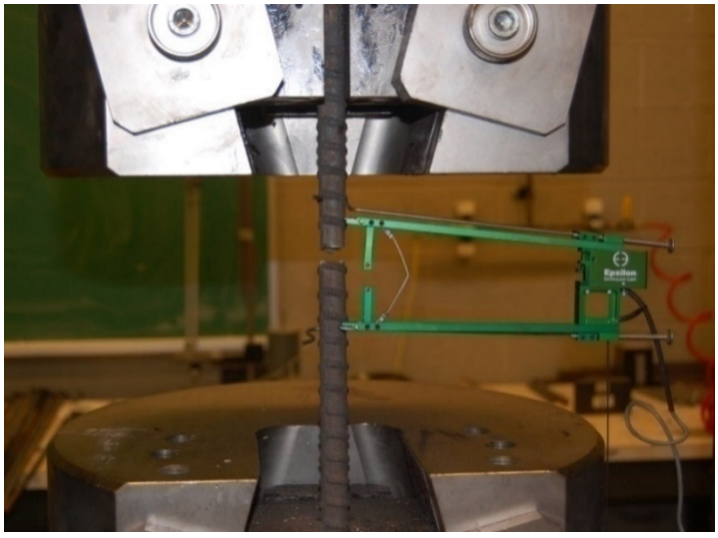

Figure 3.2 Reinforcing Steel Bar Coupon Test

The coupon test results showed $f_y = 460\ MPa\ (67\ ksi)$ and $f_u = 710\ MPa\ (103\ ksi)$ at peak of strain hardening. The coupon sample maintained a capacity of over 700 MPa up to 16.4% elongation. The sample subsequently exhibited significant necking and ruptured at 20.6% elongation. The elastic portion of the stress-strain relationship shown in Figure 3.1 indicates elastic modulus of $E_s = 198\ GPA$.

3.3 Concrete

Twelve (12) 100 mm diameter concrete cylinders were taken for each wall and tested after 7, 14 and 28 days under axial compression up to failure. Typical concrete cylinder failure modes in compression are shown in Figure 3.3. The compressive strength – time relationship of concrete samples over time is depicted in Figures 3.4(a), 3.5(a) and 3.6(a) for concrete used in shear walls No. 1 to No. 3, respectively.

The complete concrete stress-strain relationship was established using popovics model (1973). The concrete theoretical stress-strain graphs for shear walls No.1 to No. 3 are presented in Figures 3.4(b), 3.5(b) and 3.6(b). The 28-day concrete strength and the corresponding strain ε_0 was used to generate the stress-strain relationships. Popovics' expression for unconfined concrete is given below:

$$f = f'_c \frac{\varepsilon}{\varepsilon_0} \cdot \frac{n}{n - 1 + \left(\frac{\varepsilon}{\varepsilon_0}\right)^n}$$

Where n and ε_0 values are obtained from the following equations. Note that imperial units (PSI for pressure) were used in the expressions given below.

$$n = 0.4 \times 10^{-3} f'_c + 1$$

$$\varepsilon_0 = 2.7 \times 10^{-4} \sqrt[4]{f'_c}$$

Figure 3.3 Concrete Cylinder Sample under Axial Compression

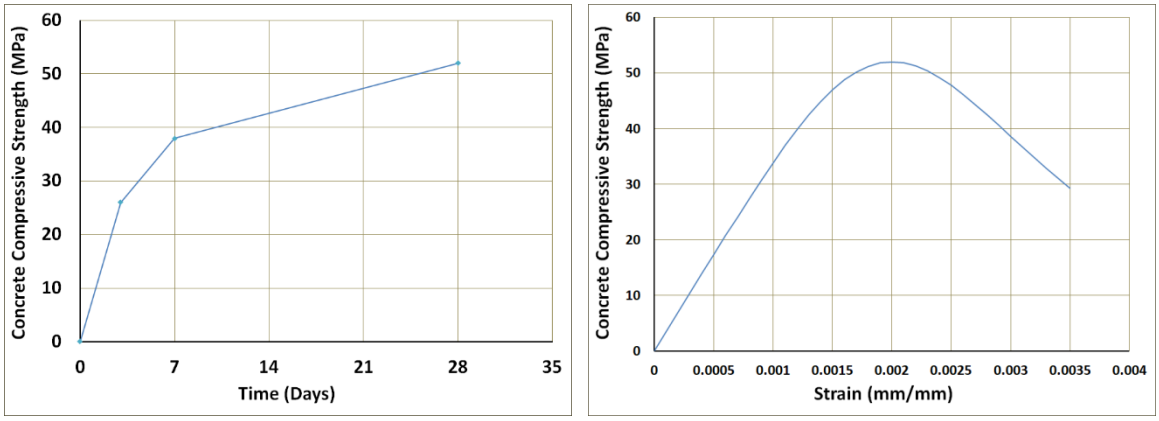

(a) (b)

Figure 3.4 Concrete Used in Shear Wall No. 1; a) Strength vs. Time; b) Stress vs. Strain

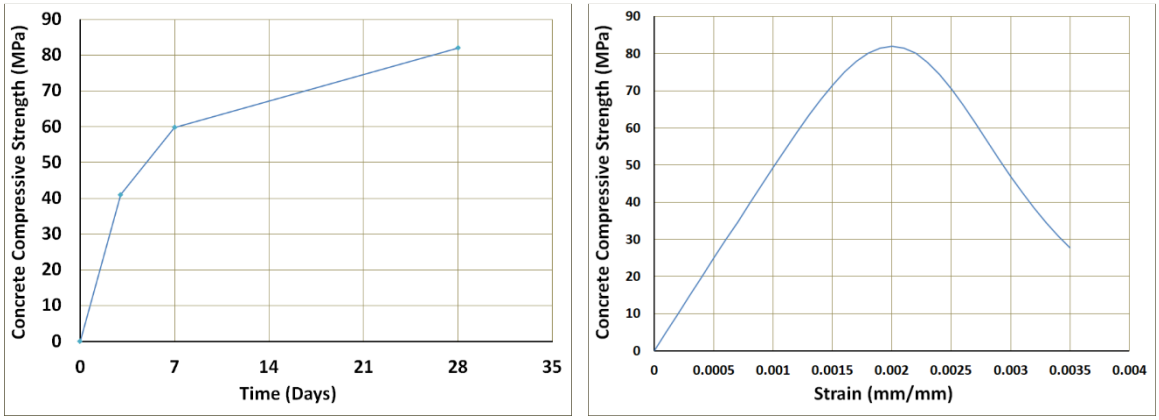

(a) (b)

Figure 3.5 Concrete Used in Shear Wall No. 2; a) Strength vs. Time; b) Stress vs. Strain

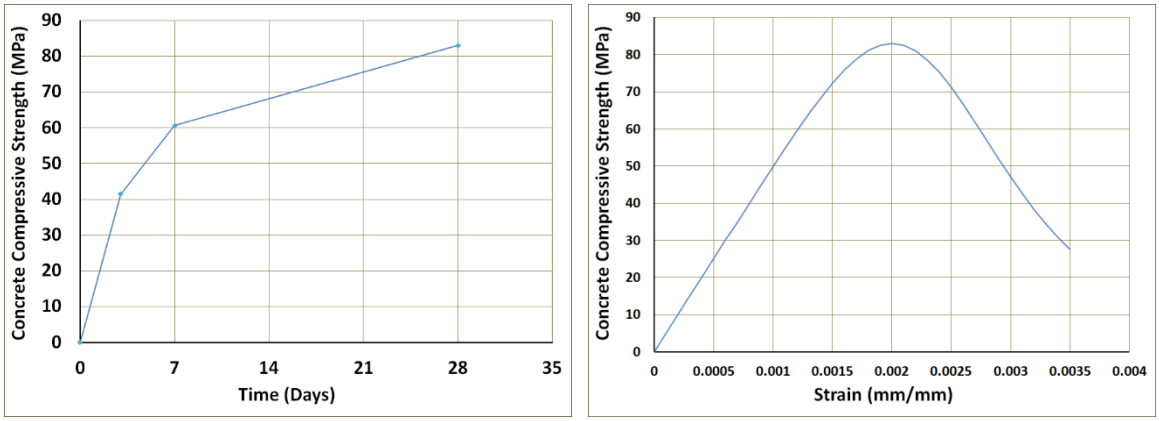

(a) (b)

Figure 3.6 Concrete Used in Shear Wall No. 3; a) Strength vs. Time; b) Stress vs. Strain

Concrete prism specimens used for WWR tests in concrete, reported in Chapter 4, were cast using high-early strength concrete mix. Once again, concrete cylinders samples were tested on 3, 7 and 28 days after casting. Figures 3.7(a) and (b) shows concrete strength gain over time and concrete stress-strain relationship using Popovics model respectively. The 28-day concrete strength was used to generate the stress-strain diagram.

In addition to the grids embedded in concrete, a series of small concrete columns were cast using SIKA premix concrete to assess grid potential against controlling bar buckling in axially loaded columns. The concrete cylinders taken from these columns, behavior of which is also discussed in Chapter 4, reached 80 MPa after 28 days. The concrete cylinder test data for the experimental phase is summarized in Table 3.1.

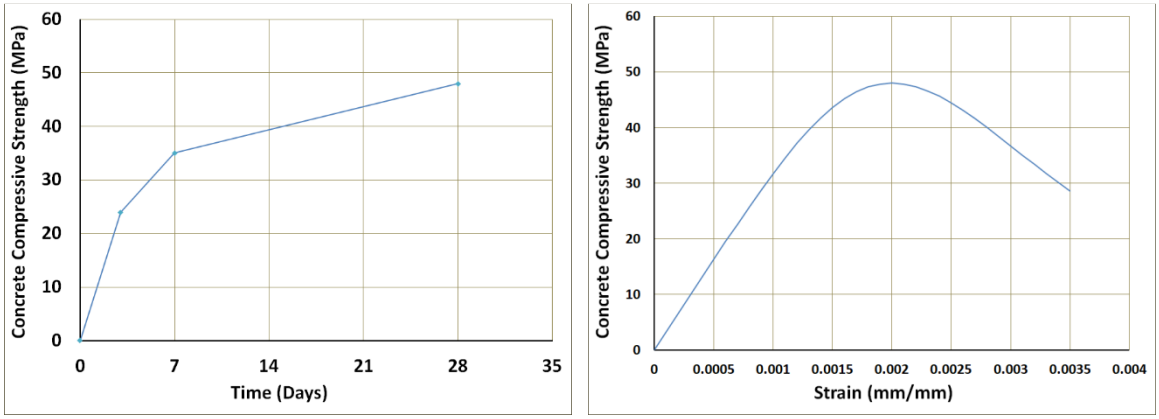

(a) (b)

Figure 3.7 Concrete Used in WWR Prisms; a) Strength vs. Time; b) Stress vs. Strain

Table 3.1 – Standard Concrete Cylinder Test Results

Specimen	Sample No.	Recorded Force	Sample Diameter	Concrete Strength
Shear Wall No. 1 3 Days	Cylinder 1	199	100	25.3
	Cylinder 2	205	100	26.1
	Cylinder 3	220	101	27.5
Shear Wall No. 1 7 Days	Cylinder 1	295	99	38.3
	Cylinder 2	299	100	38.1
	Cylinder 3	309	100	39.3
Shear Wall No. 1 28 Days	Cylinder 1	406	100	51.7
	Cylinder 2	413	100	52.6
	Cylinder 3	422	101	52.7
Shear Wall No. 2 3 Days	Cylinder 1	320	100	40.7
	Cylinder 2	322	100	41.0
	Cylinder 3	331	100	42.1
Shear Wall No. 2 7 Days	Cylinder 1	452	99	58.7
	Cylinder 2	475	100	60.5
	Cylinder 3	477	101	59.5
Shear Wall No. 2 28 Days	Cylinder 1	640	100	81.5
	Cylinder 2	648	100	82.5
	Cylinder 3	655	101	81.8
Shear Wall No. 3 3 Days	Cylinder 1	321	99	41.7
	Cylinder 2	313	100	39.9
	Cylinder 3	330	100	42.0
Shear Wall No. 3 7 Days	Cylinder 1	467	100	59.5
	Cylinder 2	477	100	60.7
	Cylinder 3	484	101	60.4
Shear Wall No. 3 28 Days	Cylinder 1	647	100	82.4
	Cylinder 2	640	99	83.1
	Cylinder 3	664	100	84.5

Table 3.1 – Standard Concrete Cylinder Test Results (Cont'd)

Specimen	Sample No.	Recorded Force	Sample Diameter	Concrete Strength
Concrete Prisms 3 Days	Cylinder 1	185	100	23.6
	Cylinder 2	190	101	24.2
	Cylinder 3	203	101	25.3
Concrete Prisms 7 Days	Cylinder 1	275	99	35.7
	Cylinder 2	281	100	35.8
	Cylinder 3	300	102	36.7
Concrete Prisms 28 Days	Cylinder 1	377	100	48.0
	Cylinder 2	380	101	47.4
	Cylinder 3	395	101	49.3

3.4 Welded Wire Reinforcement (WWR) Grid Wires

The mechanical properties of smooth steel wire were used in WWR grids were determined by performing six (6) coupon tests. The wires had 9.5 mm diameter (3/8"). The steel coupons were obtained by cutting the un-welded straight portions of WWR grids, which were supplied from the same shipment of grids used in a companion project that studied the use of WWR grids in coupling beams, because they had longer un-welded segments. The WWR grids used in the current research project and the companion coupling beam research project were exactly the same materials, and were manufactured and shipped from the same batch of steel. Figure 3.8 shows the layout of the coupon samples that were obtained from the WWR grids. The results of these tests should provide an understanding of the behavior of the base steel material in locations were the properties were not affected by the welding process.

Figure 3.8 Undisturbed Coupon Samples, Cut from WWR Grids

The coupon samples were tested under uniaxial tension according to the general guidelines provided by the relevant ASTM standard, with the prescribed loading rate. The test setup is shown in Figure 3.9. The test results showed a yield strength of $f_y = 550\ MPa$ $(80\ ksi)$ and ultimate strength of $f_u = 640\ MPa$ $(144\ ksi)$. The yield strength was determined using a tangential offset from 0.2% strain deformation. The coupon test samples elongated from 4.15% to 4.55% prior to loosing strength beyond their ultimate capacity.

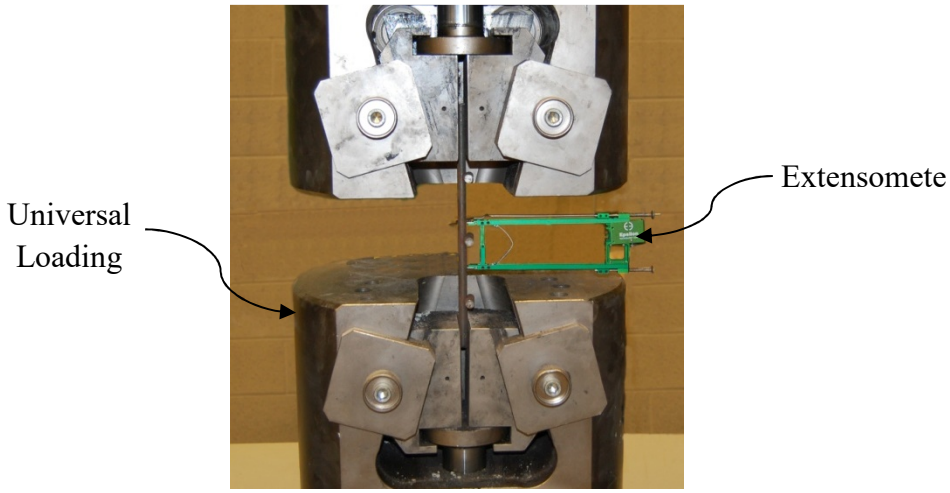

Figure 3.9 WWR Tension Coupon Sample using Universal Loading Machine

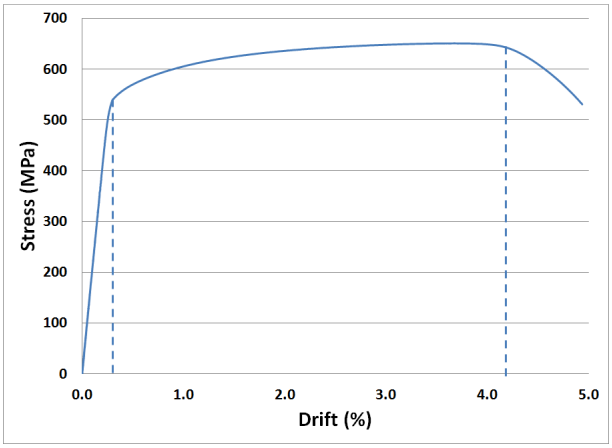

Figure 3.10 Stress – Strain Diagram of Un-welded 9.5 mm (3/8") Diameter Steel Wire in WWR grids

The strain values in the elastic range were measured using both strain gauges as well as an external extensometer with a gauge length of 50 mm. The readings using both the strain gauges and the extensometer consistently showed the same modulus of elasticity of $E_s = 200\ GPa$. This is shown

in Figure 3.10. The post-yield portion of the graph was obtained from the readings based on the movement of the loading head of the universal testing machine.

The WWR grids were produced by arranging round smooth steel wires in pre-selected spacing according to the manufacturer's requirements using robots and then concurrently subjecting these pieces to high current and substantial compressive forces. This process resulted in melting of the pieces together, forming a steel grid. The effect of this process on steel stress-strain relationship was established by means of additional six (6) coupon tests, where the coupons this time included the welded portions. Figure 3.11 shows the layout of the cut samples from WWR grids. The test results showed similar behavior to those that did not contain welded segments, both in terms of load capacity and ductility. Typical stress-strain graph for such samples is illustrated in Figure 3.12.

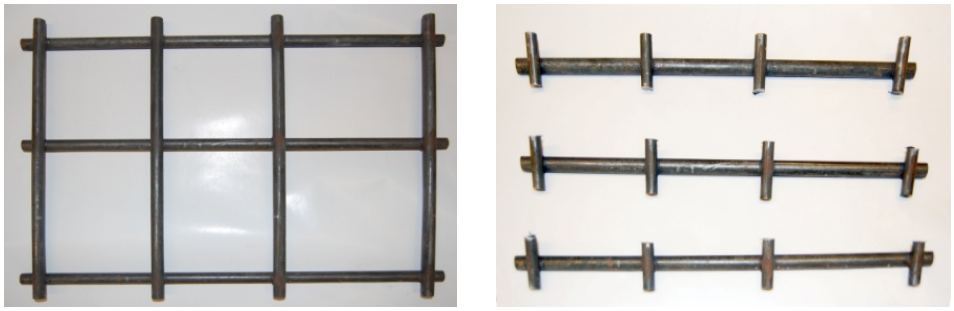

Figure 3.11 Steel Coupon Samples Including Welded Joints of WWR grid

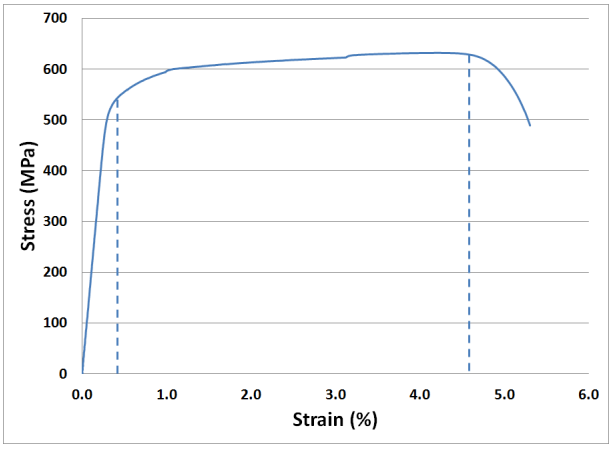

Figure 3.12 Stress – Strain Diagram of 9.5 mm (3/8") Diameter Steel Wire Including Welded Joints of WWR Grids

Close-up pictures of the failure surface at the rupture point of both types of coupons, with and without welded segments, are presented in Figure 3.13. All coupons exhibited necking, followed by rupturing. None of the samples failed in the proximity of the welds. The location of the failure was random; some coupons failed within the middle third whereas others failed closer to the supporting grips of the universal testing machine.

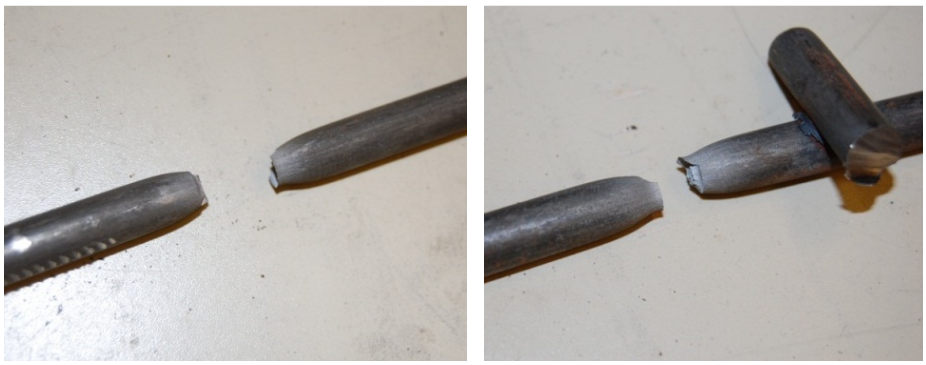

Figure 3.13 Close up Image of Necking of Coupons with and without Welded Segments

3.5 Seven-Wire Strands

A series of post-tensioned strands were used vertically as part of the shear wall test setup to apply axial compressive forces on the web and the boundary elements. The strands were sequentially tensioned to achieve uniform load distribution over the wall length. It was essential to establish the stress-strain characteristics of these strands to assess the axial forces applied.

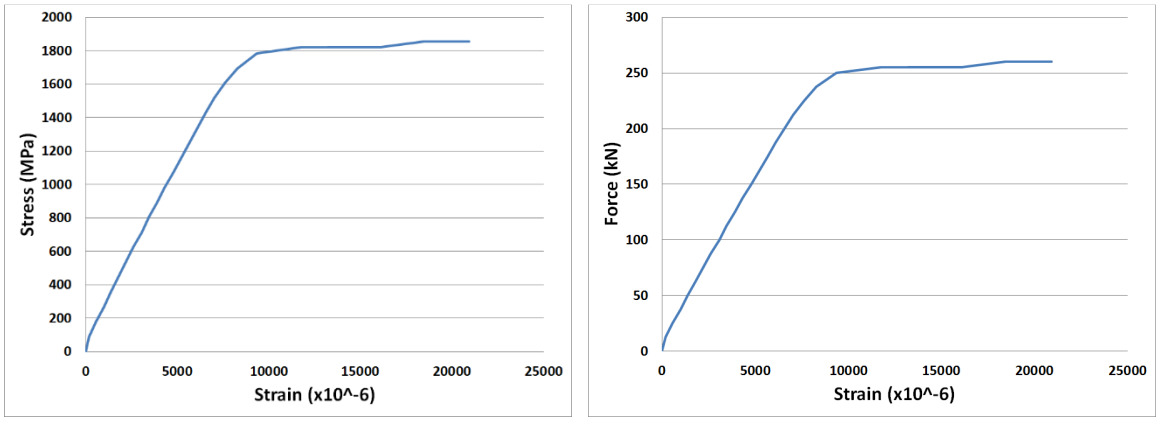

Figure 3.14 Seven Wire Strand Tension Coupon Test Result

Three coupons were taken from the shipment of strands to establish force – strain diagram of the strands, which was then used as a calibration chart to obtain forces from measured strains. This is

shown in Figure 3.14. The strands had a 15-mm nominal diameter with a sectional area of $A = 140\ mm^2$, and a tensile strength of $f_u = 1860\ MPa\ (270\ ksi)$.

Chapter 4

Experimental Research – Small Scale Specimens for WWG Material Testing

4.1 General

Series of small scale specimens were constructed and tested to assess the performance of WWR grids prior to assessing their performance in shear walls. The tests subjected WWR grids with 9.5 mm (3/8") diameter wires to various loading conditions to simulate stresses generated in grids when extreme loading scenarios are created in shear walls. The tests also helped verify the minimum weld capacity as required by ASTM standards. The terms WWR grids and grids are used interchangeably in the thesis.

The initial series of grid testing included bare steel grids under two loading scenarios, simulating two possible directions in which compression reinforcement could force the grids laterally as they develop tendency to buckle in wall boundary elements. The longitudinal bar buckling tendency is followed by outward movement of the bar away from the concrete core and the movement can be either perpendicular or angular relative to the grid corners. The two test procedures simulating these two scenarios are referred to as "direct shear test" and "burst test." The direct shear test applies a force parallel to the long side of the grid by pulling the two adjacent corners away from the corresponding corners at opposite ends of the grid through a universal testing machine. The direct shear test is analogous to that required by the applicable ASTM Standard, with the exception that the test is performed on a grid instead of a single welded joint. The burst test pulls one of the

grid corners diagonally against the opposite corner while the transverse legs are restrained against collapse by means of a rigid link. The details of these tests, including pictures illustrating test set-ups, are provided in this Chapter.

The above tests were repeated on WWR embedded in concrete to simulate a similar environment as shear wall boundary elements. This set of tests included direct shear tests and burst tests on concrete samples with cast-in grids, where a single grid is placed in a concrete prism, representing a slice of a shear wall boundary element. These samples were intended to simulate more realistic boundary conditions for grids in reinforced concrete structural elements.

The final set of material tests involved tests of small scale columns loaded to failure under concentric and eccentric compression. These tests were used to provide insight into the performance of grids in controlling longitudinal compression bars against buckling when placed with different grid spacing.

4.2 Welded Wire Reinforcement (WWR) Grid Tests According to ASTM

ASTM Standards sets the minimum manufacturing requirements for WWR grids, including but not limited to minimum yield and ultimate strength of the steel wires and minimum shear capacity of the joints formed by resisting welds. The ASTM standards have evolved since the initiation of the research program in 2008. The reference documents are listed below in a descending chronological order based on the publication date:

- ***ASTM A1022/A1022M – 13***: "Standard Specification for Deformed and Plain Stainless-Steel Wire and Welded Wire for Concrete Reinforcement"
- ***ASTM A1064/1064M – 12***: "Standard Specification for Carbon-Steel Wire and Welded Wire Reinforcement, Plain and Deformed, for Concrete"
- ***ASTM A185/A185M – 07***: "Standard Specification for Steel Welded Wire Reinforcement, Plain, for Concrete"

4.2.1 ASTM Mechanical Property Requirements

ASTM A1064/A1064M – 12: "*Standard Specification for Carbon-Steel Wire and Welded Wire Reinforcement, Plain and Deformed, for Concrete*" outlines the most recent ASTM mechanical property requirements applicable to WWR grids. Section 7 of ASTM 1064-12 defines the "*Mechanical Property Requirements – Wire, Plain and Deformed"* in which the minimum required yield and tensile strength of the wires used in manufacturing WWR grids is tabulated in Table 6 (ASTM 1064-12). This requirement is reproduced in Table 4.1 below. The table refers to W1.2 wire which is a standard size wire with a nominal diameter of 0.124" (3.15 mm). BauGrid WWR grids used in the current research program use 3/8" (9.5 mm) diameter smooth bars with a sectional area of $A_s = 71mm^2$. The yield and tensile strength of BauGrids are presented in Chapter 3 and meet the minimum strength requirement shown in Table 4.1.

Table 4.1 Tension Test Requirements – Plain Wire for Welded Wire Reinforcement (ASTM 1064-12 – Table 6)

	Size W1.2 [MW7.7] And Larger	**Smaller than Size W1.2 [MW7.7]**
Tensile Strength, min, ksi [MPa]	75 [515]	70 [485]
Yield Strength, min, ksi [MPa]	65 [450]	56 [385]
Reduction of Area, min, %	30 *	30 *

* For material testing over 100 ksi [690 MPa] tensile strength, the reduction of area shall be not less than 25%.

Section 8.3 of ASTM 1064-12 identifies the minimum required shear capacity of the welded joints: "*Weld Shear Strength: The weld shear strength between longitudinal and transverse wires shall be tested as described in Section 9. The minimum average shear value in pound-force shall not be less than 35,000 multiplied by the nominal area of the larger wire in square inches [in Newton, it shall not be less than 241 multiplied by the nominal area of the larger wire in square millimeters], where the smaller wire has an area of 40% or more of the area of the larger wire. For deformed welded wire reinforcement, the smaller wire shall not be less than D4 [MD 26]"*. ASTM 1064 also provides a recommended test set-up to establish the shear capacity of the welded joint The test set-up, is shown in Figure 4.1.

The ASTM requirement indicated above corresponds to welded joints of 3/8" (9.5 mm) BauGrid WWR to exceed 3,850 lbs [17.1 kN]. This capacity requirement is verified through the tests presented in Section 4.3.

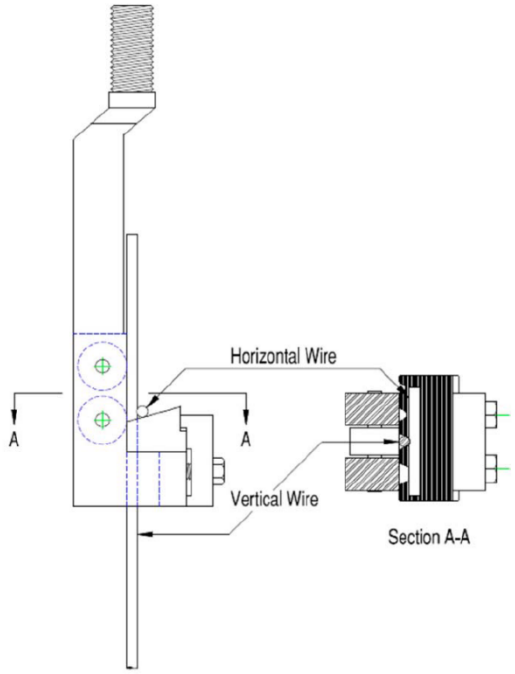

Figure 4.1 Welded Wire Reinforcement Weld Tester (ASTM 1064 – Fig. 1)

4.3 WWR Grid Tests – Steel Grid Experiments

WWR grid tests were conducted up to failure under direct tension applied by a universal loading machine. The following test procedures were used:

- Joint shear capacity test following the ASTM 1064 recommended test set-up
- Direct shear test of a WWR grid
- Burst test of a WWR grid

The joint shear capacity test was conducted on cross shaped grid samples with a welded joint at the intersection of the two perpendicular bars, as shown in Figure 4.1. The samples were prepared by cutting large grids and isolating the joint. Various grid layouts of single-cell, 2-cell, 3-cell and 8-cell configurations were tested to reach a better understanding of grid behavior with different layouts. The test set-up was adjusted accordingly to accommodate each layout. The details of each experimental program and the recorded results follow.

4.3.1 WWR Grid Dimensions

The test was not limited to a single grid shape. Different grid arrangements were considered, including: 2-cell, 3-cell and 8-cell WWR grids, as shown in Figure 4.2. Each test condition was repeated on multiple samples of different grid arrangement. This, not only provided an insight on grid weld performance, but also indicated potential impact of grid arrangement on performance. All the grids were shipped from the same batch of production.

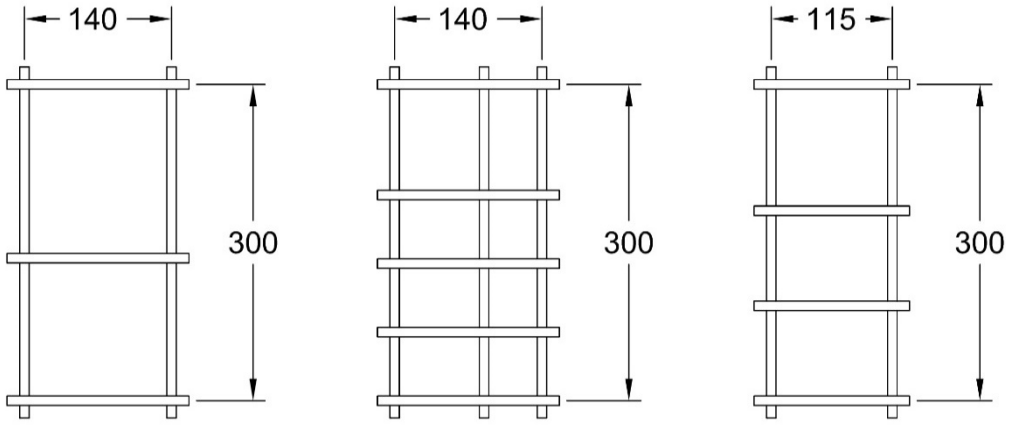

Figure 4.2 Grid Dimensions for Small-Scale Experiments

4.3.2 WWR Grid Tests – Joint Shear Capacity as per ASTM 1064

ASTM 1064 provides a recommended test setup to test the shear capacity of joints in a WWR grid as illustrated in Figure 4.1. The setup provides a continuous support underneath the horizontal member of the joint which helps to minimize local bending of intersecting members while establishing the shear capacity of the welded interface of the joint. In addition, the universal testing machine's moving head should align with the restrained end of the vertical leg of the joined members. Pictures of a specimen before and after the test are shown in Figure 4.3. This setup is replicated in the lab as shown in Figure 4.4, and three (3) samples were tested accordingly. The three samples exhibited similar failure modes. The force-displacement readings are presented in Figure 4.5. The test results are summarized in Table 4.2. It is noted that all the recorded loads are in excess of 17.1 kN, minimum required shear capacity of the joint as identified by ASTM 1064.

Table 4.2 Shear Capacity of a Welded Joint per ASTM 1064 Recommended Set-up

Specimen ID	Load at Failure (kN)	Displacement at Failure (mm)*
J1	30.1	5.9
J2	31.7	4.9
J3	32.0	5.6

* The recorded displacements at failure include the initial gap of up to 1mm between the loading instrument and the specimens. These gaps were then overcome as the loading started and the loading at full contact took place. The net deformation of the joint is estimated between 4.6mm to 4.9mm. The length of the vertical leg of the sample is measured at 310 mm. The initial soft slope in the load-deformation graphs is caused by this initial gap.

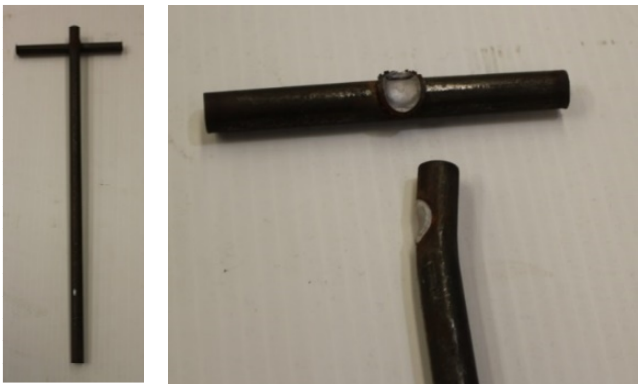

Figure 4.3 WWR Grid Joint Specimen (Left); Failed Specimen (Right)

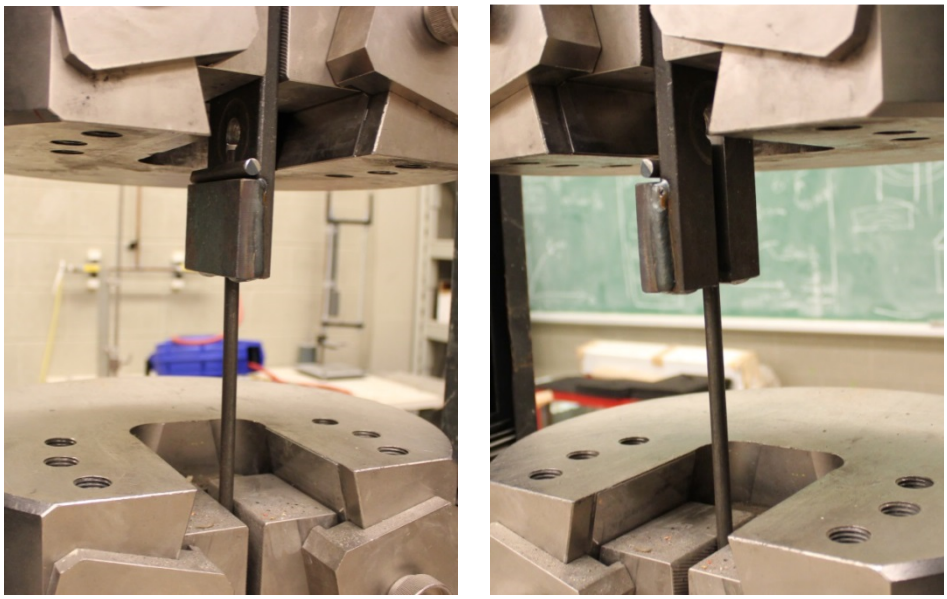

Figure 4.4 ASTM 1064 Recommended Test Set-up for Joint Shear Capacity Verification

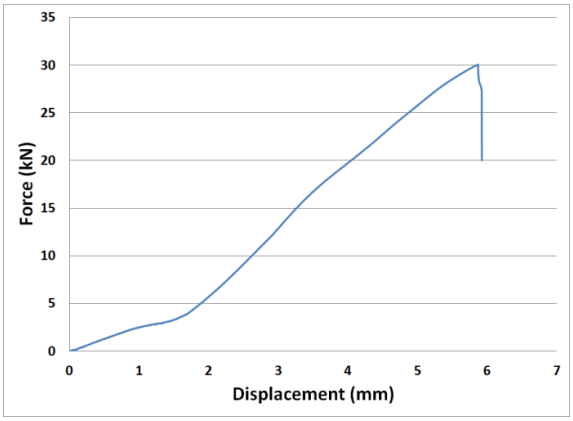

J1 Specimen

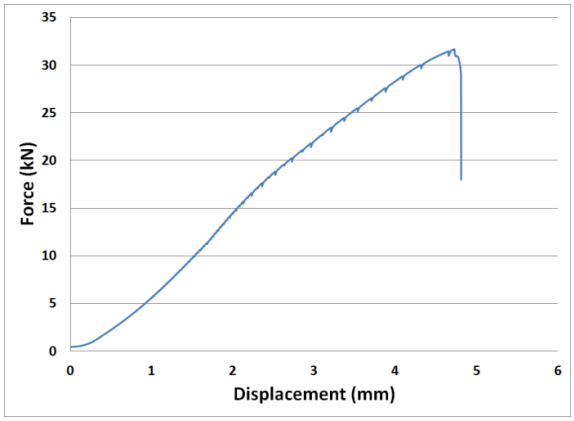

J2 Specimen

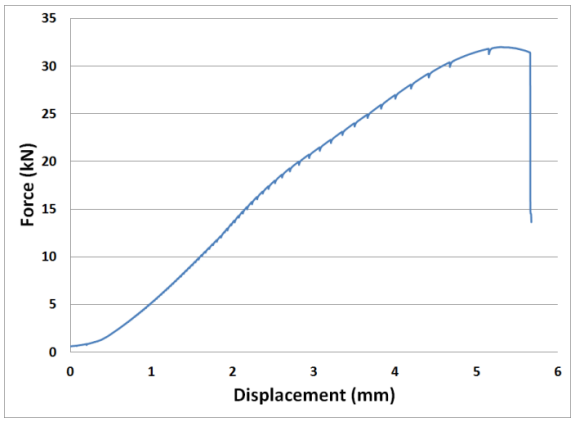

J3 Specimen

Figure 4.5 Force – Displacement Graphs of WWR Grids Tested per ASTM 1064 Test Set-up

The ASTM standards discussed above outline the recommended test procedure to verify the minimum required mechanical properties for grids. It should be noted, however that the requirements do not reflect a comprehensive understanding of grid performance in reinforced concrete structural elements, and specifically in shear wall boundary elements. Therefore, additional tests were proposed and conducted by the author, and presented in this Chapter to provide further insight into the grid performance in concrete when the grid corners are subjected to lateral loads exerted by longitudinal compression reinforcement. Further structural testing is conducted to assess grid performance in large-scale shear walls under more realistic loading conditions. These tests are discussed in Chapter 5.

The measured loads, which were recorded for the ASTM tests, are compared with the yield capacity of wire used in manufacturing the WWR grids. The comparison indicates that welded joints failed before reaching the yield capacity of steel wire as summarized in Table 4.3.

Table 4.3 Joint Shear Capacity per ASTM 1064 Compared to Yield Strength of an Individual Steel Bar

Specimen ID	Failure Load (kN)	Yield Load (kN)	Failure Load / Yield Load (%)
J1	30.1	39.0	77.2%
J2	31.7	39.0	81.2%
J3	32.0	39.0	82.0%

4.3.3 WWR Grid Tests – Direct Shear Test

Two pairs of WWR grids with 2-cell and 8-cell configurations were tested under direct shear. In a direct shear test four corner bars are placed, one in each corner representing longitudinal compression bars in shear wall boundary elements. The bars are then pulled apart by applying tensile forces parallel to the longitudinal side of the grids. This way of applying tensile forces assumes rebar tendency of buckling outwards parallel to the longitudinal side of the grid. The test set-up for direct shear tests is illustrated in Figure 4.6.

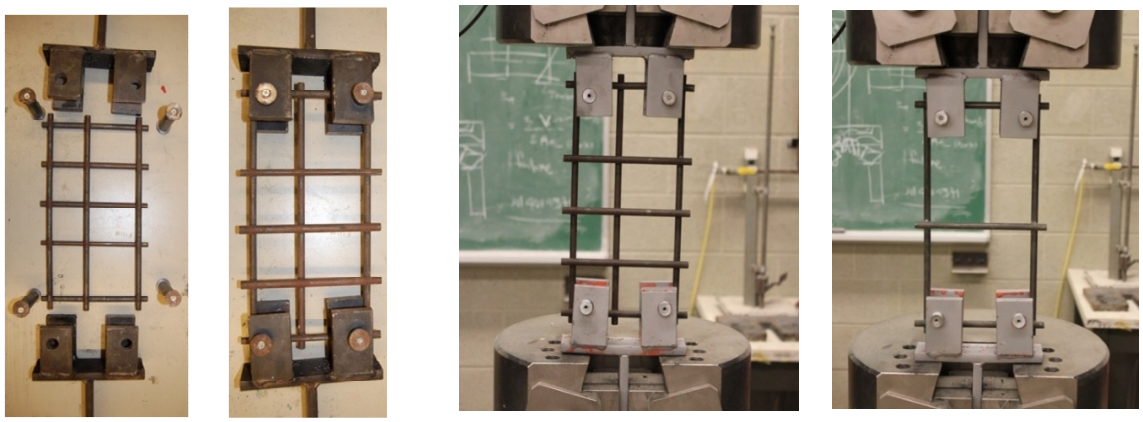

Figure 4.6 Direct Shear Test Set-up

The direct shear tests were conducted at a speed of 2 mm/min. The gaps between the corner bars and the joints were minimized to avoid bending of the grid wire due to accidental eccentricities. Observations during testing, however, indicated that some degree of rotation was visible around welded joints near failure loads. The performance of grids, including recorded force-displacement

relationships, are presented in Figures 4.7 to 4.10 for 2-cell and 8-cell samples, respectively. The test results are summarized in Table 4.4. The prefix "SH" in specimen label refers to direct shear, the first number refers to the number of cells, and the second number identifies the specimen number for that particular grid configuration. All the grids exhibited similar failure patterns with failure being initiated by welded steel pieces separating from each other at weld interfaces.

Figure 4.7 Direct Shear Test – Failed 2-Cell Grid

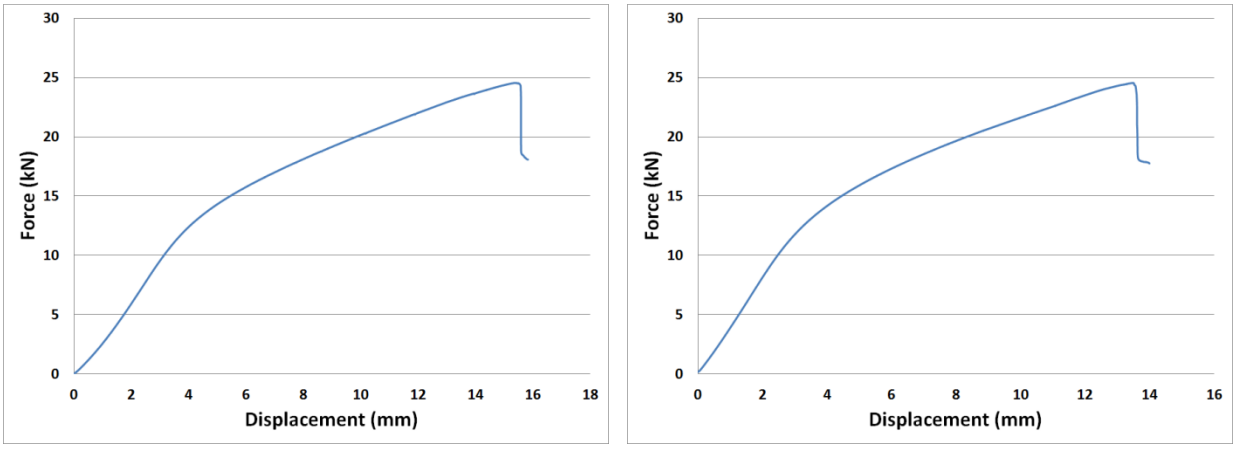

SH-2-1 Specimen

SH-2-2 Specimen

Figure 4.8 Force – Displacement Graphs; Direct Shear Testing on 2-Cell Grids

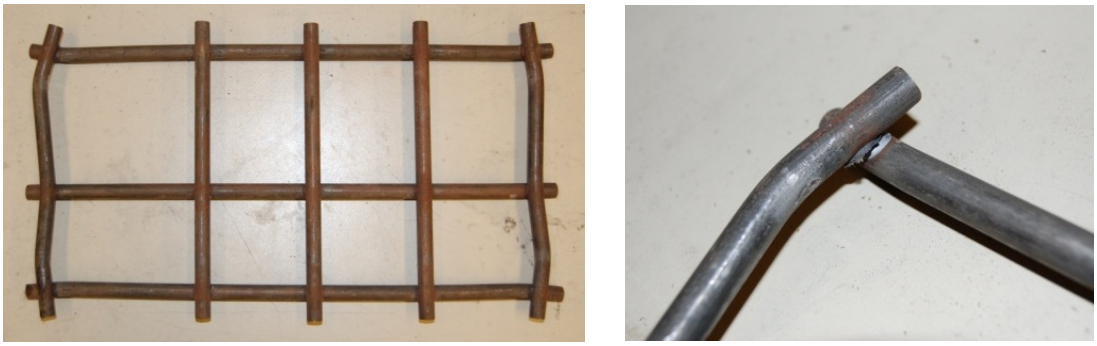

Figure 4.9 Direct Shear Test – Failed 8-Cell Grid

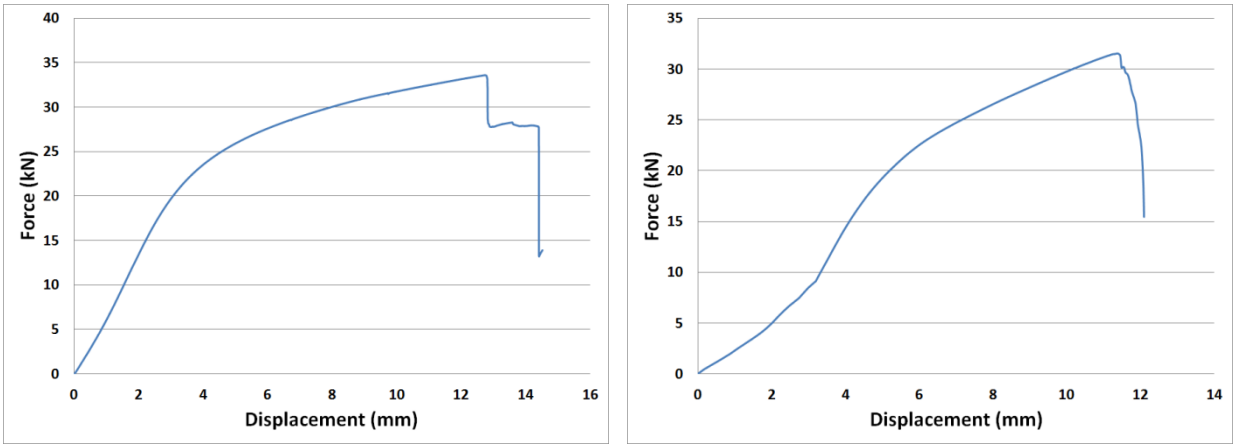

SH-8-1 Specimen SH-8-2 Specimen

Figure 4.10 Force – Displacement Graphs; Direct Shear Tests on 8-Cell Grids

Table 4.4 WWR grids Direct Shear Test Results

Specimen ID	Load at Failure (kN)	Displacement at Failure (mm)
SH-2-1	24.6	15.5
SH-2-2	24.5	13.6
SH-8-1	33.6	12.8
SH-8-2	31.6	11.6

The failure loads shown in Table 4.4 are total loads applied by the testing machine. Average force resistance per grid leg may be computed by assuming equal distribution of forces among the resisting grid legs. Average load per leg is tabulated in Table 4.5. As the failure load was approached, however, it was observed that one of the joints developed excessive deformation and slight rotation, leading to the failure of the grid by the separation of welded joint, indicating that the load may not have been shared equally. The average load per leg is compared with the yield

strength of single wire in tension. The results indicate that the grid welds failed at a significantly lower load than that corresponding to yield force during coupon tests.

Table 4.5 Comparing WWR grids Direct Shear Test Results with Yield Strength of Steel bars

Specimen ID	Load at Failure (kN)	Average Load Per Bar (kN)	Yield Strength (kN)	Average Load/ Yield Strength (%)
SH-2-1	24.6	12.3	39.0	31.5%
SH-2-2	24.5	12.25	39.0	31.4%
SH-8-1	33.6	11.2	39.0	28.7%
SH-8-2	31.6	10.53	39.0	27.0%

4.3.4 WWR Grid Tests – Burst Test

Three pairs of WWR grids with 2-cell, 3-cell and 8-cell configurations were subjected to burst tests along grid diagonals until failure. In a burst test, the samples are loaded along grid diagonals. One grid corner is fixed to the stationary end of the test machine, and the opposite corner is pulled away by moving the head of the universal test machine at a speed of 2 mm/min. The corners on the opposite diagonal are restrained against movement by means of a rigid link to maintain the original rectangular shape during testing. This is intended to simulate, to a degree, the behavior of grids in a concrete member where the deformations in the grid would be controlled by the surrounding concrete. The rigid link consists of two-25mm diameter round metal pieces connected by two 3/8" threaded rods, as illustrated in Figure 4.11. The round bars are placed snug tight in the corners prior to placing the grids in the universal testing machine. Figures 4.12 to 4.17 illustrate the specimen behavior and force-displacement graphs for 2-cell, 3-cell and 8-cell grids, respectively. The results of burst tests are summarized in Table 4.6. The prefix "B" in test labels refers to the burst test set-up, the first number refers to the number of grid cells and the last number identifies the specimen number for that particular grid configuration. All WWR grids exhibited a similar failure mode, and failed at welded joint locations where the weld interface got separated.

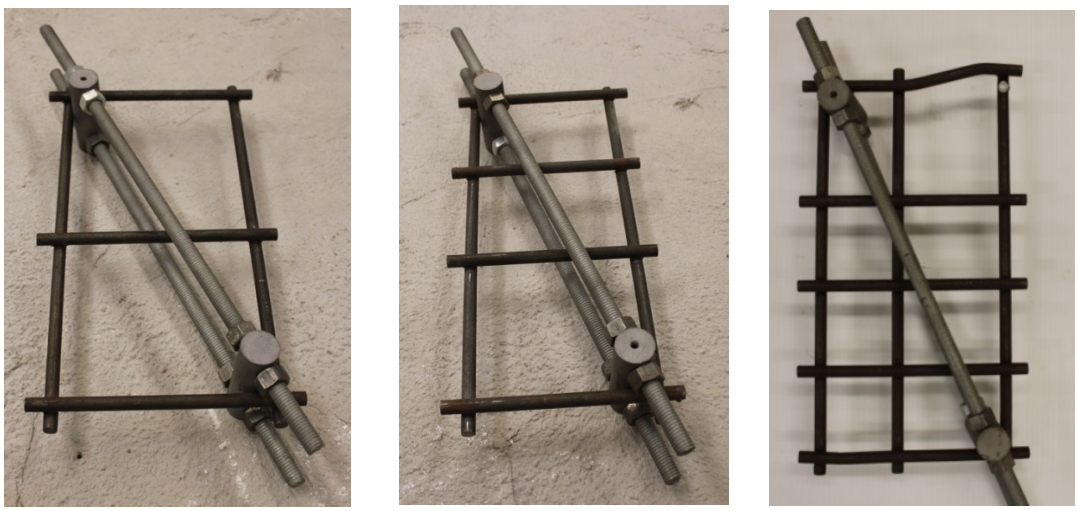

(a) 2-Cell; 3-Cell and 8-Cell Grid Configurations

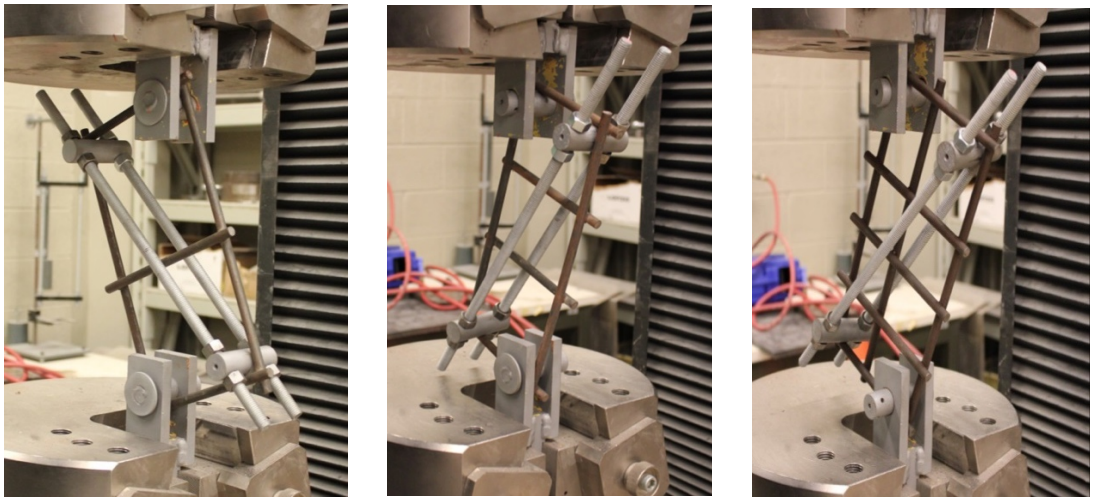

(b) Test Setup

Figure 4.11 Burst Tests

Table 4.6 WWR Grids – Burst Test Results

Specimen ID	Load at Failure (kN)	Displacement at Failure (mm)
B-2-1	14.9	13.5
B-2-2	16.0	16.1
B-3-1	10.2	6.7
B-3-2	12.9	10.4
B-8-1	9.6	19.7
B-8-2	9.5	19.4

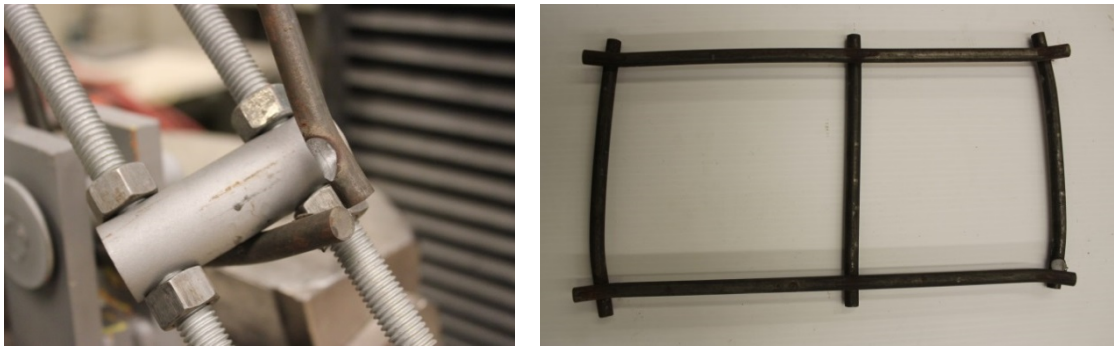

Figure 4.12 Burst Test – Failed 2-Cell Grid

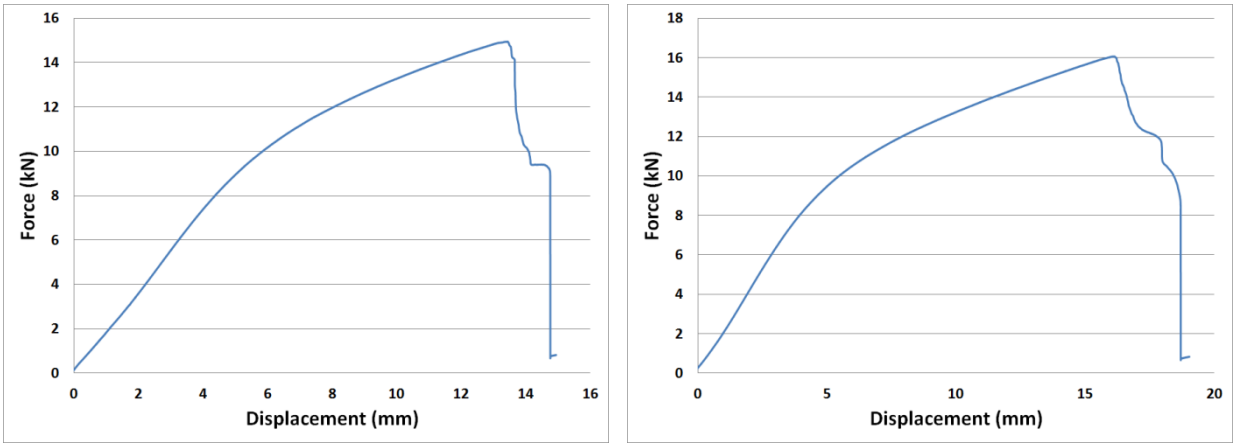

B-2-1 Specimen B-2-2 Specimen

Figure 4.13 Force – Displacement Graphs; Burst Test of 2-Cell Grids

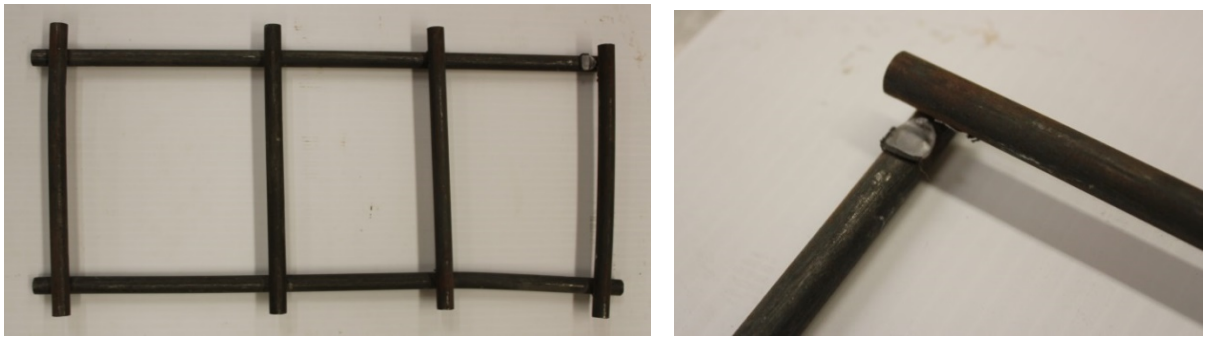

Figure 4.14 Burst Test – Failed 3-Cell Grid

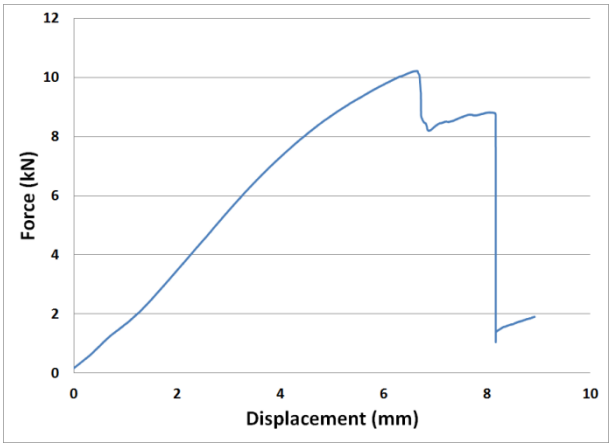

B-3-1 Specimen

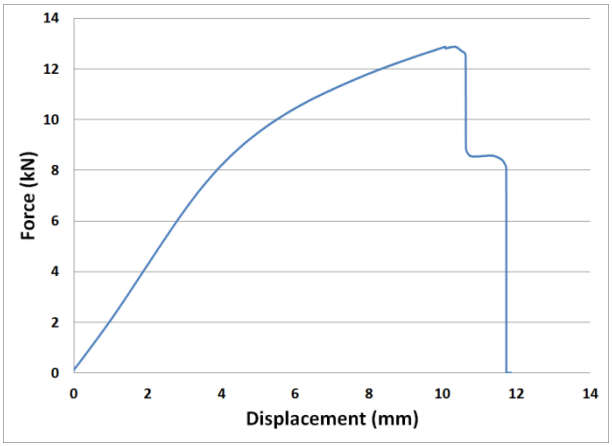

B-3-2 Specimen

Figure 4.15 Force – Displacement Graphs; Burst Tests on 3-Cell Grids

Figure 4.16 Burst Test – Failed 8-Cell Grid

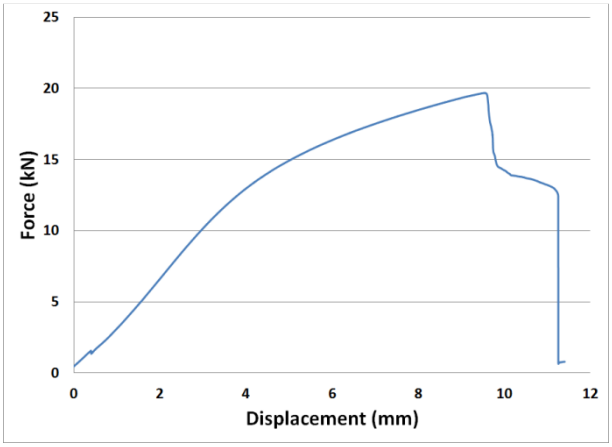

B-8-1 Specimen

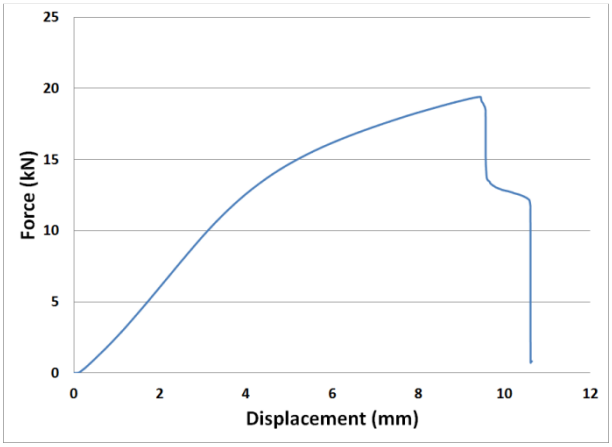

B-8-2 Specimen

Figure 4.17 Force – Displacement Graphs; Burst Tests on 8-Cell Grids

The tension force in burst tests can be resolved into its components along the direction of grid wires. The free-body-diagram of a grid joint during a burst test is shown in Figure 4.18. The larger force component is developed along the long direction of the grid due to the smaller angle it makes with the diagonal. The tensile force that is generated in each one of these grid legs is computed and compared with the yield force obtained by coupon tests. The results are summarized in Table 4.7. It becomes evident that the forces developed in grid legs were much lower than those corresponding to steel yield level, indicating that the welded joint failed prior to steel yielding.

Table 4.7 WWR Grids Burst Test – Force Components

Specimen ID	Load at Failure (kN)	Angle (Degrees)	F1 (kN)	F2 (kN)	Fy (kN)	F1/Fy (%)	F2/Fy (%)
B-2-1	14.9	68□	13.82	5.58	39.0	35.4%	14.3%
B-2-2	16.0	68□	14.83	5.99	39.0	38.0%	15.4%
B-3-1	10.2	73□	9.75	2.98	39.0	25.0%	7.6%
B-3-2	12.9	73□	12.34	3.77	39.0	31.6%	9.7%
B-8-1	9.6	68□	8.90	3.60	39.0	22.8%	9.2%
B-8-2	9.5	68□	8.81	3.56	39.0	22.6%	9.1%

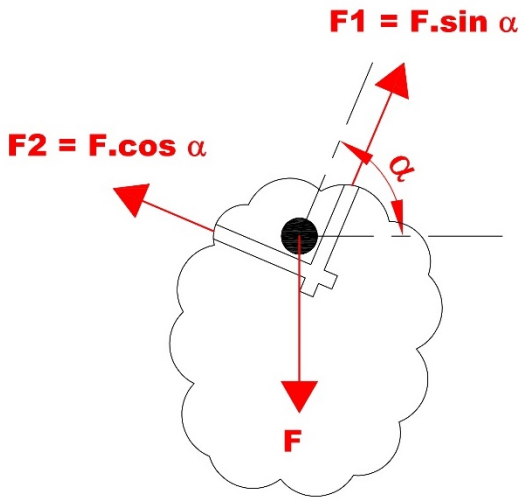

Figure 4.18 WWR Grid Burst Test Force Components

4.4 Concrete Prisms with Cast-in WWR Grids

In air testing of bare grids indicated bending of grid legs prior to weld failures. This behavior was believed to be prevented in actual reinforced concrete structural elements where the grids would be embedded in concrete. To simulate grids in concrete, a new set of material tests was devised using WWRs cast-in concrete prisms. This type of material testing involved direct shear tests and burst tests of WWR embedded in 100 mm thick concrete prisms. The grids were placed in the center of concrete prisms that represented a slice of concrete shear wall boundary element with a thickness equal to the tie spacing. The grids were instrumented with strain gauges. Four rebars were placed in perimeter grid corners, representing longitudinal reinforcement in prototype structural elements. The specimens were divided into two groups; one group for direct shear tests, and the other group for burst tests. In all cases the load was increased monotonically until failure.

4.4.1 Preparation of Concrete Prisms with Cast-in WWR Grids

A total of thirteen (13) concrete specimens with embedded WWR grids were prepared for testing. The grids were instrumented with strain gauges prior to concrete casting. Wooden formwork was built for casting multiple specimens as shown in Figure 4.19. Holes were drilled in the formwork to allow for the placement of short 25M re-bars, representing longitudinal reinforcement in prototype structural elements. The grids were tied to the 25M bars and held in place at mid-depth of concrete prisms. The bars were placed in a precise manner to have a minimum gap between the longitudinal bars and the grid corners. Minimum concrete cover of 50 mm was provided, measured to the center of 25M bars.

The layout of steel strain gauges varied depending on the intended test procedure, i.e., whether direct shear test or burst test. The strain gauge layout matched the internal load path of the specimen. It was important to ensure that the corner (25M) bars would remain elastic and did not bend during testing; hence, the selection of a large diameter 25M bars. The concrete was moist-cured for 7 days, and covered with wet burlaps afterwards. Standard concrete cylinders were cast from each batch of concrete. The results of cylinder test are presented in Chapter 2.

Figure 4.19 Cast-in Grid Steel Cage (Left); Freshly Poured Concrete Prisms (Right)

4.4.2 Direct Shear Tesst of Concrete Prism Specimens

Direct shear tests were conducted using a similar test procedure as that employed for the bare grid testes explained in Section 4.3.3 with parallel forces applied at grid corners through the 25M bars. The main difference between this test set up and the one used earlier was the presence of concrete surrounding the grids. This was believed to provide a more realistic simulation of grid behavior in shear wall boundary elements. The magnitude of applied force, machine head movement, and strain values were recorded using a data acquisition system. The direct shear test set-up and the schematic view of the applied load is shown in Figure 4.20. The grid layout for each concrete specimen for direct shear tests is shown in Tables 4.8.

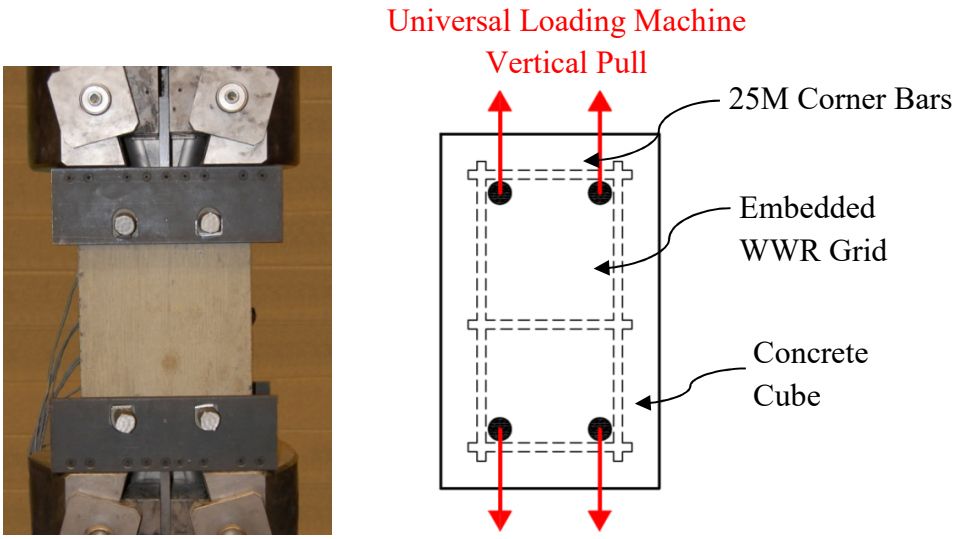

Figure 4.20 Concrete Cube with Cast-in WWR Grid – Direct shear test set-up

Table 4.8 Direct Shear Prism Specimen Information

Specimen Information	*Grid Picture*	*Grid Layout*	*Loading Diagram*
SHC-2-1 and SHC-2-2 Direct Shear Test 2-Cell Grid Configuration		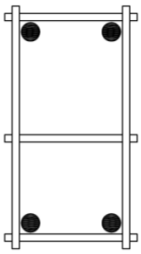	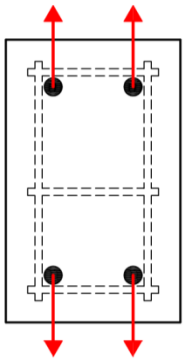
SHC-3-1, SHC-3-2 and **SHC-3-3** Direct Shear Test 3-Cell Grid Configuration	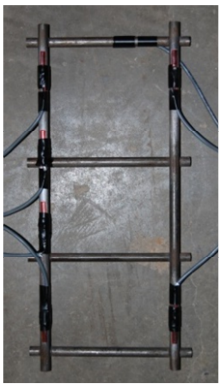	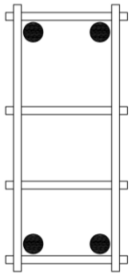	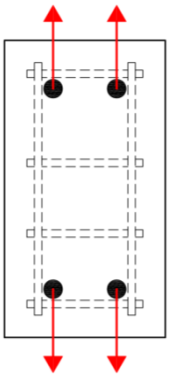
SHC-8-1 and **SHC-8-2** Direct Shear Test 8-Cell Grid Configuration	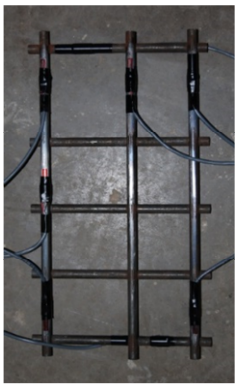	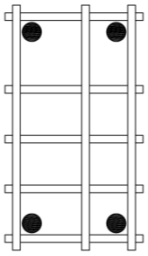	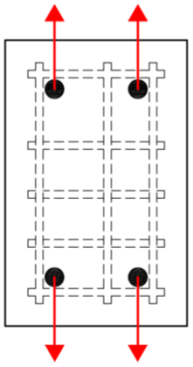

During the initial loading, concrete and WWR grid shared the applied tensile load until the concrete reached its tensile capacity and cracked. These tensile cracks appeared as full-depth horizontal cracks within the immediate vicinity of 25M bars. This is shown in Figure 4.21. Upon cracking, a drop was observed in load resistance as shown in the Force-Displacement graphs. The free-body diagram of the cracked end segment of concrete is shown in Figure 4.22. Because of the full-depth

of cracks, which caused separation of cracked end segments, the average load per vertical leg of grid in the post-cracking phase was calculated assuming steel resistance only. Hence, the applied total tensile load was divided by the number of resisting vertical legs. This assumption may have small conservatism in estimating the maximum resistance provided by the grids since it assumes perfectly even distribution of load between the vertical steel members, whereas the actual distribution could be slightly different due to possible redistribution of forces resulting from bending of individual legs at later stages of loading.

Figure 4.21 Typical Cracking and spalling of Concrete During Direct Shear Loading

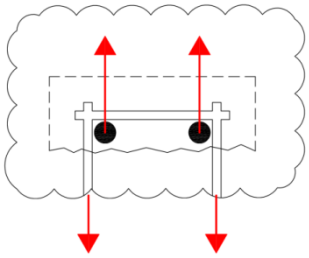

Figure 4.22 Cracked Concrete Cube Free Body Diagram for Direct Shear Test

All specimens exhibited weld failures, which resulted in the separation of welded joints at their interface. The results are summarized in Table 4.9. The layout of concrete prisms with 2-cell, 3-cell and 8-cell grids were presented earlier in Table 4.8. The prefix “SHC” in specimen labels refers to “direct shear” test of concrete prisms, the second number in the label refers to the number of cells in the grid and the last number identifies the specimen number having the same grid configuration. The experimentally recorded force-displacement relationships are shown in Figure 4.23.

Table 4.9 Direct Shear Test results for Concrete Prism Specimens with Cast-in WWR Grids

Specimen ID	Load at Failure (kN)	Average load per vertical leg (kN / connection)	Yield Strength (kN)	Average Load/ Yield Strength (%)
SH-2-1	45.8	22.9	39.0	58.7%
SH-2-2	40.0	20.0	39.0	51.2%
SH-3-1	42.5	21.3	39.0	54.6%
SH-3-2	44.8	22.4	39.0	57.4%
SH-3-3	41.4	20.7	39.0	53.1%
SH-8-1	74.8	24.9	39.0	63.8%
SH-8-2	69.9	23.3	39.0	59.7%

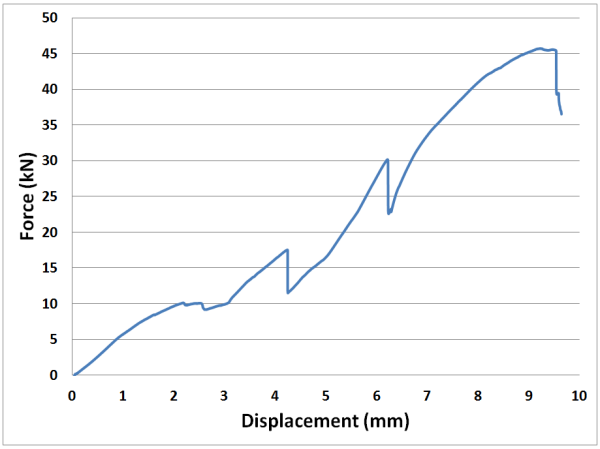

SHC-2-1 Specimen

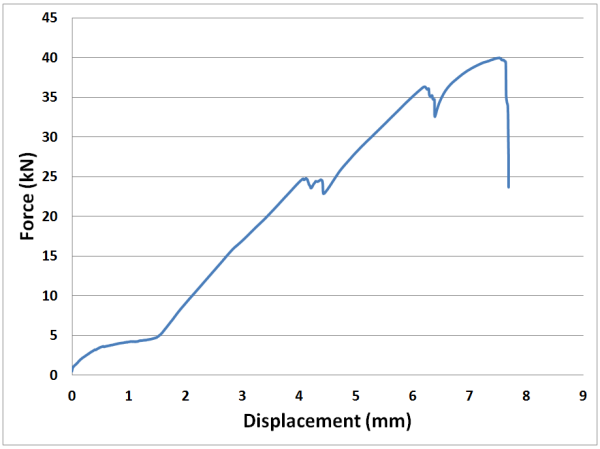

SHC-2-2 Specimen

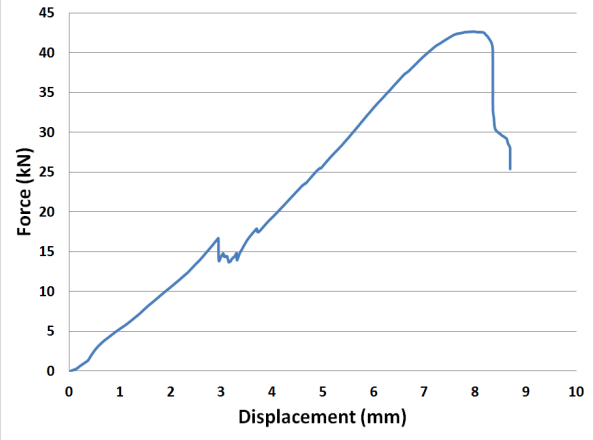

SHC-3-1 Specimen

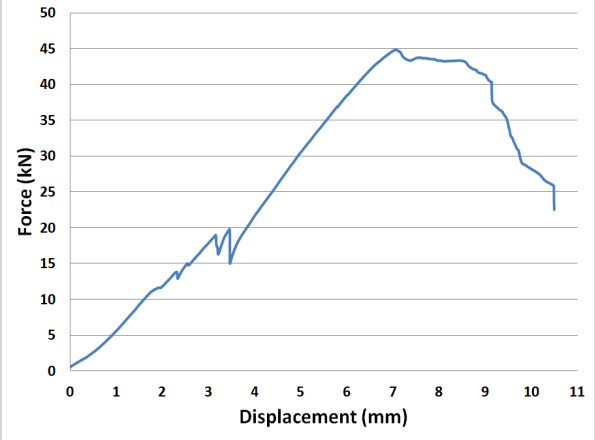

SHC-3-2 Specimen

Figure 4.23 Direct Shear Tests; Force – Displacement Relationships for Concrete Prisms

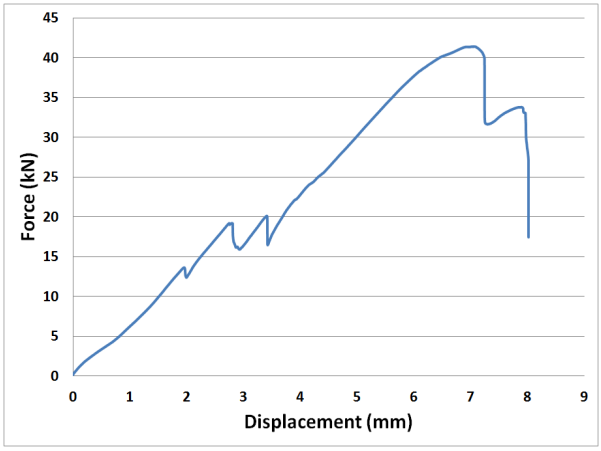

SHC-3-3 Specimen

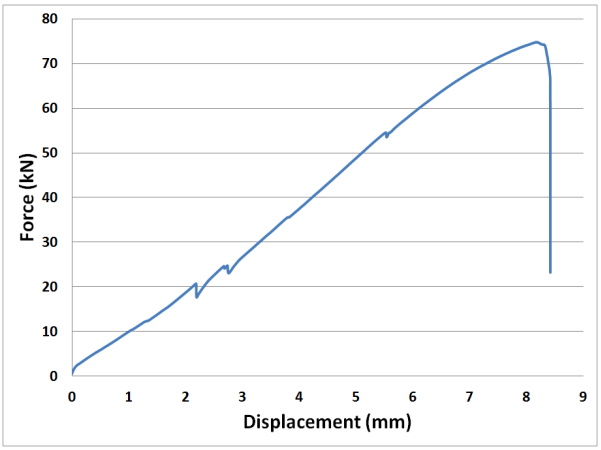

SH8-1 Specimen

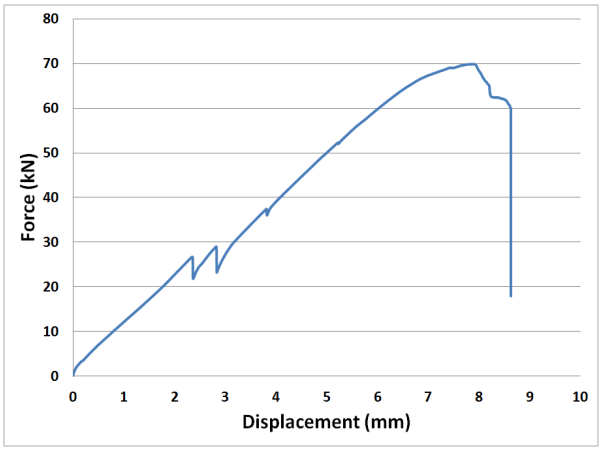

SH8-2 Specimen

Figure 4.23 (Cont'd) Direct Shear Tests; Force – Displacement Relationships for Concrete Prisms

The load recorded by the test machine was assumed to be divided approximately equally between the vertical legs of the WWR grid at failure. However, it was observed that one of the joints showed excessive deformation and slight rotation before the welded wires were separated at the weld interface, indicating unequal forces resisted by the wirers. The presence of concrete provided better support for the grid and minimized the out-of-plane deformation under lower loads. The average load in each resisting wire is tabulated in Table 4.10 and compared with steel yield strength. The results indicated that the welds failed prior to yielding of the wire.

The WWR grids were instrumented with strain gauges to monitor strains in steel. Figure 4.24 shows the strain gauge layout and labelling of the grids. It should be noted that the strain gauges

not only measured axial tension, but also captured strains associated with bending of the ends, especially near failure loads. Therefore, the strain readings, although showed some indication of tensile forces, could not be taken as accurate representation of actual forces in wires. Some strain gauges were damaged and did not provide proper readings and were eliminated from Appendix A.1, where the strain-deformation graphs are presented.

Table 4.10 Direct Shear Test results for Concrete Prisms with Cast-in WWR Grids

Specimen ID	Load at Failure (kN)	Displacement at Failure (mm)	Average load per vertical leg (kN / connection)
SH-2-1	45.8	9.5	22.9
SH-2-2	40.0	7.6	20.0
SH-3-1	42.5	8.4	21.3
SH-3-2	44.8	7.1	22.4
SH-3-3	41.4	7.0	20.7
SH-8-1	74.8	8.2	24.9
SH-8-2	69.9	7.9	23.3

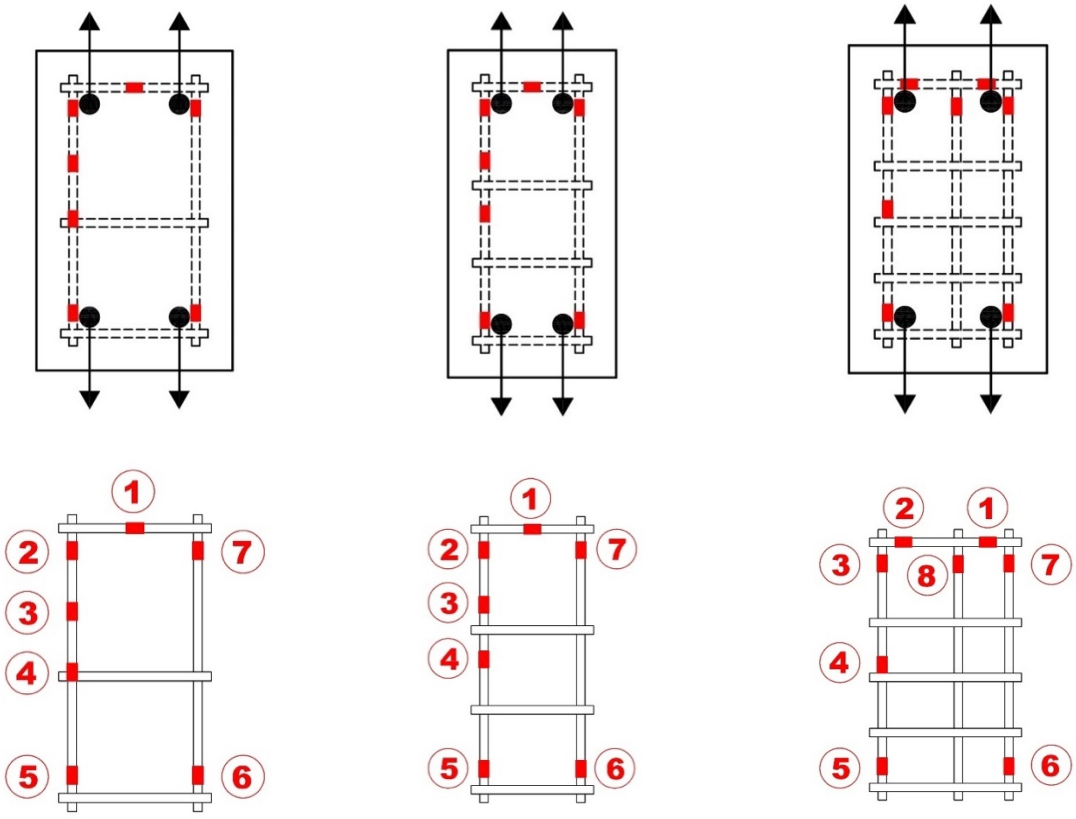

Figure 4.24 Strain Gauge Locations for Concrete Prisms Tested under Direct Shear

4.4.3 Burst Tests of Concrete Prism Specimens

Burst tests were conducted using a similar test procedure as that used earlier for bare grid testes described in Section 4.3.4. The tensile force was applied along the grid diagonal through the corner 25M bar. The main difference between the bare grid tests and the current tests was the presence of concrete, which eliminated the need to provide a rigid link along the opposite diagonal. The embedment of grids in concrete was believed to provide a more realistic representation of the actual behavior of grids in structural elements. The data recorded during these tests by a data acquisition system include the magnitude of applied force, machine head movement, and steel strains. The burst test set-up is shown in Figure 4.25.

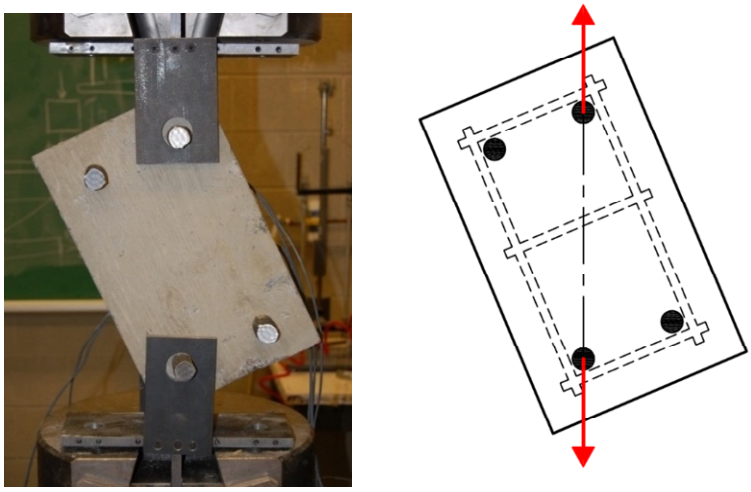

Figure 4.25 Concrete Prism with Cast-in WWR Grid and Burst Test Set-up

During the initial stage of loading, the concrete and WWR grid shared the applied tensile load together until the concrete reached its tensile capacity and cracked. The cracks appeared to be as full-depth cracks, taking place perpendicular to the direction of the load. This is shown in Figure 4.26. At this stage of loading a drop in load resistance was recorded. The free-body diagram of the cracked segment is illustrated in Figure 4.27. The layout and geometric details of concrete prisms with embedded 2-cell, 3-cell and 8-cell grids are shown in Table 4.11. The specimens were labelled such that the prefix “BC” refers to the burst test of concrete prism specimens, the second number refers to the number of cells in the grid and the last number identifies the specimen number of for the grid configuration.

Tensile forces across the crack were transmitted through two steel wires that crossed the crack, as shown in the free body diagram of Figure 4.27 with a force component resisted by each. The angle between the load and the grid members varied slightly as the geometry of the grids changed for each configuration. All the specimens exhibited grid weld failures with welded steel wires separating at the weld interface. The results of direct shear tests of concrete specimens are summarized in Table 4.12. Applied diagonal load versus displacement relationships are plotted in Fig. 4.28.

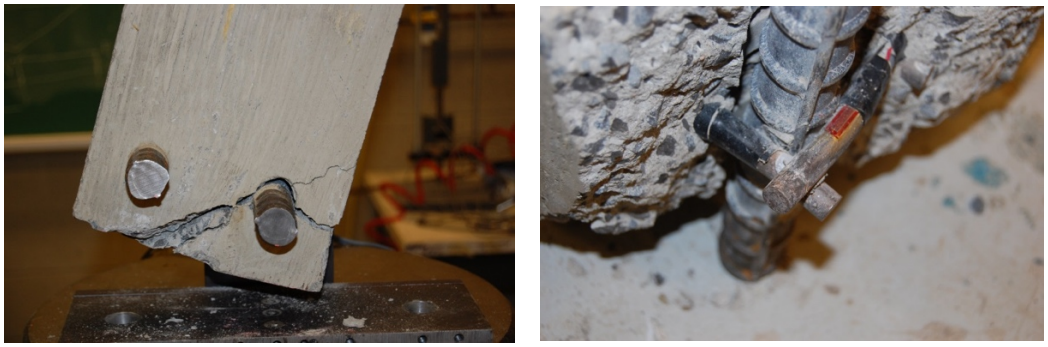

Figure 4.26 Typical Failed Concrete Cube Specimen under Burst Test Loading

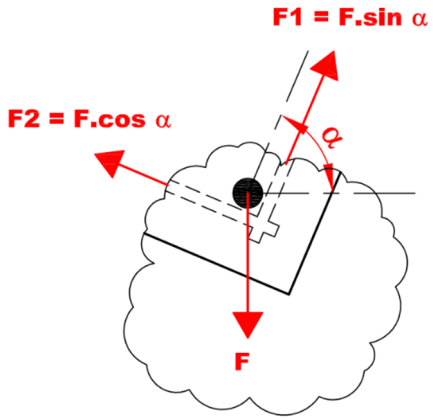

Figure 4.27 Cracked Concrete Cube Free Body Diagram for Burst Test

Table 4.11 Burst Test Specimen Information

Specimen Information	*Grid Picture*	*Grid Layout*	*Loading Diagram*
BC-2-1 and **BC-2-2** Burst Test 2-Cell Grid Configuration		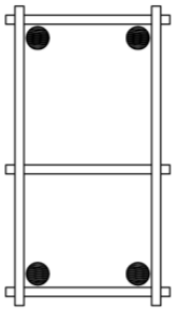	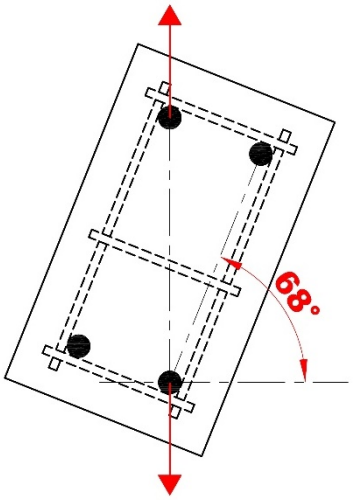
BC-3-1 and **BC-3-2** Burst Test 3-Cell Grid Configuration		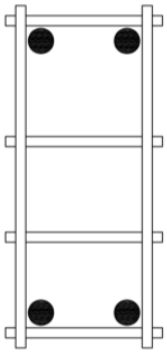	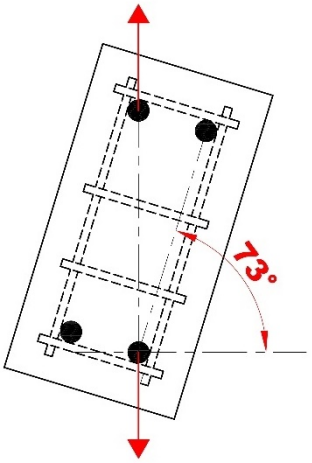
BC-8-1 Burst Test 8-Cell Grid Configuration	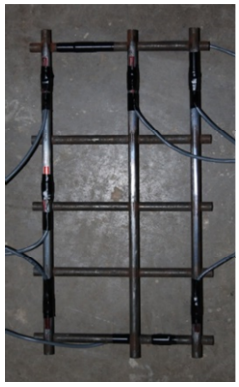	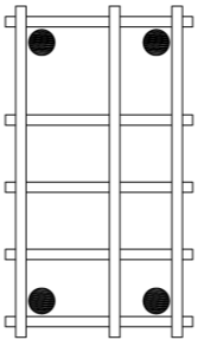	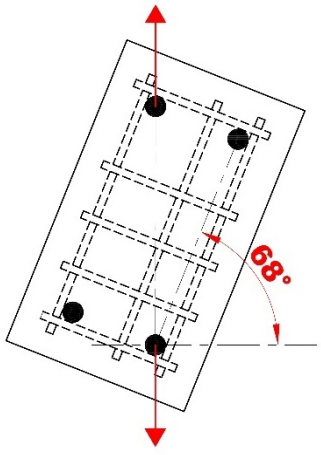

Table 4.12 Burst Test results for Concrete Cubes Specimens with Cast-in WWR Grids

Sample ID	Load at Failure (kN)	Displacement at Failure (mm)
BC-2-1	33.9	7.0
BC-2-2	33.3	6.0
BC-3-1	26.1	6.4
BC-3-2	26.7	8.5
BC-8-1	38.0	7.2

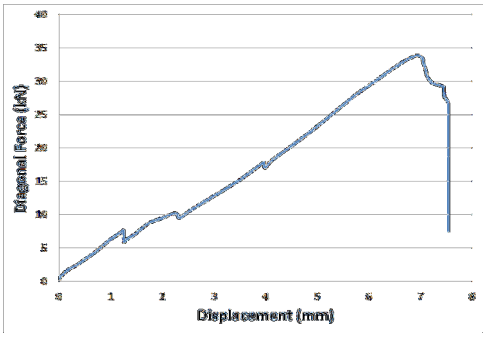

BC-2-1 Specimen

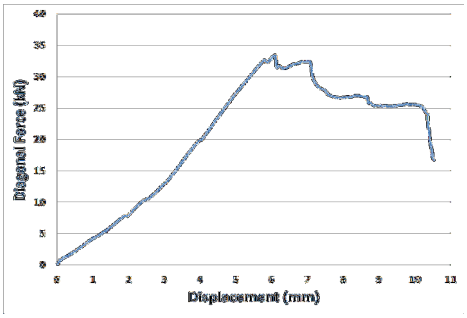

BC-2-2 Specimen

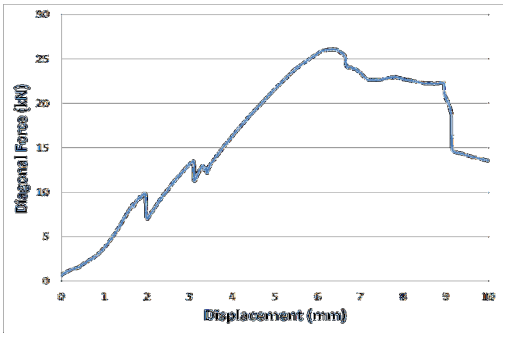

BC-3-1 Specimen

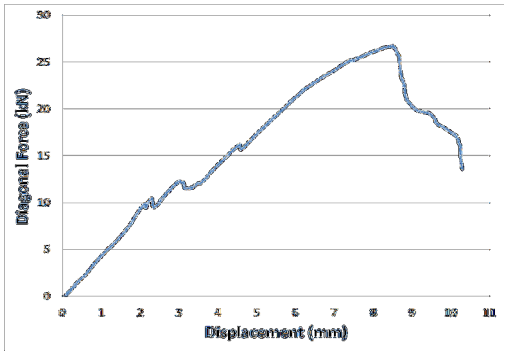

BC-3-2 Specimen

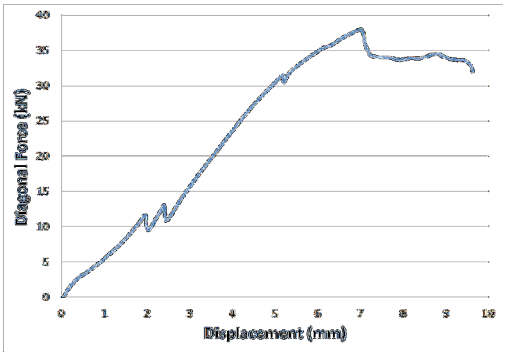

BC-8-1 Specimen

Figure 4.28 Force – Displacement Relationships; Burst Tests on Concrete Prisms

The applied load was decomposed into its components in each direction of intersecting grid wires using the free-body-diagram shown on Figure 4.27. The values of these force components are tabulated in Table 4.13. They are also compared with yield force in the same table. The results indicate that the welds failed in all cases prior to the yielding of wire.

Table 4.13 WWR Grids Burst Test – Force Components

Specimen ID	Load at Failure (kN)	Angle (Degrees)	F1 (kN)	F2 (kN)	Fy (kN)	F1/Fy (%)	F2/Fy (%)
BC-2-1	33.9	68	31.43	12.70	39.0	80.6%	32.6%
BC-2-2	33.3	68	30.88	12.47	39.0	79.2%	32.0%
BC-3-1	26.1	73	24.96	7.63	39.0	64.0%	19.6%
BC-3-2	26.7	73	25.53	7.81	39.0	65.5%	20.0%
BC-8-1	38.0	68	35.23	14.24	39.0	90.3%	36.5%

The WWR grids were instrumented with strain gauges to monitor strains in grid wires. It should be noted that the strain gauges not only measured axial tension, but also captured strains associated with bending of the ends, especially near failure loads. Therefore, the strain readings, although showed some indication of tensile forces, could not be taken as accurate representation of actual forces in wires. Figure 4.29 shows the strain gauge layout and labelling of the grids. Some strain gauges were damaged and did not provide proper readings and were eliminated from Appendix A.2, where the strain-deformation graphs are presented.

4.5 Small-Scale Column Specimens

In addition to the material tests reported in previous sections, six (6) small scale columns with a 150 mm square cross-section were built using WWR as transverse reinforcement to assess the grid capacity for restraining compression bars against buckling. The columns were instrumented and tested under axial compression until failure. The axial compression was applied either as a concentric or eccentric loading. The grid spacing varied between 35 and 70 millimeters. The eccentricity of load was; zero, 9 mm and 18 mm, resulting in bending moments in some columns. The strain gauge layout was implemented according to the loading condition to capture behavior

near the highly stressed regions. The reinforcement layout for column specimens is shown in Figure 4.30. The columns were labelled such that the prefix "SC" refers to short column specimens, the first number in the label refers to the eccentricity level and the second number identifies the grid spacing. Figure 4.31 shows the manufacturing process of the small-scale columns.

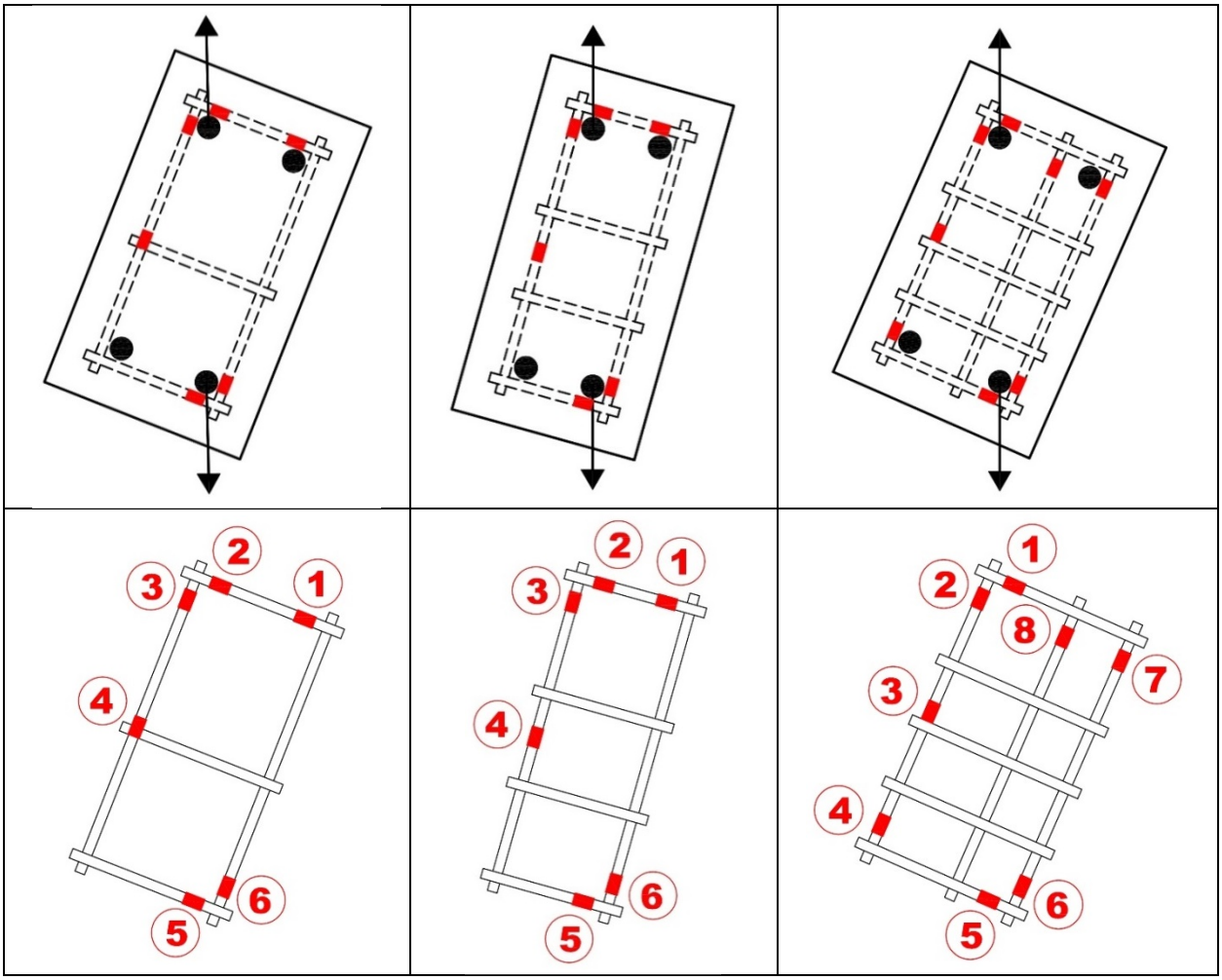

Figure 4.29 Strain Gauge Locations for Concrete Prisms Subjected to Burst Tests

The test set up and the damaged specimens are shown in Figure 4.32. All columns failed in a similar fashion by buckling of the longitudinal bars, which coincided with the failure of the corner grid welds. The results are summarized in Table 4.14 and indicate higher capacity for columns with 35 mm grid spacing in comparison with columns with 70 mm grid spacing. This was attributed to improved concrete confinement. Experimentally obtained load-versus displacement relationships are shown in Figure 4.33 to 4.35 for concentrically and eccentrically loaded columns.

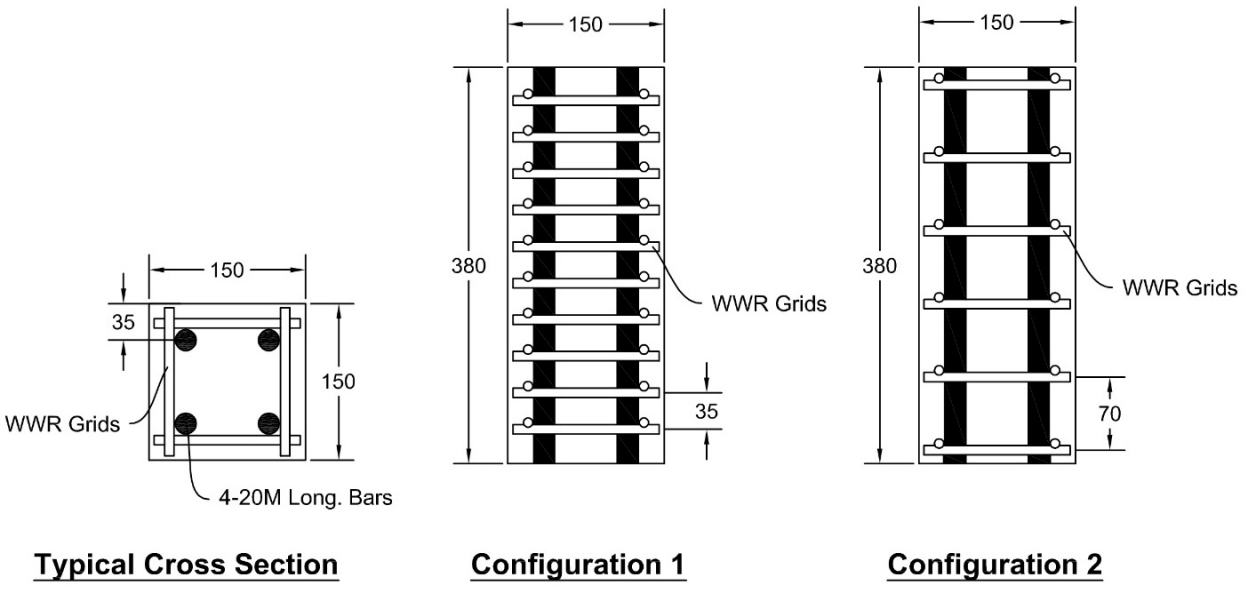

Figure 4.30 Small Column Specimen Layout and Dimensions

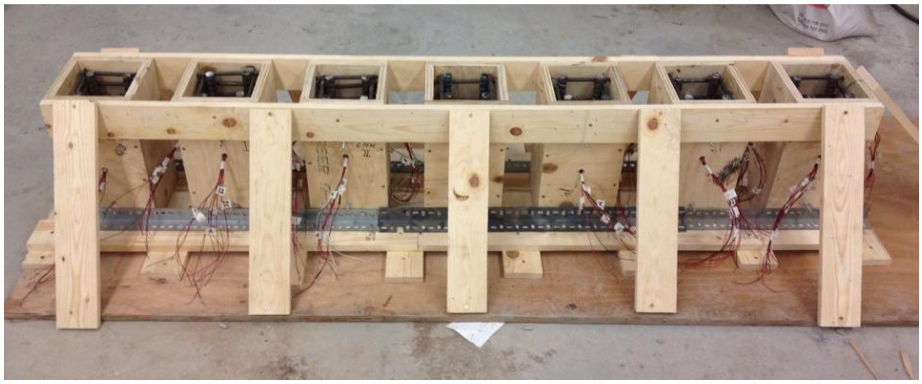

Figure 4.31 Manufacturing of Small Column Specimens

Figure 4.32 Small Scale Column Test Setup (LEFT) and Failed Specimen (Right)

Table 4.14 Small Scale Column Specimens

Specimen ID	Cross Section (mm x mm)	Height (mm)	Eccentricity (mm)	Tie Spacing (mm)	Maximum Load (kN)
SC-0-35	150x150	380	0	35	2052
SC-0-70	150x150	380	0	70	1831
SC-9-35	150x150	380	9	35	1420
SC-9-70	150x150	380	9	70	1170
SC-18-35	150x150	380	18	35	1289
SC-18-70	150x150	380	18	70	1222

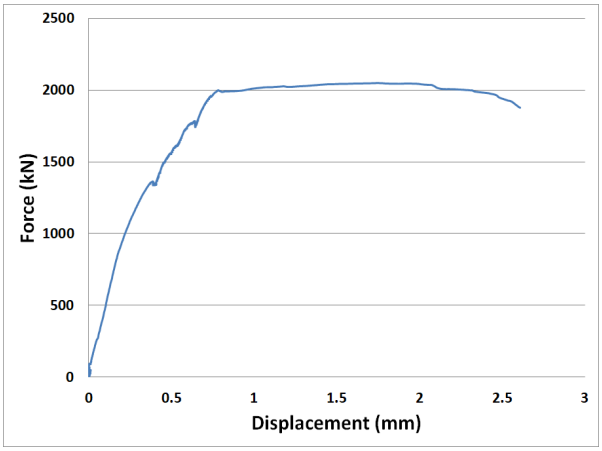

SC-0-35 Specimen

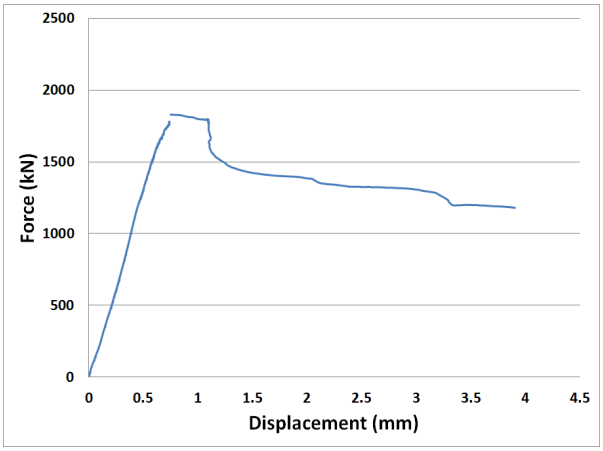

SC-0-70 Specimen

Figure 4.33 Force – Displacement Relationships for Concentrically Loaded Columns

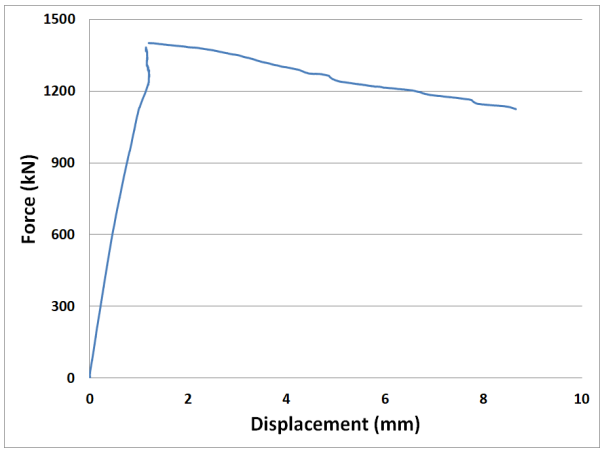

SC-9-35 Specimen – LVDT 1 (Compression Side)

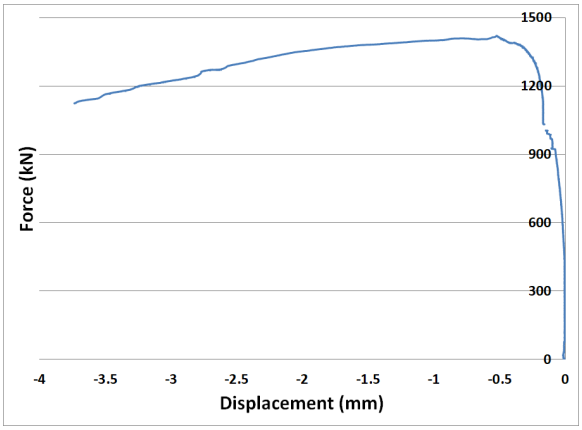

SC-9-35 Specimen – LVDT 2 (Tension Side)

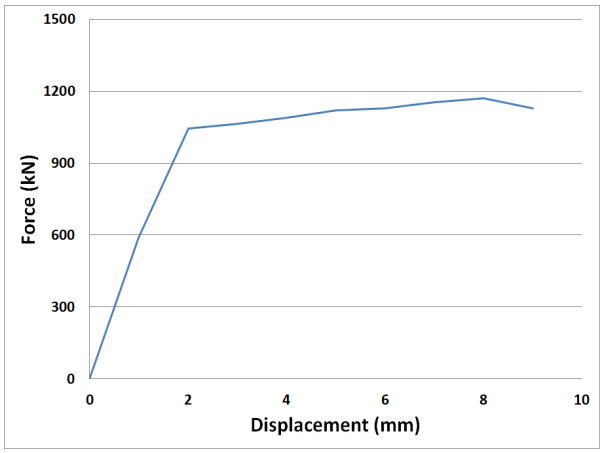

SC-9-70 Specimen – LVDT 1 (Compression side)

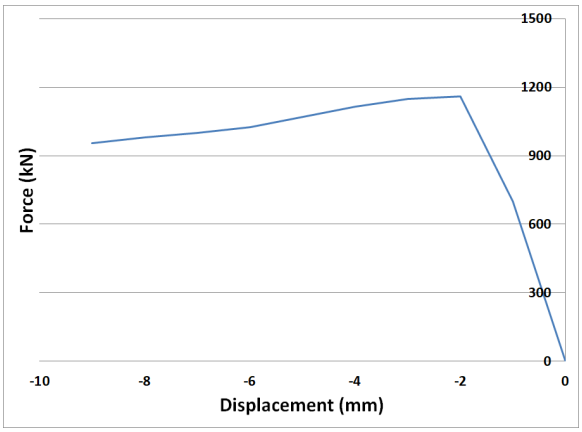

SC-9-70 Specimen – LVDT 2 (Tension Side)

Figure 4.34 Force – Displacement Relationships for Eccentrically Loaded Columns; e = 9 mm

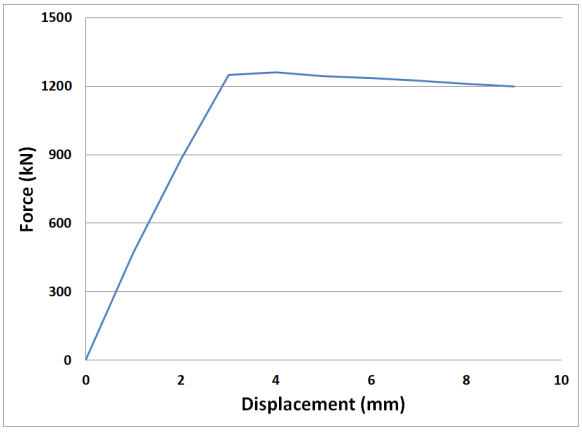

SC-18-35 Specimen – LVDT 1 (Compression side)

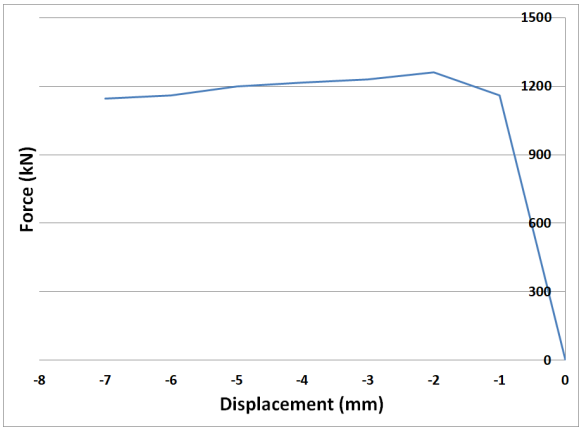

SC-18-35 Specimen – LVDT 2 (Tension Side)

Figure 4.35 Force – Displacement Relationships for Eccentrically Loaded Columns; e = 18 mm

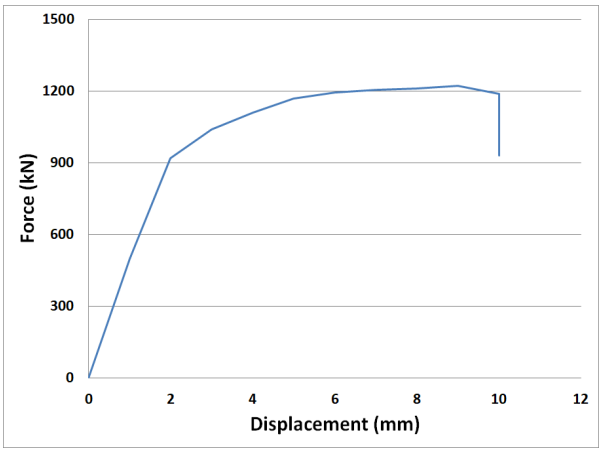

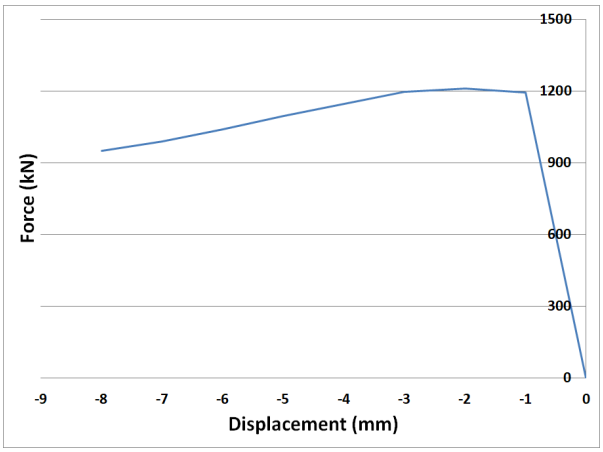

SC-18-70 Specimen – LVDT 1 (Compression side) SC-18-70 Specimen – LVDT 2 (Tension Side)

Figure 4.35 (Cont'd) Force–Displacement Relationships for Eccentrically Loaded Columns; e = 18 mm

The location of instrumented grids for concentrically loaded columns and the layout and labelling of strain gauges on these grids are depicted in Figure 4.36. The longitudinal bars were instrumented with strain gauges at half the column height. The force-strain graphs are presented in Appendix A.3. The positive strain readings indicate elongation of the surface where the strain gauge is adhered to, and the negative reading indicates shortening of the steel fiber on the surface. The strain readings on grids may include additional strains associated with twisting/bending of the wires, in addition to axial straining. Bending of the wires may be introduced due the eccentricity generated by welding two off-center bars together.

The strain gauges on longitudinal bars showed readings in excess of 2000 microstrain in compression, indicating yielding. The grids maintained their integrity beyond yield. The columns then failed by buckling of the longitudinal bars which coincided with the grid weld failure. The maximum strain values recorded during the experiments are tabulated in Tables 4.15 and 4.16. It should be noted that some strain gauges were showing out-of-range readings while the specimen was still being loaded. Therefore, the maximum strain readings shown in the tables are not necessarily the maximum strains experienced by steel members. Further details of steel strains can be found in Appendix A.3 for concentrically loaded columns. Several strain gauges graphs are excluded from Appendix A.3 as they showed out-of-range errors.

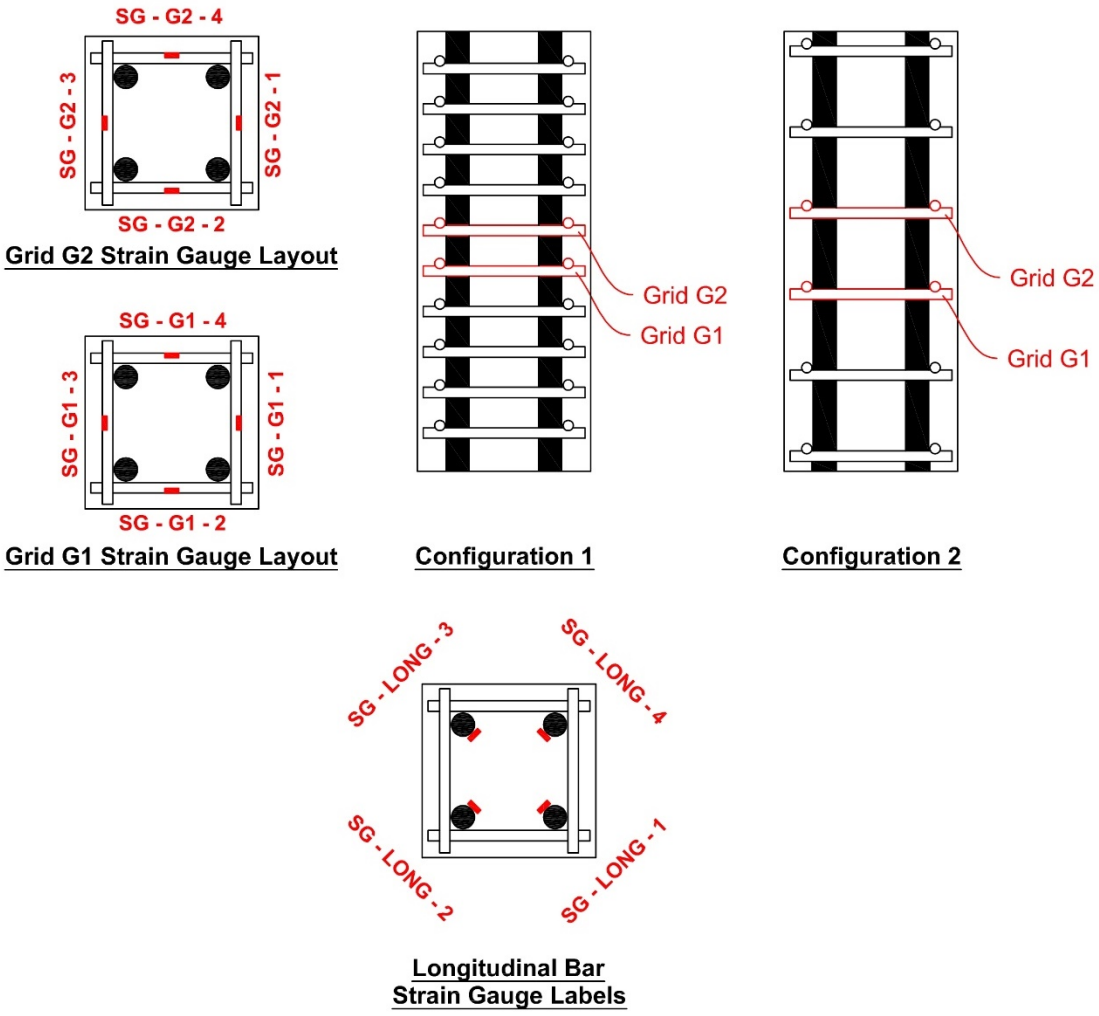

Figure 4.36 Strain Gauges Locations for Concentrically Loaded Columns

The locations of strain gauges and their labels for eccentrically loaded columns are shown in Figure 4.37. The longitudinal bars were instrumented with strain gauges at column mid-height. The Force-strain graphs are presented in Appendix A.4. The strain gauges on longitudinal bars showed strain readings in excess of 2000 microstrain, indicating yielding in compression. The grids initially maintained their integrity, but failed at welded connections, at which time the compression bars buckled. The maximum strain values recorded by strain gauges are tabulated in Tables 4.17 to 4.20. It should be noted that some strain gauges were out-of-range, and some of the very high strain values may not be reliable. Further details of strain readings and their plots are provided in Appendix A.4.

Table 4.15 Maximum Recorded Strains for Specimen SC-0-35

Strain Gauge ID	Maximum Recorded Strain	Strain Gauge ID	Maximum Recorded Strain
SG – LONG – 1	-13600	SG – LONG – 2	-14000
SG – LONG – 3	-5800	SG – LONG – 4	-15800
SG – G1 – 1	1870	SG – G1 – 2	2550
SG – G1 –3	4820	SG – G1 – 4	2430
SG – G2 – 1	9850	SG – G2 – 2	7100
SG – G2 – 3	5830	SG – G2 – 4	3450

Note: Force-Strain graphs for concentrically loaded columns are provided in Appendix A.3.

Table 4.16 Maximum Recorded Strains for Specimen SC-0-70

Strain Gauge ID	Maximum Recorded Strain	Strain Gauge ID	Maximum Recorded Strain
SG – LONG – 1	-16300	SG – LONG – 2	-16700
SG – LONG – 3	-16500	SG – LONG – 4	-16600
SG – G1 – 1	3000	SG – G1 – 2	5850
SG – G1 –3	2680	SG – G1 – 4	3040
SG – G2 – 1	2900	SG – G2 – 2	6350
SG – G2 – 3	5060	SG – G2 – 4	3100

Note: Force-Strain graphs for concentrically loaded columns are provided in Appendix A.3.

Table 4.17 Maximum Recorded Strains for Specimen SC-9-35

Strain Gauge ID	Maximum Recorded Strain	Strain Gauge ID	Maximum Recorded Strain
SG – LONG – 1	-970	SG – LONG – 2	-17800
SG – LONG – 3	-18100	SG – LONG – 4	-940
SG – G1 – 1	1650	SG – G1 – 2	-2750
SG – G1 – 4	-8300	SG – G1 – 5	-2700
SG – G1 – 6	1720	SG – G2 – 1	3400
SG – G2 – 2	-2300	SG – G2 – 3	-3400
SG – G2 – 5	-2700	SG – G2 – 6	1740

Note: Force-Strain graphs for eccentrically loaded columns are provided in Appendix A.4.

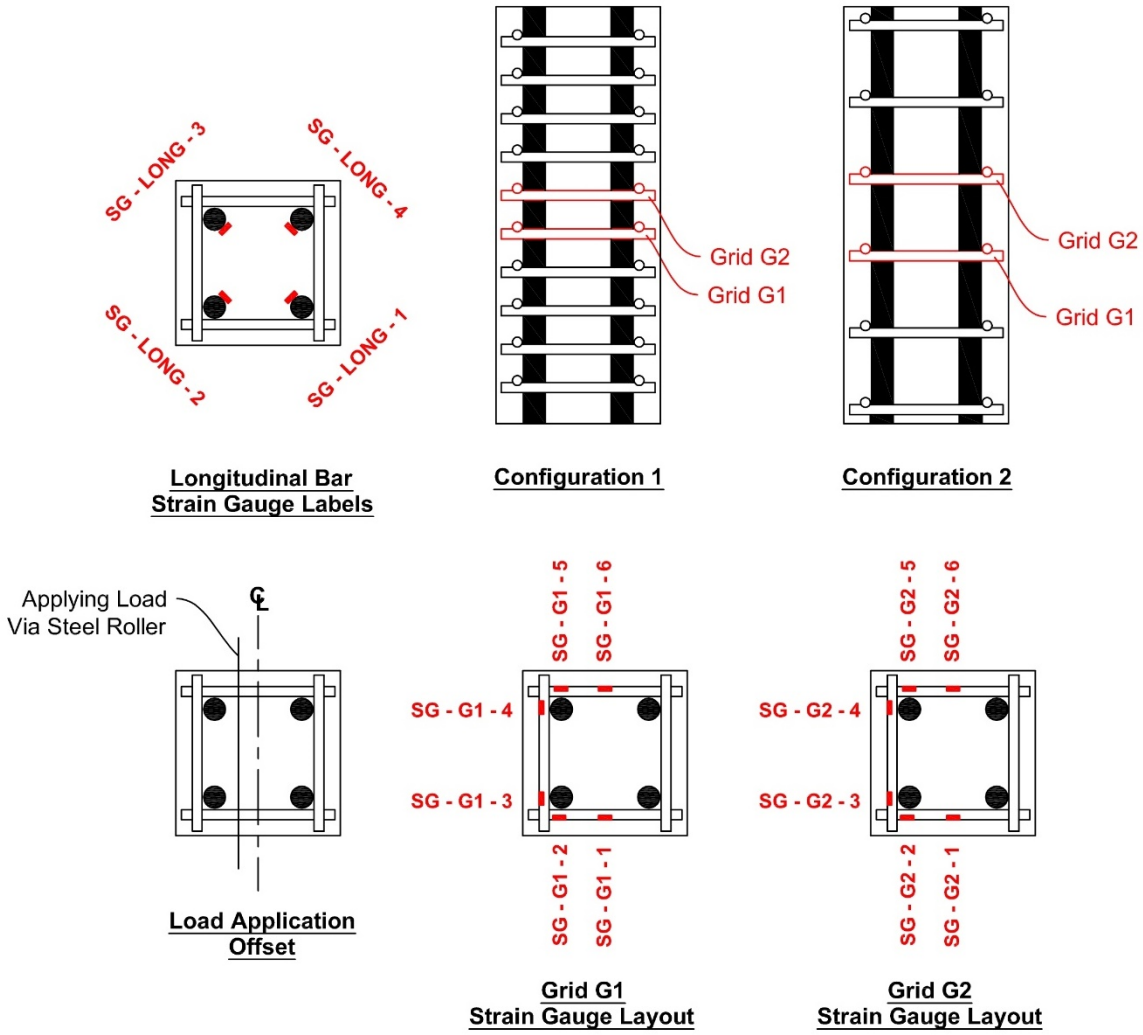

Figure 4.37 Strain Gauges Locations for Eccentrically Loaded Columns

Table 4.18 Maximum Recorded Strains for Specimen SC-9-70

Strain Gauge ID	Maximum Recorded Strain	Strain Gauge ID	Maximum Recorded Strain
SG – LONG – 1	-1030	SG – LONG – 2	-13400
SG – LONG – 3	-13900	SG – LONG – 4	-900
SG – G1 – 1	3020	SG – G1 – 2	-2280
SG – G1 – 3	-760	SG – G1 – 4	330
SG – G1 – 5	-4830	SG – G1 – 6	4970
SG – G2 – 1	11100	SG – G2 – 2	-5260
SG – G2 – 3	-1340	SG – G2 – 4	-8700
SG – G2 – 5	-6600	SG – G2 – 6	3300

Note: Force-Strain graphs for eccentrically loaded columns are provided in Appendix A.4.

Table 4.19 Maximum Recorded Strains for Specimen SC-18-35

Strain Gauge ID	Maximum Recorded Strain	Strain Gauge ID	Maximum Recorded Strain
SG – LONG – 1	-840	SG – LONG – 2	-16000
SG – LONG – 3	-13800	SG – LONG – 4	-810
SG – G1 – 1	2100	SG – G1 – 2	-2050
SG – G1 – 3	1400	SG – G1 – 4	2740
SG – G1 – 6	1340	SG – G2 – 2	-4650
SG – G2 – 3	-3220	SG – G2 – 4	800
SG – G2 – 5	-2100	SG – G2 – 6	500

Note: Force-Strain graphs for eccentrically loaded columns are provided in Appendix A.4.

Table 4.20 Maximum Recorded Strains for Specimen SC-9-70

Strain Gauge ID	Maximum Recorded Strain	Strain Gauge ID	Maximum Recorded Strain
SG – LONG – 1	-1740	SG – LONG – 2	-16400
SG – LONG – 3	-15700	SG – LONG – 4	-1410
SG – G1 – 1	4800	SG – G1 – 2	-2740
SG – G1 – 3	-6440	SG – G1 – 4	-12600
SG – G1 – 5	-3400	SG – G1 – 6	5250
SG – G2 – 1	3000	SG – G2 – 2	-1000
SG – G2 – 3	-4300	SG – G2 – 4	-2950
SG – G2 – 5	-2260	SG – G2 – 6	6100

Note: Force-Strain graphs for eccentrically loaded columns are provided in Appendix A.4.

Chapter 5

Experimental Research – Large Scale Shear Walls

5.1 General

Three (3) large scale shear walls were constructed using WWR grids as transverse reinforcement in boundary elements. The design philosophy and aspect ratio of each wall was selected differently to determine the performance of walls under various design and loading conditions. The following variables were considered as test parameters: concrete strength, transverse reinforcement volumetric ratio, WWR grid spacing, wall length, wall height (height-to length ratio), wall thickness, and wall cross-sectional shape (rectangular or barbell). The walls were subjected to reverse cyclic loading up to failure. The details of the wall specimens are provided in this Chapter.

5.2 Test Set-up and Loading Program

The components of test set-up consist of two A-frames, a connection beam, actuators, load cells, lateral restraining elements, external displacement monitoring support, and the top loading beam. These components, as well as the test wall were all supported by the laboratory strong wall at the University of Ottawa. The schematic view of the test setup elevation and plan views are illustrated in Figures 5.1 and 5.2, respectively. The A-Frames consist of a steel wide flange section positioned vertically and supported by a diagonal HSS section to provide rigidity. Stiffener plates were added

to the wide flange section to provide local strengths where required. The A-frame was connected to the strong floor using 3" diameter high strength threaded bolts. The Laboratory strong floor is a 900 mm (3') thick reinforced concrete structural slab with a matrix of pre-located sleeves spaced at 900 mm (3') o/c in both directions for fixing test elements. These holes were used to tie down both the A-Frame and the shear wall specimens. Figures 5.1 and 5.2 illustrate the test setup.

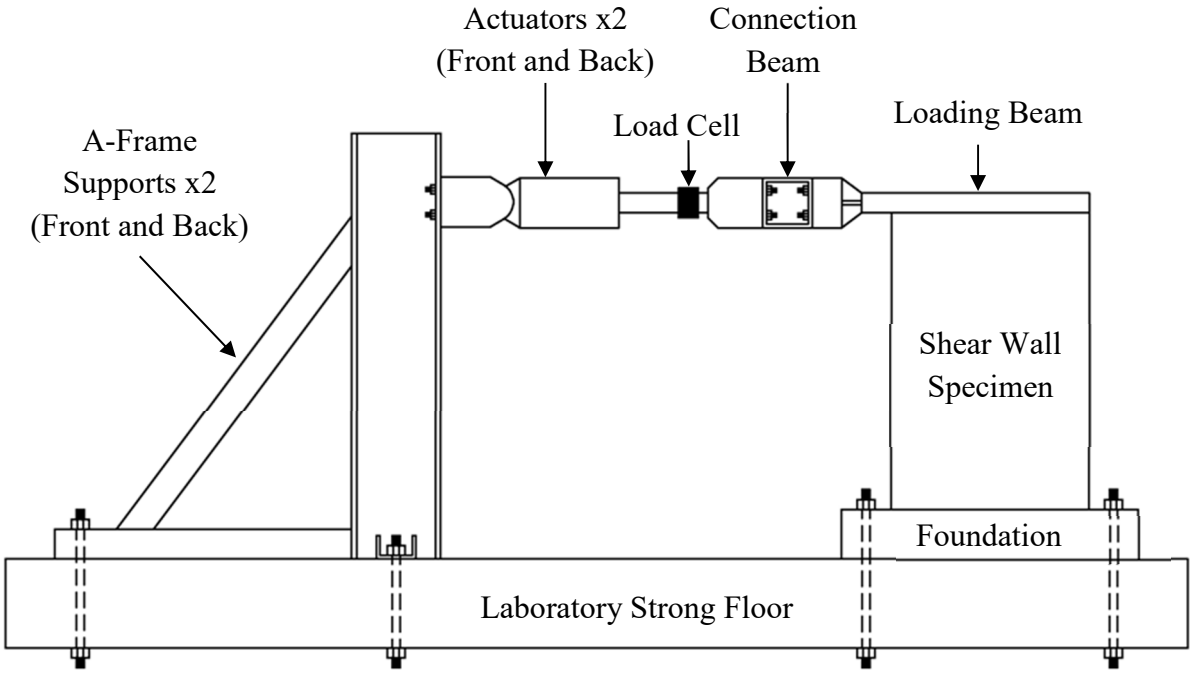

Figure 5.1 Schematic View of Test Set-up Elevation

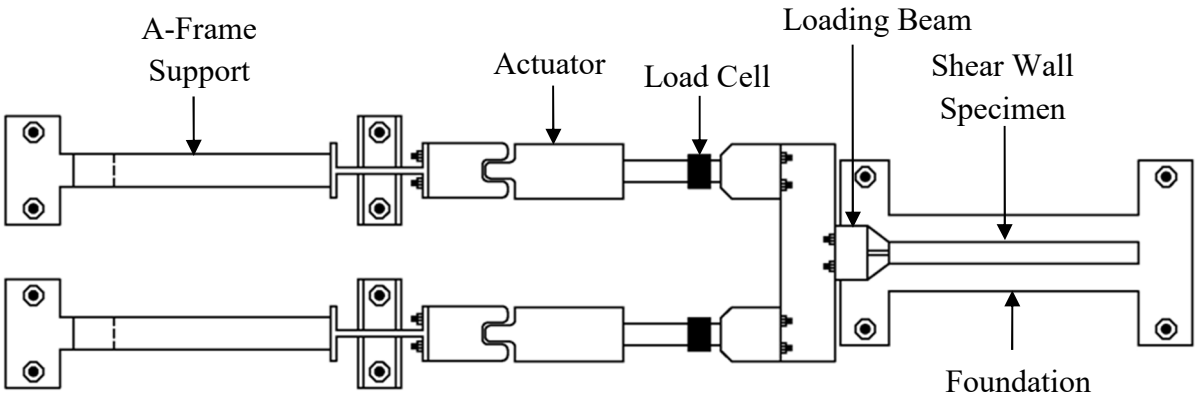

Figure 5.2 Schematic View of Test Set-up Top View

Two actuators, each with +/- 1000 kN capacity were used to apply lateral deformations/forces, except for the tallest third wall, which could be tested by one actuator. Because of the size and capacity of the first two shear wall specimens, one actuator would not provide sufficient load capacity. The two actuators were connected to specimens via a connection beam and a loading beam. The connection beam connects the ends of the actuators to the loading beam, which was cast integrally with the shear walls. The actuator has its own controlling unit which is directly connected to the load cell and an internal LVDT that monitors the movement of the actuator. This allows the user to move the actuator to any desired load or displacement level. The tests are mostly conducted in the deformation mode (except for the initial elastic load cycles). When two actuators were used, the emphasis during testing was to ensure equal displacement in each actuator. It should be noted that the wall deformation would not exactly match the movement of the actuator since the actuator movement includes elastic movement of the A-frame and any potential sliding and lifting of the supports and the wall foundation.

A series of equally spaced vertical prestressing tendons were used on both sides of the walls to apply gravity loads. These strands were anchored to the foundation at the base and to the loading beam at the top. The prestressing operation was done in increments to achieve a uniform load distribution until the desired level of gravity loading was attained. During the initial prestressing process, the strands were loaded up to about 50% of their tensile capacity.

The shear walls were tested under incrementally increasing reversed cyclic loading until failure. Tests were conducted in displacement controlled mode. After the initial elastic cycles, pre-selected lateral displacement increments were applied and the corresponding loads were recorded. Loading was stopped at the end of each deformation level for observations of damage and crack patterns. The walls were cycled three times at each of the incrementally increasing displacement level.

5.3 WWR Grid Dimensions for Shear Wall Specimens

The layout and geometry of WWR grids, which were used as boundary element transverse reinforcement, are shown in Figure 5.3. Shear wall specimens 1, 2 and 3 used 2-cell, 6-cell and 4-cell grids, respectively.

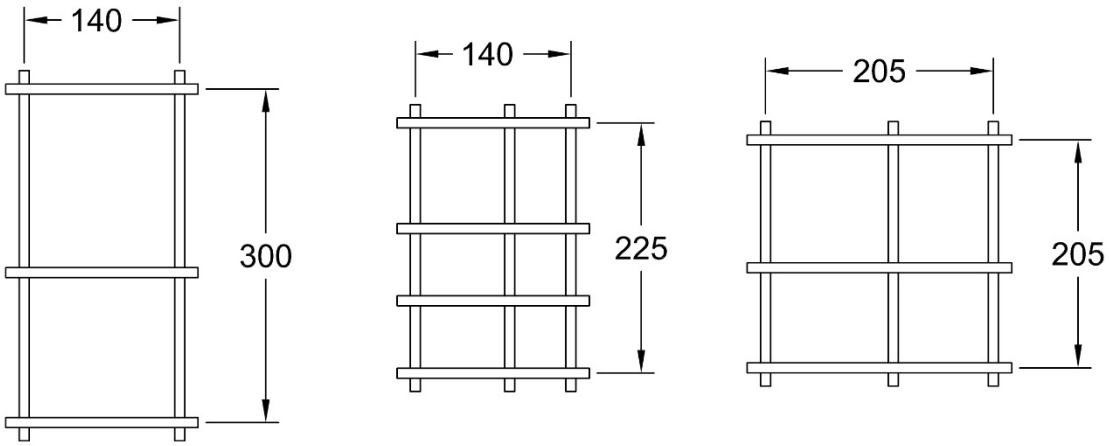

Figure 5.3 Grid Dimensions for Shear Wall Specimens: Walls 1 to 3 from left to right

5.4 Shear Wall No. 1

Shear wall No. 1 was a rectangular wall with a height to length aspect ratio of 1.55:1 (3.1m height to 2m length). The wall thickness was 200 mm. Concentrated end reinforcement was used near the ends of the section to create boundary elements as shown in Figures 5.4 and 5.5. The wall was designed following the seismic requirements of ACI-318-11, which identifies walls with aspect ratios of 1.5 or less to be categorized as shear-dominant walls. The same code defines walls with aspect ratios of 2.0 or higher to be flexure dominant. The aspect ratios between 1.5 and 2.0 is considered as a transition zone, as the wall gradually shifts from shear dominant to flexure dominant behavior. Elevation and cross-sectional views of Wall 1 are illustrated in Figures 5.4 and 5.5. These figures provide geometric and reinforcement details of Wall 1.

The wall was cast integrally with a pre-fabricated steel loading beam at the top. It was cast with shear keys and high strength steel rods at the top to prevent any sliding or tensile separation of the loading beam. The wall was subjected to 1600 kN axial compression using sixteen (16) prestressing strands divided equally on two sides of the wall. The web horizontal reinforcement was placed as straight bars outside of vertical bars. The wall shear span was defined as the distance from the base of the wall to the center of the loading beam, coinciding with the centerline of actuators (point of application of lateral load).

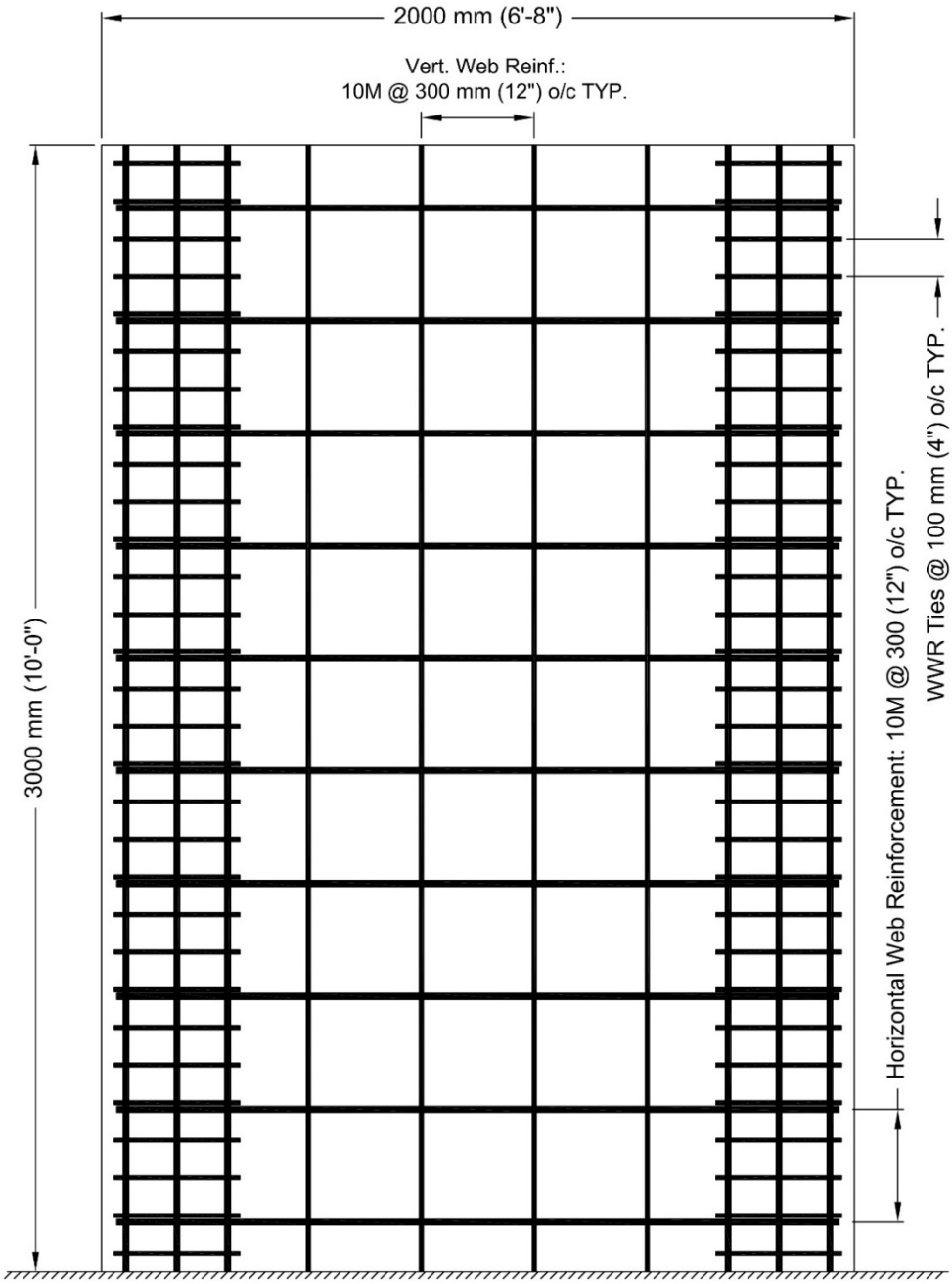

Figure 5.4 Shear Wall No. 1 Elevation

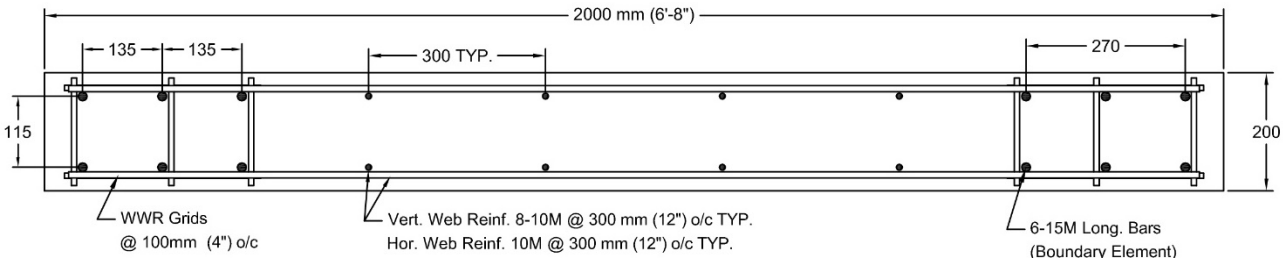

Figure 5.5 Shear Wall No. 1 Cross-Section

Among the three walls tested, Wall 1 was designed to have nominal shear and flexural capacities to be approximately equal to assess the performance of a wall and the WWR grids when flexure and shear were equally critical. The subsequent two walls (Walls 2 and 3) were designed to perform predominantly in flexure, with higher wall aspect ratios. The initial design of Wall 1, as presented in the following section, was based on 40 MPa concrete. The concrete strength was not identical to design concrete strength. On the day of testing, cylinder tests indicated 52 MPa concrete. Therefore, the design calculations were made one more time based on the actual concrete strength. These calculations are labelled as "wall as-built calculations," and presented after the initial design. The design calculations provide requirements for web horizontal and vertical reinforcement (both amount and spacing), as well as the boundary element reinforcement, including WWR grids and their spacing.

5.4.1 Shear Wall No. 1 – Design Notes

The first step in designing the wall requires a sectional analysis to determine the moment capacity of the wall for the selected geometry and longitudinal reinforcement, as illustrated in Figure 5.5. "RC-Section" software was used to perform sectional analysis. A screenshot of the modelled wall is provided in Figure 5.6.

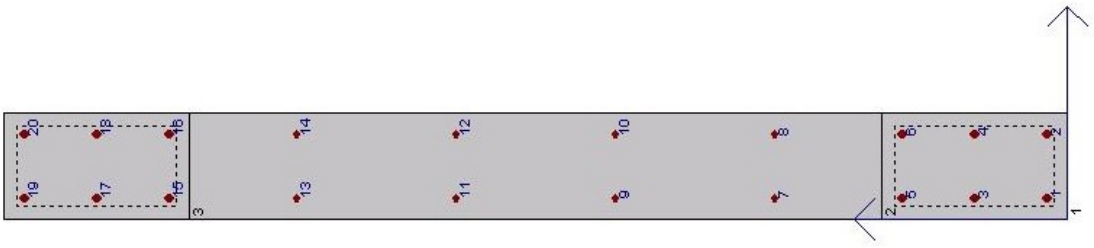

Figure 5.6 Screenshot of Shear Wall No. 1 Model in RC-Section Software

RC-Section software allows for various concrete models to be defined and assigned to different segments of the cross section. For shear wall No. 1, two concrete models were introduced: Hognestad's (1951) model for unconfined concrete cover and Saatcioglu and Razvi (1992) model for confined core concrete in boundary elements. A bilinear stress-strain relationship was assumed for the reinforcing steel. The design assumptions and calculations are summarized below. ACI 318-11 equations were used in design.

Design Assumptions:

$f'_c = 40\ MPa = 5{,}800\ psi$

$fy = 460\ MPa = 66{,}700\ psi$: for all rebars;

$fyt = 550\ MPa = 80{,}000\ psi$: for WWR grids;

$\sqrt{f'_c} = 76.1\ < 100\ psi \qquad OK.$

$l_w = 2.0\ m \cong 80"$

$h_w = 3.1\ m \cong 124"$

$h = 0.2\ m \cong\ 8"$

$d = 0.8 l_w \cong 64"$ Cl. 21.9.2.3(c)

$A_{cv} = l_w h = 80" \times 8" = 640\ in^2$ Cl. 21.9.4.1

$\alpha_c = 2.9 \qquad : Wall\ No.1\ with\ aspect\ ratio\ of\ 1.55$ Cl. 21.9.4.1

Boundary element longitudinal reinforcement ratio: $\frac{6\times200}{200\times350} = 1.71\%$

The concrete confinement parameter, K, for Saatcioglu and Razvi model is calculated below:

Tie Spacing: $s = 100\ mm$

$b_{cx} = 300\ mm$

$b_{cy} = 140\ mm$

$S_{lx} = 135\ mm$

$S_{ly} = 115\ mm$

$f_{lx} = \frac{\sum A_{sx}\, f_{yt}}{s b_{cx}} = \frac{3(71)550}{100(300)} = 3.91\ MPa$

$f_{ly} = \frac{\sum A_{sy}\, f_{yt}}{s b_{cy}} = \frac{2(71)550}{100(140)} = 5.58\ MPa$

$K_{2x} = 0.26\sqrt{\frac{b_{cx}}{s}\frac{b_{cx}}{s_{lx}}\frac{1}{f_{lx}}} \leq 1.0$

$K_{2x} = 0.26\sqrt{\frac{300}{100}\frac{300}{135}\frac{1}{4.34}} = 0.322$

$K_{2y} = 0.26\sqrt{\frac{b_{cy}}{s}\frac{b_{cy}}{s_{ly}}\frac{1}{f_{ly}}} \leq 1.0$

$K_{2y} = 0.26\sqrt{\frac{140}{100}\frac{140}{115}\frac{1}{5.58}} = 0.143$

$f_{lex} = K_{2x} f_{lx} = 0.322 \times 3.91 = 1.26\ MPa$

$f_{ley} = K_{2y} f_{ly} = 0.143 \times 5.58 = 0.80\ MPa$

$$f_{le} = \frac{f_{lex}b_{cx}+f_{ley}b_{cy}}{b_{cx}+b_{cy}}$$

$$f_{le} = \frac{1.26\times300+0.80\times140}{300+140} = 1.11\ MPa$$

$$K_1 = 6.7(f_{le})^{-0.17} = 6.7(1.11)^{-0.17} = 6.58$$

$$K = \frac{K_1 f_{le}}{f"_{co}} = \frac{6.58(1.11)}{0.85(40)} = 0.21$$

Web Horizontal Reinforcement:

Wall No. 1 was designed to have nominal shear and flexural capacities to be approximately equal to assess the performance of a wall and the WWR grids when flexure and shear were equally critical. For the initial design of the wall, the concrete strength of 40 MPa was assumed and the horizontal web reinforcement was determined using the nominal moment. RC-Section software output for nominal moment capacity, while sustaining 1600kN axial load, is tabulated in Table 5.1.

Table 5.1 Nominal Moment Capacity of Shear Wall No. 1 under 1600 kN Axial Load (RC-Section output)

Nominal Capacity in Metric Units			**Nominal Capacity in Imperial Units**		
$\boldsymbol{P\ (kN)}$	$M_N\ (kN.m)$	$c\ (mm)$ *	$P\ (kips)$	$M_N\ (kip.ft)$	$c\ (in)$ *
14963.2	2647.8	304.3	3363.9	1952.9	11.98

* *c is the distance to the N.A.*

The horizontal lateral force corresponding to nominal moment was obtained by dividing the nominal moment by the shear span, which is the distance between the center line of the actuator arm to the top of foundation.

$$V_N = \frac{M_N}{h} \quad \rightarrow \quad V_{pr} = \frac{2647.8}{3.1} = 796.1\ kN\ \ (178.9\ kips)$$

$$V_N \geq V_{pr} = 796.1\ kN\ \ (178.9\ kips)$$

$$V_{N,max} = 10\sqrt{f'_c}\ hd = 10 \times 76.1 \times 8 \times 64 = 389.6\ kips\ (1733\ kN) \qquad \text{Cl. 11.9.3}$$

$$V_N = V_c + V_s \geq 178.9\ kips \quad \longrightarrow \quad V_s \geq 178.9 - V_c$$

$$V_{c,max} = A_{cv}\ \alpha_c \lambda \sqrt{f'_c} = 640 \times 2.90 \times 1.0 \times 76.1 = 141.2\ kips\ \ (628.1\ kN) \quad \text{Cl. 21.9.4.1}$$

The concrete shear capacity is calculated per ACI 318 Cl. 11.9.5.

$$V_c = 2\lambda\sqrt{f'_c}hd = 2 \times 1.0 \times 76.1 \times 8 \times 64 = 77.9\ kips\ (346.5\ kN)$$

$$V_s \geq 178.9 - 77.9 = 101.0\ kips\ (449.3\ kN)$$

$$V_s = \frac{A_v f_y d}{s_v} \geq 101.0 \longrightarrow \frac{A_v}{s_v} \geq \frac{101.0}{66.7\times 64} = 0.0236$$

Provide two curtains of 10M horizontal web reinforcements: $A_v = 200\ mm^2 = 0.31\ in^2$

$$s_v \leq \frac{A_v}{0.0236} = \frac{0.31}{0.0236} = 13.1"$$

Select $s_v = 12"$, where s_v is vertical spacing between web horizontal reinforcement.

Checking maximum allowable spacing per Cl. 11.9.9.3:

$$s_v \leq \begin{cases} l_w/5 = 80"/5 = 16" \\ 3h = 3\times 8" = 24" \\ 18" \end{cases}$$

Checking minimum web horizontal reinforcement ratio:

$$\rho_t = \frac{A_v}{s_v \times h} = \frac{0.31}{12\times 8} = 0.0032 \qquad \longrightarrow \quad \rho_{t,min} = 0.0025 \qquad \text{Ok.}$$

Web Vertical Reinforcement:

The maximum allowable horizontal spacing between web vertical shear reinforcement, s_h, is expressed in ACI 318, Cl. 11.9.9.5:

$$s_h \leq \begin{cases} l_w/3 = 80"/3 = 26.6" \\ 3h = 3\times 8" = 24" \\ 18" \end{cases}$$

ACI 318, Cl. 11.9.9 indicates that the vertical shear reinforcement area to gross concrete area of horizontal section, ρ_l, shall be the larger of the two values indicated below:

$$\rho_l \geq \begin{cases} 0.0025 + 0.5\left(2.5 - \frac{h_w}{l_w}\right)(\rho_t - 0.0025) \\ \rho_{l,min} = 0.0025 \end{cases}$$

$$\rho_l \geq 0.0025 + 0.5\left(2.5 - \frac{3.1}{2.0}\right)(0.0032 - 0.0025) = 0.00283$$

Provide two curtains of 10M vertical web reinforcements: $A_v = 0.31\ in^2$

$$\rho_l = \frac{A_v}{s_h \times h} \rightarrow s_h = \frac{A_v}{\rho_l \times h} = \frac{0.31}{0.00283\times 8} = 13.7"$$

Two curtains of 10M vertical rebars spaced at 12" o/c satisfies the design requirements.

Boundary Element Transverse Reinforcement:

The minimum volumetric reinforcement ratio for shear wall boundary elements is provided in ACI 318-11, Cl. 21.9.6.4, 21.6.4.3 and 21.6.4.4. It should be noted that Cl. 21.9.6.4 modifies the wall requirements by changing 21.6.4.3(a) from one-quarter to one-third of the least dimension of the boundary element. In addition, only the following equation is required to determine the volumetric reinforcement ratio:

$$A_{sh} \geq 0.09 \frac{s b_c f'_c}{f_{yt}} \longrightarrow s \leq \frac{A_{sh} f_{yt}}{0.09 b_c f'_c}$$

The above equation should be satisfied in both cross-sectional directions of the rectangular core.

$$A_{sh,provided-x} = 3\ bars\ in\ a\ WWR\ Grid = 3 \times 71 = 213\ mm^2\ (0.33\ in^2)$$

$$A_{sh,provided-y} = 2\ bars\ in\ a\ WWR\ Grid = 2 \times 71 = 142\ mm^2\ (0.22\ in^2)$$

The yield strength of the WWR grids, f_{yt}, was determined as 80 ksi (550 MPa) by performing tension coupon tests. Details of Material Properties are provided in Chapter 3 of this thesis.

$$s_x \leq \frac{A_{sh-x} f_{yt}}{0.09 b_{cx} f'_c} = \frac{213 \times 550}{0.09 \times 300 \times 40} = 108\ mm\ (4.25")$$

$$s_y \leq \frac{A_{sh-y} f_{yt}}{0.09 b_{cy} f'_c} = \frac{142 \times 550}{0.09 \times 140 \times 40} = 155\ mm\ (6.1")$$

Checking for maximum allowable spacing between transverse reinforcements:

$$s \leq \begin{cases} one\ third\ of\ min.member\ dimension \\ six\ times\ the\ diameter\ of\ the\ smallest\ long.bar \\ 4" < s_0 < 6" \end{cases}$$

$$s \leq \begin{cases} \frac{200\ mm}{3} = 66.7\ mm\ (2.67") \\ 6 \times 16 = 96\ mm\ (3.78") \\ 4" < s_0 < 6" \end{cases}$$

Because the wall was a scaled test specimen, the maximum tie spacing is defined as wall thickness divided by three (3) was relaxed to allow for the maximum allowed tie spacing per confinement requirement. This also tests the grids (ties) in the wall in a more stringent and critical fashion. It should also be noted that the maximum tie spacing allowance for minimum member size dimension is defined differently in CSA A23.3 – 04 where the maximum tie spacing is defined as least dimension divided by two (2) which would translate into 4" maximum tie spacing. The

spacing of s = 100 mm (4") between WWR transverse reinforcements in the boundary elements is selected.

5.4.2 Shear Wall No. 1 – As-Built Calculations

The calculations in this section provide a more accurate understanding of shear wall capacity, as they are based on actual material properties. The concrete strength, f'_c , which was assumed as 40 MPa during the design phase, but it was 52 MPa during the test period. The concrete confinement parameter, K, was revised based on the actual recorded concrete strength. The reinforcement bi-linear stress-strain model was replaced with a model which included strain hardening effect, where $f_y = 460\ MPa$ and $f_u = 710\ MPa$. RC-Section software model was revised and re-ran to determine the moment capacity of the section using the actual recorded material strength. The shear capacity of the as-built wall was determined by dividing the moment capacity by the shear span (wall height). The details of the calculations are summarized here.

Revised Concrete Confinement Parameter

Tie Spacing: $s = 100\ mm$

$b_{cx} = 300\ mm$

$b_{cy} = 140\ mm$

$S_{lx} = 135\ mm$

$S_{ly} = 115\ mm$

$$f_{lx} = \frac{\sum A_{sx}\, f_{yt}}{s b_{cx}} = \frac{3(71)550}{100(300)} = 3.91\ MPa$$

$$f_{ly} = \frac{\sum A_{sy}\, f_{yt}}{s b_{cy}} = \frac{2(71)550}{100(140)} = 5.58\ MPa$$

$$K_{2x} = 0.26\sqrt{\frac{b_{cx}}{s}\frac{b_{cx}}{s_{lx}}\frac{1}{f_{lx}}} \leq 1.0$$

$$K_{2x} = 0.26\sqrt{\frac{300}{100}\frac{300}{135}\frac{1}{4.34}} = 0.322$$

$$K_{2y} = 0.26\sqrt{\frac{b_{cy}}{s}\frac{b_{cy}}{s_{ly}}\frac{1}{f_{ly}}} \leq 1.0$$

$$K_{2y} = 0.26\sqrt{\frac{140}{100}\frac{140}{115}\frac{1}{5.58}} = 0.143$$

$$f_{lex} = K_{2x} f_{lx} = 0.322 \times 3.91 = 1.26\ MPa$$

$$f_{ley} = K_{2y} f_{ly} = 0.143 \times 5.58 = 0.80\ MPa$$

$$f_{le} = \frac{f_{lex} b_{cx} + f_{ley} b_{cy}}{b_{cx} + b_{cy}}$$

$$f_{le} = \frac{1.26 \times 300 + 0.80 \times 140}{300 + 140} = 1.11\ MPa$$

$$K_1 = 6.7(f_{le})^{-0.17} = 6.7(1.11)^{-0.17} = 6.58$$

$$K = \frac{K_1 f_{le}}{f"_{co}} = \frac{6.58(1.11)}{0.85(52)} = 0.165$$

The moment capacity of the section calculated by RC-Section is tabulated in Table 5.2.

Table 5.2 Moment Capacity of As-Built Shear Wall No. 1 under 1600 kN Axial Load (RC-Section output)

Moment Capacity in Metric Units			**Moment Capacity in Imperial Units**		
***P* (*kN*)**	$M\ (kN.m)$	$c\ (mm)$ *	$P\ (kips)$	$M\ (kip.ft)$	$c\ (in)$ *
19010	2865	261.6	4274	2113	10.3

* *c is the distance to the N.A.*

The theoretical shear force that will generate the moment capacity of the as-built wall is calculated as $\frac{2865}{3.1} = 924\ kN\ (207.7\ kips)$.

The shear capacity of the as-built wall is calculated as followed.

$$V_N = V_c + V_s$$

$$V_c = 2\lambda\sqrt{f'_c}hd = 2 \times 1.0 \times \sqrt{7540} \times 8 \times 64 = 88.9\ kips\ (395.4\ kN)$$

$$V_s = \frac{A_v f_y d}{s_v} = \frac{0.31 \times 66.7 \times 64}{12} = 110\ kips\ \ (489\ kN)$$

$$V_N = 88.9 + 110 = 198.9\ kips\ \ (885\ kN)$$

5.4.3 Shear Wall No. 1 – Wall Construction

Shear wall No. 1 was constructed using normal-strength concrete. The concrete was poured in two stages; foundation first, followed by the wall, which was integrally casted with the steel loading beam on the top. The foundation was I-shaped with an overall dimensions of 3300 mm (L) x 1500 mm (W) x 500 mm (T), (~11’ x 5’ x 1’-8”). Four (4) pre-formed sleeves were placed at four extreme corners of the foundation to match the locations of the existing holes in the laboratory strong floor. High-strength 3” diameter (75mm) threaded steel rods were placed in these sleeved holes to tie the foundation to the laboratory strong floor and provide fixity at the base. The holes

were spaced at 2700 mm (9') along the length of the wall and 900 mm (3') in the perpendicular direction. The surface of the foundation was roughened and cleaned prior to pouring the wall concrete. The steel loading beam was constructed using two stacked 4"x4" (102x102) HSS sections and has five (5) 50 mm wide by100 mm deep steel shear keys welded underneath. In addition, eight (8) straight pieces of one inch (1") diameter high-strength threaded rods were inserted 500 mm (20") into the upper segment of the wall and bolted to the loading beam. The loading beam was drilled with sixteen (16) holes (eight on each side) to allow for the installation of prestressing tendons. The cables were loaded in small increments until all of the cables were loaded to 100 kN, applying a total axial load of 1600 kN.

The foundation also had eight (8)–1" Diameter (25mm) high-strength threaded rods on each side of the wall, which were embedded and anchored in concrete. Each one of these doweled threaded rods was used to support one pre-stressing cable, applying vertical gravity load.

The shear wall was constructed using conventional reinforcing steel bars, except where high strength WWR grids were used as transverse reinforcement in boundary elements. Figure 5.7 illustrates Wall No. 1 during construction.

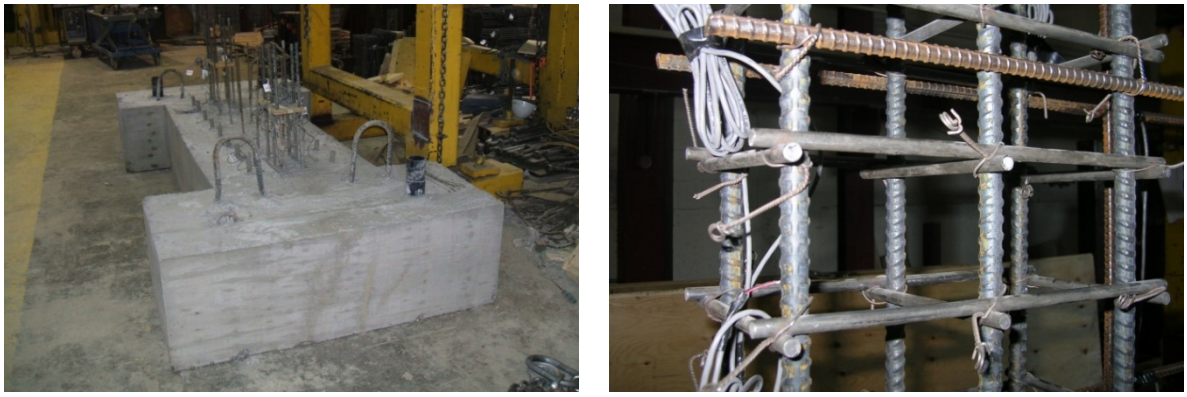

Figure 5.7 Shear Wall No. 1 during Construction

Figure 5.7 (Cont'd) Shear Wall No. 1 during Construction

5.4.4 Shear Wall No. 1 – Test Set up and Instrumentation

The overall test setup, shown in Figure 5.8, was modified to add a secondary A-Frame to provide out-of-plane support. Two HSS sections were mounted on top of the secondary A-frame on two sides of the wall specimen at the top. A small gap was placed between the loading beam and the out-of-plane support where the steel surfaces were covered with grease to facilitate sliding, should the wall move out of plane. The out-of-plane support represents the stiff support provided by the floor slabs in a building floor diaphragm.

Two data acquisition systems were used to collect data. Figure 5.8 illustrates the layout and location of externally installed transducers/gauges. The following data was recorded during the test:

- Magnitude of the applied lateral force by the MTS actuator;
- Top displacement of the wall at the level of horizontal force line-of-action. Two cable-transducers were placed to provide back-up readings.
- Strain values of steel reinforcement and WWR grids, as outlined in the next section.

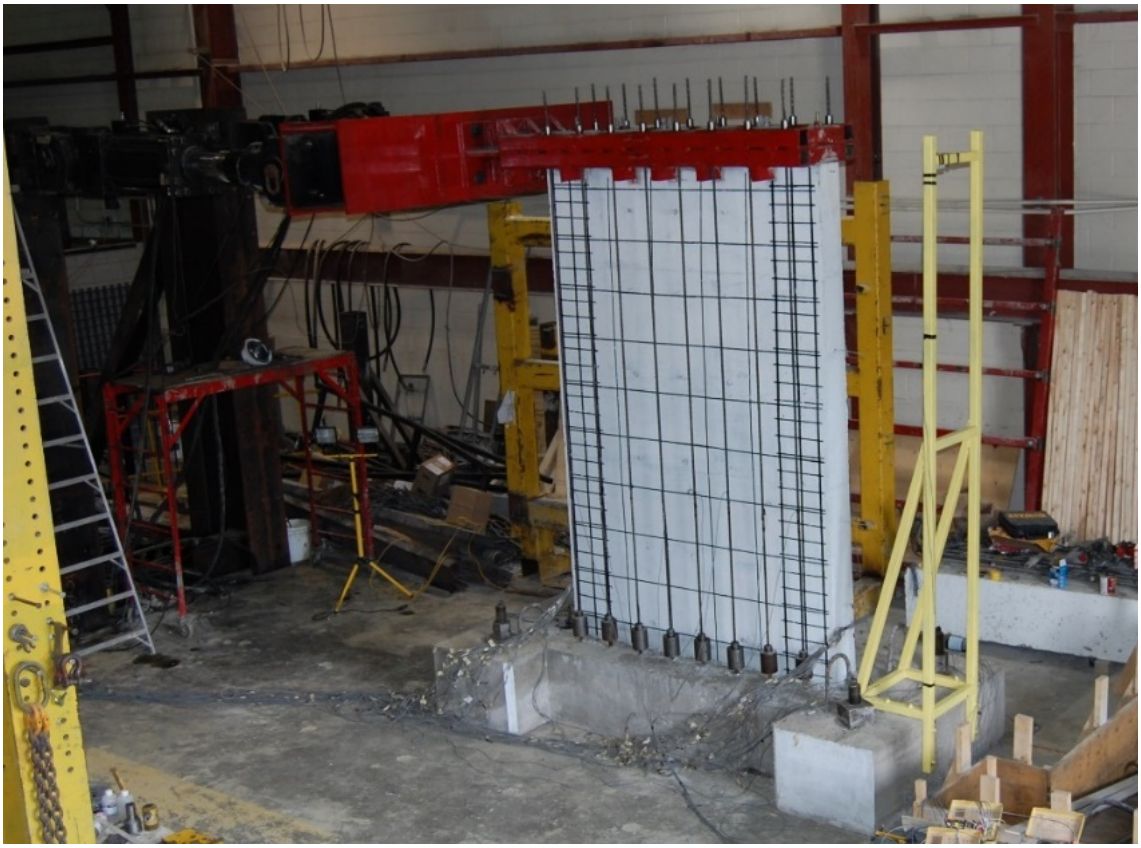

Figure 5.8 Shear Wall No. 1 Test Set-up

5.4.4.1 Shear Wall No. 1 – Strain Gauges

A series of strain gauges were installed on reinforcement to monitor steel strains. Strain – lateral deformation graphs were generated and presented in Appendix B.1. Figures 5.9 and 5.10 illustrate the locations of strain gauges, as well as the labelling scheme used to identify each gauge. It should be noted that several strain gauges were damaged. Depending on the timing of the damage, the strain graph data was either omitted or partial readings were used.

The following steel members were instrumented with strain gauges:

- Longitudinal bars in the boundary elements ; shown in Figure 5.9;
- Dowels in the foundation ; shown in Figure 5.9;
- WWR grids in boundary elements ; shown in Figures 5.10 and 5.11;
- Horizontal web reinforcement in the web ; shown in Figure 5.11;

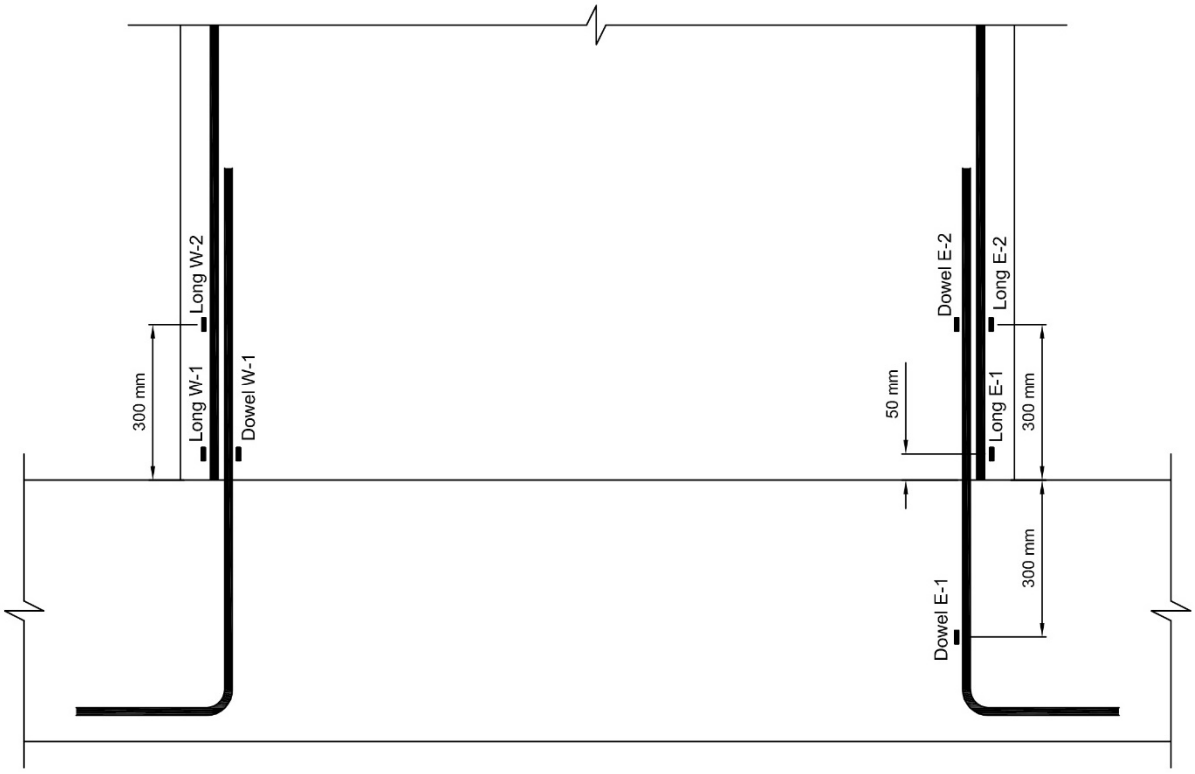

Figure 5.9 Shear Wall No. 1 – Dowels and Longitudinal Bars Strain Gauges

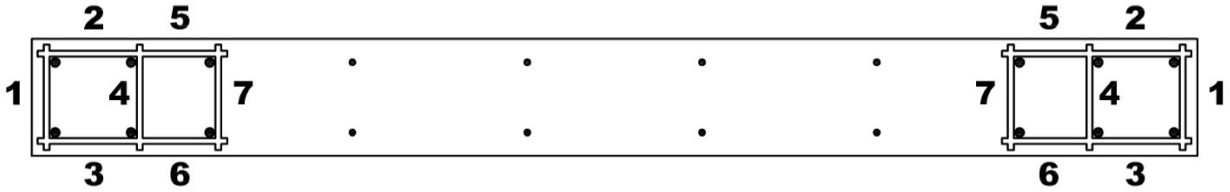

Figure 5.10 Shear Wall No. 1 – Key Map for Strain Gauge Locations on WWR Grids

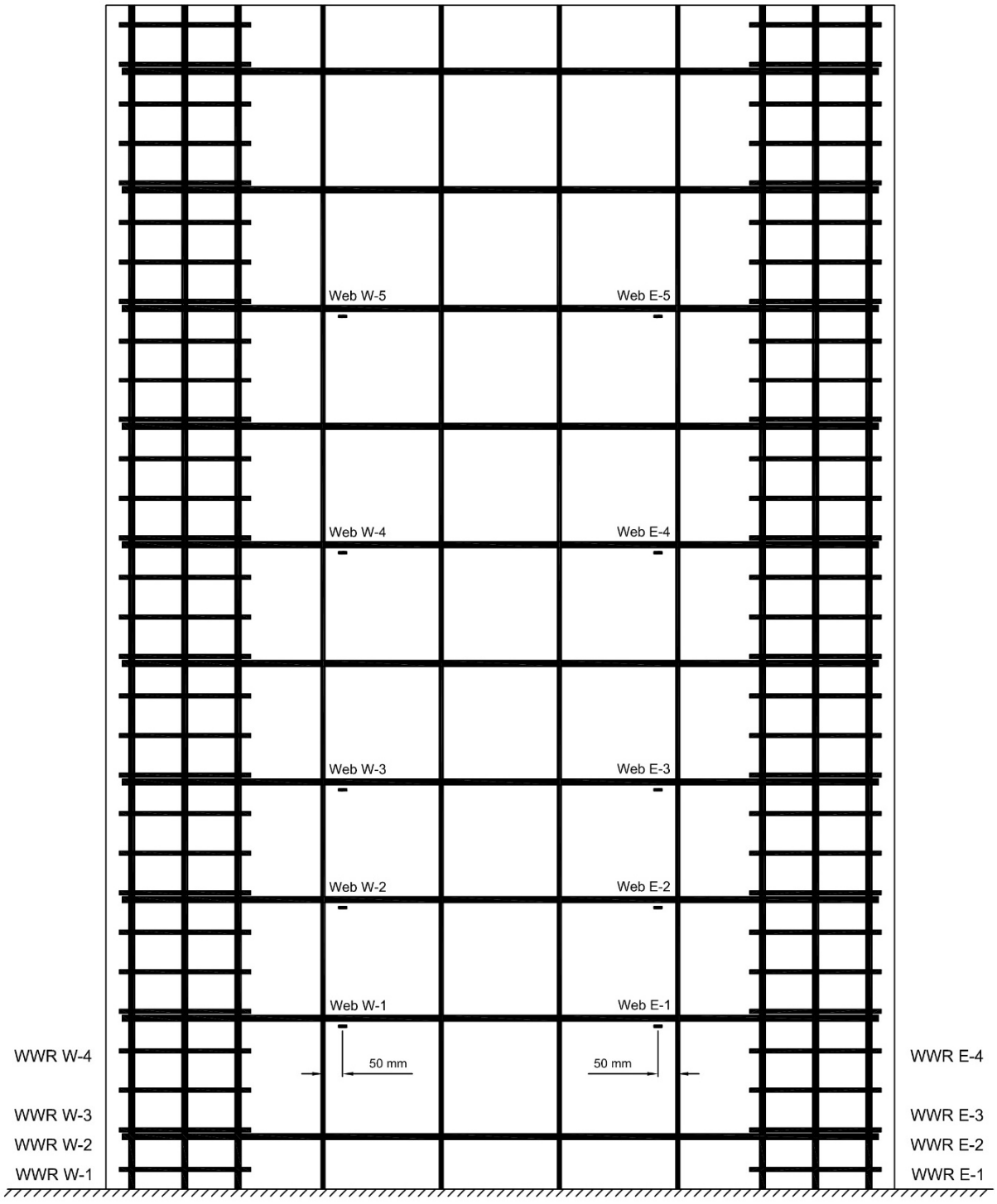

Figure 5.11 Shear Wall No. 1 – WWR Grids Labels and Web Reinforcement Strain Gauges

The maximum strain values recorded by strain gauges are tabulated in Table 5.3. It should be noted that some of the strain gauges stopped recording during the test prior to wall failure. The tabulated values refer to the highest strain value that was successfully recorded.

Table 5.3 Maximum Recorded Strains for Shear Wall No. 1

Strain Gauge ID	Maximum Recorded Strain	Strain Gauge ID	Maximum Recorded Strain
Dowel W-1	1200	Dowel E-1	5080
Dowel E-2	5460	Long W-1	1300
Long W-2	10000	Long E-1	1290
Long E-2	-3400		
WWR W1-6	1450	WWR W2-1	360
WWR W2-5	1260	WWR W3-2	650
WWR W3-7	530	WWR W4-6	920
WWR E1-1	1000	WWR E2-3	1070
WWR E2-4	550	WWR E3-3	1200
WWR E4-7	-540		
Web W-1	900	Web E-1	2440
Web W-2	1540	Web E-2	1280
Web W-3	1130	Web E-3	760
Web W-4	730	Web E-4	1570
Web W-5	1330	Web E-5	640

Note: Force-Strain graphs for Shear Wall No. 1 strain gauges are provided in Appendix B.1.

5.4.5 Shear Wall No. 1 – Test Result

Wall No. 1 developed shear and flexural cracking under increasing lateral deformation reversals. The shear wall specimen was successfully loaded under load reversals until 0.36% lateral drift level (yield load) without having any horizontal sliding supports installed at the top of the wall with the assumption that the use of two actuators would maintain out-of-plane stability of the wall. However, during the experiment, as the wall entered inelastic regions, the wall specimen distorted and it was noticed that the wall had twisted as the load was applied. The test was stopped and bracing against lateral movement at the top of the wall was added. It was subsequently observed that the Wall had already been damaged in shear and it never recovered its expected capacity after the placement of out-of-plane bracing. Therefore, while the results are valid for initial strength and deformation capacity, they are not reliable in the inelastic range of deformation cycles. The wall failed in a brittle manner due to diagonal tension, after developing flexural yielding. The final

inclined shear crack that led to wall failure is shown in Figure 5.12. The hysteretic Force-Displacement relationship for applied horizontal actuator force versus lateral displacement (and drift) is shown in Figure 5.13. The Lateral force was then further adjusted to account for the horizontal components of vertical prestressing forces to compute the net horizontal force that was imposed on the wall. The net lateral force vs. top lateral displacement (and drift) relationship is shown in Figure 5.14. Finally, the applied moment vs. lateral displacement (and drift) relationship is shown in Figure 5.15. The lateral moment is the summation of the moment generated by the net lateral load and the secondary moment caused by the vertical components of prestressing tendons (axial force times lateral displacement).

Figure 5.12 Shear Wall No. 1 Failure Photos

Figure 5.12 (Cont'd) Shear Wall No. 1 Failure Photos

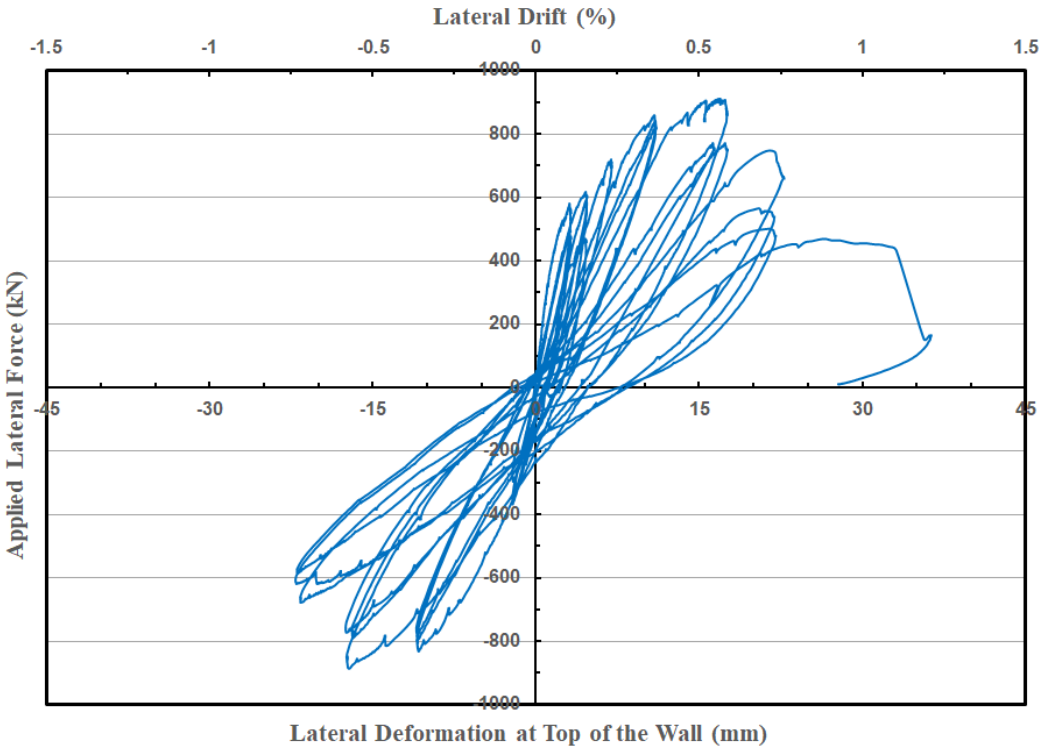

Figure 5.13 Shear Wall No. 1 – Applied Lateral Force by Actuator vs. Lateral Deformation

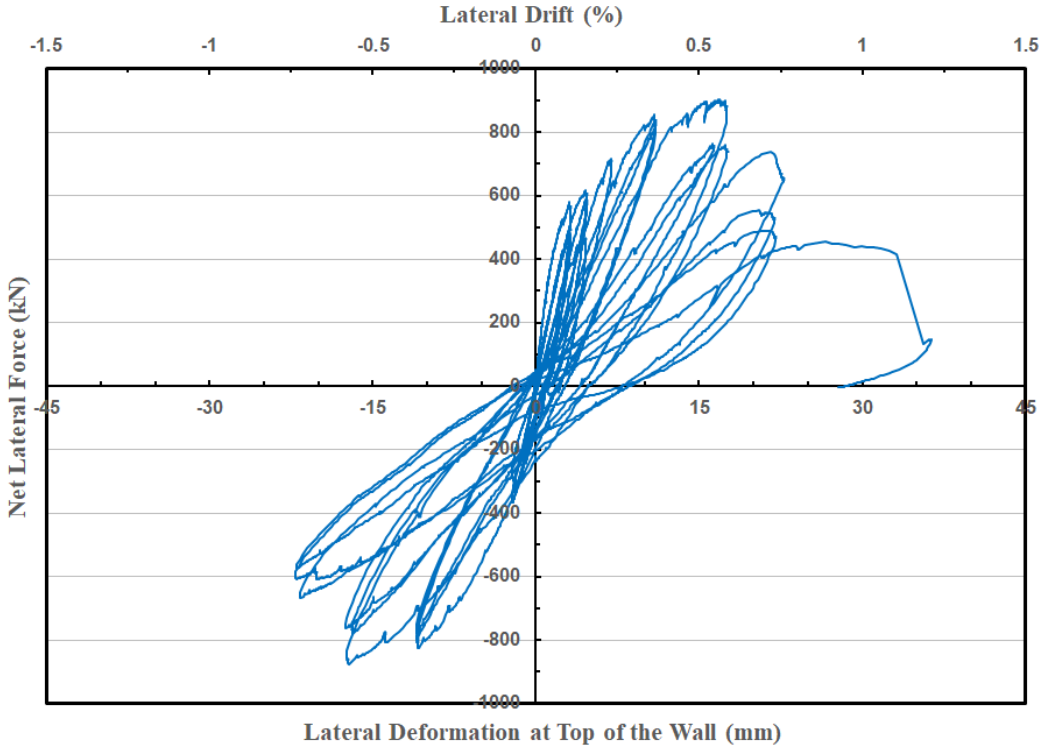

Figure 5.14 Shear Wall No. 1 – Net Lateral Force vs. Lateral Deformation

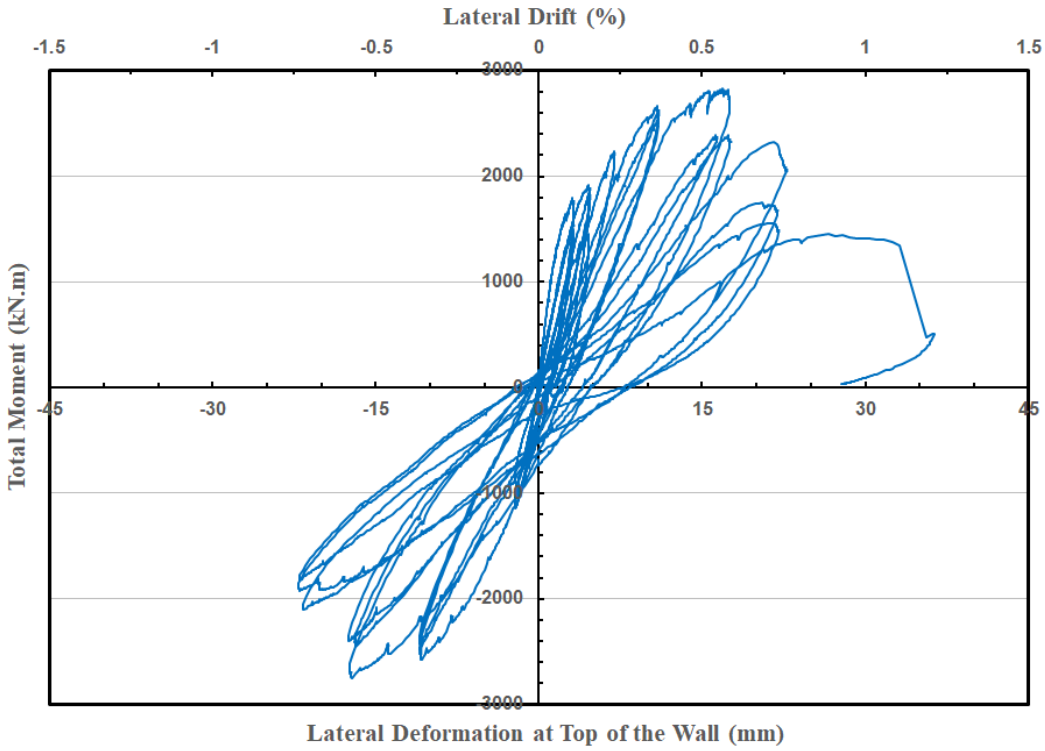

Figure 5.15 Shear Wall No. 1 – Applied Moment vs. Lateral Deformation

5.5 Shear Wall No. 2

Shear Wall No. 2 is a rectangular wall with a height-to-length aspect ratio of 1.94:1 (3.1m height to 1.6m length). This wall has a thickness of 200 mm with concentrated vertical reinforcement forming boundary elements within the section as shown in Figure 5.17. This wall has the same wall thickness as Wall No. 1, but the aspect ratio is increased from 1.55 in Shear Wall No. 1 to 1.94 in Shear Wall No. 2. The increase in wall aspect ratio is expected to increase flexural action on Wall No. 2. This also has implications on the wall shear design. The shear wall elevation view and wall cross section, illustrated in Figures 5.16 and 5.17, provide the details of wall geometry and reinforcement details.

The wall was cast integrally with the pre-fabricated steel loading beam used for Wall No. 1. The wall was subjected to 1600 kN axial compression by using sixteen (16) prestressing cables, 8 on each side, simulating gravity loading. The web horizontal reinforcements had 90º bends at the ends, well anchored into the boundary elements. The wall was designed following the seismic design requirements of ACI 318-11, as presented in Section 5.5.1. The initial design was

performed based on the assumption of 80 MPa concrete. The design was fine-tuned subsequently using the actual material properties attained during the test period. The revised design is presented in Section 5.5.2 under "as-built calculations." The wall was designed with the intent of preventing premature failure under shear while promoting ductile flexural behaviour. The detailed design notes for this wall are presented in the following sections.

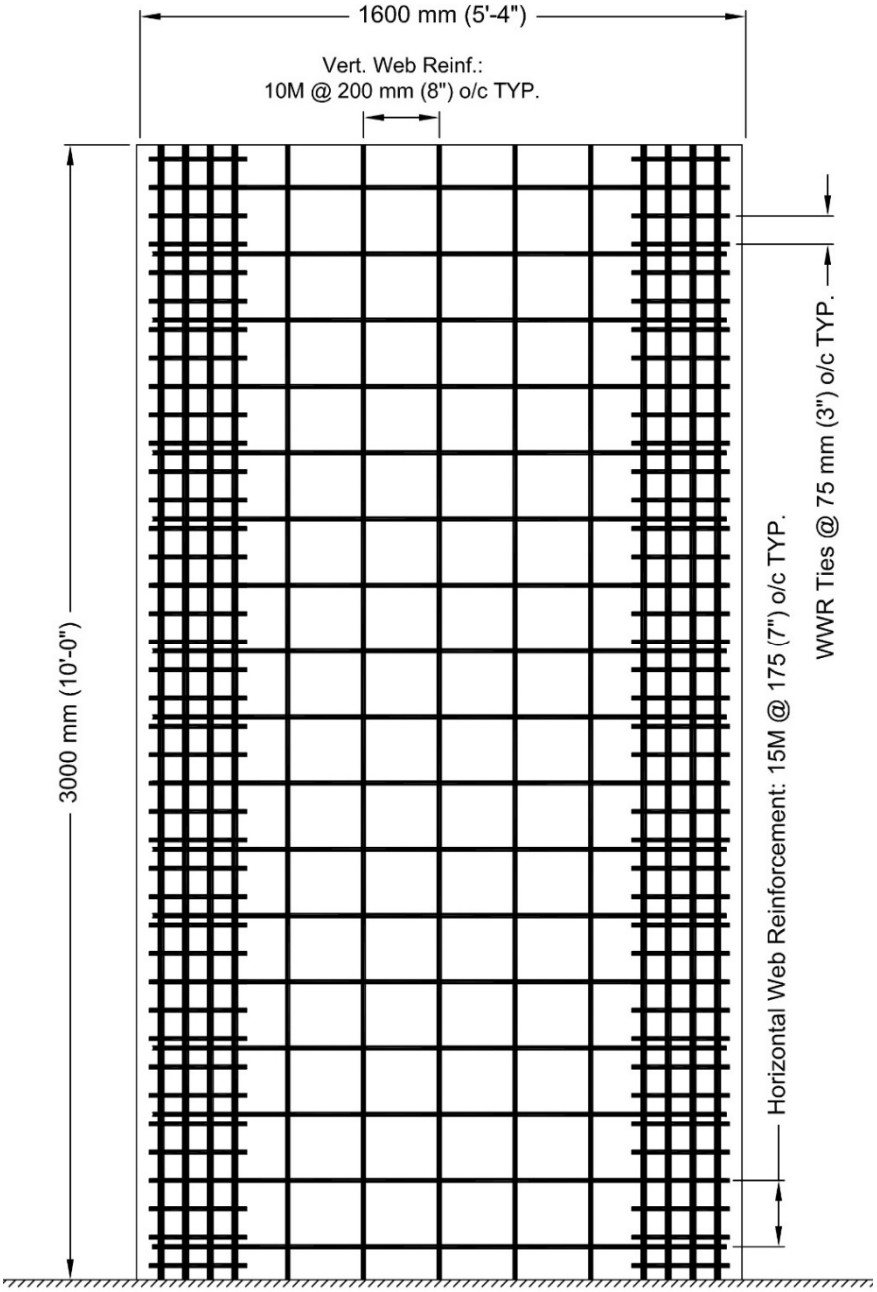

Figure 5.16 Shear Wall No. 2 Elevation

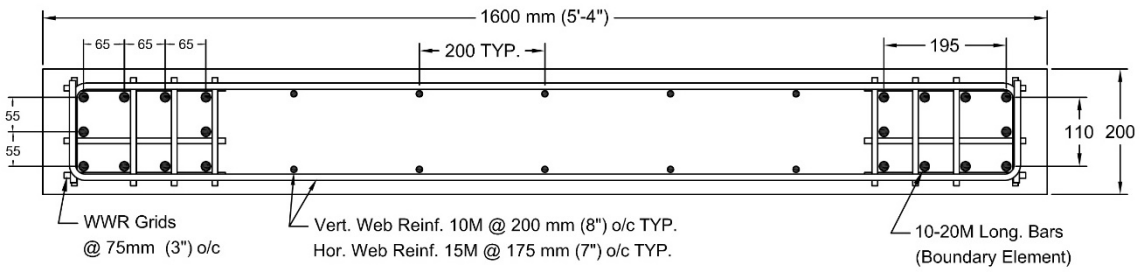

Figure 5.17 Shear Wall No. 2 Cross-Section

5.5.1 Shear Wall No. 2 – Design Notes

"RC-Section" sectional analysis software was employed to calculate wall capacities. Figure 5.18 shows the screenshot of the wall model. Two concrete models were used to define concrete stress-strain characteristics: Hognestad (1951) model for unconfined cover concrete and Saatcioglu and Razvi (1992) for confined core concrete. A bilinear stress-strain relationship was assumed for all reinforcement.

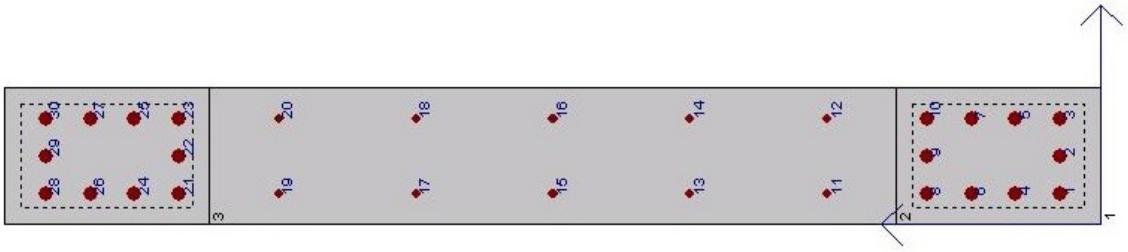

Figure 5.18 Screenshot of Shear Wall No. 2 Model in RC-Section Software

The design assumptions and calculations are summarized below. ACI 318-11 equations are used for the calculations.

Design Assumptions:

$f'_c = 80\ MPa = 11{,}600\ psi$

$fy = 460\ MPa = 66{,}700\ psi$: for all rebars;

$fyt = 550\ MPa = 80{,}000\ psi$: for WWR grids;

$\sqrt{f'_c} = 107.8 \xrightarrow{exceeds\ \max\ allowable} \sqrt{f'_c} = 100psi$ Cl. 11.1.2

$l_w = 1.6\ m \cong 64"$

$h_w = 3.1\ m \cong 124"$

$h = 0.2\ m \cong\ 8"$

$d = 0.8l_w \cong 51.2"$ Cl. 21.9.2.3(c)

$A_{cv} = l_w h = 64" \times 8" = 512\ in^2$ Cl. 21.9.4.1

$\alpha_c = 2.12$ $: Wall\ with\ aspect\ ratio\ of\ 1.94$ Cl. 21.9.4.1

Boundary element longitudinal reinforcement ratio: $\frac{10\times300}{200\times315} = 4.7\%$

The concrete confinement parameter, K, for Saatcioglu and Razvi model is calculated below:

Tie Spacing: $s = 75\ mm$

$b_{cx} = 225\ mm$

$b_{cy} = 140\ mm$

$S_{lx} = 65\ mm$

$S_{ly} = 55\ mm$

$f_{lx} = \frac{\sum A_{sx} f_{yt}}{sb_{cx}} = \frac{4(71)550}{75(225)} = 9.26\ MPa$

$f_{ly} = \frac{\sum A_{sy} f_{yt}}{sb_{cy}} = \frac{3(71)550}{75(140)} = 11.16\ MPa$

$K_{2x} = 0.26\sqrt{\frac{b_{cx}}{s}\frac{b_{cx}}{s_{lx}}\frac{1}{f_{lx}}} \leq 1.0$

$K_{2x} = 0.26\sqrt{\frac{225}{75}\frac{225}{65}\frac{1}{9.26}} = 0.275$

$K_{2y} = 0.26\sqrt{\frac{b_{cy}}{s}\frac{b_{cy}}{s_{ly}}\frac{1}{f_{ly}}} \leq 1.0$

$K_{2y} = 0.26\sqrt{\frac{140}{75}\frac{140}{55}\frac{1}{11.16}} = 0.170$

$f_{lex} = K_{2x} f_{lx} = 0.275 \times 9.26 = 2.55\ MPa$

$f_{ley} = K_{2y} f_{ly} = 0.170 \times 11.16 = 1.90\ MPa$

$f_{le} = \frac{f_{lex} b_{cx} + f_{ley} b_{cy}}{b_{cx} + b_{cy}}$

$f_{le} = \frac{2.55\times225 + 1.90\times140}{225+140} = 2.30\ MPa$

$K_1 = 6.7(f_{le})^{-0.17} = 6.7(2.30)^{-0.17} = 5.82$

$K = \frac{K_1 f_{le}}{f"_{co}} = \frac{5.82(2.30)}{0.85(80)} = 0.197$

Web Horizontal Reinforcement:

It was decided that the wall should have sufficient horizontal web reinforcement to prevent premature shear failure. It was assumed that the highest moment that the wall could resist in the post-yield state could be approximated by the probable moment capacity of the wall. RC-Section software output for probable moment capacity under 1600 kN axial compression is tabulated in Table 5.4.

Table 5.4 Probable Moment Capacity of Shear Wall No. 2 under 1600 kN Axial Load (RC-Section output)

Probable Capacity in Metric Units			**Probable Capacity in Imperial Units**		
$\boldsymbol{P\ (kN)}$	$M_{Pr}\ (kN.m)$	$c\ (mm)$ *	$P\ (kips)$	$M_{Pr}\ (kip.ft)$	$c\ (in)$ *
25309	3857.5	227.4	5689	2845.1	8.95

* c is the distance to the N.A.

The horizontal force corresponding to probable moment was obtained by dividing the moment by the shear span.

$$V_{pr} = \frac{M_{pr}}{h} \quad \rightarrow \quad V_{pr} = \frac{3857.5}{3.1} = 1244.3\ kN\ \ (279.7\ kips)$$

$$V_N \geq V_{pr} = 1244.3\ kN\ \ (279.7\ kips)$$

$$V_{N,max} = 10\sqrt{f'_c}\ hd = 10 \times 100 \times 8 \times 51.2 = 409.6\ kips\ (1822\ \text{kN}) \quad \text{Cl. } 11.9.3$$

$$V_N = V_c + V_s \geq 279.7\ kips \quad \longrightarrow \quad V_s \geq 279.7 - V_c$$

$$V_{c,max} = A_{cv}\ \alpha_c \lambda \sqrt{f'_c} = 512 \times 2.12 \times 1.0 \times 100 = 108.5\ kips\ \ (482.6\ kN)$$

The concrete shear capacity was calculated as per ACI 318 Cl. 11.9.5.

$$V_c = 2\lambda\sqrt{f'_c}hd = 2 \times 1.0 \times 100 \times 8 \times 51.2 = 81.9\ kips\ (364.3\ kN)$$

$$V_s \geq 279.7 - 81.9 = 197.8\ kips\ (879.8\ kN)$$

$$V_s = \frac{A_v f_y d}{s_v} \geq 197.8 \longrightarrow \frac{A_v}{s_v} \geq \frac{197.8}{66.7 \times 51.2} = 0.058$$

Provide two curtains of 15M horizontal web reinforcements: $A_v = 400\ mm^2 = 0.62\ in^2$.

$$s_v \leq \frac{A_v}{0.050} = \frac{0.62}{0.058} = 10.7"$$

Select $s_v = 7"$: Where s_v is vertical spacing between web horizontal reinforcement.

Checking maximum allowable spacing per Cl. 11.9.9.3:

$$s_v \leq \begin{cases} l_w/5 = 64"/5 = 12.8" \\ 3h = 3 \times 8" = 24" \\ 18" \end{cases}$$

Checking minimum web horizontal reinforcement ratio:

$$\rho_t = \frac{A_v}{s_v \times h} = \frac{0.62}{7 \times 8} = 0.011 \qquad \longrightarrow \quad \rho_{t,min} = 0.0025 \qquad \text{Ok.}$$

Web Vertical Reinforcement:

The maximum allowable horizontal spacing between web vertical shear reinforcement, s_h, is expressed in ACI 318, Cl. 11.9.9.5:

$$s_h \leq \begin{cases} l_w/3 = 64"/3 = 21.3" \\ 3h = 3 \times 8" = 24" \\ 18" \end{cases}$$

ACI 318, Cl. 11.9.9 indicates that the vertical shear reinforcement area to gross concrete area of horizontal section, ρ_l, shall be the larger of the two values indicated below:

$$\rho_l \geq \begin{cases} 0.0025 + 0.5\left(2.5 - \frac{h_w}{l_w}\right)(\rho_t - 0.0025) \\ \rho_{l,min} = 0.0025 \end{cases}$$

$$\rho_l \geq 0.0025 + 0.5\left(2.5 - \frac{3.1}{1.6}\right)(0.011 - 0.0025) = 0.0048$$

Provide two curtains of 10M vertical web reinforcements: $A_v = 0.31\ in^2$.

$$\rho_l = \frac{A_v}{s_h \times h} \rightarrow s_h = \frac{A_v}{\rho_l \times h} = \frac{0.31}{0.0048 \times 8} = 8.1"$$

Two curtains of 10M vertical rebars spaced at 8" o/c satisfies the design requirements.

Boundary Element Transverse Reinforcement:

The minimum volumetric reinforcement ratio for shear wall boundary elements is provided in ACI 318, Cl. 21.9.6.4, 21.6.4.3 and 21.6.4.4. It should be noted that Cl. 21.9.6.4 modifies the wall requirements by changing 21.6.4.3(a) from one-quarter to one-third of the least dimension of the boundary element. In addition, only the following equation is required to determine the volumetric reinforcement ratio:

$$A_{sh} \geq 0.09 \frac{s b_c f'_c}{f_{yt}} \quad \longrightarrow s \leq \frac{A_{sh} f_{yt}}{0.09 b_c f'_c}$$

The above equation should be satisfied in both cross-sectional directions of the rectangular core.

$$A_{sh,provided-x} = 3\ bars\ in\ a\ WWR\ Grid = 4 \times 71 = 284\ mm^2\ (0.44\ in^2)$$

$$A_{sh,provided-y} = 2\ bars\ in\ a\ WWR\ Grid = 3 \times 71 = 213\ mm^2\ (0.33\ in^2)$$

The yield strength of the WWR grids, f_{yt}, was determined as 80 ksi (550 MPa) by performing tension coupon tests. Details of Material Properties are provided in Chapter 3 of this research document.

$$s_x \leq \frac{A_{sh-x} f_{yt}}{0.09 b_{cx} f'_c} = \frac{284 \times 550}{0.09 \times 225 \times 80} = 96.4\ mm\ (3.80")$$

$$s_y \leq \frac{A_{sh-y} f_{yt}}{0.09 b_{cy} f'_c} = \frac{213 \times 550}{0.09 \times 140 \times 80} = 116\ mm\ (4.57")$$

Checking for maximum allowable spacing between transverse reinforcements:

$$s \leq \begin{cases} one\ third\ of\ min.member\ dimension \\ six\ times\ the\ diameter\ of\ the\ smallest\ long.bar \\ 4" < s_0 < 6" \end{cases}$$

$$s \leq \begin{cases} \frac{200\ mm}{3} = 66.7\ mm\ (2.67") \\ 6 \times 20 = 120\ mm\ (4.8") \\ 4" < s_0 < 6" \end{cases}$$

The maximum tie spacing requirement, defined as wall thickness divided by three (3), was relaxed to allow for maximum allowed tie spacing per confinement requirement because of the use of scaled wall specimens. This resulted in testing the wall grids (ties) in a more stringent and critical fashion, because of the increased grid spacing. It should also be noted that the maximum tie spacing allowance for minimum member size dimension is defined differently in CSA A23.3 – 04 where the maximum spacing is defined as the least dimension divided by two (2) which would translate into 100 mm (4") maximum tie spacing. The grid spacing of s = 75 mm (3") was selected for boundary element design in Wall No. 2.

5.5.2 Shear Wall No. 2 – As-Built Calculations

The calculations in this section provide a more accurate understanding of shear wall capacity based on the actual material properties attained through material testing. The concrete strength, f'_c, which was assumed as 80 MPa during the design phase, was determined to be 82 MPa at the time of testing. The concrete confinement parameter, K, was revised based on the actual recorded concrete strength. The reinforcement bi-linear stress-strain model was replaced with a model which included strain hardening with $f_y = 460\ MPa$ and $f_u = 710\ MPa$. The shear capacity of the as-built wall was calculated as shown below.

Revised Concrete Confinement Parameter

Tie Spacing: $s = 75\ mm$

$b_{cx} = 225\ mm$

$b_{cy} = 140\ mm$

$S_{lx} = 65\ mm$

$S_{ly} = 55\ mm$

$$f_{lx} = \frac{\sum A_{sx}\, f_{yt}}{s b_{cx}} = \frac{4(71)550}{75(225)} = 9.26\ MPa$$

$$f_{ly} = \frac{\sum A_{sy}\, f_{yt}}{s b_{cy}} = \frac{3(71)550}{75(140)} = 11.16\ MPa$$

$$K_{2x} = 0.26\sqrt{\frac{b_{cx}}{s}\frac{b_{cx}}{s_{lx}}\frac{1}{f_{lx}}} \leq 1.0$$

$$K_{2x} = 0.26\sqrt{\frac{225}{75}\frac{225}{65}\frac{1}{9.26}} = 0.275$$

$$K_{2y} = 0.26\sqrt{\frac{b_{cy}}{s}\frac{b_{cy}}{s_{ly}}\frac{1}{f_{ly}}} \leq 1.0$$

$$K_{2y} = 0.26\sqrt{\frac{140}{75}\frac{140}{55}\frac{1}{11.16}} = 0.170$$

$$f_{lex} = K_{2x} f_{lx} = 0.275 \times 9.26 = 2.55\ MPa$$

$$f_{ley} = K_{2y} f_{ly} = 0.170 \times 11.16 = 1.90\ MPa$$

$$f_{le} = \frac{f_{lex} b_{cx} + f_{ley} b_{cy}}{b_{cx} + b_{cy}}$$

$$f_{le} = \frac{2.55 \times 225 + 1.90 \times 140}{225 + 140} = 2.30\ MPa$$

$$K_1 = 6.7(f_{le})^{-0.17} = 6.7(2.30)^{-0.17} = 5.82$$

$$K = \frac{K_1 f_{le}}{f"_{co}} = \frac{5.82(2.30)}{0.85(82)} = 0.192$$

Table 5.5 Moment Capacity of As-Built Shear Wall No. 2 under 1600 kN Axial Load (RC-Section output)

Moment Capacity in Metric Units			**Moment Capacity in Imperial Units**		
$\boldsymbol{P\ (kN)}$	$M\ (kN.m)$	$c\ (mm)$ *	$P\ (kips)$	$M\ (kip.ft)$	$c\ (in)$ *
25036	3596.5	218.9	5628	2652.6	8.6

* c is the distance to the N.A.

The theoretical shear force corresponding to the moment capacity of the as-built wall is calculated as $\frac{3596.5}{3.1} = 1160\ kN\ (260.8)$.

The shear capacity of the as-built wall was calculated below. It should be noted that the ACI 318-11 equation for shear capacity of concrete puts a cap on the contribution of high-strength concrete and does not recognize the full capacity of the wall concrete due to lack of sufficient research on this topic.

$$V_N = V_c + V_s$$

$$V_c = 2\lambda\sqrt{f'_c}hd = 2 \times 1.0 \times 100 \times 8 \times 51.2 = 81.9\ kips\ (364.3\ kN)$$

$$V_s = \frac{A_v f_y d}{s_v} = \frac{0.62 \times 66.7 \times 51.2}{8} = 264.7\ kips\ \ (1177.4\ kN)$$

$$V_N = 81.9 + 264.7 = 346.6\ kips\ \ (1541.7\ kN)$$

5.5.3 Shear Wall No. 2 – Wall Construction

Shear Wall No. 2 was constructed using high-strength concrete, which was poured in two stages; foundation followed by the wall which was integrally cast with the top steel loading beam. The foundation was selected to be of rectangular shape, in comparison to the I-shape foundation used for Shear Wall No. 1 to provide additional strength and stiffness as the wall would be subjected to higher lateral forces and moments. The foundation had an overall dimension of 3300 m (L) x 1500 mm (W) x 500 mm (T), (~11’ x 5’ x 1’-8”). Four (4) pre-formed sleeves were placed near the extreme corners to match the locations of the existing holes in the strong floor. High-strength 3” diameter (75mm) threaded rods were placed in these sleeved holes to secure the foundation on the strong floor and to provide fixity at the base. The holes were spaced at 2700 mm (9’) along the

length of the wall and 900 mm (3') in the perpendicular direction. The surface of the foundation was roughened and cleaned prior to pouring the wall concrete. The steel loading beam, consisting of two stacked 4"x4" (102x102) HSS sections and five (5) 50 mm wide by100 mm deep welded steel shear keys was placed on the top of the wall. A total of eight (8) one inch (1") diameter high strength threaded rods were inserted 500 mm (20") into the upper segment of the wall and bolted to the loading beam. The loading beam was drilled with sixteen (16) holes (eight on each side) to allow for the installation of prestressing tendons. The cables were loaded in small increments until all the cables were loaded to 100 kN, applying a total axial load of 1600 kN on the specimen.

Figure 5.19 Shear Wall No. 2 during Construction

The foundation also had eight (8) – 1" Diameter (25mm) high strength threaded rods cast in concrete on each side of the wall with a continuous steel plate underneath. Each one of these doweled threaded rods was used to support a pre-stressing cable for the application of gravity loads. The shear wall was constructed using conventional reinforcing steel bars except for the high strength WWR grids used as transverse boundary element reinforcement. Figure 5.19 illustrates Wall No. 2 during construction.

5.5.4 Shear Wall No. 2 – Test Set up and Instrumentation

The overall test setup used for Shear Wall No. 2 is shown in Figure 5.20. A secondary A-Frame support was placed perpendicular to the plane of shear wall to restrain the wall against out-of-plane movement. Two HSS sections provided out-of-plane sliding supports at the top of the wall. A small gap was placed between the loading beam of the wall and the out-of-plane support where the steel surfaces were covered with grease to facilitate sliding, should the wall move out of plane. The out-of-plane support represents the stiff support provided by floor slabs in a building floor diaphragm.

Three data acquisition systems were used to collect data during the test. Figure 5.21 illustrates the layout and location of the externally installed transducers/gauges. The following information was collected during the test:

- Magnitude of applied force by the MTS actuator;
- Lateral displacement of wall at the line of action of horizontal force. The cable transducer used for this purpose was identified as CT-01.
- Horizontal movement at the top of the foundation, measured by cable transducer C-02;
- Vertical movements of the foundation relative to the Laboratory strong floor, measured by LVDTs at five (5) intervals spaced at 450mm o/c. The LVDTs were located at the center span of the foundation, labelled as LVDT FND-01 to LVDT FND-05.
- Vertical movement of the wall measured at elevations 50 and 300 mm on both sides of the wall using cable transducers LVDT-E-1, LVDT-E-2, LVDT-W-1, and LVDT-W-2. These measurements were used to create wall rotation graphs at the base of the wall.
- Strain values of the steel reinforcement and WWR grids, as outlined in the next section.

Figure 5.20 Shear Wall No. 2 Test Set-up

The horizontal displacement measurements in this test were taken relative to the laboratory strong floor to avoid any potential errors that could be introduced by the slight bending of the foundation under applied moments. As the lateral load magnitude increases, the foundation is likely to lift up on one side (the heel) and is pushed down on the opposite side (the toe). This causes the foundation to bend and crack, affecting lateral displacement measurement taken relative to the foundation. In the current test the reference point was moved to the strong floor for all displacement measurements. The net horizontal movement of the wall was obtained by subtracting the foundation movement from the horizontal displacement recorded at the top of the wall. Also, the error due to the rotation of the foundation base in the measurement of the top displacement was corrected using the foundation vertical movement readings.

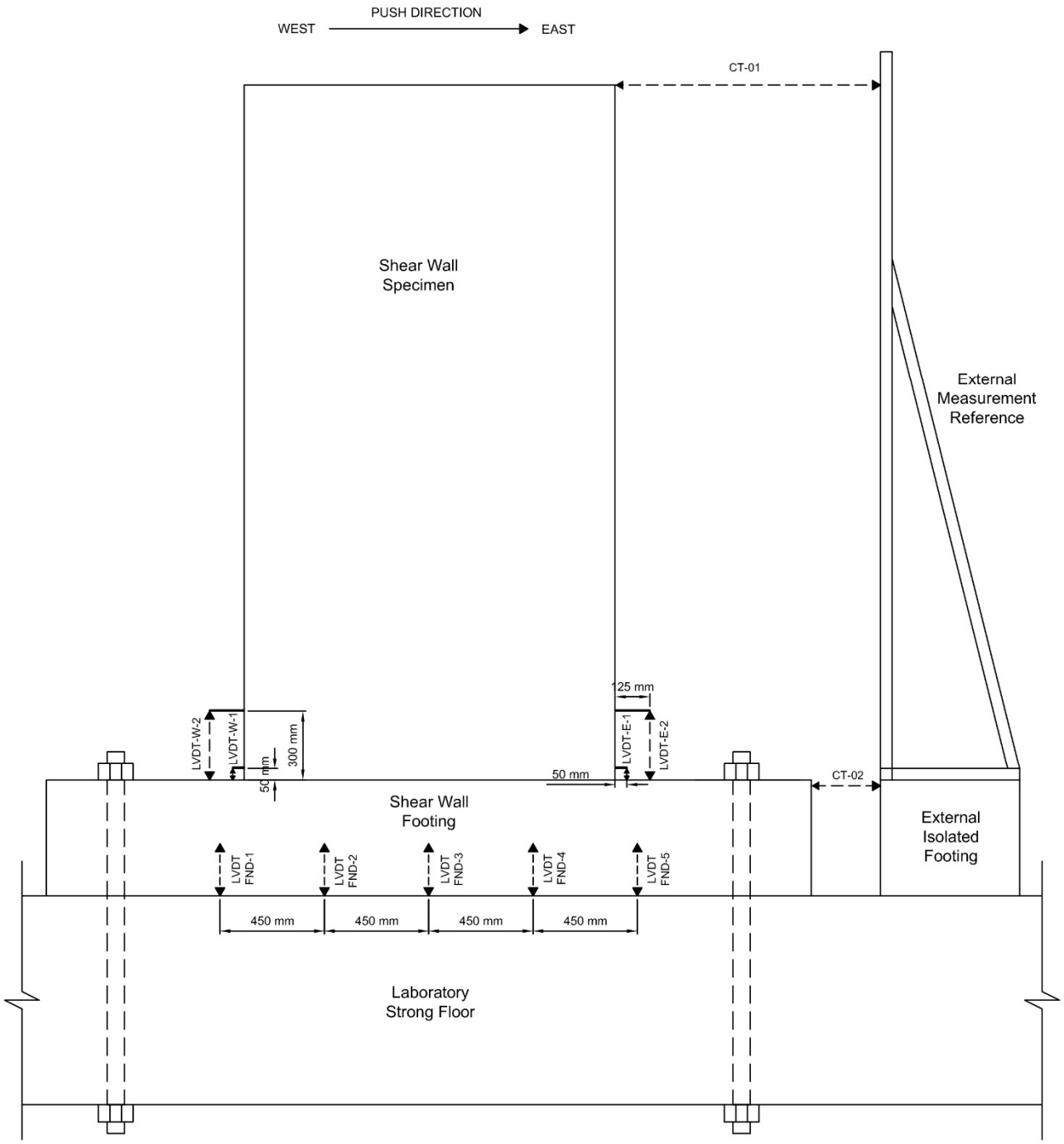

Figure 5.21 Shear Wall No. 2 – Measurement Devices Layout

5.5.4.1 Shear Wall No. 2 – Strain Gauges

A series of strain gauges were installed to monitor the strains in reinforcement. Strain – Lateral deformation graphs were generated and are presented in the thesis. Figures 5.22 to 5.24 illustrate the locations of strain gauges, as well as the labelling scheme that was used to identify each gauge. It should be noted that several strain gauges were damaged during casting and were removed from the list of strain gauges.

The following steel members were instrumented with strain gauges:

- Longitudinal bars in the boundary elements ; shown in Figure 5.22;
- Dowels in the foundation ; shown in Figure 5.22;
- WWR grids in boundary elements ; shown in Figures 5.23 and 5.24;
- Horizontal web reinforcement in the web ; shown in Figure 5.23;

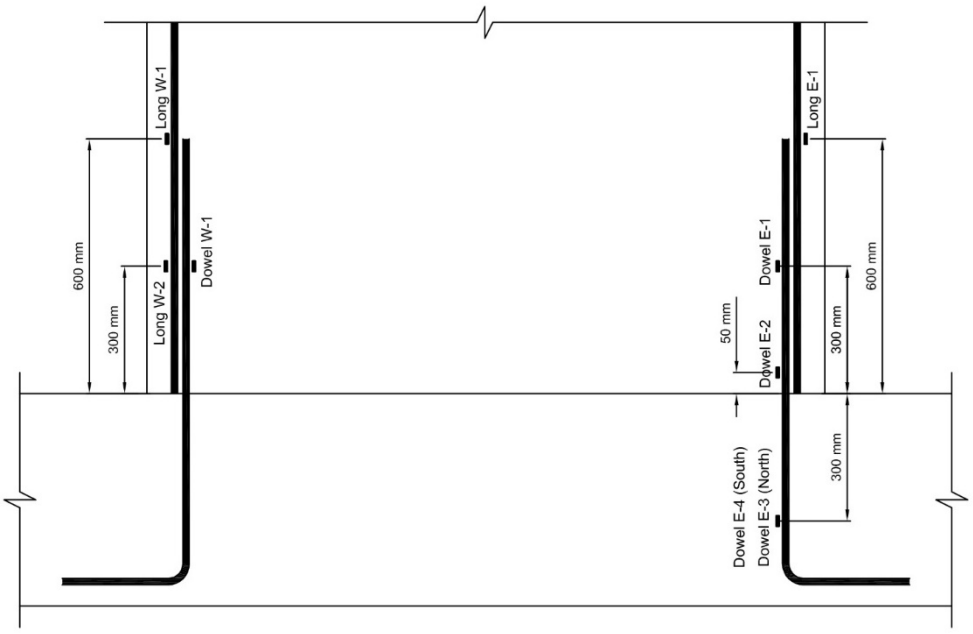

Figure 5.22 Shear Wall No. 2 – Dowels and Longitudinal Bars Strain Gauges

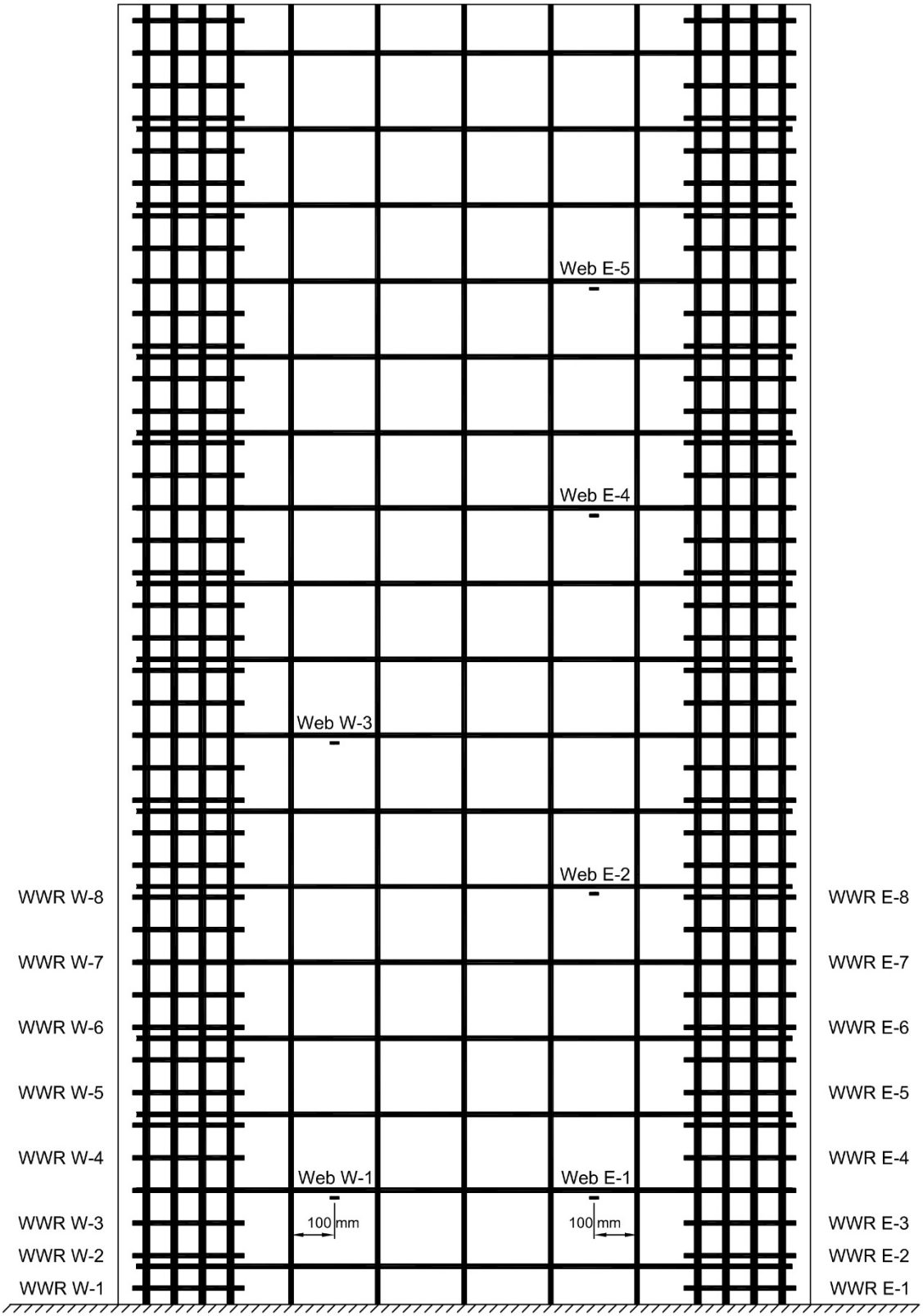

Figure 5.23 Shear Wall No. 2 – WWR Grids Labels and Web Reinforcement Strain Gauges

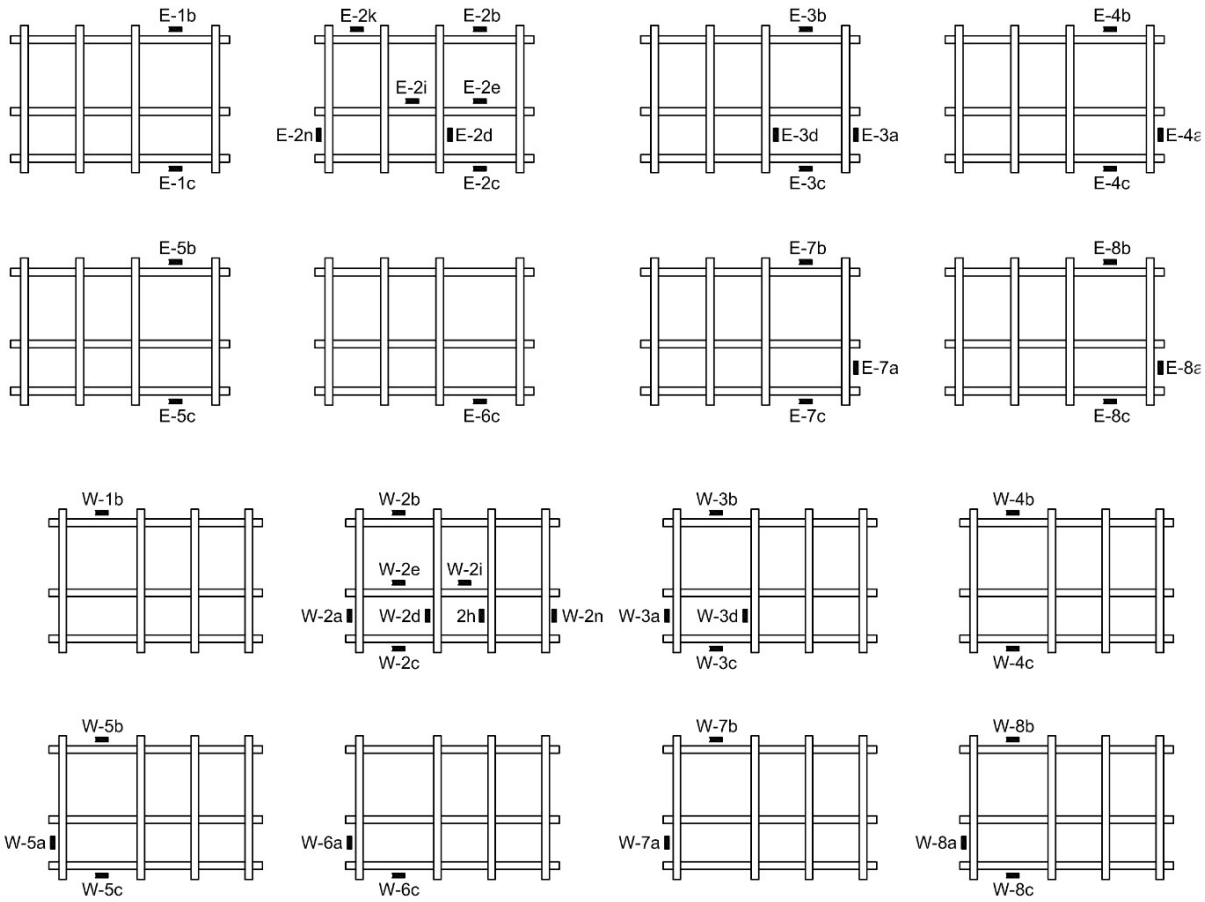

Figure 5.24 Shear Wall No. 2 – WWR Grid Strain Gauge Labels

The maximum strain values recorded by strain gauges are tabulated in Table 5.6. It should be noted that some of the strain gauges stopped recording during the test prior to wall failure. The tabulated values refer to the highest strain value that was successfully recorded.

Table 5.6 Maximum Recorded Strains for Shear Wall No. 2

Strain Gauge ID	**Maximum Recorded Strain**	**Strain Gauge ID**	**Maximum Recorded Strain**
Dowel W-1	2000	Dowel E-1	2050
Dowel E-2	2050	Dowel E-3	4100
Dowel E-4	16000	Long W-1	1700
Long W-2	1650	Long E-1	1860
W-1b	580		
W-2a	-720	W-2b	-470
W-2c	280	W-2d	230
W-2e	280	W-2h	320

Note: Force-Strain graphs for Shear Wall No. 2 strain gauges are provided in Appendix B.2.

Table 5.6 Maximum Recorded Strains for Shear Wall No. 2 (Cont'd)

Strain Gauge ID	Maximum Recorded Strain	Strain Gauge ID	Maximum Recorded Strain
W-2i	-170	W-2n	240
W-3a	135	W-3b	215
W-3c	390	W-3d	410
W-4b	360	W-4c	170
W-5a	290	W-5b	350
W-5c	270		
W-6a	220	W-6c	430
W-7a	390	W-7b	500
W-8a	195	W-8b	215
W-8c	205		
E-1b	1230	E-1c	780
W-2b	620	E-2c	480
E-2d	1240	E-2e	950
E-2i	1000	E-2k	1130
E-2n	1030		
E-3a	440	E-3b	650
E-3c	180	E-3d	480
E-4a	400	E-4b	700
E-4c	380		
E-5b	340	E-5c	370
E-6c	220		
E-7a	350	E-7b	350
E-7c	320		
E-8a	145	E-8b	260
E-8c	2400		
Web W-1	1000	Web W-3	700
Web E-1	930	Web E-2	1700
Web E-4	950	Web E-5	320

Note: Force-Strain graphs for Shear Wall No. 2 strain gauges are provided in Appendix B.2.

5.5.5 Shear Wall No. 2 – Test Result

The shear wall was subjected to inelastic displacement reversals until failure. The wall behaved in a ductile manner and failed by rupturing of the longitudinal bars as shown in Figure 5.25. The hysteretic Force-Displacement graphs, using applied force by the actuators vs. top lateral displacement (and drift) is shown in Figure 5.26. The Lateral force was then revised to include the effects of the horizontal force components of gravity load prestressing strands. This resulted in the

net lateral force. Net lateral force-top lateral displacement (and drift) relationship is shown in Figure 5.27. Finally, the applied moment vs. lateral displacement (and drift) relationship is shown in Figure 5.28. The applied moment was obtained by multiplying the net lateral force by shear span (wall height), plus the secondary moment caused by the vertical component (gravity load effect) of prestressing tendons multiplied by lateral displacement.

Figure 5.25 Shear Wall No. 2 Failure Photos (bottom two after the failure, when the wall was turned over to expose the bottom section)

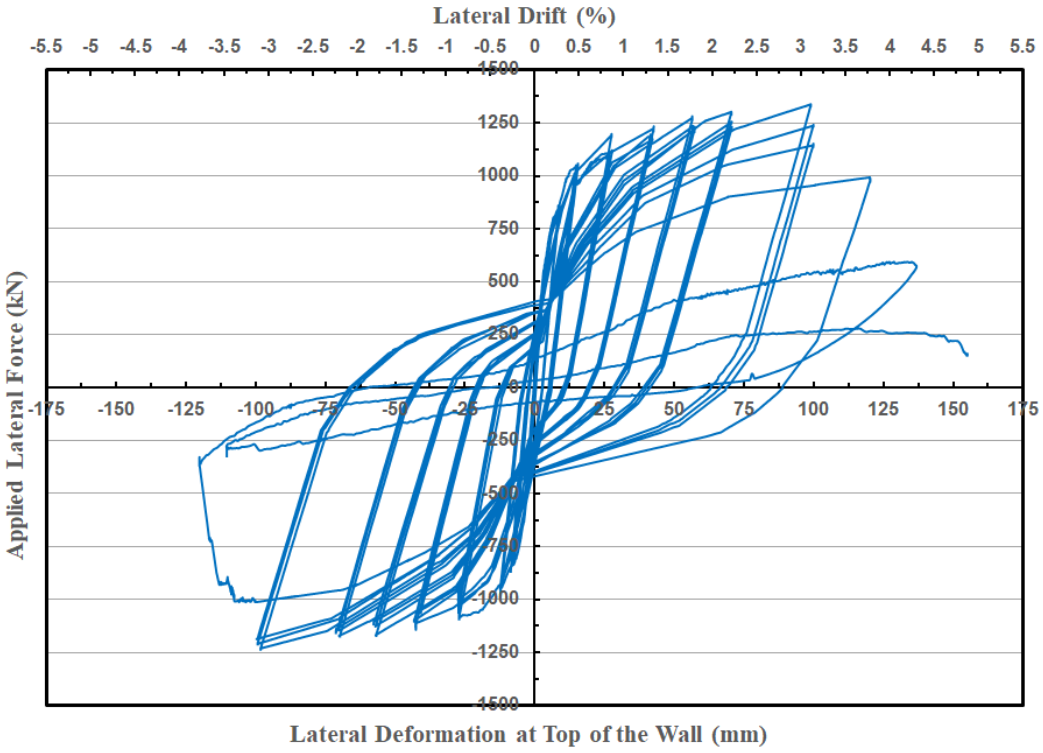

Figure 5.26 Shear Wall No. 2 – Applied Lateral Force by Actuator vs. Lateral Deformation

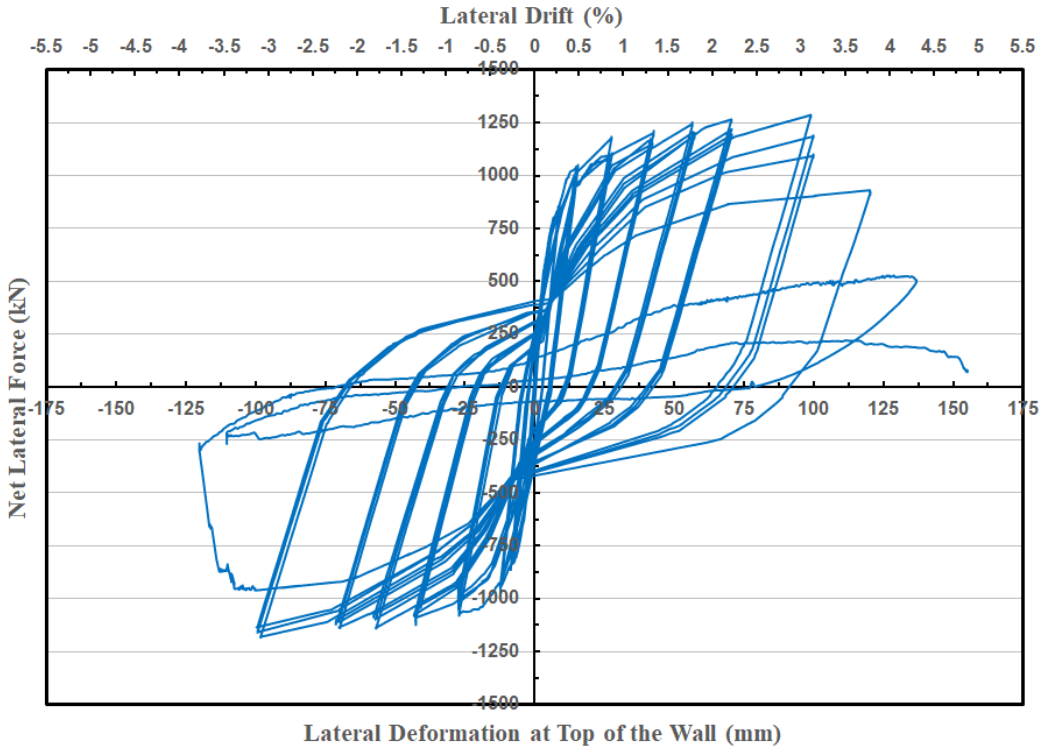

Figure 5.27 Shear Wall No. 2 – Net Lateral Force vs. Lateral Deformation

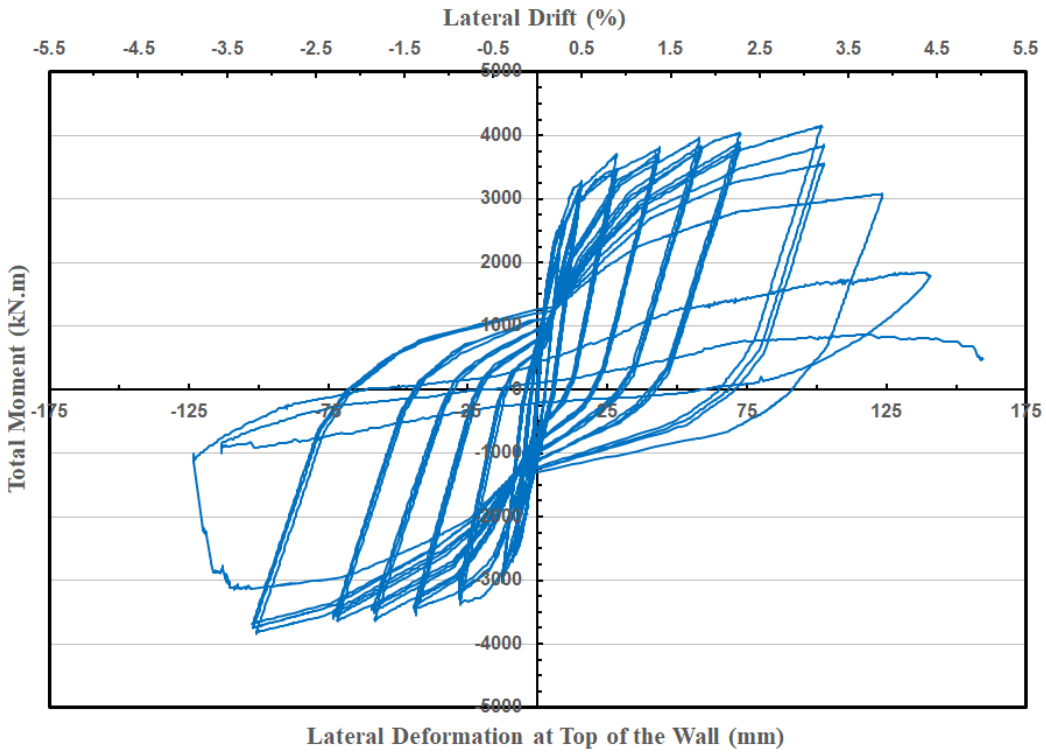

Figure 5.28 Shear Wall No. 2 – Applied Moment vs. Lateral Deformation

5.5.6 Shear Wall No. 2 – Foundation Deformation and Movement

During the Shear Wall No. 1 test, it was observed that the foundation experienced cracking during loading, with crack sizes increasing with the magnitude of applied load. It was also noted that the foundation lifted up from the laboratory strong floor on the tension side in spite of the fact the bolts used to secure the foundation to the strong floor were tightened prior to and during testing. The lifting side of the foundation switched sides as the direction of the force reversed during reversed loading. Few spot measurements were made but no continuous instrumented measurements were taken as it was noted in the later stages of the experiment. The lifting of the foundation caused the wall to develop slight rigid-body rotation. In addition, the bending of the foundation introduced further rotation of the wall which had a small but sizeable effect on measured wall displacements at the top of the wall. In order to confirm and quantify these observations, the foundation of Shear Wall No. 2 was instrumented with five (5) LVDTs along the long direction of the wall to measure vertical movements as shown in Figure 5.29. The signs of foundation cracking during the wall test is illustrated in Figure 5.30.

Figure 5.29 Shear Wall No. 2 – Monitoring of Foundation Vertical Movement During Testing

Figure 5.30 Shear Wall No. 2 – Visual Signs of Foundation Cracking

The vertical deformation recording confirmed that the wall bent under the applied load. The measurements also showed that the maximum foundation bending occurred underneath the boundary element where the highest tensile forces were developed and pulled the foundation upward. This location switched sides as the loading direction was reversed. Graphs in Figure 5.31 shows the measured trend on foundation deformation. Two corrections were introduced to the wall lateral measurement at the top of the wall to take into account foundation rotation due to foundation lift up and foundation bending. It was noted that the foundation bending has become constant after the yielding of wall boundary element reinforcement (yielding of the wall).

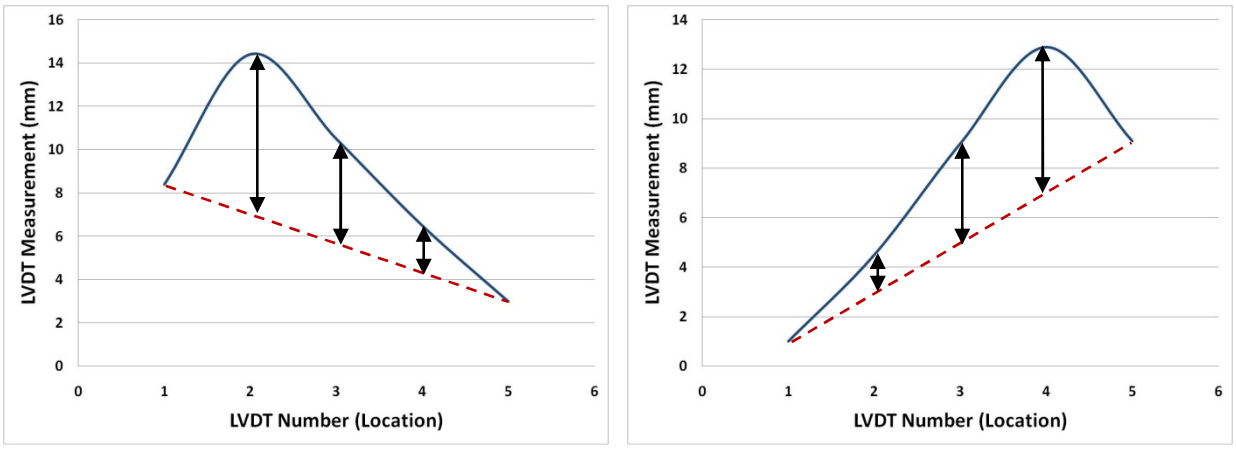

Figure 5.31 Shear Wall No. 2 Foundation Vertical Movement under Push (Left) and Pull (Right)

5.6 Shear Wall No. 3

Shear wall No. 3 is a barbell shaped wall with a height to length aspect ratio of 3:1 (4.35 m Height: 1.45 m length). The boundary elements are 250 mm x 250 mm and the web is 100 mm thick. The wall was constructed using 83 MPa concrete and conventional reinforcement, except for the high-strength WWR grids used as boundary element transverse reinforcement. The wall concrete was poured in multiple stages; i) lower wall segment and ii) upper wall segment with concrete loading beam. A consistent concrete mix was used and concrete cylinders were taken and tested to determine the compressive strength of concrete. The material test results are presented in Chapter 3. The wall elevation and cross section views are shown in Figures 5.32 and 5.33, respectively. It was first designed using the specified concrete strength of 80 MPa and rebar yield strength of 400 MPa. The wall was designed with the intent of preventing premature shear failure to promote ductile behaviour. It was subjected to 1500 kN axial force using vertical prestressing tendons. Horizontal web reinforcement and transverse boundary element WWR grids reinforcement were designed to attain the intended ductile flexural response. The design notes are shown in the following section.

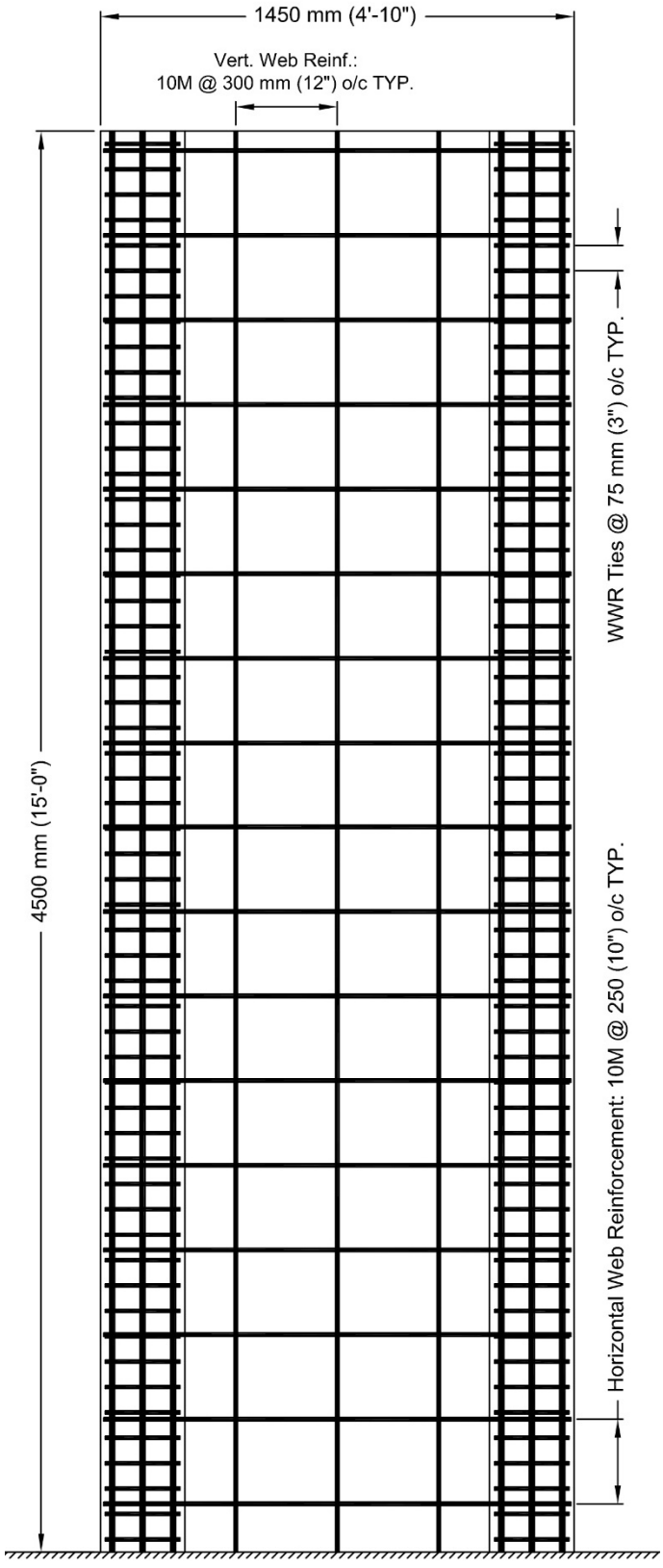

Figure 5.32 Shear Wall No. 3 Elevation

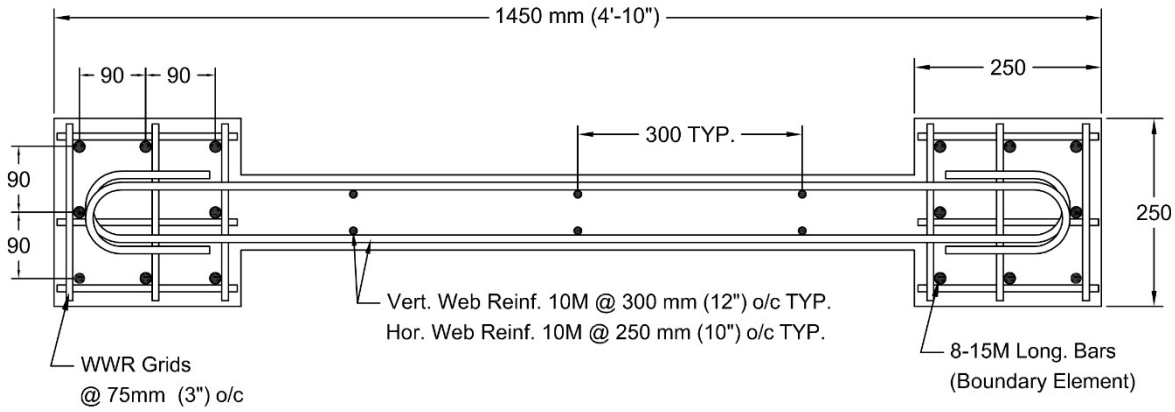

Figure 5.33 Shear Wall No. 3 Cross-Section

5.6.1 Shear Wall No. 3 – Design Notes

The first step in designing the shear wall was sectional analysis to determine the moment capacity for the selected geometry and longitudinal reinforcement. RC-Section software was used to perform the sectional analysis, and a screenshot of the model is depicted in Figure 5.34.

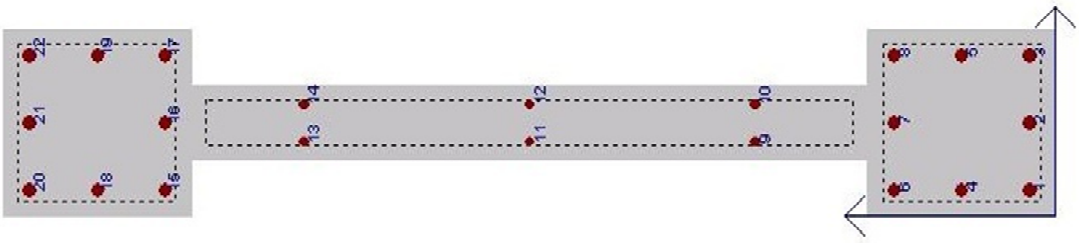

Figure 5.34 Screenshot of Shear Wall No. 3 Model in RC-Section Software

RC-Section software allows for various concrete models to be assigned to different segments of the cross section. For Shear Wall No.3, two concrete models were introduced: Hognestad (1951) model for unconfined cover concrete and Saatcioglu and Razvi (1992) model for confined core concrete. A bilinear stress-strain relationship was assumed for the reinforcing steel. The design assumptions and calculations are summarized below. ACI 318-11 approach for ductile wall design was used as design guidelines.

Design Assumptions:

$f'_c = 80\ MPa = 11{,}600\ psi$

$fy = 460\ MPa = 66{,}700\ psi$: for all rebars;

$fyt = 550\ MPa = 80{,}000\ psi$: for WWR grids;

$\sqrt{f'_c} = 107.7 \xrightarrow{exceeds\ \max\ allowable} \sqrt{f'_c} = 100psi$ Cl. 11.1.2

$l_w = 1.45m \cong 58"$

$h_w = 4.35\ m \cong 174"$

$h = 0.1m \cong\ 4"$

$d = 0.8l_w \cong 46.4"$ Cl. 21.9.2.3(c)

$A_{cv} = l_w h = 58 \times 4 = 232\ in^2$ Cl. 21.9.4.1

$\alpha_c = 2.0$: $Walls\ with\ aspect\ ratio\ of$ 3.0 $or\ higher$ Cl. 21.9.4.1

Boundary element longitudinal reinforcement ratio: $\frac{8\times200}{250^2} = 2.56\%$

The concrete confinement parameter, K, for Saatcioglu and Razvi model is calculated below:

Tie Spacing: $s = 75\ mm$

$b_c = 204.5\ mm$

$S_l = 90\ mm$

$f_l = \frac{\sum A_s f_{yt}}{sb_c} = \frac{3(71)550}{75(204.5)} = 7.64\ MPa$

$K_2 = 0.26\sqrt{\frac{b_c}{s}\frac{b_c}{s_l}\frac{1}{f_l}} \leq 1.0$

$K_2 = 0.26\sqrt{\frac{204.5}{75}\frac{204.5}{90}\frac{1}{7.64}} = 0.234$

$f_{le} = K_2 f_l = 0.234 \times 7.64 = 1.788\ MPa$

$K_1 = 6.7(f_{le})^{-0.17} = 6.7(1.788)^{-0.17} = 6.07$

$K = \frac{K_1 f_{le}}{f"_{co}} = \frac{6.07(1.788)}{0.85(80)} = 0.160$

Web Horizontal Reinforcement:

It was decided that Wall 3 should have sufficient horizontal web reinforcement to prevent premature shear failure. The highest moment that the wall could experience in the post-yield region was approximated by the probable moment resistance of the wall. RC-Section software provided output for probable moment capacity under a constant axial compressive load, which in this case was 1500 kN. Table 5.7 provides the details of probable moment capacity calculations for the wall. The horizontal web reinforcement was designed to provide shear capacity in excess of that

corresponding to probable moment resistance. The horizontal web reinforcement was well anchored into the boundary elements with 180º hooks.

Table 5.7 Probable Moment Capacity of Shear Wall No. 3 under 1500 kN Axial Load (RC-Section output)

Probable Capacity in Metric Units			**Probable Capacity in Imperial Units**		
$\boldsymbol{P\ (kN)}$	$M_{Pr}\ (kN.m)$	$c\ (mm)$ *	$P\ (kips)$	$M_{Pr}\ (kip.ft)$	$c\ (in)$ *
16887	2416.3	148.4	3796	1782.2	5.84

* c is the distance to N.A.

The horizontal lateral force corresponding to probable moment resistance was obtained by dividing the probable moment by shear span, which was taken as the distance between the center line of the actuator arm and the wall base at the foundation interface.

$$V_{pr} = \frac{M_{pr}}{h} \quad \rightarrow \quad V_{pr} = \frac{2416.3}{4.35} = 555.5\ kN\ \ (124.9\ kips)$$

$$V_N \geq V_{pr} = 555.5\ kN\ \ (124.9\ kips)$$

$$V_{N,max} = 10\sqrt{f'_c}\ hd = 10 \times 100 \times 4 \times 46.4 = 185.6\ kips\ (825.6\ kN) \quad \text{Cl. 11.9.3}$$

$$V_N = V_c + V_s \geq 124.9\ kips \quad \longrightarrow \quad V_s \geq 124.9 - V_c$$

$$V_{c,max} = A_{cv}\ \alpha_c \lambda \sqrt{f'_c} = 232 \times 2.0 \times 1.0 \times 100 = 46.4\ kips\ \ (206.4\ kN)$$

The concrete shear capacity is calculated per ACI 318 Cl. 11.9.5.

$$V_c = 2\lambda\sqrt{f'_c}hd = 2 \times 1.0 \times 100 \times 4 \times 46.4 = 37.1\ kips\ (165.0\ kN)$$

$$V_s \geq 124.9 - 37.1 = 87.8\ kips$$

$$V_s = \frac{A_v f_y d}{s_v} \geq 87.8 \ \longrightarrow \ \frac{A_v}{s_v} \geq \frac{87.8}{66.7 \times 46.4} = 0.0283$$

Provide two curtains of 10M horizontal web reinforcements: $A_v = 200\ mm^2 = 0.31\ in^2$.

$$s_v \leq \frac{A_v}{0.0259} = \frac{0.31}{0.0283} = 10.9"$$

Select $s_v = 10"$: Where s_v is vertical spacing between web horizontal reinforcement.

Checking maximum allowable spacing per Cl. 11.9.9.3:

$$s_v \leq \begin{cases} l_w/5 = 58"/5 = 11.6" \\ 3h = 3 \times 4" = 12" \\ 18" \end{cases}$$

Checking minimum web horizontal reinforcement ratio:

$$\rho_t = \frac{A_v}{s_v \times h} = \frac{0.31}{10 \times 4} = 0.0078 \longrightarrow \rho_{t,min} = 0.0025 \quad \text{Ok.}$$

Web Vertical Reinforcement:

The maximum allowable horizontal spacing between web vertical shear reinforcement, s_h, is expressed in ACI 318, Cl. 11.9.9.5:

$$s_h \leq \begin{cases} l_w/3 = 58"/3 = 19.3" \\ 3h = 3 \times 4" = 12" \\ 18" \end{cases}$$

ACI 318, Cl. 11.9.9 commentary indicates that in case of a shear wall with an aspect ratio of larger than 2.5 (Height: Length), only a minimum amount of web vertical reinforcement is required. This specimen has an aspect ratio of 3:1 and, therefore:

$$\rho_l = \rho_{l,min} = 0.0025$$

Provide two curtains of 10M vertical web reinforcements: $A_v = 0.31\ in^2$

$$\rho_l = \frac{A_v}{s_h \times h} \rightarrow s_h = \frac{A_v}{\rho_l \times h} = \frac{0.31}{0.0025 \times 4} = 31"$$

Two curtains of 10M vertical rebars spaced at 12" o/c satisfies the design requirements.

The minimum volumetric reinforcement ratio for shear wall boundary elements is provided in ACI 318, Cl. 21.9.6.4, 21.6.4.3 and 21.6.4.4. It should be noted that Cl. 21.9.6.4 modifies the wall requirements by changing 21.6.4.3(a) from one-quarter to one-third of the least dimension of the boundary element. In addition, only the following equation is required to determine the volumetric reinforcement ratio:

$$A_{sh} \geq 0.09 \frac{s b_c f'_c}{f_{yt}} \longrightarrow s \leq \frac{A_{sh} f_{yt}}{0.09 b_c f'_c}$$

The above equation should be satisfied in both cross-sectional directions of the rectangular core.

$$A_{sh,provided-x} = 3\ bars\ in\ a\ WWR\ Grid = 3 \times 71 = 213\ mm^2\ (0.33\ in^2)$$

$$A_{sh,provided-y} = 3\ bars\ in\ a\ WWR\ Grid = 3 \times 71 = 213\ mm^2\ (0.33\ in^2)$$

The yield strength of the WWR grids, f_{yt}, was determined as 80 ksi (550 MPa) by performing tension coupon tests. Details of Material Properties are provided in Chapter 3 of this research document.

$$s_x \leq \frac{A_{sh-x} f_{yt}}{0.09 b_{cx} f'_c} = \frac{213 \times 550}{0.09 \times 204.5 \times 80} = 79.5\ mm\ (3.1")$$

$$s_y \leq \frac{A_{sh-y} f_{yt}}{0.09 b_{cy} f'_c} = \frac{213 \times 550}{0.09 \times 204.5 \times 80} = 79.5\ mm\ (3.1")$$

Checking for maximum allowable spacing between transverse reinforcements:

$$s \leq \begin{cases} one\ third\ of\ min.member\ dimension \\ six\ times\ the\ diameter\ of\ the\ smallest\ long.bar \\ 4" < s_0 < 6" \end{cases}$$

$$s \leq \begin{cases} \frac{250\ mm}{3} = 83.3\ mm\ (3.28") \\ 6 \times 15 = 90\ mm\ (3.54") \\ 4" < s_0 < 6" \end{cases}$$

Provide s = 75 mm (3") between WWR transverse reinforcements in the boundary elements.

5.6.2 Shear Wall No. 3 – As-Built Calculations

The calculations in this section provide more accurate understanding of the shear wall capacity based on the actual material properties obtained by materials testing. The concrete strength, f'_c, which was assumed as 80 MPa during the design phase, was found to be 83 MPa at the time of wall test. The concrete confinement parameter K was revised based on the actual recorded concrete strength. The reinforcement bi-linear stress-strain model was replaced with a model, which included the strain hardening effect, where $f_y = 460\ MPa$ and $f_u = 710\ MPa$. RC-Section software model was revised and re-ran to determine the moment capacity of the section using accurately recorded material behaviour. The shear capacity of as-built wall was determined by dividing the moment capacity by the shear span (wall height). The details of the calculations are summarized below.

Revised Concrete Confinement Parameter

Tie Spacing: $s = 75\ mm$

$b_c = 204.5\ mm$

$S_l = 90\ mm$

$f_l = \frac{\sum A_s\ f_{yt}}{s b_c} = \frac{3(71)550}{75(204.5)} = 7.64\ MPa$

$$K_2 = 0.26\sqrt{\frac{b_c}{s}\frac{b_c}{s_l}\frac{1}{f_l}} \leq 1.0$$

$$K_2 = 0.26\sqrt{\frac{204.5}{75}\frac{204.5}{90}\frac{1}{7.64}} = 0.234$$

$$f_{le} = K_2 f_l = 0.234 \times 7.64 = 1.788 MPa$$

$$K_1 = 6.7(f_{le})^{-0.17} = 6.7(1.788)^{-0.17} = 6.07$$

$$K = \frac{K_1 f_{le}}{f"_{co}} = \frac{6.07(1.788)}{0.85(83)} = 0.154$$

The moment capacity of the section calculated by RC-Section is tabulated in Table 5.8.

Table 5.8 Moment Capacity of As-Built Shear Wall No. 3 under 1500 kN Axial Load (RC-Section output)

Moment Capacity in Metric Units			**Moment Capacity in Imperial Units**		
$\boldsymbol{P\ (kN)}$	$M\ (kN.m)$	$c\ (mm)$ *	$P\ (kips)$	$M\ (kip.ft)$	$c\ (in)$ *
17001	2388.0	144.7	3822	1761.3	5.70

* c is the distance to the N.A.

The theoretical shear force that will generate the moment capacity of the as-built wall is calculated as $\frac{2388}{4.35} = 549\ kN\ (123.4\ kips)$.

The shear capacity of the as-built wall is calculated as followed. It should be noted that the ACI 318 equation for shear capacity of the concrete puts a cap on the contribution of the high-strength concrete and does not recognize the full capacity of the wall due to lack of sufficient research on this topic.

$$V_N = V_c + V_s$$

$$V_c = 2\lambda\sqrt{f'_c}hd = 2 \times 1.0 \times 100 \times 4 \times 46.4 = 37.1\ kips\ (165.0\ kN)$$

$$V_s = \frac{A_v f_y d}{s_v} = \frac{0.31 \times 66.7 \times 46.4}{10} = 95.9\ kips\ \ (426.6\ kN)$$

$$V_N = 37.1 + 95.9 = 133.0\ kips\ \ (591.6\ kN)$$

5.6.3 Shear Wall No. 3 – Wall Construction

Shear Wall No. 3 was constructed using a uniform concrete mix design for the foundation and the wall segments. The foundation was selected to have a rectangular shape, compared to the I-shape that was used in Wall No. 1, to provide additional rigidity and minimize bending during testing

under high levels of applied moment. In addition, a more uniform support was provided by increasing the number of connection points to the strong floor from four (4) in the first two walls to eight (8) in Wall No. 3. The connection points were provided by tying the foundation through 75mm (3") sleeved holes using large diameter steel bolts. The foundation was tied to the strong floor using 75mm (3") diameter steel bolts at the far end and 50mm (2") diwydag bars at the interior holes. The overall foundation size was 3300mm x 1500 mm x 500 mm (~11' x 5' x 1'-8") where the thickness was governed by the length of the 75mm (3") steel bolts available in the structural lab.

The specimen was subjected to 1500 kN of axial load using prestressing tendons, which were placed at 150 mm (6") offset from each face of the wall using a total of ten (10) prestressing tendons. The tendons were connected to a series of 25mm (1") high-strength steel threaded rods, which were embedded and anchored in the foundation using a double nut connection on a 75mm x 12.5 mm (3" x ½") flat steel plate.

5.6.4 Shear Wall No. 3 – Test Set up and Instrumentation

The overall test setup for Wall No. 3 is shown in Figure 5.35. A secondary A-Frame support was placed perpendicular to the shear wall to restrain the wall against out-of-plane movements by means of two HSS sections against which the wall would slide at the top. A small gap was placed between the wall and the HSS's with the steel surfaces greased to facilitate sliding. The out-of-plane support simulated the effects of stiff support provided by floor slabs in actual building floor diaphragms.

Three data acquisition systems were used to collect the data. Figure 5.36 illustrates the layout and location of externally installed istrumentation. The following information was collected during the test:

- Magnitude of the applied force by the MTS actuator;
- Lateral displacement at the top of the wall coinciding with the line-of-action of the horizontal force. A back up cable-transducer was installed at the same location to provide redundancy for this key data. The two cable transducers used for this purpose were identified as CT-01 and CT-02.
- Horizontal movement at the top of the foundation, measured by cable transducer C-03;

- Horizontal movement of the wall at 1450 mm above the foundation level, measured by cable transducer CT-04;
- Vertical movements of the foundation relative to the Laboratory strong floor, measured at the two extreme ends of the foundation by cable transducers CT-FE and CT-FW;
- Vertical movement of the wall measured at elevations 700, 1050 and 1400 mm on both sides of the wall using cable transducers CT-E-1, CT-E-2, CT-E-3, CT-W-1, CT-W-2 and CT-W-3. These measurements were used to create wall rotation graphs at the base of the wall.
- Strain values of steel reinforcement and WWR grids, as outlined in the next section.

The reference point for all measurements was taken as the laboratory strong floor to eliminate any inaccuracies that could generate from bending of the foundation, however small it may be. As the lateral load magnitude increased, the foundation lift-up was observed on the heel side, while the wall was compressed to the floor on the toe side. The net horizontal movement of the wall was obtained by correcting for foundation movement from the horizontal displacement at the top of the wall.

Figure 5.35 Shear Wall No. 3 Test Set up Overview

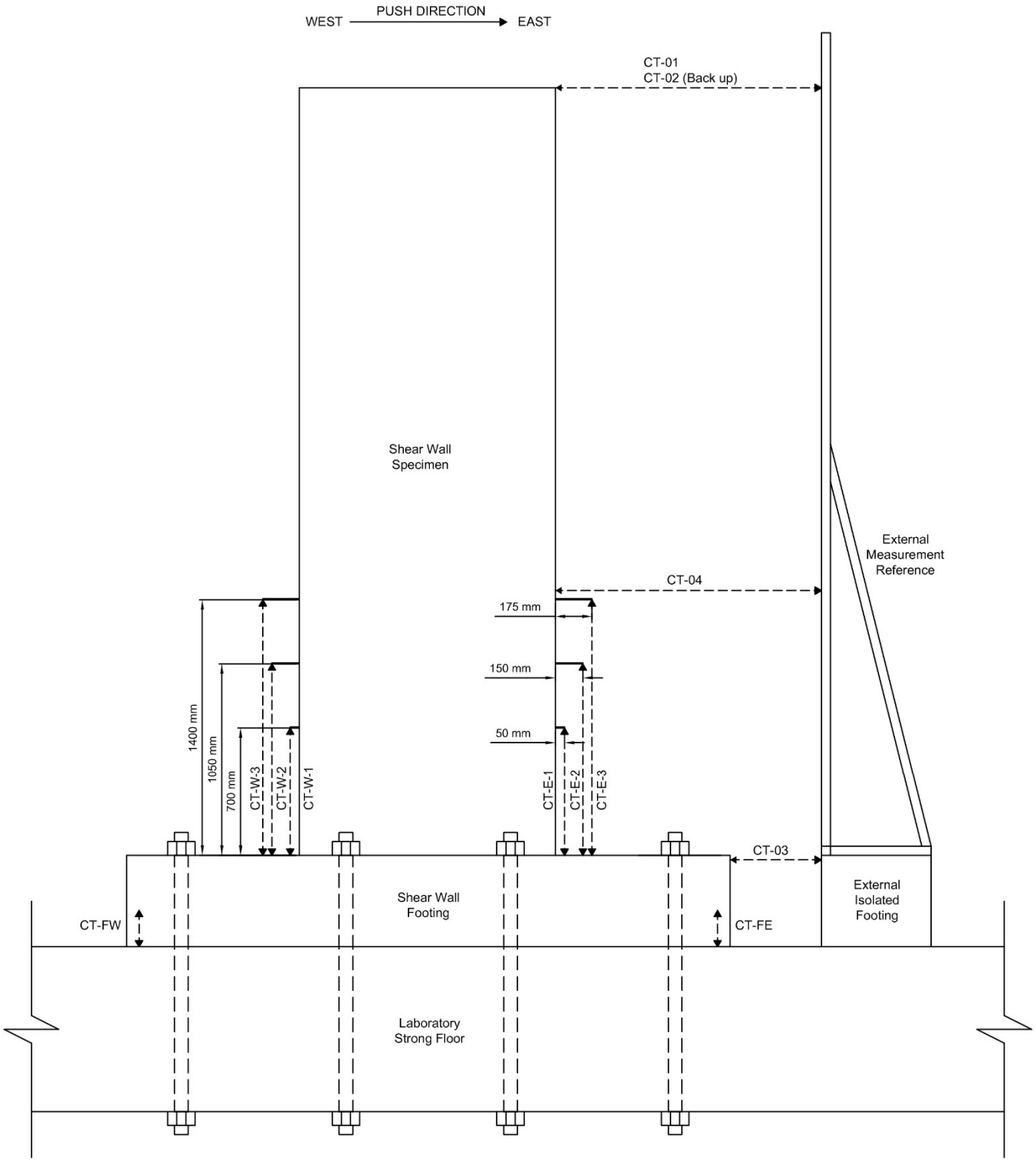

Figure 5.36 Shear Wall No. 3 – Cable Transducer Layout

5.6.4.1 Shear Wall No. 3 – Strain Gauges

A series of strain gauges were installed to monitor steel strains. Strain – lateral deformation graphs were generated and presented in Appendix B.3 of the thesis. Figures 5.37 to 5.39 illustrate the locations of strain gauges, as well as the labelling scheme that was used to identify each gauge. It should be noted that several strain gauges were damaged during casting, and were removed from the strain gauges list.

The following steel members were instrumented with strain gauges:

- Longitudinal bars in the boundary elements ; shown in Figure 5.37;
- Dowels in the foundation ; shown in Figure 5.37;
- WWR grids in boundary elements ; shown in Figures 5.38 and 5.39;
- Horizontal web reinforcement in the web ; shown in Figure 5.39;
- Vertical prestressing tendons ; shown in Figure 5.40;

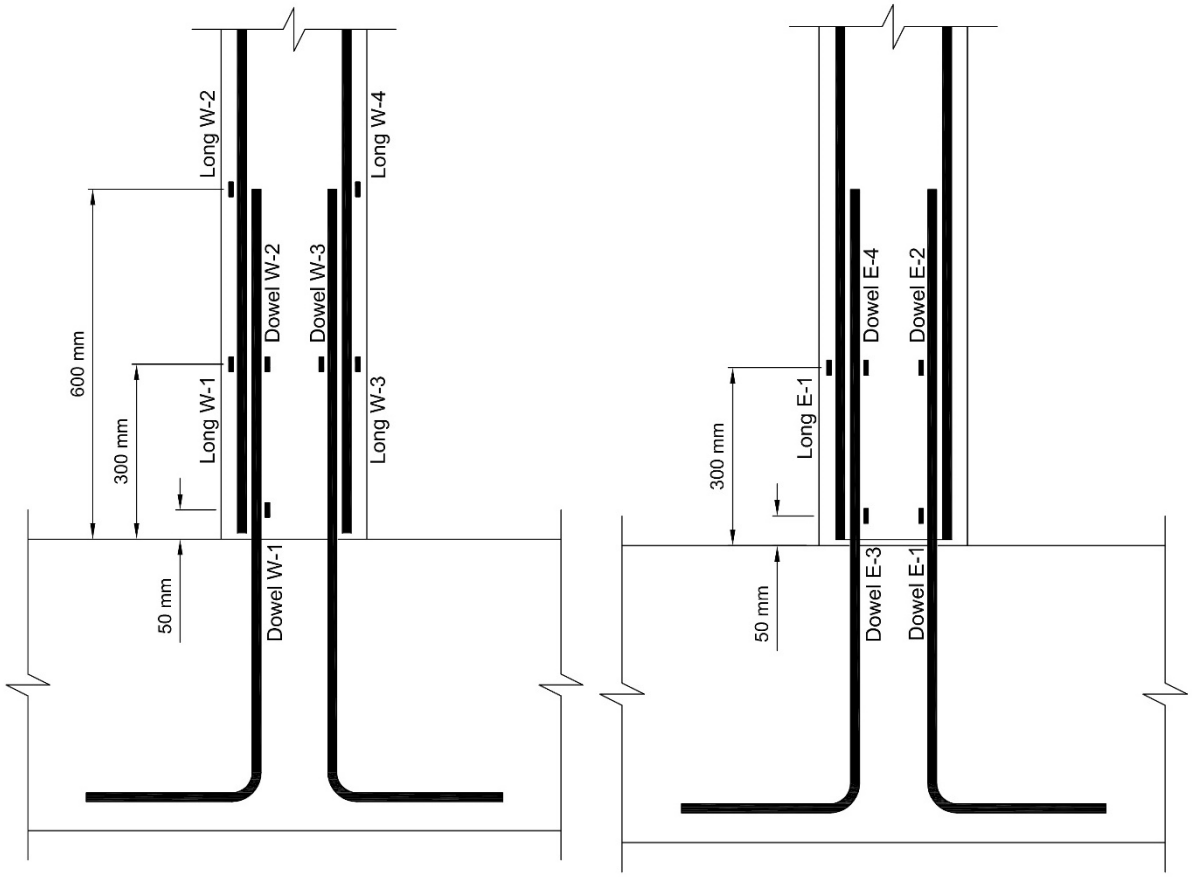

Figure 5.37 Shear Wall No. 3 – Dowel and Longitudinal Bar Strain Gauges

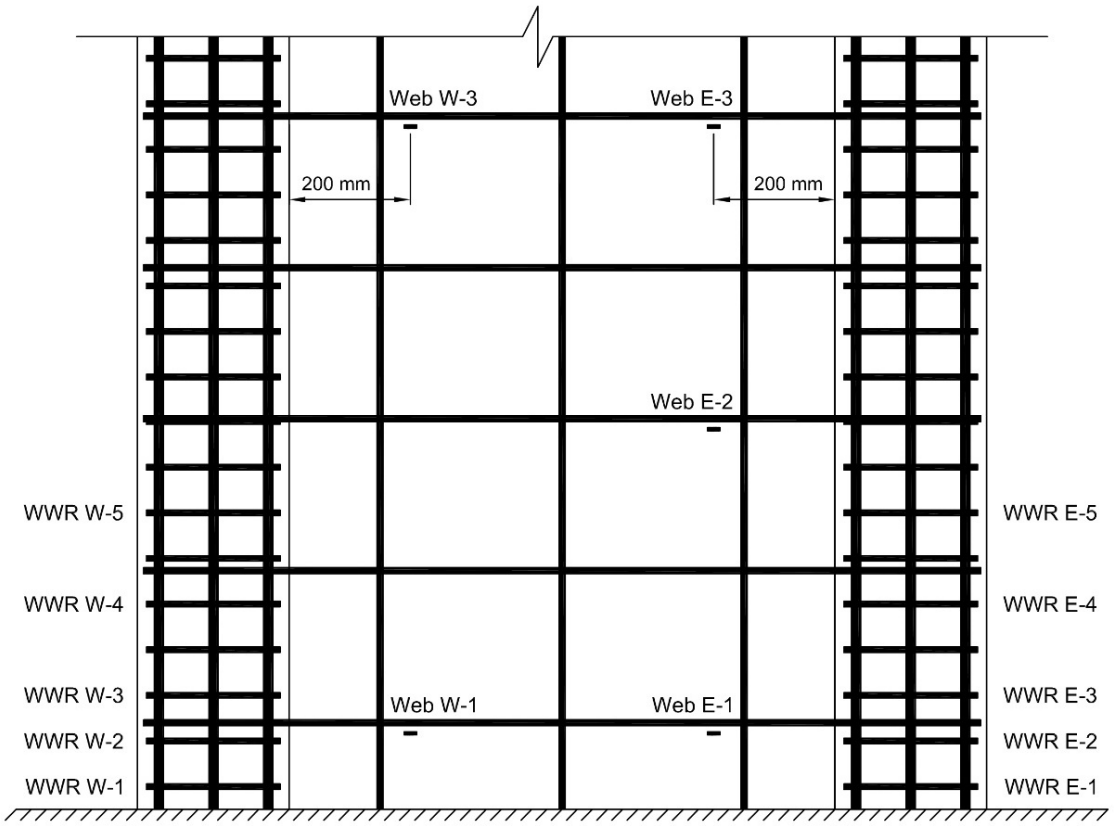

Figure 5.38 Shear Wall No. 3 – WWR Grid Labels and Web Reinforcement Strain Gauges

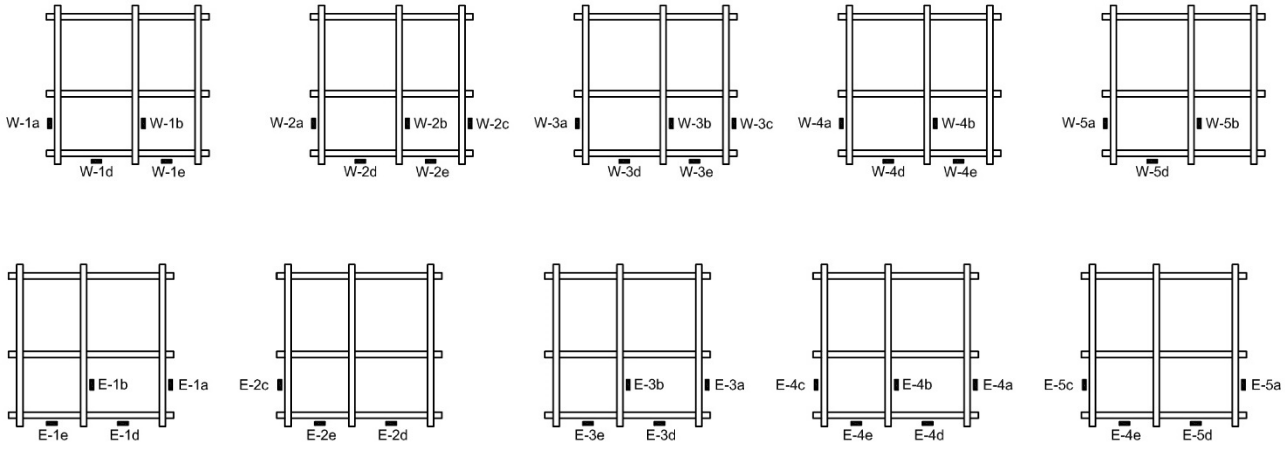

Figure 5.39 Shear Wall No. 3 – WWR Grid Strain Gauge Labels

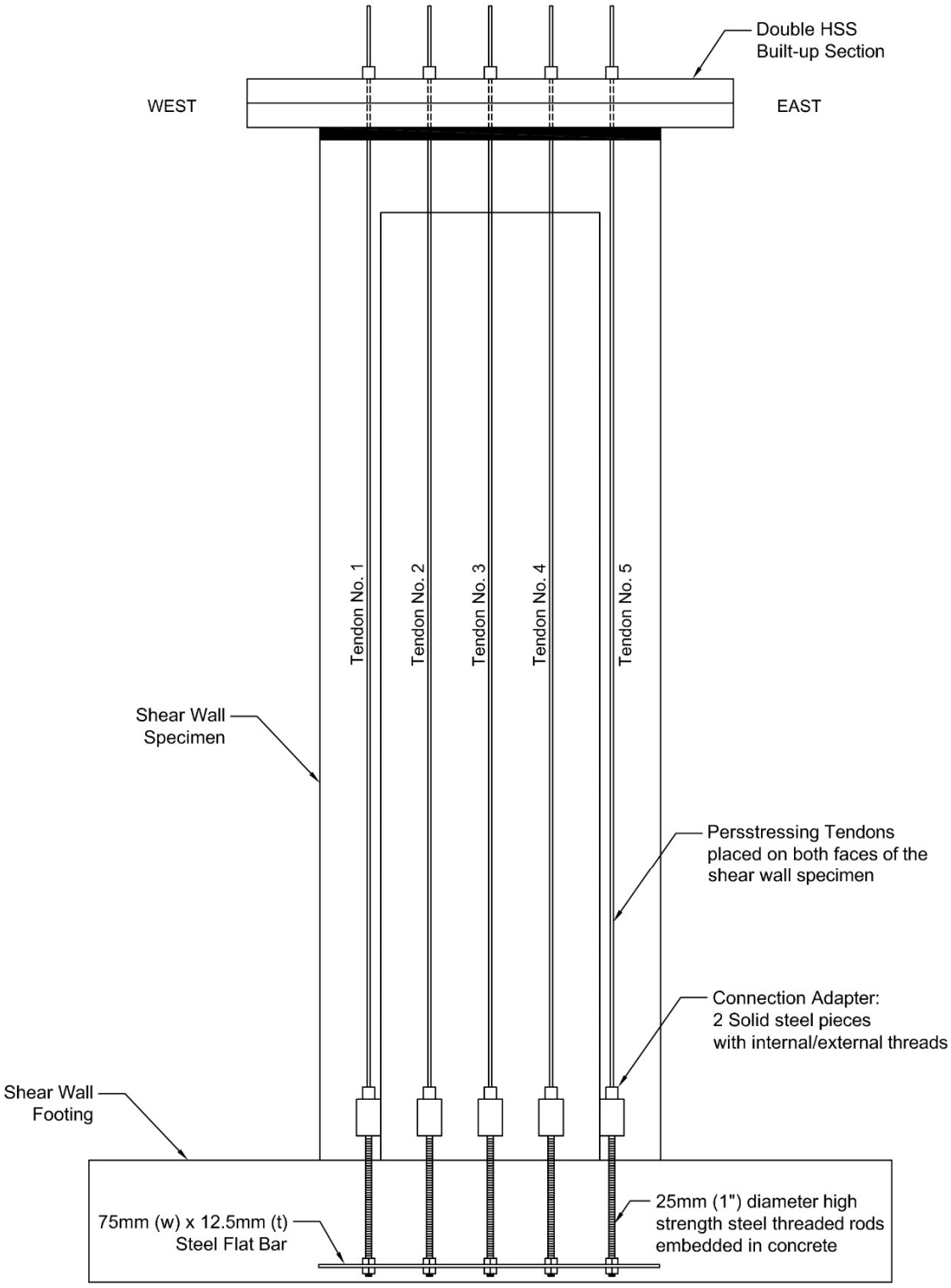

Figure 5.40 Shear Wall No.3 – Prestressing Tendon Layout

The maximum strain values recorded by strain gauges are tabulated in Table 5.9. It should be noted that some of the strain gauges stopped recording during the test prior to wall failure. The tabulated values refer to the highest strain value that was successfully recorded.

Table 5.9 Maximum Recorded Strains for Shear Wall No. 3

Strain Gauge ID	Maximum Recorded Strain	Strain Gauge ID	Maximum Recorded Strain
Dowel W-1	-1400	Dowel W-2	-3750
Dowel W-3	2400	Long W-1	-2300
Long W-2	17000	Long W-3	17000
Long W-4	2800	Dowel E-1	-12500
Dowel E-2	6500	Dowel E-3	12300
Dowel E-4	-2350	Long E-1	2050
WWR W-1a	-1700	WWR W-1b	-1850
WWR W-1d	900	WWR W-1e	550
WWR W-2a	780	WWR W-2b	1900
WWR W-2c	1950	WWR W-2d	1230
WWR W-2e	2780		
WWR W-3a	280	WWR W-3b	-300
WWR W-3c	-420	WWR W-3d	-640
WWR W-3e	910		
WWR W-4a	-230	WWR W-4b	240
WWR W-4e	-3400		
WWR W-5a	-320	WWR W-5b	-380
WWR W-5d	-2150		
WWR E-1a	700	WWR E-1b	2100
WWR E-1d	300	WWR E-1e	1330
WWR E-2c	1300	WWR E-2d	-520
WWR E-2e	-1650		
WWR E-3a	3540	WWR E-3b	1650
WWR E-3d	-1000	WWR E-3e	-1820
WWR E-4a	-610	WWR E-4b	-820
WWR E-4c	-400	WWR E-4d	-1420
WWR E-4e	-720		
WWR E-5a	-410	WWR E-5c	-800
WWR E-5e	-1930		
Web W-1	750	Web W-3	1850
Web E-1	920	Web E-2	1800
Web E-3	1860		

Note: Force-Strain graphs for Shear Wall No. 3 strain gauges are provided in Appendix B.3.

5.6.5 Shear Wall No. 3 – Test Results

Wall 3 behaved in a ductile manner and eventually failed by the buckling of longitudinal bars under compression, as shown in Figure 5.41. The hysteretic Force-Displacement relationship based on the applied actuator force and lateral top displacement (and drift) is shown in Figure 5.42. The lateral force was then refined to exclude the horizontal force component of vertical prestressing force during lateral displacements. The net lateral force vs. top lateral displacement (and drift) relationship is depicted in Figure 5.43. Finally, the applied moment vs. lateral displacement (and drift) relationship is plotted as shown in Figure 5.44. The lateral moment was obtained by adding the net lateral load times the shear span to the secondary moment due to the vertical prestressing tendon forces. The cable transducer measuring the top of the wall horizontal deformation malfunctioned as the wall started failing rapidly. The force-displacement relationship at this failure point is shown as dotted line.

Figure 5.41 Shear Wall No. 3 Failure Photos

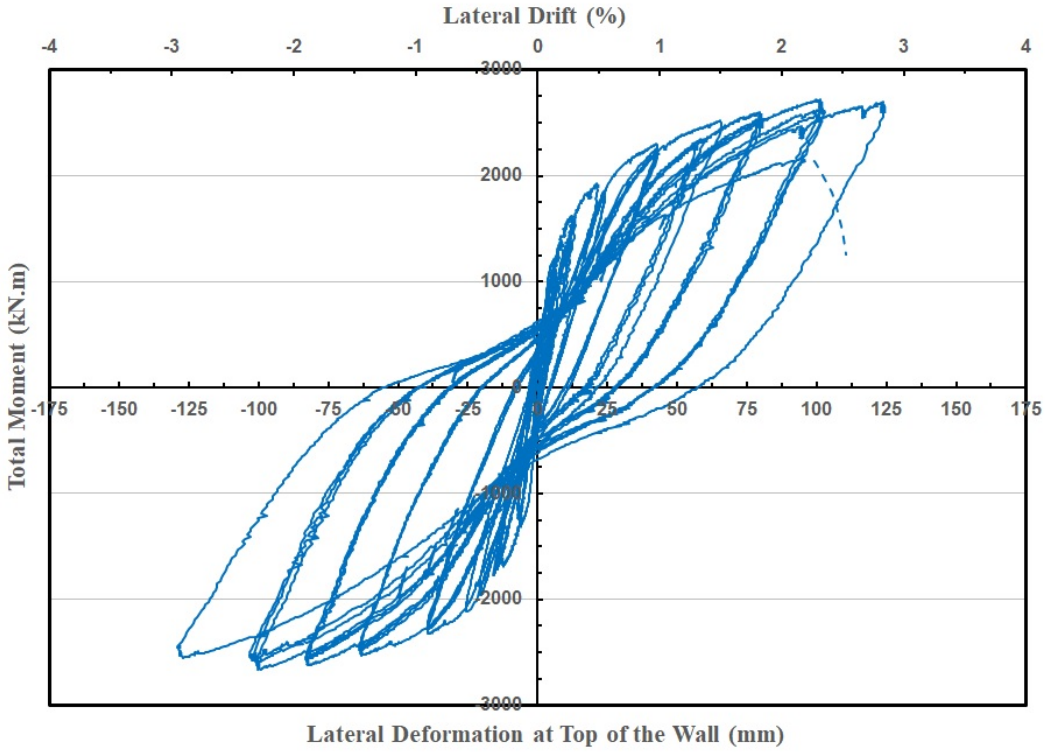

Figure 5.42 Shear Wall No. 3 – Applied Lateral Force by Actuator vs. Lateral Deformation

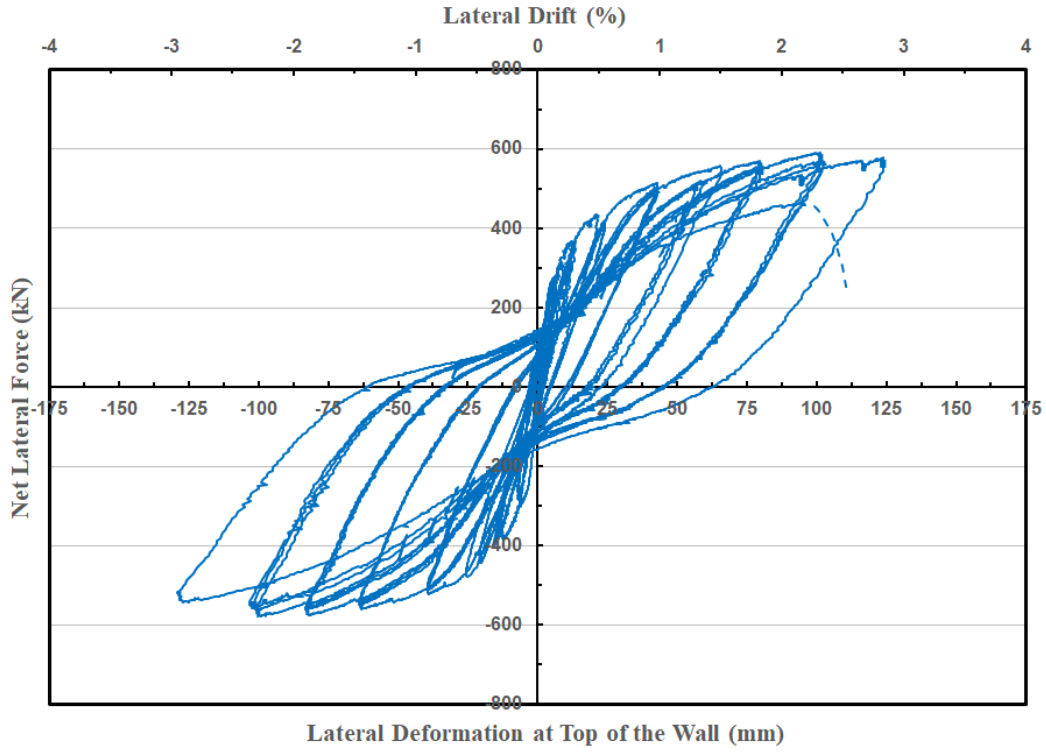

Figure 5.43 Shear Wall No. 3 – Net Lateral Force vs. Lateral Deformation

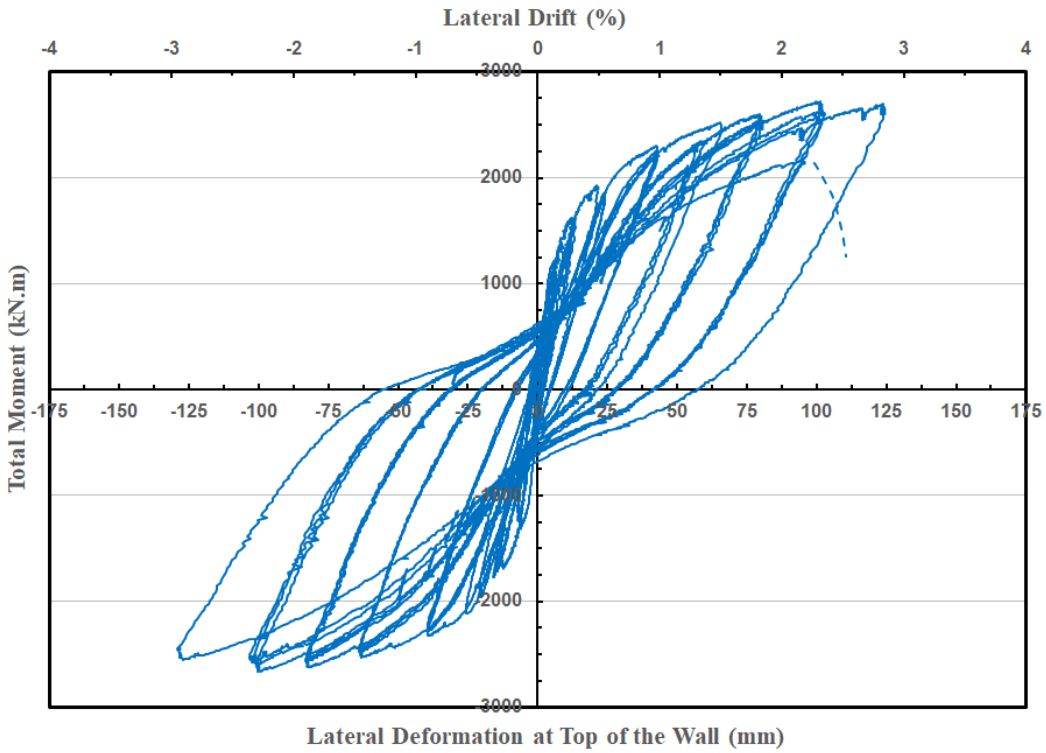

Figure 5.44 Shear Wall No. 3 – Applied Moment vs. Lateral Deformation

Chapter 6

Analytical Research – Computer Modelling

6.1 General

Analytical research was conducted to expand the experimental results and develop a design procedure for use of WWGs as boundary element transverse reinforcement. The shear wall specimens tested were modelled in VecTor2 finite element analysis software bundle. The software provided capabilities for modelling non-linear behavior of reinforced concrete elements under reversed cyclic loading, while incorporating shear-flexure interaction. This capability of the analytical tool is of utmost importance especially for shear walls as they are typically subjected to significant shear stresses, even if the walls were designed to fail in flexure. The analytical research is divided into two phases: i) Validation of analytical models; ii) Analytical parametric investigations.

The test walls were modelled and analyzed under the loading history applied during the experimental phase. This would generate inelastic static analysis under reversed cyclic loading. Experimental and analytical hysteretic relationships were then compared to validate the models.

Upon the validation of wall models, stress-strain characteristics of WWR grids were varied to conduct analytical parametric investigation. Currently there are concerns on the use of WWR in earthquake resistant structural elements as welds could show premature failure. ACI318-14 has recently disallowed the use of WWR in earthquake resisting construction because of mixed performance reports. The wall tests reported in Chapter 5 indicate adequate member ductility.

However, weld failures were observed in wall tests when the grids engaged in restraining the longitudinal compression bars against buckling and maintaining bond stresses between concrete and steel in lap regions. Earlier tests on columns conducted by Saatcioglu and Grira (1999) indicated favorable performance of grids, with ductile post-yield behavior of grid welds. Tests on coupling beams reinforced with WWR grids as transverse shear reinforcement (Ozkan and Saatcioglu 2018), and the shear wall tests reported in Chapter 5 show limited, but perhaps adequate deformability. It appears that lack of inelastic deformability may be offset in design by reduced design strength. These aspects of the design process were assessed analytically by conducting wall analysis with reduced weld strengths. The grids were modelled with due consideration given to their stress-strain characteristics with implications on bar buckling and concrete confinement in shear wall boundary elements. The analysis results shed more light on the ability of WWR steel strains, as the test results indicated higher strains in grid crossties, though weld failures occurred around the perimeter weld connections.

6.2 Analysis Software – VecTor2 Bundle

Analytical investigation requires computer software that incorporates inelastic material characteristics for reinforced concrete shear walls under combined flexure and shear. The selected software should have the capability of processing post-yield non-linear behavior of concrete as a composite material under shear-flexure interaction. It should also be able to implement post-yield behavior of longitudinal steel reinforcement and simulate confinement of concrete in core regions of boundary elements. VecTor2 software bundle which was developed at University of Toronto is selected for the analytical research. VecTor2 software bundle was introduced as a "complete package for the Nonlinear Analysis of Two-Dimensional Reinforced Concrete Membrane Structures". The software bundle includes the following modules: ***VecTor2, FormWorks and Augustus*** (University of Toronto website, 2017).

Formworks module has multiple interfaces to allow the user to create the geometry of the model, create finite element mesh, define and assign composite materials, select analytical models for material behavior, define and assign reinforcement, define load types (gravity, axial and lateral loads in current study), define load magnitudes and loading steps.

A computer model of each shear wall was generated to validate the expected inelastic static behavior of walls under reverse cyclic loading. Upon completion of the model, ***Vector2 Processor module*** is run using the model and analyze the structure. The output of the numerical calculation is accessed and reviewed using ***Augustus Post-Processing Module***. The following shear wall analysis output data is reported in this Chapter: i) Top wall lateral force-lateral displacement hysteretic response, ii) vertical stress of the finite element in unconfined concrete cover of boundary element's outside face, iii) vertical stress of the finite element in confined concrete core of boundary element, iv) horizontal stress of smeared reinforcement in boundary elements, and v) vertical stresses of the longitudinal bars placed at wall extreme ends at wall/foundation interface.

6.3 Validation of Analytical Models

The test walls are modelled and analyzed under the loading history applied during the experimental phase. This will result in inelastic static analyses under reversed cyclic loading. Experimental and analytical hysteretic relationships are compared to validate the models. VecTor2 Software provides a range of numerical modelling techniques for modelling the behavior of materials under various loading conditions and types of material used. The modelled shear walls mostly require the suggested default models with the exception of a few adjustments to better address the specifics of current research study. Below is the summary of the selected material behavior models. Figure 6.1 depicts the screenshot of Model Interface in the FormWorks module.

Concrete Models:

- ***Compression Pre-Peak:*** Hognestad (Parabola)
- ***Compression Post-Peak:*** Modified Park-Kent
- ***Compression Softening:*** Vecchio 1992-A
- ***Tension Stiffening:*** Vecchio 1982
- ***Tension Softening:*** Bilinear
- ***FRC Tension:*** SDEM – Cyclic
- ***Confined Strength:*** Kupfer/Richart
- ***Dilation:*** Variable – Isotropic
- ***Crack Criterion:*** Mohr-Coulomb (Stress)

- ***Hysteretic Response:*** Palermo 2002 (w/ Decay)

Reinforcement Models:

- ***Hysteretic Response:*** Bauschinger Effect (Seckin)
- ***Dowel Action:*** Tassios (Crack Slip)
- ***Buckling:*** Akkaya 2012 (Modified Dhakal-Maeka)

Bond Model:

- ***Concrete Bond:*** Eligehausen

Analysis Modes:

- ***Strain History:*** Previous Loading Considered
- ***Structural Damping:*** Not Considered
- ***Geometric Nonlinearity:*** Considered

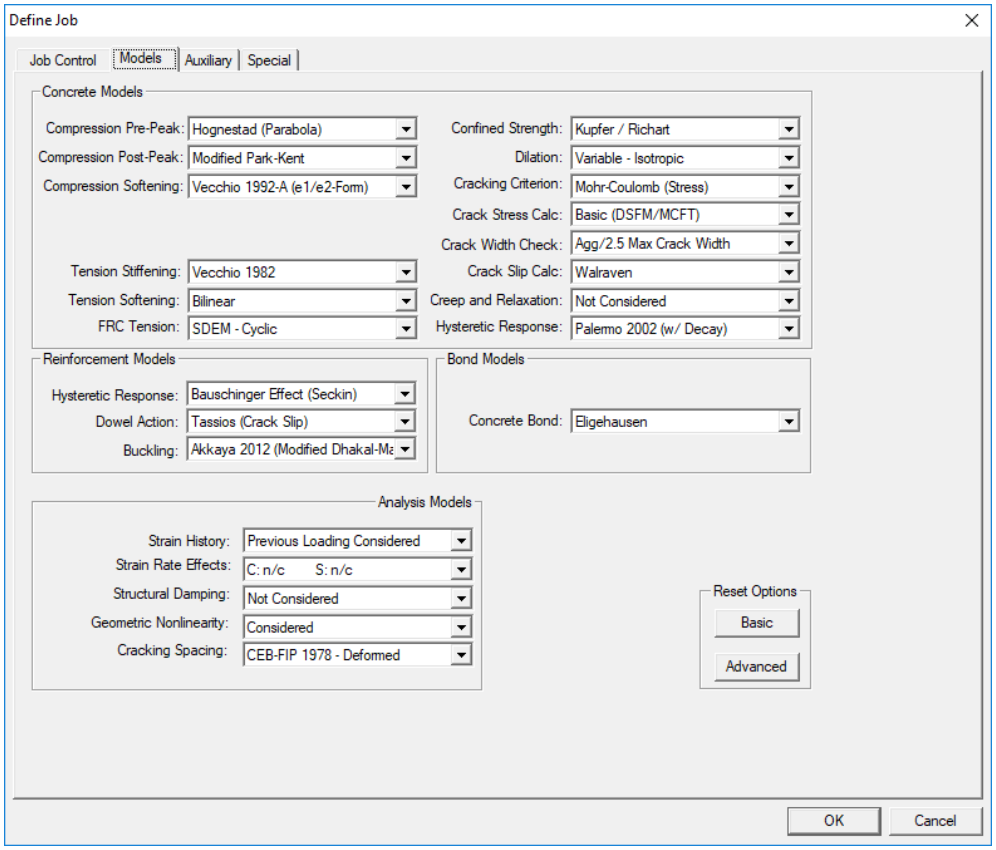

Figure 6.1 Material Behavior Model Interface in FormWorks Software

VecTor2 shear wall models are comprised of a series of finite elements, interacting and influencing each other through common nodes. The models are subjected to vertical loads, representing the axial load applied by prestressing tendons and horizontal loads applied by MTS hydraulic actuator(s). The vertical loads are applied as a series of point loads on nodes along the loading beam on top of the wall. In the VecTor2 model, the vertical loads remain vertical throughout the analyses as modelled walls are deformed laterally, unlike the loads from the prestressing cables in the experimental program where the force magnitude in cables vary slightly while a small horizontal force component in the opposite direction of the applied load is produced. The hysteretic response of the wall tests presented in Chapter 5, Figures 5.14, 5.27 and 5.43 illustrate net horizontal force vs. lateral displacement relationships of shear walls. The net horizontal force takes into consideration the correction for horizontal force component in the cables. Therefore, the results of the VecTor2 analyses are compared with the net force-displacement graphs. The vertical loads also included as gravity loads.

The horizontal load is assigned as a single point load at the centerline of the MTS actuator on the loading beam on top of the shear wall. The horizontal load is displacement controlled, which means the load is gradually increased until the pre-selected displacement step is achieved. The horizontal load is defined as "reverse cyclic" and the wall is subjected to incrementally increasing push-pull load cycles until the wall is reached its ultimate capacity.

6.3.1 VECTOR2 Model – Shear Wall No. 1

Shear Wall No. 1 is modelled in VecTor2 Software using the material properties which were established in Chapter 3 through standard material testing. The model includes three (3) segments: i) Foundation, ii) Loading beam, and iii) Shear Wall. The geometry of the wall is divided and meshed manually to maintain a height to length aspect ratio of between 1 and 2. The steel reinforcement is introduced as smeared reinforcement with the exception of longitudinal bars which are modelled individually. The mechanical properties, as well as reinforcement ratio of each segment of the wall is presented below. Figure 6.2 shows a screenshot of the modelled shear wall No. 1 in VecTor2 Software.

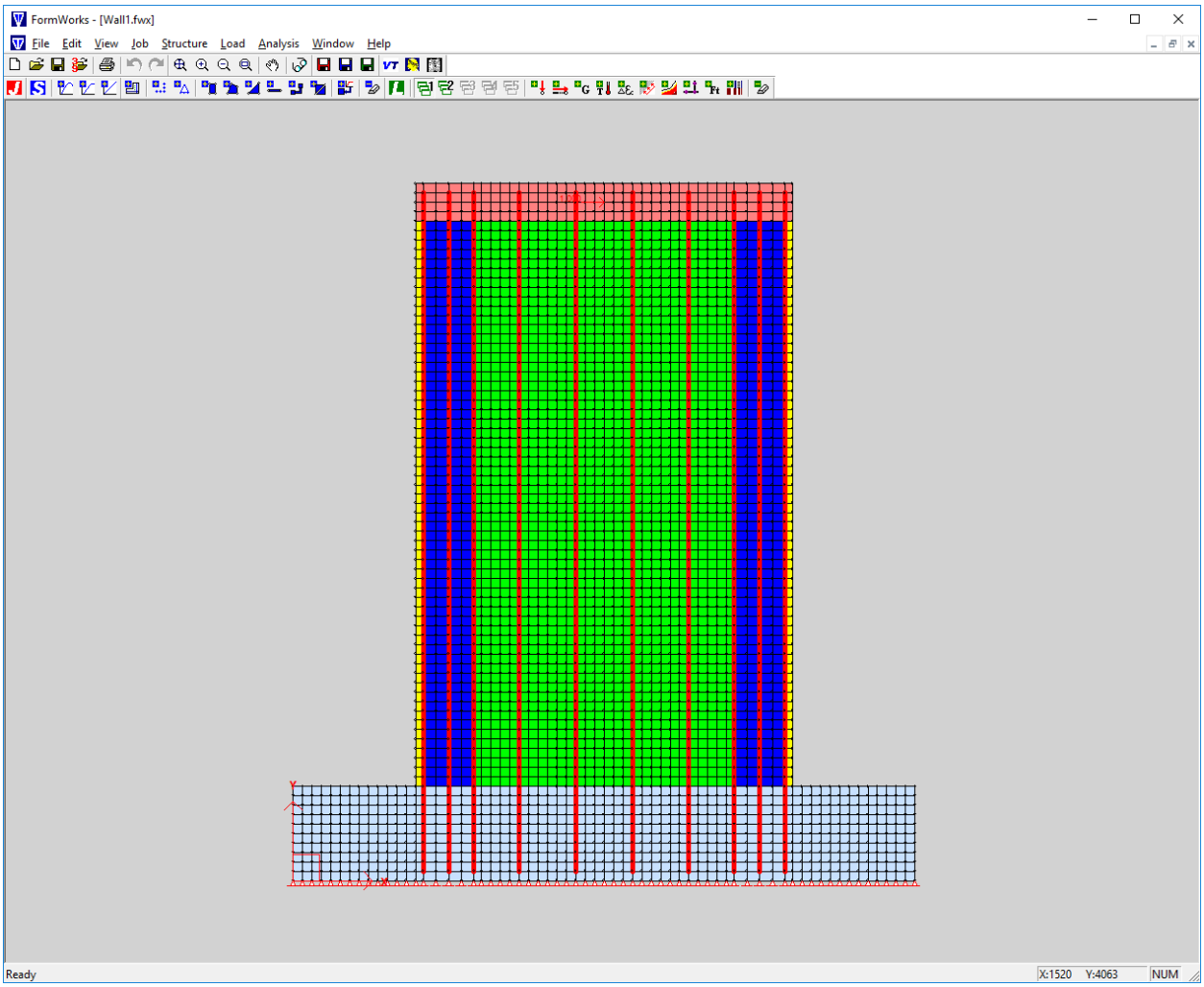

Figure 6.2 VecTor2 Model of Shear Wall No. 1 using FormWork Modelling Interface

Element Properties – Web Reinforcement:

Web horizontal reinforcement is modelled as smeared reinforcement having 0.333% steel

Web vertical reinforcement is modelled as individual bars with an unsupported length to diameter (b/t) ratio of 30. These vertical bars are modelled as unconfined bars.

Element Properties – Boundary element:

Web horizontal reinforcement is extended into boundary element as smeared reinforcement having 0.333% steel.

Horizontal component of WWR grid reinforcement is modelled as having 0.71% steel.

Out-of-Plane component of WWR grid reinforcement is modelled as having 0.79% steel.

Boundary element longitudinal bars are modelled as individual bars with an unsupported length to diameter (b/t) ratio of 6.67. These vertical bars are modelled as confined bars.

The concrete cover is modelled as unreinforced, unconfined concrete.

The initial VecTor2 model is developed with the assumption that the grids were able to exhibit a fully ductile behavior where the welds have sufficient capacity to allow the grids to yield and reach their post-yield ultimate capacity as shown in Chapter 3 tension coupon tests. This provides an overall benchmark as to the best-case scenario of a wall that is designed and built with these grids. The parametric study, which is presented later in this Chapter, considers the full range of grid capacities, including revised models to illustrate the consequence of weld failure. Figure 6.3 illustrates the hysteretic response of Shear Wall No. 1 model using ductile WWR grids with a yield strength of $F_y = 550\ MPa$ and an ultimate strength of $F_u = 640\ MPa$ corresponding to an average strain of 4.35%. The hysteretic response of Shear Wall No. 1 is presented in Figure 6.3 with experimental and VecTor2 analysis results, respectively.

The experimental research showed maximum recorded forces of +905 kN and -880 kN in push and pull directions, respectively. In addition, the specimen exhibited yielding at 0.36% drift and failed in shear (diagonal tension) at 0.78% drift cycle after completing the 0.59% drift cycle successfully. In comparison, the VecTor2 analysis showed +958 kN and -955 kN maximum forces in push and pull directions, respectively. The VecTor2 model yielded at 0.33% drift and failed during the 1.62% drift cycles after successfully completing the 1.29% drift cycles. The shear failure in Shear Wall No. 1 is associated with the detailing of shear reinforcement in the web of the wall where straight bars were placed on the outside face of the boundary elements without bend or hooks. These horizontal bars were not able to achieve their development capacity within the boundary element and caused inadequate shear capacity as the shear demand increased. Shear Wall No. 1 was designed with the intent of promoting shear failure to assess the performance of the grids in boundary elements with extensive shear cracks. The analysis output showed a maximum concrete stress value of 52.9 MPa and 70.0 MPa for the unconfined skin concrete element and confined core concrete element respectively. The unconfined, unreinforced concrete cover element spalled off after being pushed to the recorded stress value for the first time and then

carried almost no load for the rest of the analysis. The analysis also showed a maximum horizontal tensile stress of 460 MPa in the smeared reinforcement at the wall/foundation interface of the boundary element. The longitudinal bars in the extreme ends of the wall showed maximum tensile stress of 617.8 MPa and maximum compressive stress of 529.9 MPa.

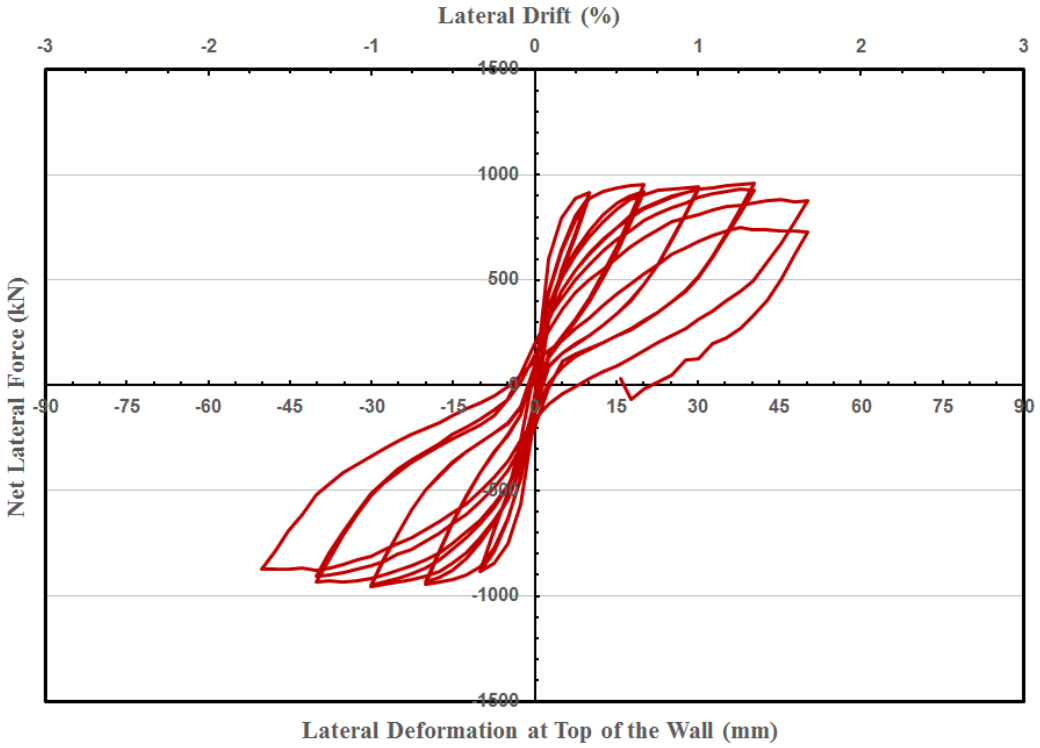

Figure 6.3 Shear Wall No. 1 Hysteretic Response – Analytical Vs. Experimental
Fy =550 MPa, Fu = 640 MPa

6.3.2 VECTOR2 Model – Shear Wall No. 2

Shear Wall No. 2 is modelled in VecTor2 Software using the material properties established in Chapter 3 through standard material testing. The model includes three (3) segments: i) Foundation, ii) Loading beam, and iii) Shear Wall. The geometry of the wall is divided and meshed manually to maintain a height to length aspect ratio of between 1 and 2. The steel reinforcement is introduced as smeared reinforcement with the exception of longitudinal bars which are modelled individually. The mechanical properties, as well as the reinforcement ratio of each segment of the wall is presented below. Figure 6.4 shows a screenshot of the Shear Wall No. 2 model in VecTor2 Software.

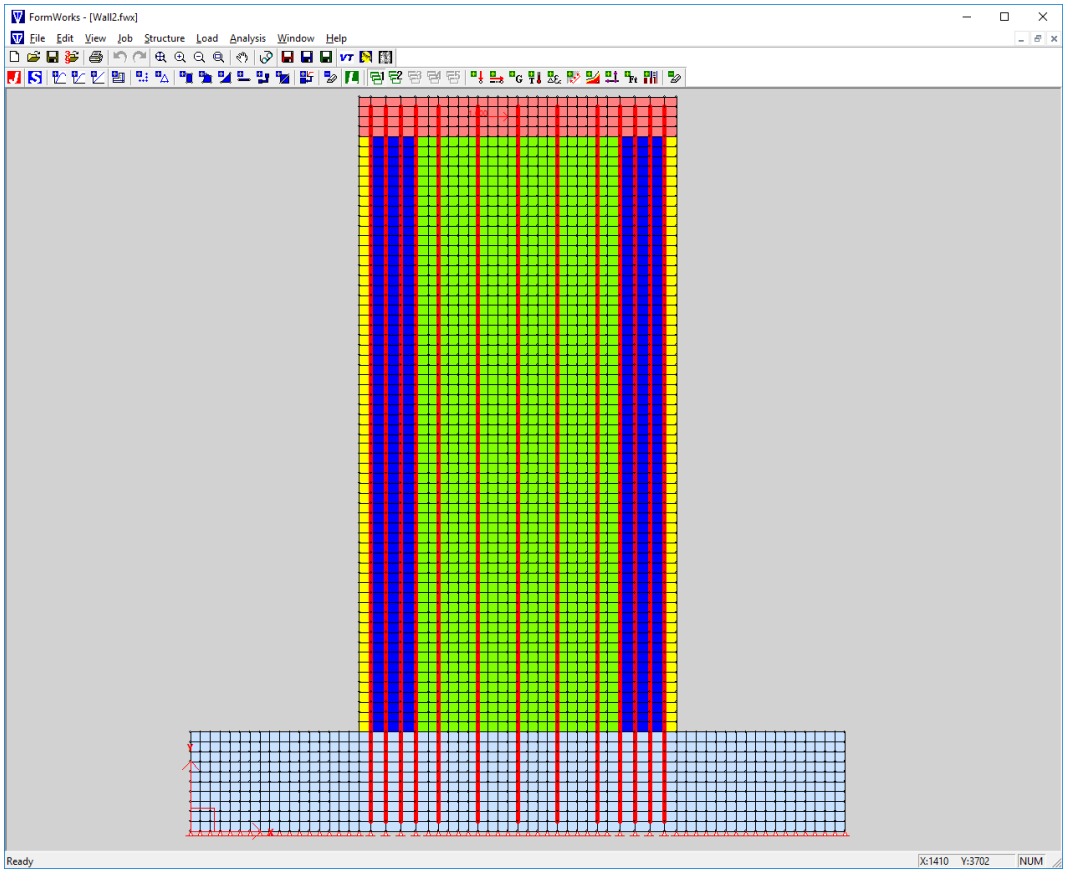

Figure 6.4 VecTor2 Model of Shear Wall No. 2 using FormWork Modelling Interface

Element Properties – Web Reinforcement:

Web horizontal reinforcement is modelled as smeared reinforcement having 1.14% of steel.

Web vertical reinforcement is modelled as individual bars with an unsupported length to diameter (b/t) ratio of 17.5. These vertical bars are modelled as unconfined bars.

Element Properties – Boundary element:

Web horizontal reinforcement is extended into the boundary element as smeared reinforcement having 1.14% steel.

Horizontal component of WWR grid reinforcement with 1.42% steel.

Out-of-Plane component of WWR grid reinforcement with 1.94% steel.

Boundary element longitudinal bars are modelled as individual bars with an unsupported length to diameter (b/t) ratio of 3.75. These vertical bars are modelled as confined bars.

The concrete cover is modelled as unreinforced concrete.

The initial VecTor2 model is developed with the assumption that the grids were able to exhibit a fully ductile behavior where the welds have sufficient capacity to allow the grids to yield and reach their post-yield ultimate capacity as shown in Chapter 3 tension coupon tests. This provides an overall benchmark as to the best-case scenario of a wall that is designed and built with these grids. The parametric study presented later in this Chapter, considers the full range of grid capacities, with revised models to illustrate the consequence of weld failure. Figure 6.5 illustrates the hysteretic response of the model for Shear Wall No. 2 using ductile WWR grids having a yield strength of $F_y = 550\ MPa$ and an ultimate strength of $F_u = 640\ MPa$ corresponding to an average strain of 4.35%. The experimentally obtained hysteretic response is also included in Figure 6.5 for comparison.

The test data indicated maximum recorded forces of +1288 kN and -1185 kN in push and pull directions respectively. In addition, the specimen yielded at 0.42% drift and failed at 3.78% drift cycle after completing the 3.16% drift cycle successfully. In comparison, the VecTor2 analysis showed +1243 kN and -1223 kN maximum forces in push and pull directions, respectively. The VecTor2 model yielded at 0.41% drift and failed during 3.50% drift cycle after successfully completing the 2.86% drift cycle. Shear Wall No. 2 behaved in a ductile manner and failed by rupturing of the longitudinal bars because of excessive lateral dift. The analysis output showed a maximum concrete stress value of 92.5 MPa and 137.8 MPa for the unconfined skin concrete element and confined core concrete element, respectively. The unconfined, unreinforced concrete cover element spalled off after being pushed to the recorded stress value for the first time and then carried almost no load for the rest of the analysis. The analysis also showed a maximum horizontal tensile stress of 460 MPa in the smeared reinforcement at the wall/foundation interface of the boundary element. The longitudinal bars in the extreme ends of the wall showed maximum tensile stress of 687.3 MPa and maximum compressive stress of 634.2 MPa. The computed maximum tensile stress in longitudinal reinforcement is comparable to the ultimate tensile rupturing strength of 710 MPa obtained from the coupon tests as reported in Fig. 3.1, explaining the experimentally observed failure mode by rupturing of longitudinal reinforcement.

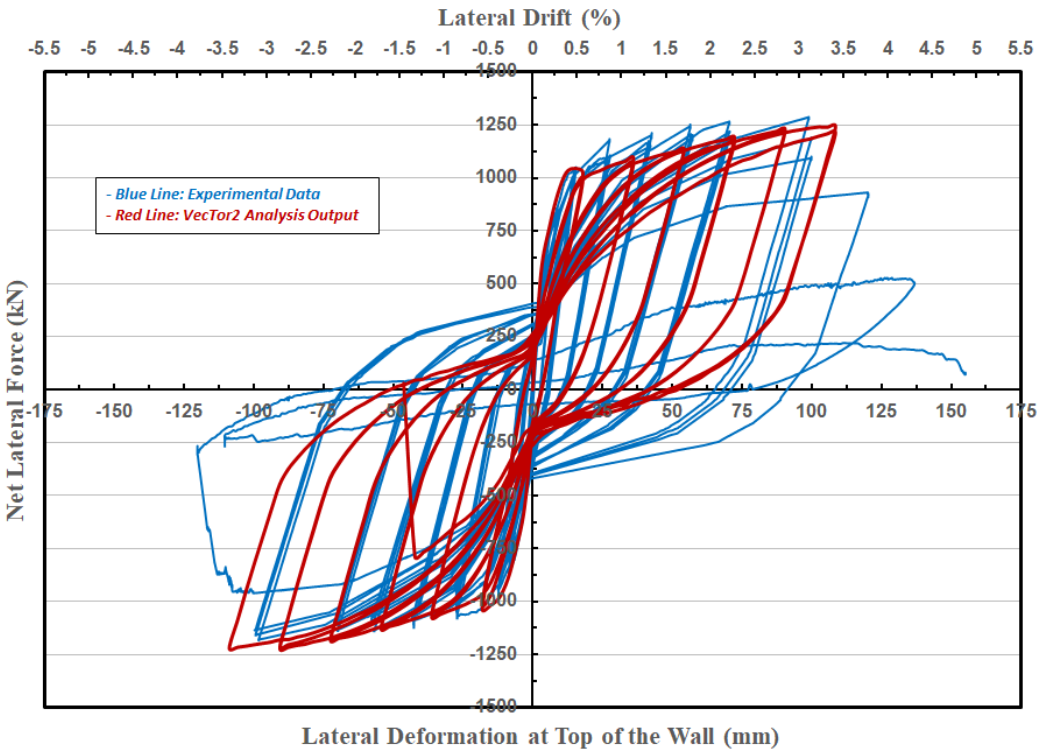

Figure 6.5 Shear Wall No. 2 Hysteretic Response – Analytical Vs. Experimental
Fy =550 MPa, Fu = 640 MPa

6.3.3 VECTOR2 Model – Shear Wall No. 3

Shear Wall No. 3 is modelled in VecTor2 Software using the material properties which were established in Chapter 3 through standard material testing. The model includes three (3) segments: i) Foundation, ii) Loading beam, and iii) Shear Wall. The geometry of the wall is divided and meshed manually to maintain a height to length aspect ratio of between 1 and 2. The steel reinforcement is introduced as smeared reinforcement with the exception of longitudinal bars which are modelled individually. The mechanical properties, as well as the reinforcement ratio for each segment of the wall is presented below. Figure 6.6 shows a screenshot of the Shear Wall No. 3 model in VecTor2 Software.

Element Properties – Web Reinforcement:

Web horizontal reinforcement is modelled as smeared reinforcement having 0.8% steel.

Web vertical reinforcements are modelled as individual bars with an unsupported length to diameter (b/t) ratio of 25. These vertical bars are modelled as unconfined bars.

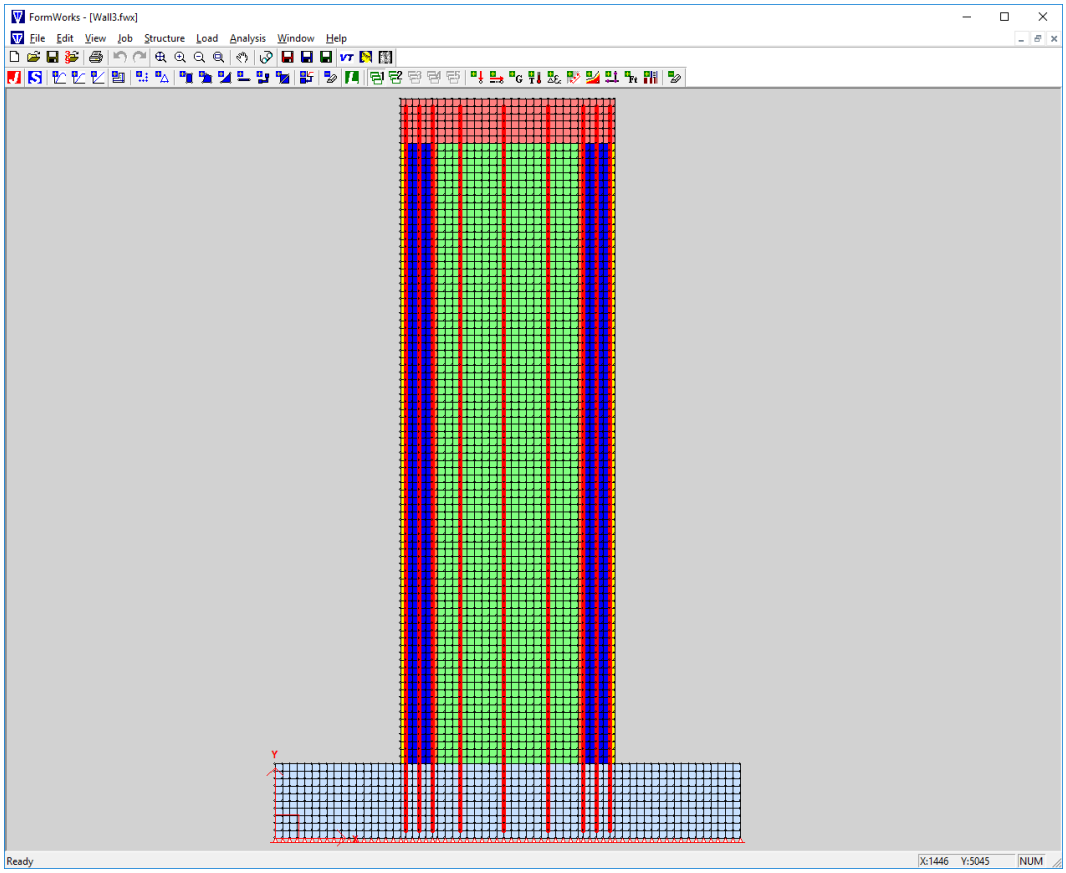

Figure 6.6 VecTor2 Model of Shear Wall No. 3 using FormWork Modelling Interface

Element Properties – Boundary element:

Web horizontal reinforcement is extended into boundary element as smeared reinforcement having 0.8% steel.

Horizontal component of WWR grid reinforcement with 1.14% steel.

Out-of-Plane component of WWR grid reinforcement with 1.58% steel.

Boundary element longitudinal bars are modelled as individual bars with an unsupported length to diameter (b/t) ratio of 5. These vertical bars are modelled as confined bars.

The concrete cover is modelled as unreinforced concrete.

The initial VecTor2 model is developed with the assumption that the grids were able to exhibit a fully ductile behavior where the welds have sufficient capacity to allow the grids to yield and reach their post-yield ultimate capacity as shown in Chapter 3 tension coupon tests. This provides an

overall benchmark as to the best-case scenario of the wall that is designed and built with these grids. The parametric study segment presented later in this Chapter, considers the full range of grid capacities, with revised models illustrating the consequences of weld failure. Figure 6.7 illustrates the computed hysteretic response of Shear Wall No. 3 model using ductile WWR grids with a yield strength of $F_y = 550\ MPa$ and an ultimate strength of $F_u = 640\ MPa$ corresponding to an average strain of 4.35%. The experimentally recorded hysteretic response of Shear Wall No. 3 is also presented in the same figure for comparison.

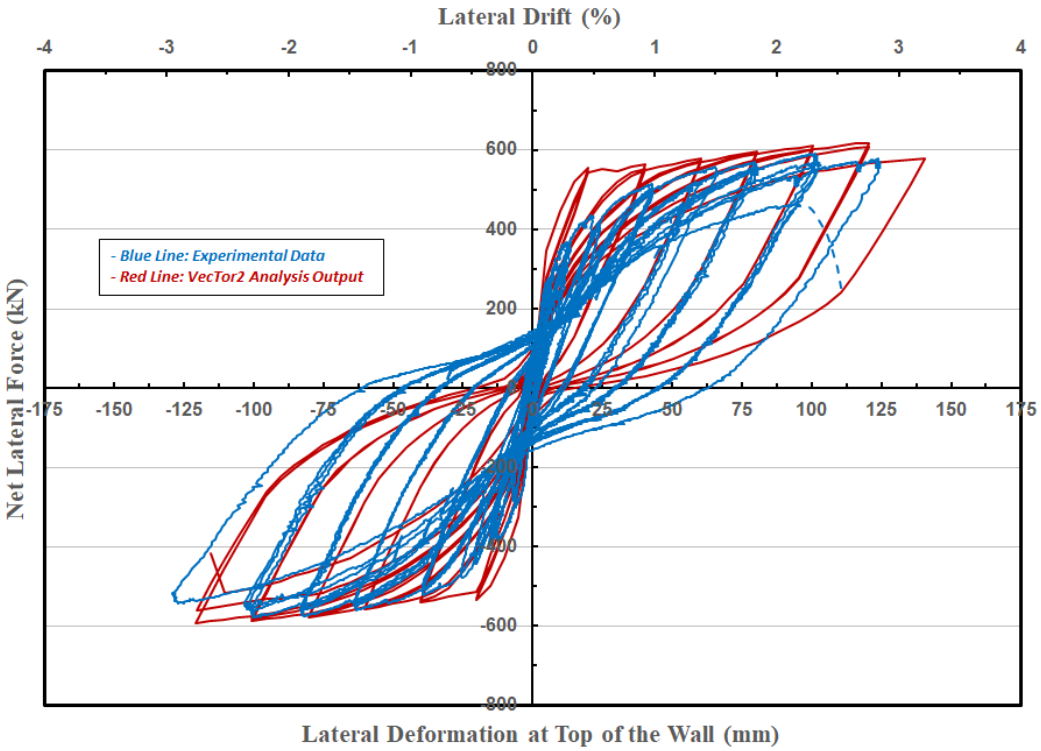

Figure 6.7 Shear Wall No. 3 Hysteretic Response – Analytical Vs. Experimental
Fy =550 MPa, Fu = 640 MPa

The experimental research showed maximum recorded forces of +592 kN and -578 kN in push and pull direction, respectively. In addition, the specimen yielded at 0.52% drift and failed during 2.84% drift cycle after completing the 2.39% drift cycle successfully. In comparison, the VecTor2 analysis showed +618 kN and -592 kN maximum forces in push and pull directions, respectively. The VecTor2 model yielded at 0.46% drift and failed during 3.25% drift cycles after successfully completing the 2.82% drift cycles. Shear Wall No. 3 behaved in a ductile manner and failed by buckling of the longitudinal bars in compression. The analysis output showed a maximum concrete stress value of 89.9 MPa and 133.4 MPa for the unconfined skin concrete element and confined

core concrete element respectively. The unconfined, unreinforced concrete cover element spalls after being pushed to the recorded stress value for the first time and then carries almost no load for the rest of the analysis. The analysis also showed a maximum horizontal tensile stress of 460 MPa in the smeared reinforcement at the wall/foundation interface of the boundary element. The longitudinal bars in the extreme ends of the wall showed maximum tensile stress of 649.2 MPa and maximum compressive stress of 634.2 MPa.

6.4 Analytical Parametric Investigation

Upon the validation of the wall models, the stress-strain characteristics of WWR grids were varied to conduct analytical parametric investigation. The possibility of offsetting lack of inelastic deformability due to premature weld failure by reducing steel design strength was investigated analytically. The grids were modelled by capping their ultimate capacity at assumed weld failure strength. This was done by reducing the yield strength of transverse steel in the analytical model (to reflect premature weld failure), and setting the ultimate capacity of steel equal to the yield strength.

ASTM 1064 considers 241 MPa as the minimum weld strength for WWR to be acceptable for use in structural applications in earthquake resistant structures. This strength limit was used as the lower bound strength in the parametric investigation. In addition, grid capacities of 400 MPa and 500 MPa were modelled to provide an understanding of the sensitivity of wall behavior to grid strength. The upper bound strength used in the parametric investigation corresponded to the use of the stress-strain relationship obtained from the wire coupon tests reported in Chapter 3 (yield strength of 550 MPa with an ultimate strength of 640 MPa) assuming the welds would not fail prematurely and the grid steel would follow the stress-strain relationship established by the wire coupon tests. The computed hysteretic relationships for the latter case are presented in Figures 6.3, 6.5 and 6.7 for the three shear walls tested.

The effect of a weld failure at a grid joint, while the grids above and below remain intact as observed in some tests, was also studied as the second parameter. This time the spacing of grids was increased by a factor of two. This had an implication on the volumetric ratio of transverse reinforcement for the smeared reinforcement model, as well as the buckling length of longitudinal

bars between the ties. Hence, the volumetric ratio was reduced by a factor of 2 and the unsupported length of the longitudinal bars in the boundary elements was increased by a factor of two. This parameter also reflected the effect of using widely spaced grid reinforcement in shear wall boundary elements. The entire set of analysis included shear wall models with grid strengths of 241, 400, 500 MPa, where yield and ultimate strengths were assumed to coincide, as well as the use grids without the weld failure (ductile stress-strain relationship as obtained from wire coupon tests, i.e., f_y = 550 MPa and f_u = 640 MPa). The results of these computer models are presented in subsequent section.

6.4.1 Parametric Investigation – Shear Wall No. 1

The first set of analysis in the parametric study of Shear Wall No 1 involved the investigation of premature weld failure, as described in Section 6.4. Figures 6.8 to 6.10 show the results of Shear Wall 1 analysis with different grid strengths. The results indicate that the overall wall capacity is not affected by the variation in grid strength. However, the ductility of the wall is significantly reduced as the grid strength and the ability to confine core concrete and restrain longitudinal bars against buckling is reduced. The shear wall models with 241, 400 and 500 MPa grid strengths failed during 0.97%, 1.30%, and 1.30% drift cycles after successfully completing three cycles at 0.65%, 0.97% and 0.97% drift ratios, respectively. The shear wall model with fully ductile grids, as shown in Figure 6.3, failed during 1.62% drift cycle after successfully completing three cycles at 1.29% drift. The experimental results for Shear Wall No. 1 indicate that the wall failed during 0.78% drift cycles after completing three successful cycles at 0.59% drift.

Maximum concrete and steel stresses were also recorded in the above analyses to assess wall performance. The skin concrete element located at the exterior most compression corner of unconfined cover concrete indicated maximum compressive stresses of 52.1, 52.6 and 52.4 MPa, respectively for the three brittle grid cases considered, respectively with gradually reducing strengths. The same element in the cover showed maximum compressive stress of 52.9 MPa when the grid behavior was assumed to be ductile, corresponding to the wire stress-strain relationship recorded by coupon tests. The cover concrete spalled off immediately after experiencing these maximum stresses, and stopped providing compressive resistance for the rest of the analysis. The confined core concrete element at the extreme compression region of the boundary element showed somewhat increased compressive resistance with maximum compressive stresses of 58.4,

63.0 and 66.7 MPa when the previously indicated three brittle grids were used, respectively with reduced strengths. The same confined core concrete element showed an increased maximum compressive stress of 70 MPa when ductile grid properties were specified based on the wire stress-strain relationship.

The stresses in transverse boundary element reinforcement (WWR) were also recorded for further assessment. Maximum horizontal tensile stresses of 460, 460 and 460 MPa were obtained in smeared reinforcement at the wall/foundation interface when the three brittle grid models were employed with reduced strengths as expressed earlier, respectively. The maximum tensile stress remained the same in the same element when fully ductile grids were used assuming no weld failure. The longitudinal boundary element reinforcement at the extreme end of the wall section was also examined. They developed maximum tensile stresses of 535.5, 557.2 and 566.7 MPa; and maximum compressive stresses of 496.9, 516.0 and 519.1 MPa when the three brittle grid models were employed with reduced strengths as expressed earlier, respectively. The same longitudinal bar showed increased maximum tensile stress of 617.8 MPa and maximum compressive stress of 529.9 MPa when fully ductile grids were used with a stress-strain relationship following that of the wires.

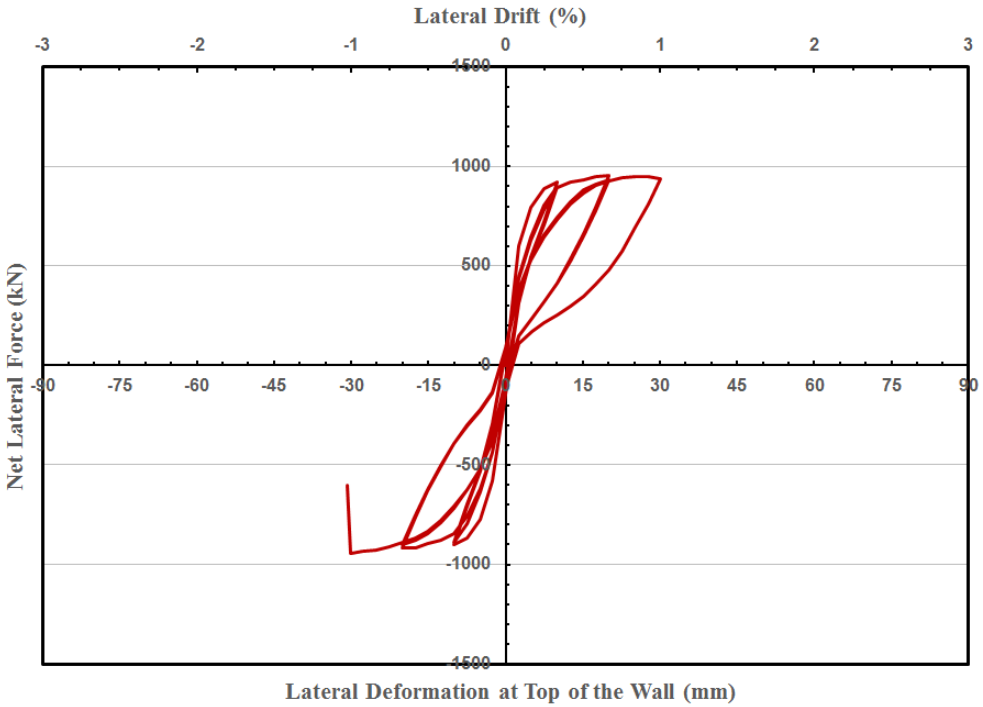

Figure 6.8 Shear Wall No. 1 – WWR Grid with $F_y = 241\ MPa$ and $F_u = 242\ MPa$

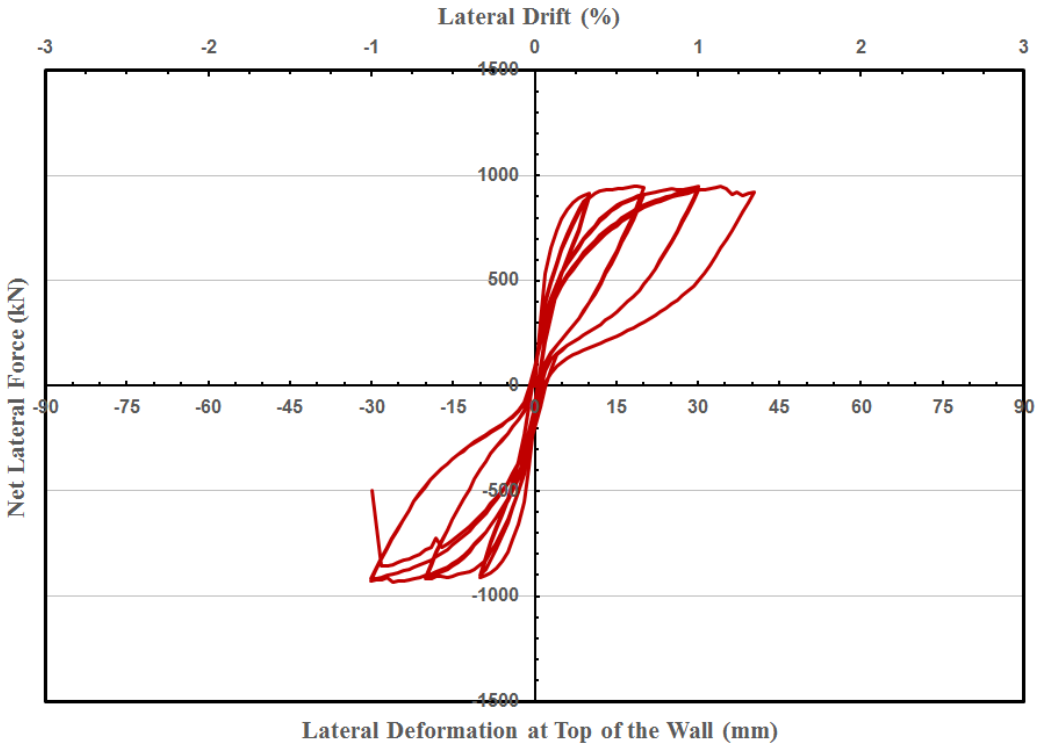

Figure 6.9 Shear Wall No. 1 – WWR Grid with $F_y = 400\ MPa$ and $F_u = 401\ MPa$

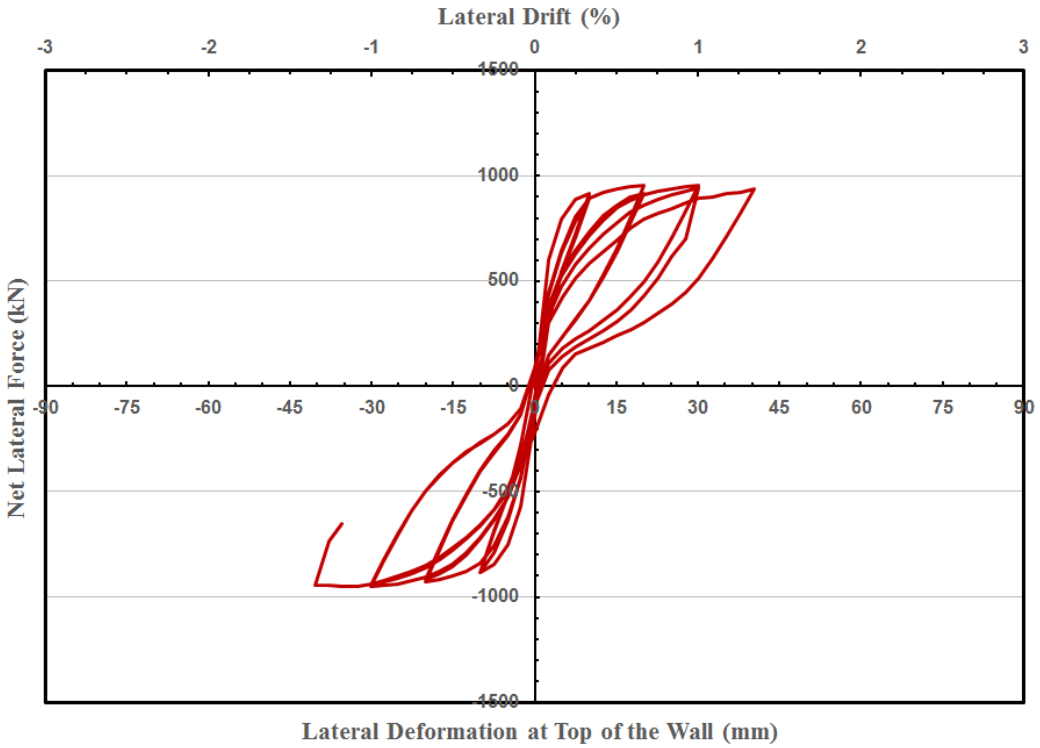

Figure 6.10 Shear Wall No. 1 – WWR Grid with $F_y = 500\ MPa$ and $F_u = 501\ MPa$

The second set of analysis in the parametric study of Shear Wall No 1 involved the investigation of weld failures at one grid location while the grids above and below remained intact. This was done by specifying reduced volumetric ratio of transverse reinforcement and increased buckling length for compression bars as explained in the Section 6.4. This set of analysis also provided insight into the use of different strength grids at increased grid spacing. The hysteretic response of the four VecTor2 models obtained are presented in Figures 6.11 to 6.14 for three brittle grid behaviour models, having 241, 400, and 500 MPa strengths and a ductile grid model having 550 MPa yield strength. The results indicate that the wall developed failure during 0.65%, 0.84%, 1.30% and 1.35% drift cycle, having completed three successful cycles at 0.32%, 0.65%, 0.97% and 1.30% drift ratios, respectively.

The VecTor2 Simulation shows that for the given material properties and weld strength, Shear Wall No. 1 would reach approximately 1.5% ductility, if it did not experience out-of-plane torsional twisting due to the initial test set-up issues and lack of lateral support at the top of the wall.

The analysis output was also examined in terms of maximum concrete and steel stresses generated in representative critical elements. Accordingly, maximum compressive stresses of 51.1, 51.3, 52.5 and 51.4 MPa were observed at wall base in the unconfined skin concrete element located in the extreme fiber of cover concrete when the four grid material models described above were used, respectively. The unconfined concrete cover spalled off shortly thereafter, and stopped carrying any load for the rest of the analysis. As for the confined core concrete in the outermost element, the analysis results showed maximum concrete stresses of 54.5, 55.8, 59.8 and 61.4 MPa when the same four grid material models were employed, respectively.

The reinforcement stresses also changed with grid material models. Maximum horizontal tensile stresses of 247.7, 449.4, 460 and 460 MPa were recorded in smeared reinforcement at the wall/foundation interface of boundary element when the same four grid material models were used, respectively. The longitudinal bars at extreme ends of walls showed maximum tensile stress of 496.1, 518.0, 570.0 and 575.4 MPa; and maximum compressive stress of 428.9, 437.0, 457.4 and 460.0 MPa with the use of the four grid material models, respectively.

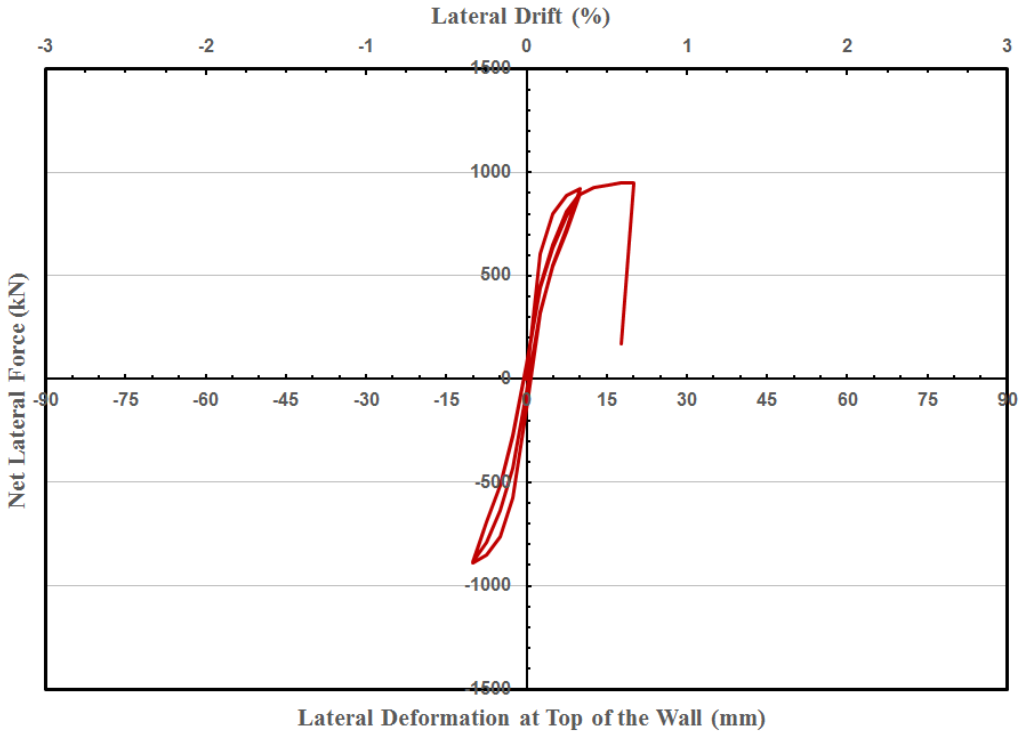

Figure 6.11 Shear Wall No. 1 – WWR Grid with Double Spacing
$F_y = 241\ MPa$ and $F_u = 242\ MPa$

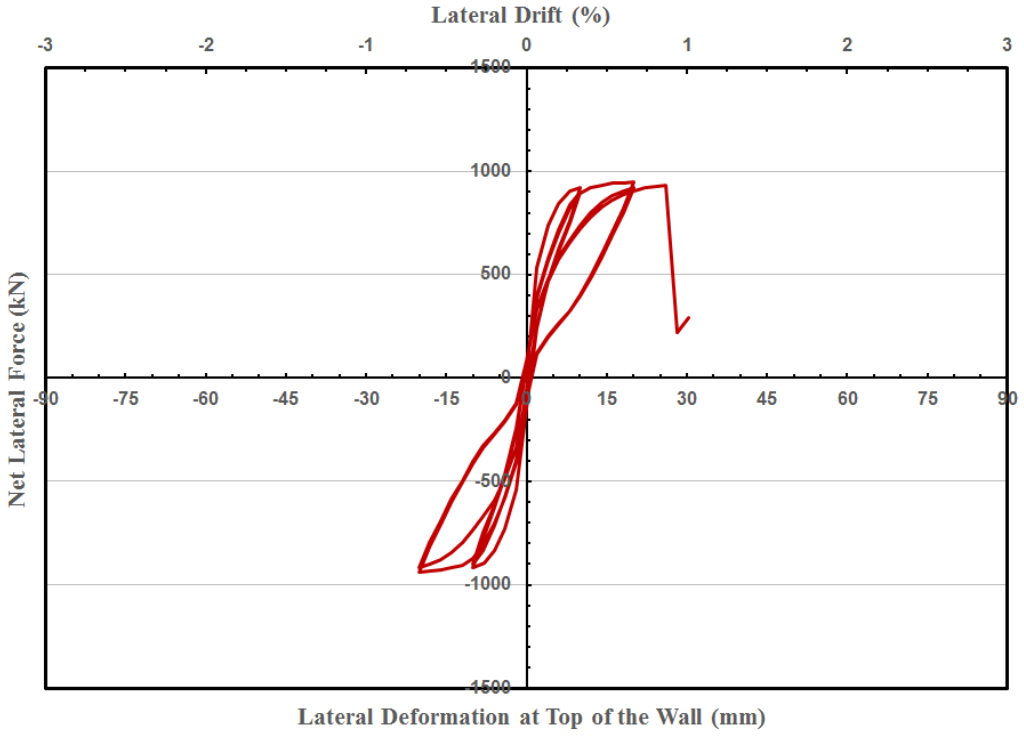

Figure 6.12 Shear Wall No. 1 – WWR Grid with Double Spacing
$F_y = 400\ MPa$ and $F_u = 401\ MPa$

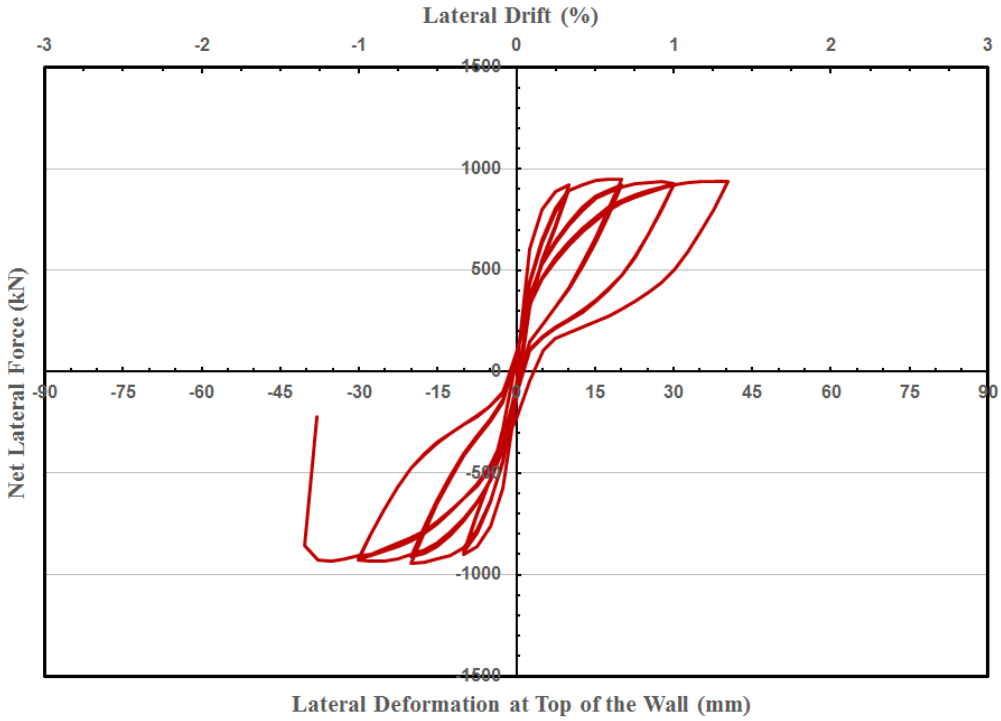

Figure 6.13 Shear Wall No. 1 – WWR Grid with Double Spacing
$F_y = 500\ MPa$ and $F_u = 501\ MPa$

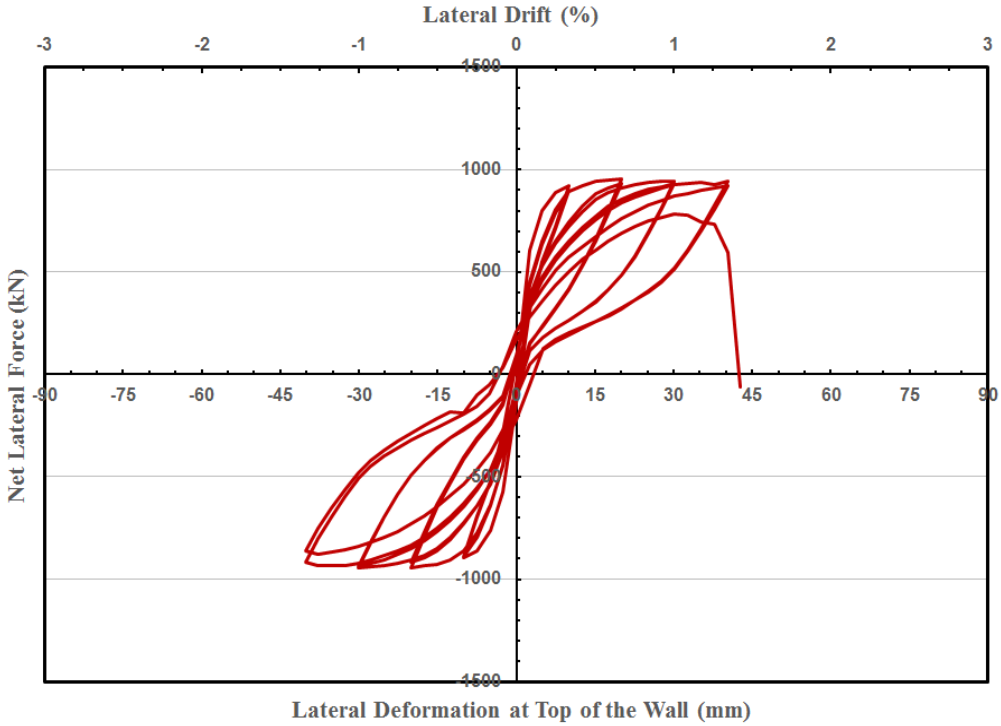

Figure 6.14 Shear Wall No. 1 – WWR Grid with Double Spacing
$F_y = 550\ MPa$ and $F_u = 640\ MPa$

6.4.2 Parametric Investigation – Shear Wall No. 2

The first set of analysis in the parametric study of Shear Wall No 2 involved the investigation of premature weld failure, as described in Section 6.4. Figures 6.15 to 6.17 show the results of Shear Wall 2 analysis with different grid strengths. The results indicate that the overall wall capacity is not affected by the variation in grid strength. However, the ductility of the wall is significantly reduced as the grid strength and the ability to confine core concrete and restrain longitudinal bars against buckling is reduced. The shear wall models with 241, 400 and 500 MPa grid strengths failed during 1.67%, 2.86%, and 3.50% drift cycles after successfully completing three cycles at 1.18%, 2.30% and 2.86% drift ratios, respectively. The shear wall model with fully ductile grids, as shown in Figure 6.3, failed during 3.50% drift cycle after successfully completing three cycles at 2.86% drift. The experimental results for Shear Wall No. 2 indicate that the wall failed during 3.78% drift cycles after completing three successful cycles at 3.16% drift.

Maximum concrete and steel stresses were also recorded in the above analyses to assess wall performance. The skin concrete element located at the exterior most compression corner of unconfined cover concrete indicated maximum compressive stresses of 91.7, 92.4 and 92.5 MPa, respectively for the three brittle grid cases considered, respectively with gradually reducing strengths. The same element in the cover showed maximum compressive stress of 92.5 MPa when the grid behavior was assumed to be ductile, corresponding to the wire stress-strain relationship recorded by coupon tests. The cover concrete spalled off immediately after experiencing these maximum stresses, and stopped providing compressive resistance for the rest of the analysis. The confined core concrete element at the extreme compression region of the boundary element showed somewhat increased compressive resistance with maximum compressive stresses of 110.6, 124.5 and 131.7 MPa when the previously indicated three brittle grids were used, respectively with reduced strengths. The same confined core concrete element showed an increased maximum compressive stress of 137.8 MPa when ductile grid properties were specified based on the wire stress-strain relationship.

The stresses in transverse boundary element reinforcement (WWR) were also recorded for further assessment. Maximum horizontal tensile stresses of 460, 460 and 460 MPa were obtained in smeared reinforcement at the wall/foundation interface when the three brittle grid models were employed with reduced strengths as expressed earlier, respectively. The maximum tensile stress

remained the same in the same element when fully ductile grids were used assuming no weld failure. The longitudinal boundary element reinforcement at the extreme end of the wall section was also examined. They developed maximum tensile stresses of 583.0, 659.9 and 681.1 MPa; and maximum compressive stresses of 540.4, 589.4 and 626.1 MPa when the three brittle grid models were employed with reduced strengths as expressed earlier, respectively. The same longitudinal bar showed increased maximum tensile stress of 687.3 MPa and maximum compressive stress of 634.2 MPa when fully ductile grids were used with a stress-strain relationship following that of the wires.

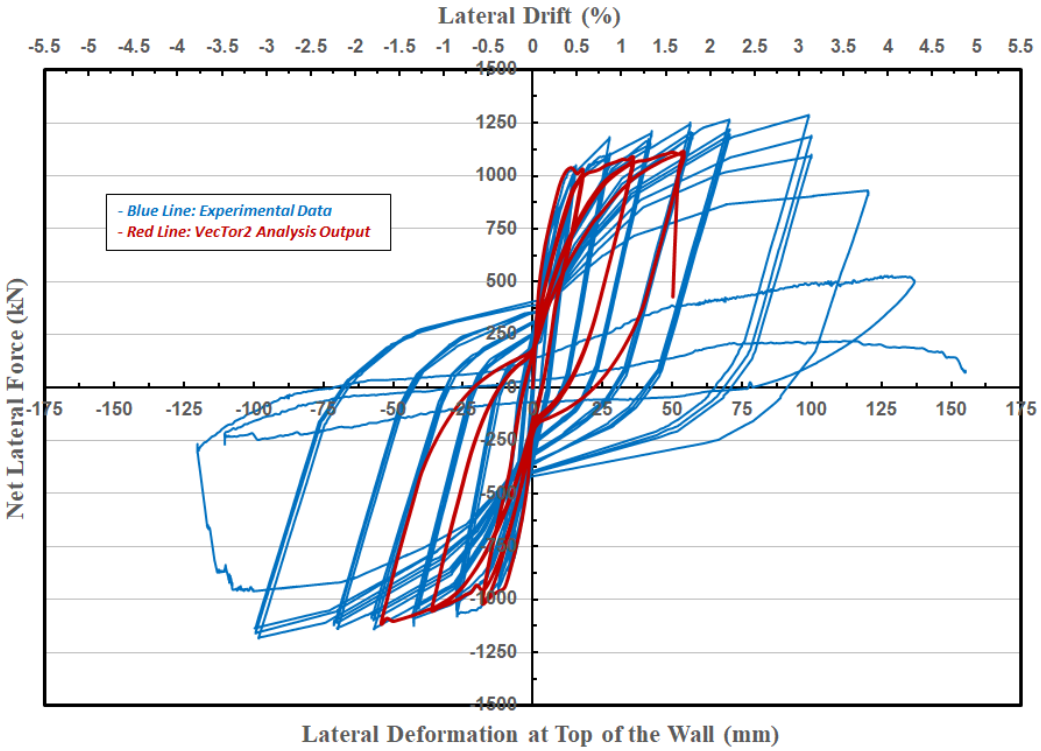

Figure 6.15 Shear Wall No. 2 – WWR Grid with $F_y = 241\ MPa$ and $F_u = 242\ MPa$

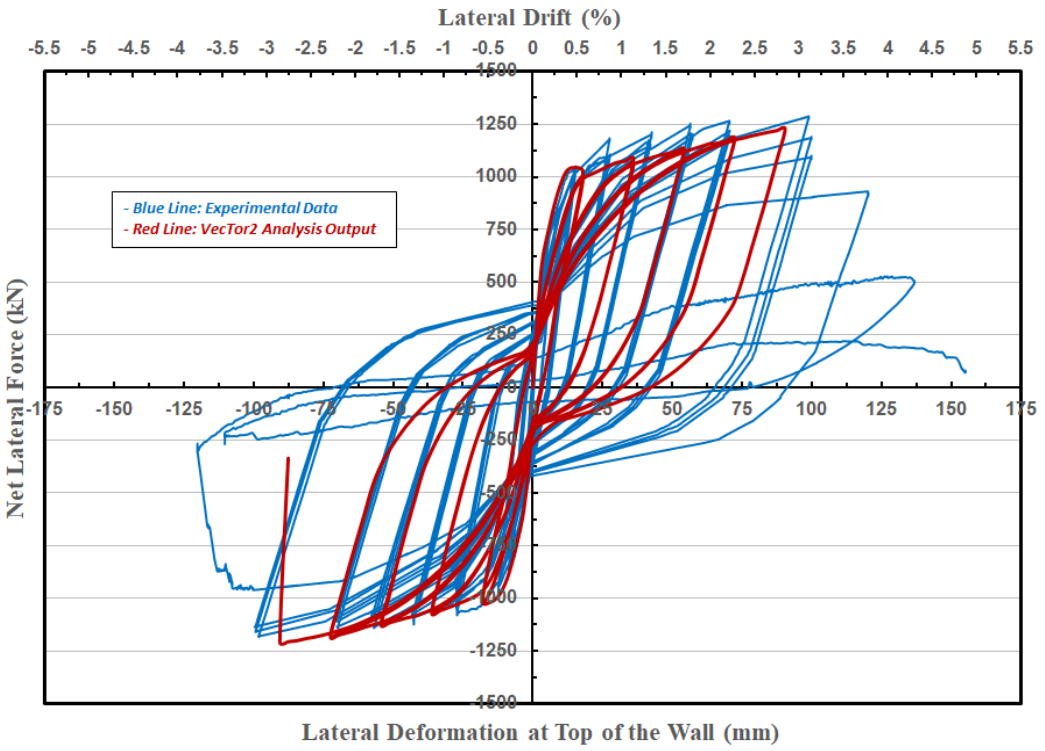

Figure 6.16 Shear Wall No. 2 – WWR Grid with $F_y = 400\ MPa$ and $F_u = 401\ MPa$

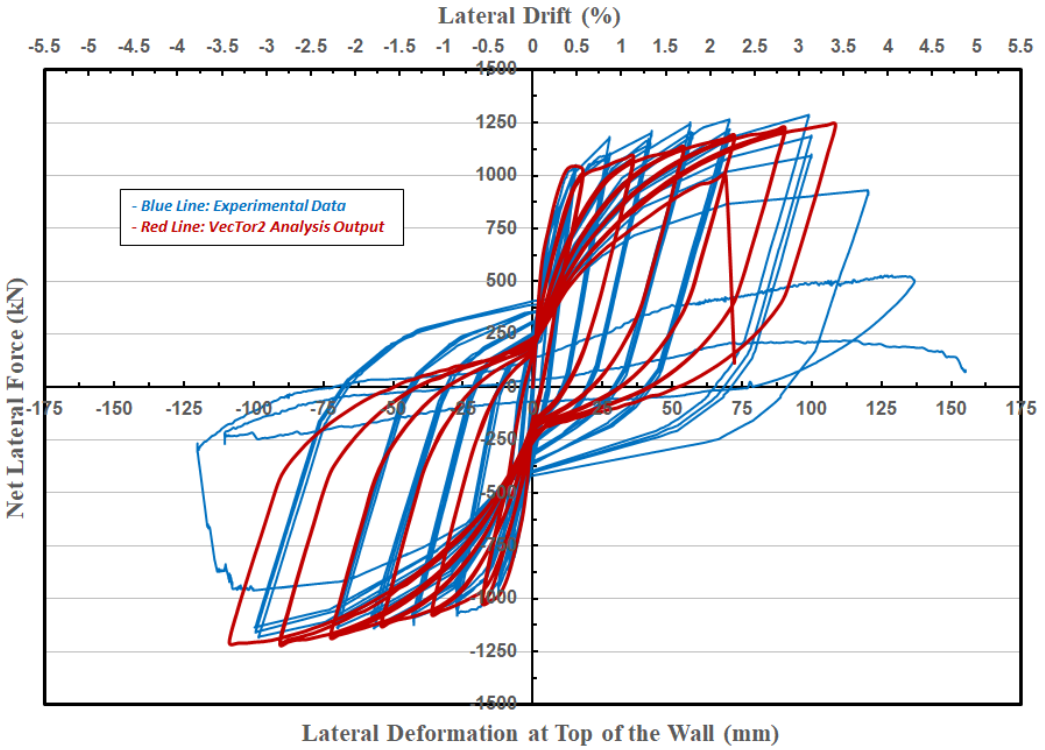

Figure 6.17 Shear Wall No. 2 – WWR Grid with $F_y = 500\ MPa$ and $F_u = 501\ MPa$

The second set of analysis in the parametric study of Shear Wall No 2 involved the investigation of weld failures at one grid location while the grids above and below remained intact. This was done by specifying reduced volumetric ratio of transverse reinforcement and increased buckling length for compression bars as explained in the Section 6.4. This set of analysis also provided insight into the use of different strength grids at increased grid spacing. The hysteretic response of the four VecTor2 models obtained are presented in Figures 6.18 to 6.21 for three brittle grid behaviour models, having 241, 400, and 500 MPa strengths and a ductile grid model having 550 MPa yield strength. The results indicate that the wall developed failure during 1.18%, 1.65%, 2.31% and 2.88% drift cycle, having completed three successful cycles at 0.61%, 1.19%, 1.67% and 2.31% drift ratios, respectively.

The analysis output was also examined in terms of maximum concrete and steel stresses generated in representative critical elements. Accordingly, maximum compressive stresses of 91.6, 92.9, 92.5 and 92.4 MPa were observed at wall base in the unconfined skin concrete element located in the extreme fiber of cover concrete when the four grid material models described above were used, respectively. The unconfined concrete cover spalled off shortly thereafter, and stopped carrying any load for the rest of the analysis. As for the confined core concrete in the outermost element, the analysis results showed maximum concrete stresses of 97.6, 109.0, 113.6 and 116.0 MPa when the same four grid material models were employed, respectively.

The reinforcement stresses also changed with grid material models. Maximum horizontal tensile stresses of 313.6, 460, 460 and 460 MPa were recorded in smeared reinforcement at the wall/foundation interface of boundary element when the same four grid material models were used, respectively. The longitudinal bars at extreme ends of walls showed maximum tensile stress of 525.3, 591.0, 629.4 and 665.0 MPa; and maximum compressive stress of 436.1, 469.2, 477.1 and 480.3 MPa with the use of the four grid material models, respectively.

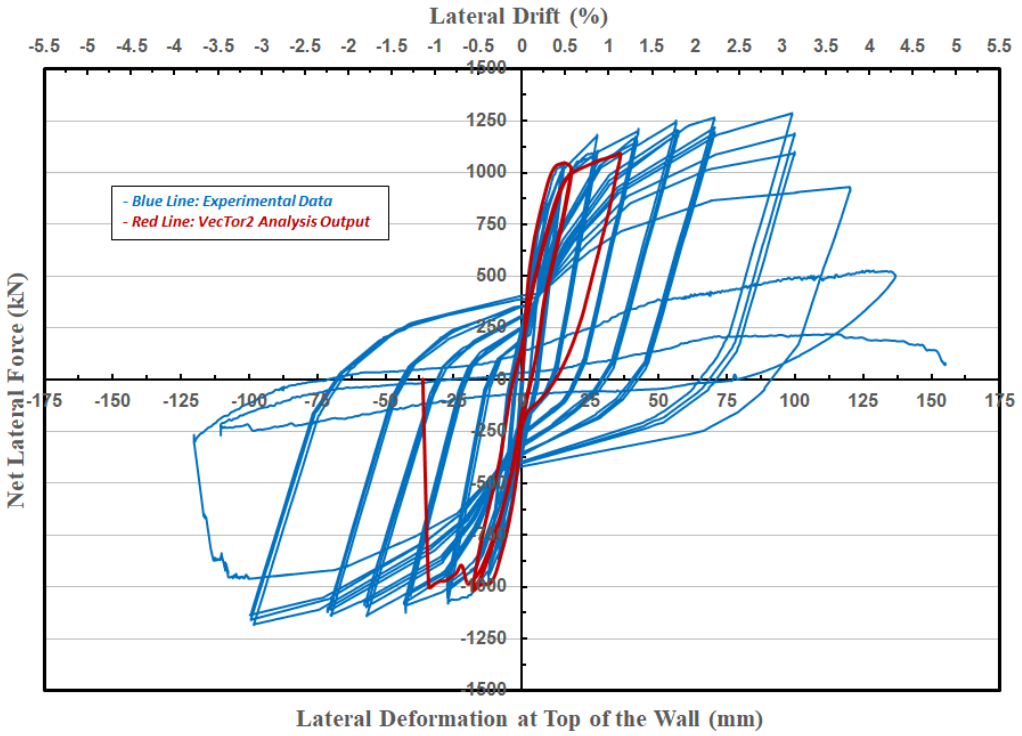

Figure 6.18 Shear Wall No. 2 – WWR Grid with Double Spacing
$F_y = 241\ MPa$ and $F_u = 242\ MPa$

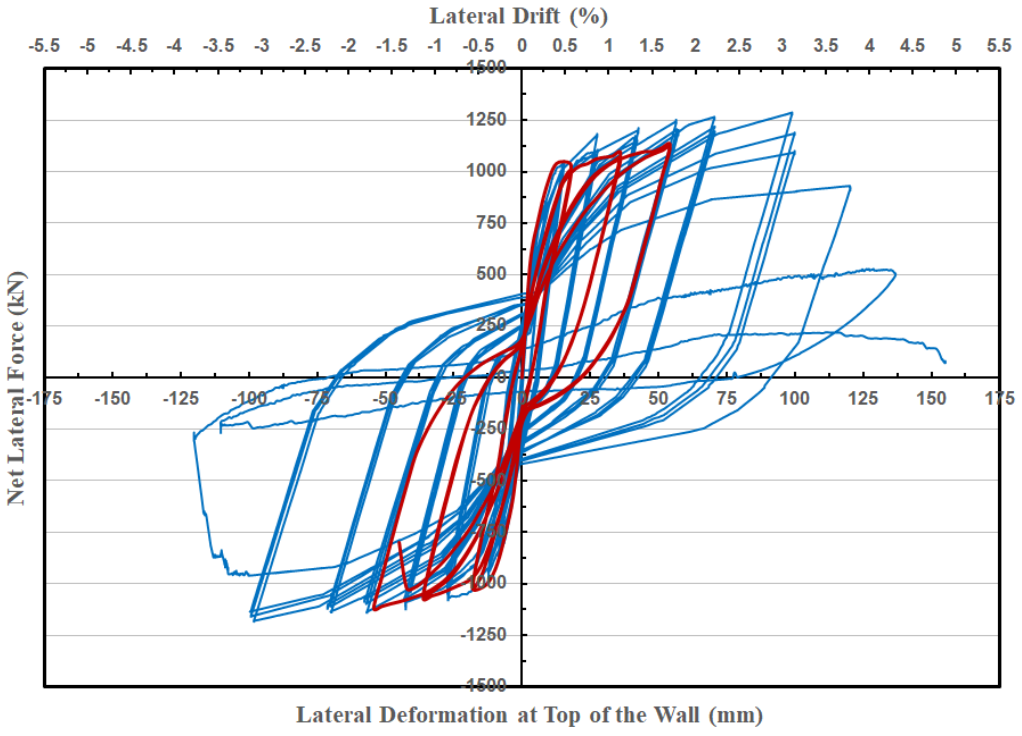

Figure 6.19 Shear Wall No. 2 – WWR Grid with Double Spacing
$F_y = 400\ MPa$ and $F_u = 401\ MPa$

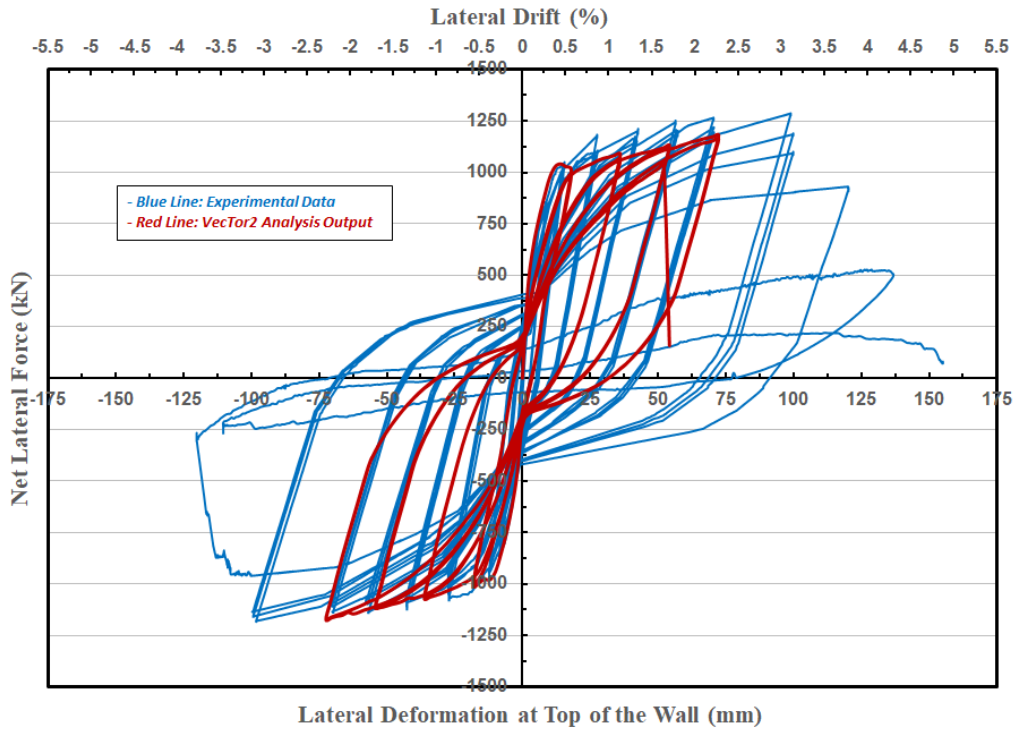

Figure 6.20 Shear Wall No. 2 – WWR Grid with Double Spacing
$F_y = 500\ MPa$ and $F_u = 501\ MPa$

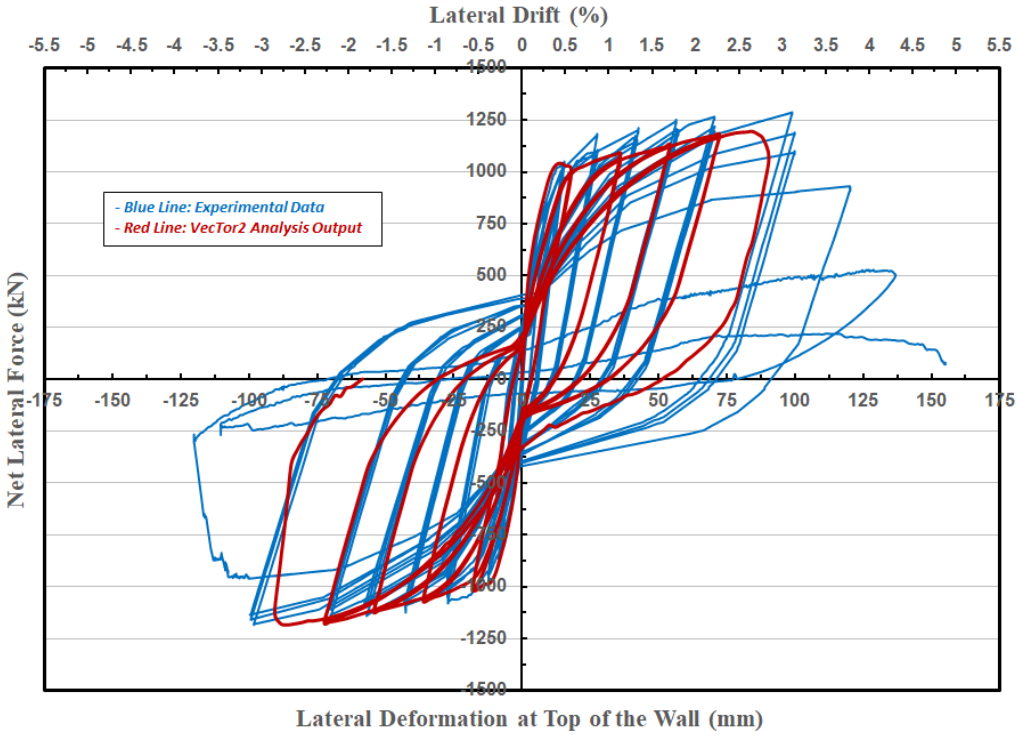

Figure 6.21 Shear Wall No. 2 – WWR Grid with Double Spacing
$F_y = 550\ MPa$ and $F_u = 640\ MP$

6.4.3 Parametric Investigation – Shear Wall No. 3

The first set of analysis in the parametric study of Shear Wall No 3 involved the investigation of premature weld failure, as described in Section 6.4. Figures 6.22 to 6.24 show the results of Shear Wall 3 analysis with different grid strengths. The results indicate that the overall wall capacity is not affected by the variation in grid strength. However, the ductility of the wall is significantly reduced as the grid strength and the ability to confine core concrete and restrain longitudinal bars against buckling is reduced. The shear wall models with 241, 400 and 500 MPa grid strengths failed during 1.39%, 1.89%, and 2.81% drift cycles after successfully completing three cycles at 0.92%, 1.42% and 2.32% drift ratios, respectively. The shear wall model with fully ductile grids, as shown in Figure 6.3, failed during 3.25% drift cycle after successfully completing three cycles at 2.82% drift. The experimental results for Shear Wall No. 3 indicate that the wall failed during 2.84% drift cycles after completing three successful cycles at 2.39% drift.

Maximum concrete and steel stresses were also recorded in the above analyses to assess wall performance. The skin concrete element located at the exterior most compression corner of unconfined cover concrete indicated maximum compressive stresses of 89.5, 93.4 and 89.9 MPa, respectively for the three brittle grid cases considered, respectively with gradually reducing strengths. The same element in the cover showed maximum compressive stress of 89.9 MPa when the grid behavior was assumed to be ductile, corresponding to the wire stress-strain relationship recorded by coupon tests. The cover concrete spalled off immediately after experiencing these maximum stresses, and stopped providing compressive resistance for the rest of the analysis. The confined core concrete element at the extreme compression region of the boundary element showed somewhat increased compressive resistance with maximum compressive stresses of 107.8, 121.4 and 127.8 MPa when the previously indicated three brittle grids were used, respectively with reduced strengths. The same confined core concrete element showed an increased maximum compressive stress of 133.4 MPa when ductile grid properties were specified based on the wire stress-strain relationship.

The stresses in transverse boundary element reinforcement (WWR) were also recorded for further assessment. Maximum horizontal tensile stresses of 460, 460 and 460 MPa were obtained in smeared reinforcement at the wall/foundation interface when the three brittle grid models were employed with reduced strengths as expressed earlier, respectively. The maximum tensile stress

remained the same in the same element when fully ductile grids were used assuming no weld failure. The longitudinal boundary element reinforcement at the extreme end of the wall section was also examined. They developed maximum tensile stresses of 548.5, 602.5 and 639.4 MPa; and maximum compressive stresses of 455.6, 472.2 and 505.4 MPa when the three brittle grid models were employed with reduced strengths as expressed earlier, respectively. The same longitudinal bar showed increased maximum tensile stress of 649.2 MPa and maximum compressive stress of 634.2 MPa when fully ductile grids were used with a stress-strain relationship following that of the wires.

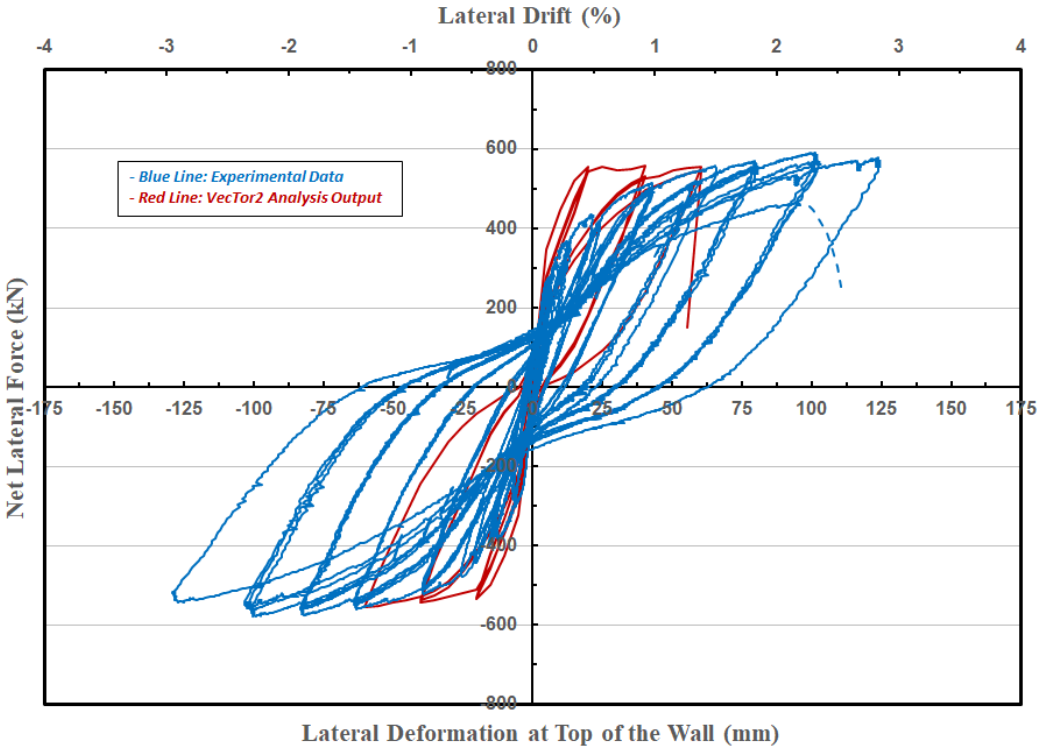

Figure 6.22 Shear Wall No. 3 – WWR Grid with $F_y = 241\ MPa$ and $F_u = 242\ MPa$

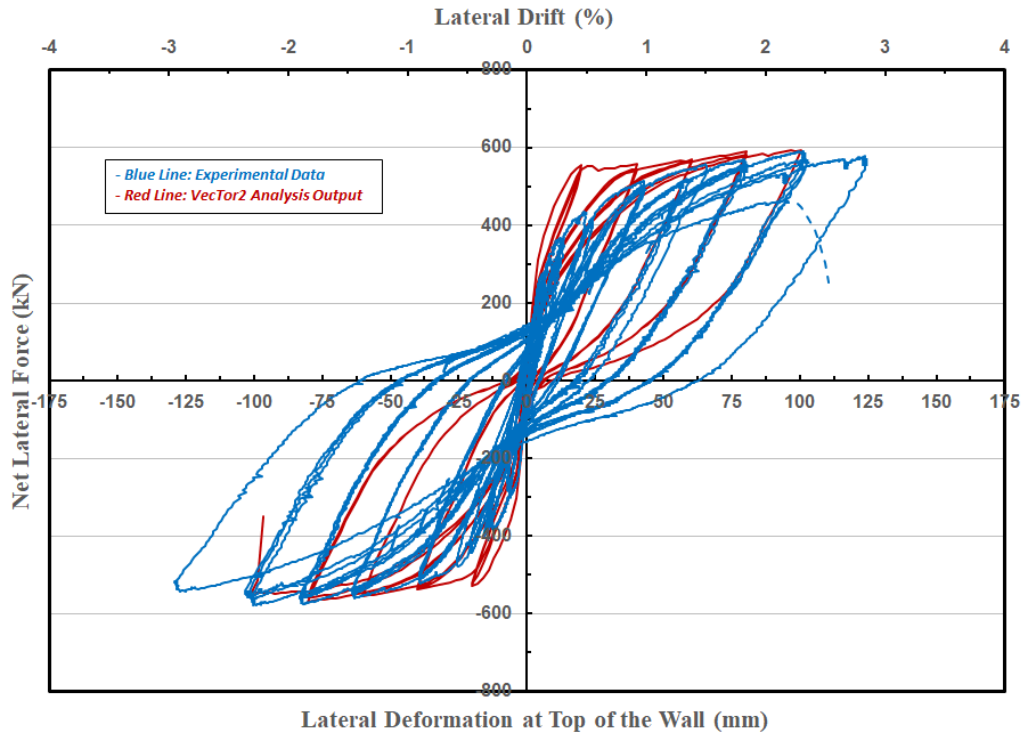

Figure 6.23 Shear Wall No. 3 – WWR Grid with $F_y = 400\ MPa$ and $F_u = 401\ MPa$

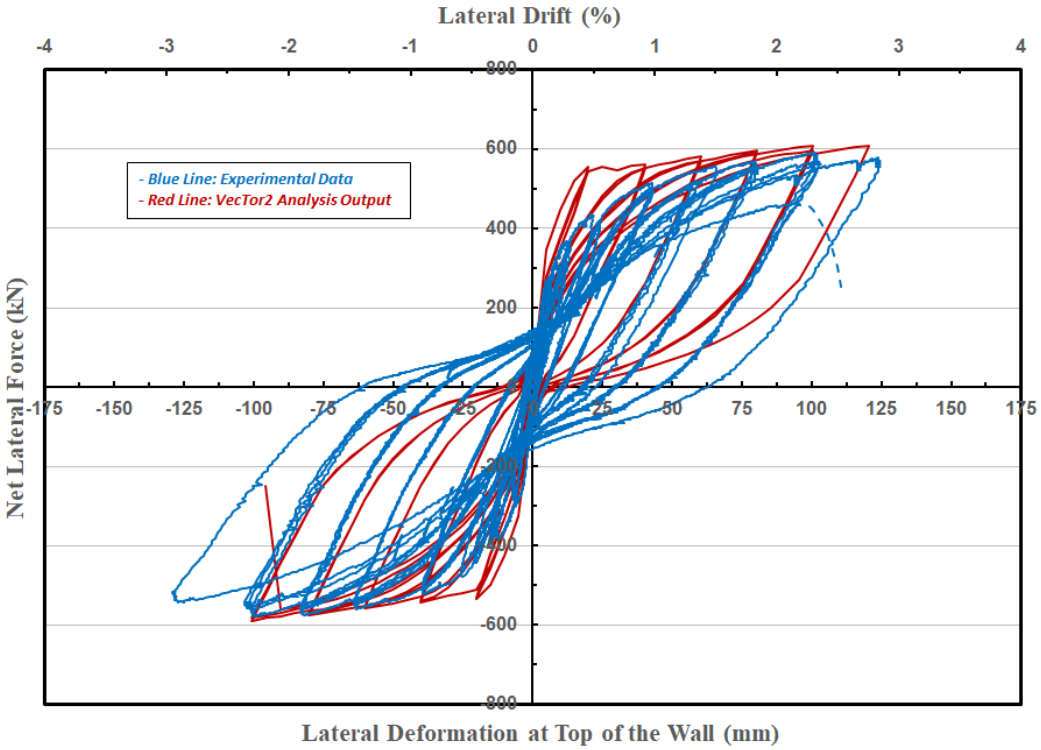

Figure 6.24 Shear Wall No. 3 – WWR Grid with $F_y = 500\ MPa$ and $F_u = 501\ MPa$

The second set of analysis in the parametric study of Shear Wall No 3 involved the investigation of weld failures at one grid location while the grids above and below remained intact. This was done by specifying reduced volumetric ratio of transverse reinforcement and increased buckling length for compression bars as explained in the Section 6.4. This set of analysis also provided insight into the use of different strength grids at increased grid spacing. The hysteretic response of the four VecTor2 models obtained are presented in Figures 6.25 to 6.28 for three brittle grid behaviour models, having 241, 400, and 500 MPa strengths and a ductile grid model having 550 MPa yield strength. The results indicate that the wall developed failure during 1.27%, 1.83%, 2.30% and 3.22% drift cycle, having completed three successful cycles at 0.92%, 1.27%, 1.83% and 2.82% drift ratios, respectively.

The analysis output was also examined in terms of maximum concrete and steel stresses generated in representative critical elements. Accordingly, maximum compressive stresses of 91.3, 91.3, 91.9 and 91.7 MPa were observed at wall base in the unconfined skin concrete element located in the extreme fiber of cover concrete when the four grid material models described above were used, respectively. The unconfined concrete cover spalled off shortly thereafter, and stopped carrying any load for the rest of the analysis. As for the confined core concrete in the outermost element, the analysis results showed maximum concrete stresses of 104.3, 108.7, 109.6 and 115.8 MPa when the same four grid material models were employed, respectively.

The reinforcement stresses also changed with grid material models. Maximum horizontal tensile stresses of 334.7, 460, 460 and 460 MPa were recorded in smeared reinforcement at the wall/foundation interface of boundary element when the same four grid material models were used, respectively. The longitudinal bars at extreme ends of walls showed maximum tensile stress of 525.1, 575.5, 614.2 and 665.5 MPa; and maximum compressive stress of 459.0, 459.7, 460.0 and 460.0 MPa with the use of the four grid material models, respectively.

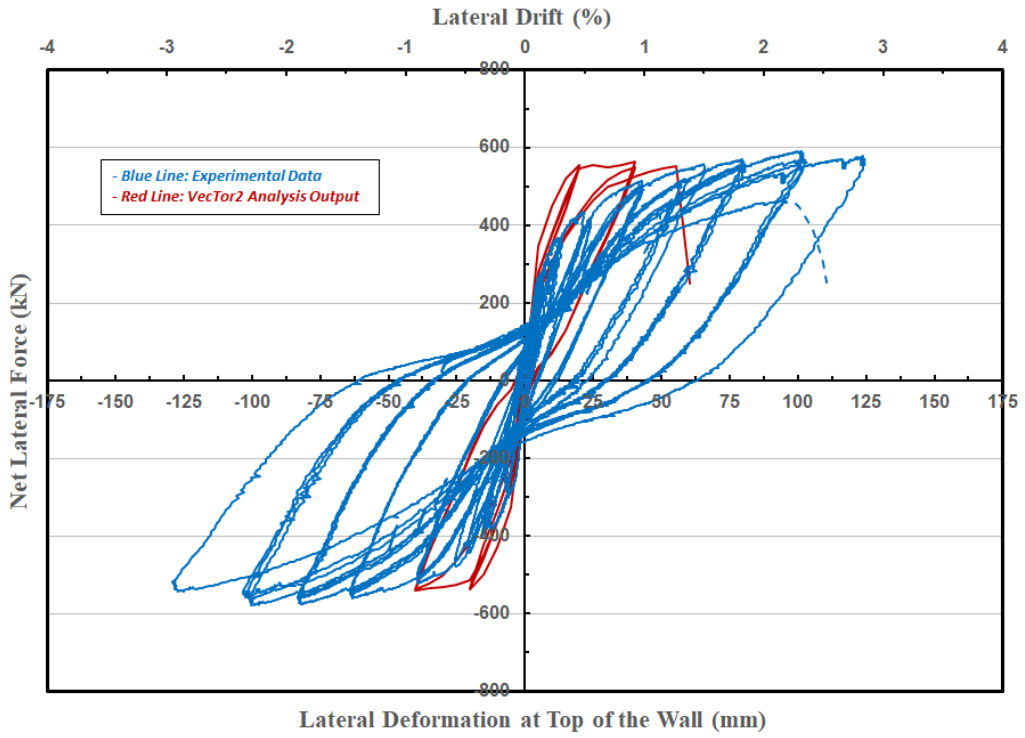

Figure 6.25 Shear Wall No. 3 – WWR Grid with Double Spacing
$F_y = 241\ MPa$ and $F_u = 242\ MPa$

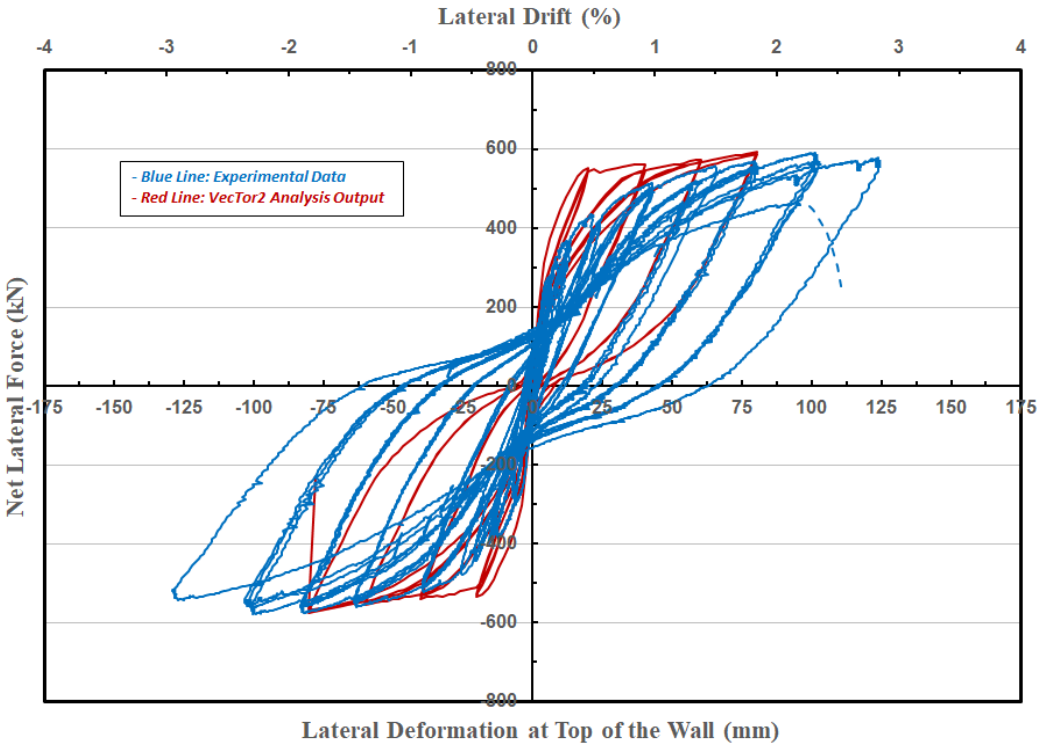

Figure 6.26 Shear Wall No. 3 – WWR Grid with Double Spacing
$F_y = 400\ MPa$ and $F_u = 401\ MPa$

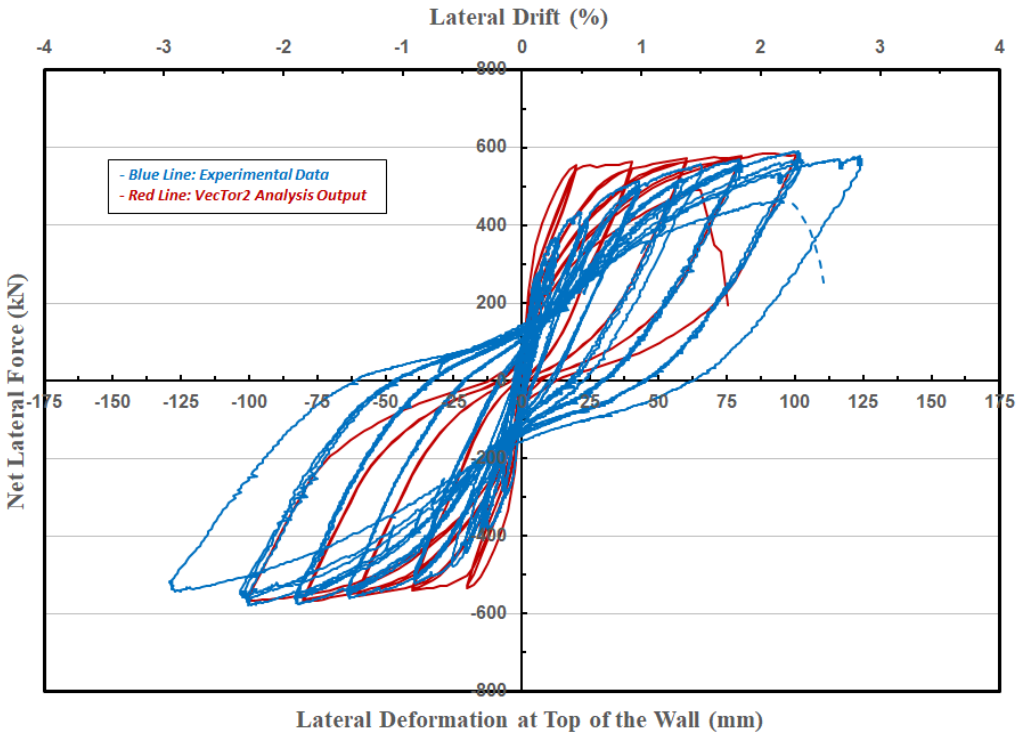

Figure 6.27 Shear Wall No. 3 – WWR Grid with Double Spacing
$F_y = 500\ MPa$ and $F_u = 501\ MPa$

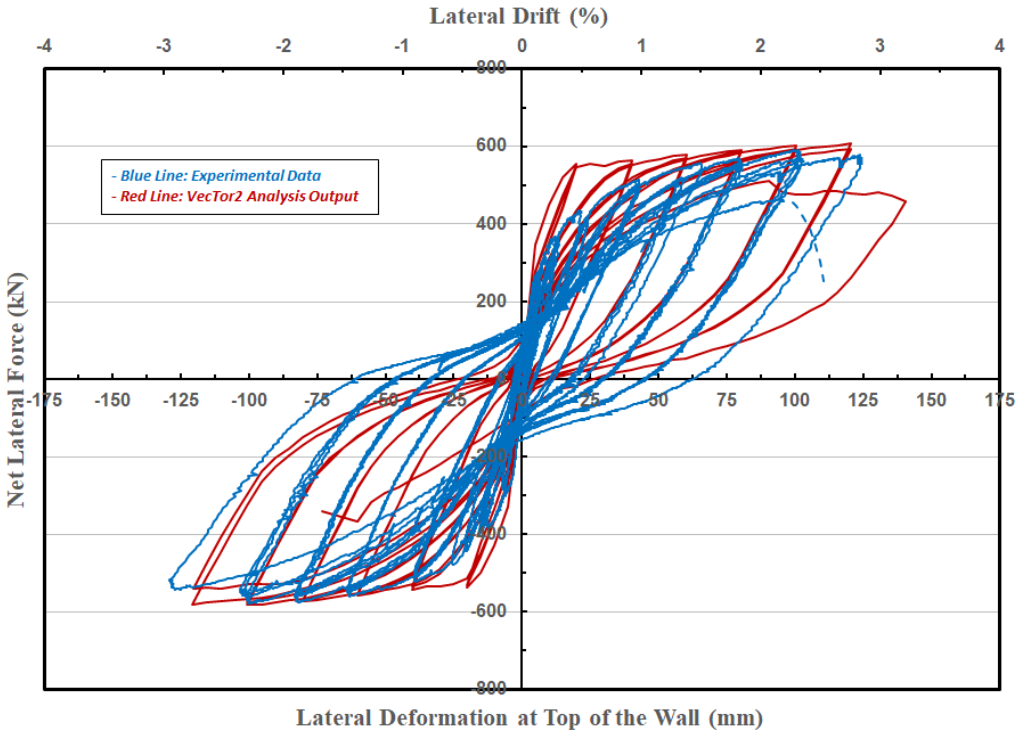

Figure 6.28 Shear Wall No. 3 – WWR Grid with Double Spacing
$F_y = 550\ MPa$ and $F_u = 640\ MPa$

6.4.4 Parametric Investigation – Summary

The results of analytical parametric investigation are summarized in Tables 6.1 and 6.2. The focus in the parametric study was placed on premature grid weld failure. The weld failure was modelled by specifying elastic strength limit for the grids. This implies that the grid reinforcement would perform elastically until the specified failure point is attained, beyond which it would fail in a brittle manner and stop contributing to the analysis. Three failure points were specified with the lowest being 240 MPa, which corresponds to the minimum acceptable weld strength as established by the applicable ASTM weld test. The other two failure points were 400 MPa and 500 MPa, arbitrarily selected between the ASTM minimum value and the steel yield strength of 550MPa that was measured through coupon tests.

Two aspects of shear wall performance with potential effects of grid behavior were of significance; i) strength and ii) ductility. Both the analysis and the wall tests indicated that the weld performance did not have a detrimental effect on shear wall strength within the strength range considered. This was expected as the grid reinforcement would engage in wall resistance at higher levels of lateral drift, beyond the flexural yielding of walls and the spalling of compression concrete. In typical flexure-dominant shear walls, concrete confinement becomes more important beyond flexural yielding as transverse strain demands would increase in this range of inelastic deformations. Buckling prevention becomes more important beyond the spalling of cover concrete, which restrains compression reinforcement against buckling. The deformation demands on welded grids were not high-enough to affect shear wall flexural strength as the walls developed their full flexural capacities shortly after their flexural yield point. The emphasis in performance assessment is placed on Shear Walls 2 and 3, as these walls performed predominantly in the flexure mode, the mode of behavior that would be affected most by grid concrete confinement and grid compression bar buckling prevention. However, the wall ductility was affected significantly by the weld strength. This was also expected, as the grid reinforcement is expected to sustain high strains in confining concrete and supporting compression bars against buckling. When the low value of 240 MPa was used as weld strength, Shear Wall No. 2 and Shear Wall No. 3 failed at 1.6% and 1.4% lateral drift prior to completing intended three cycles, respectively, both having completed three cycles successfully at about 1% drift ratio, which corresponds to twice the observed experimental yield drift level in both shear walls (ductility ratio of 2.0). When the grid strength was increased

to 400 MPa, the failure initiation point increased to 2.86% and 1.89 % drift ratios for Shear Wall No.2 and Shear Wall No. 3, respectively. The increase in lateral drift continued with the increase in weld capacity as illustrated in Figures 6.15 to 6.17 for Shear Wall No.2 and Figures 6.22 to 6.24 for Shear Wall No. 3.

The comparison of experimental and analytical hysteretic responses presented in Figures 6.5 for Shear Wall No.2 indicates good agreement when the welds were assumed to remain intact and the grid wires were allowed to yield at 550 MPa. This is not surprising because transverse strain demands on grids were not high in this wall and the grid welds did not rupture. The failure in the wall was initiated by rupturing of the longitudinal reinforcement, having developed a high drift ratio of 3.1%. The analysis based on 500 MPa weld failure strength confirmed this observation. The analytical hysteretic response shown in Figure 6.17 indicates that the deformability obtained was the same as that obtained when grid yield was assumed (no weld failure with f_y = 550 MPa and f_u = 640 MPa) because the train demand was not high enough to trigger a difference. This was not the case in Shear Wall No.3, however. The assumption of no weld failure in this wall resulted in a slight overestimation of ductility, as shown in Figure 6.7. When grid weld failure strength of 500 MPa was assumed in the analysis, the ductility was closer to that observed in the experimental response relationship. Indeed, the test revealed that the grid welds failed in this wall, albeit at a drift ratio in excess of 2.0 % (ductility ratio of approximately 4.0) in the splice region. It should be noted that the analytical modelled did not have the capability of modelling splice regions, and the analysis assumed continuous longitudinal reinforcement, complicating further the comparison between the two results.

The parametric study was extended in the second set of analysis to cover cases where every other grid suffered weld failure while the others remained intact. This was done to investigate the effects of some of the grids suffering weld failures whereas the others continue fulfilling their transverse reinforcement functions as observed in Shear Wall No. 3 and the coupling beams tested in another phase of the same research program with the same grids (Ozcan and Saatcioglu, 2018). In tests, not all the grids failed all at once as assumed in the first set of analysis presented above. The results of the second set of analysis also reflected wall behavior when the percentage of transverse reinforcement in boundary elements was reduced by one half and the buckling length of longitudinal bars between the ties was increased by a factor of 2.0. The hysteretic responses

compared in Figures 6.19 to 6.22 for Shear Wall No. 2 and Figures 6.25 to 6.28 for Shear Wall No. 3, as well as the drift capacities summarized in Table 6.2, indicate that the reduction in percentage of grid reinforcement and the increase in tie spacing resulted in reduced wall deformability as expected, although wall strengths were not affected, for reasons explained for the first set of analysis above. It was also observed that the reductions in wall deformability were not very high when the grid strength was taken to be above 400 MPa, indicating the conservatism inherent in transverse reinforcement design for shear wall boundary elements.

Table 6.1 Shear Wall Analysis Output Summary – Matching As-Built Configuration

	WWR Grid Properties (MPa)	Failure Drift Cycle	Successful Drift Cycle	Conc. Stress @ Boundary Elem. (MPa)	Steel Reinf. Stress (MPa)	
					Tension	Compression
Shear Wall No. 1	$F_{y=}240,\ F_{u=}241$	0.97%	0.65%	58.4	535.5	496.9
	$F_{y=}400,\ F_{u=}401$	1.30%	0.97%	63.0	557.2	516.0
	$F_{y=}500,\ F_{u=}501$	1.30%	0.97%	66.7	566.7	519.1
	$F_{y=}550,\ F_{u=}640$	1.62%	1.29%	70.0	617.8	529.9
Shear Wall No. 2	$F_{y=}240,\ F_{u=}241$	1.67%	1.18%	110.6	583.0	540.4
	$F_{y=}400,\ F_{u=}401$	2.86%	2.30%	124.5	659.9	589.4
	$F_{y=}500,\ F_{u=}501$	3.50%	2.86%	131.7	681.1	626.1
	$F_{y=}550,\ F_{u=}640$	3.50%	2.86%	137.8	687.3	634.2
Shear Wall No. 3	$F_{y=}240,\ F_{u=}241$	1.39%	0.92%	107.8	548.5	455.6
	$F_{y=}400,\ F_{u=}401$	1.89%	1.42%	121.4	602.5	472.2
	$F_{y=}500,\ F_{u=}501$	2.81%	2.32%	127.8	639.4	505.4
	$F_{y=}550,\ F_{u=}640$	3.25%	2.82%	133.4	649.2	643.2

Table 6.2 Shear Wall Analysis Output Summary – Twice the Tie Spacing

	WWR Grid Properties (MPa)	Failure Drift Cycle	Successful Drift Cycle	Conc. Stress @ Boundary Elem. (MPa)	Steel Reinf. Stress (MPa)	
					Tension	Compression
Shear Wall No. 1	$F_{y=}240,\ F_{u=}241$	0.65%	0.32%	54.5	496.1	428.9
	$F_{y=}400,\ F_{u=}401$	0.84%	0.65%	55.8	518.0	437.0
	$F_{y=}500,\ F_{u=}501$	1.30%	0.97%	59.8	570.0	457.4
	$F_{y=}550,\ F_{u=}640$	1.35%	1.30%	61.4	575.4	460.0
Shear Wall No. 2	$F_{y=}240,\ F_{u=}241$	1.18%	0.61%	97.6	525.3	436.1
	$F_{y=}400,\ F_{u=}401$	1.65%	1.19%	109.0	591.0	469.2
	$F_{y=}500,\ F_{u=}501$	2.31%	1.67%	113.6	629.4	477.1
	$F_{y=}550,\ F_{u=}640$	2.88%	2.31%	116.0	665.0	480.3
Shear Wall No. 3	$F_{y=}240,\ F_{u=}241$	1.27%	0.92%	104.3	525.1	459.0
	$F_{y=}400,\ F_{u=}401$	1.83%	1.27%	108.7	575.5	459.7
	$F_{y=}500,\ F_{u=}501$	2.30%	1.83%	109.6	614.2	460.0
	$F_{y=}550,\ F_{u=}640$	3.22%	2.82%	115.8	665.5	460.0

Chapter 7

Recommendations and Conclusions

7.1 General

The research project presented in this thesis had the objective of assessing reinforced concrete shear wall behavior when welded wire reinforcement (WWR) grids were used as transverse boundary element reinforcement. The goal was to develop design guidelines for earthquake-resistant shear walls while ensuring quality control for the grid material for use as confinement and buckling restraint reinforcement. Of importance was the grid weld behavior during inelastic response of shear walls when the transverse strain demands on the grids became high. The project consisted of experimental and analytical research. The experimental phase included extensive material testing, as well as large-scale shear wall tests under simulated seismic loading. The analytical research involved non-linear finite element analysis of shear walls with different properties of WWR. The following sections provide a summary of observations made during both experimental and analytical phases of research, recommendations made for design and material testing, followed by the conclusions of the research project.

7.2 Summary of Observations and Discussion

WRGs offer quick and easy cage assembly, reduced construction time, improved geometric precision and reduced congestion of steel cages when used as transverse tie reinforcement. The apparent construction advantages become assets only if the expected structural performance is attained. Tie bends and hook extension of conventional boundary element transverse reinforcement can be replaced by welded joints of WRG, provided that the welds remain intact until after the wires develop their inelastic behavior as obtained in coupon tests, with sufficient elongation capacity. Earlier research on the use of WRGs as transverse reinforcement in seismic resistant concrete columns showed favorable behavior with welds maintaining their strengths until after the wires ruptured in tension, resulting in ductile columns with inelastic drift capacities comparable to similar columns with conventional transverse reinforcement (Grira and Saatcioglu 1996, Saatcioglu and Grira 1998). The possibility of extending the applicability of WRGs to shear wall boundary elements was explored in the current research project. This was done first by material testing, followed by structural testing and structural analysis.

7.2.1 Observations Made on Material Test Results

Five types of material tests were conducted; i) steel coupon tests on wire used in producing WRGs; ii) ASTM grid weld tests; iii) grid tests under monotonically applied uniaxial pull (previously referred to as "direct shear tests" and "diagonal burst tests;" iv) tests of grids embedded in concrete prisms under monotonically applied uniaxial pull; and v) small-scale column tests with WRG ties. The following are the observations made during the material tests.

- Coupon tests conducted on 9.5 mm (3/8") diameter wires showed yield strength of 550 MPa, ultimate strength of 640 MPa and maximum elongation of 4.3%. Coupons with and without welded joint showed the same behavior.
- ASTM-1064 weld tests indicated that the weld capacity was well above the 241 MPa of minimum strength specified. The tests indicated a weld capacity between 426 MPa and 450 MPa with average weld strength of 440 MPa. The average weld strength corresponded to 80% of the wire yield capacity.
- Grids subjected to direct shear tests showed on the average 160 MPa steel stress at weld failure. This corresponds to 30% of steel yield strength. The early failure of welds under

direct shear tests were attributed to the offset between the centerlines of the two wires welded at the connection and the resulting eccentricity and associated bending of the wire end, prying the weld, causing premature weld failure. Furthermore, the strength value represents equal force distribution among the resisting grid legs. In reality one of the grids may be taking higher load with higher percentage of yield load.

- The burst tests (under diagonal pull) conducted on grids indicated similar results as the direct shear tests, with the average stress on the main grid leg equal to 160 MPa, forming 30% of the steel yield strength.
- The wire ends during grid pull tests bent and curved significantly prior to weld failure. This raised a question whether the grid pull tests (direct shear and burst tests) represented the actual grid behavior in concrete. Therefore, grids were cast in concrete prisms with concrete thickness representing grid spacing in shear wall boundary elements.
- Direct shear tests of grids embedded in concrete prisms indicated weld failures at loads corresponding to average steel stress of 313 MPa, forming 57% of the yield strength. This value represents equal force distribution among the resisting grid legs. In reality one of the grids may be taking higher load, increasing the percentage of yield load indicated.
- Burst tests of grids embedded in concrete prisms indicated weld failures at loads corresponding to average steel stress of 418 MPa in the main resisting leg, corresponding to 76% of steel yield strength. This value is closer to the ASTM-1064 weld test results.
- Small-scale columns with 4-bar arrangement and single-cell transverse grids reinforcement, tested under monotonically increasing concentric and eccentric compression indicated that the compression bars were able yield and develop in excess of 0.2% strain prior to grid failure. Strain gauges placed on the grid reinforcement indicated yielding of the grid wire. However, the column failure was initiated by concrete cover spalling, followed by the yielding of compression reinforcement. The columns failed when the grid welds failed under increasing inelastic longitudinal bar strains accompanied by compression bar buckling.

7.2.2 Observations Made on Large-Scale Shear Wall Test Results

In addition to the observations made on material performance under monotonic loading presented above, the following observations were made on the performance of two flexure dominant large-

scale shear walls with WWR used as transverse boundary element ties, tested under reversed cyclic loading.

- Shear Wall No. 2, with an aspect ratio of 1.94, designed to fail in flexure while also subjected high shear stress reversals, showed ductile response, developing a drift capacity of 3.1% while experiencing 14% strength decay at the end of the third cycle, and completely failing during the cycles at the next drift level (Figure 5.28). Using 0.5% drift ratio to be the global wall yield point, the wall displacement ductility ratio prior to failure was 3.1/0.5 = 6.2. The failure initiated by concrete crushing at the toe, followed by the rupturing of longitudinal bars in tension, having exhausted its complete flexural resistance. There was no weld failure observed in the grids. The grids maintained their integrity until the tension reinforcement ruptured. The wall developed substantial diagonal cracking due to the diagonal tension caused by shear, which was controlled by horizontal web reinforcement designed to provide shear capacity well in excess of shear resistance corresponding to probable moment resistance. The hysteretic wall behavior was comparable to those obtained by Oesterle at al (1976) at the Portland Cement Association on specimens with different material and geometric properties, shown in Figures 2.19 to 2.34, with boundary elements transversely reinforced with conventional ties.
- Shear Wall No.3, with and aspect ratio of 3.0, was designed as per ACI 318-11 requirements to perform in the flexure mode of deformations. The wall performed in a ductile manner and developed three cycles at 2.3% drift, virtually without and strength decay, and failed during the second cycle at 2.8% drift in the splice region. The failure was initiated by concrete crushing and spalling in the cover near the splice region 500 mm to 600 mm above the wall foundation interface, followed by the buckling of longitudinal compression reinforcement upon the failure of grid welds. There was no distress observed in the grids until after 2.3% lateral drift cycles, but they could not sustain high transverse strain demands at 2.8% drift and failed through the failure of grid welds as illustrated in Figure 5.41. Using 0.5% drift ratio as the global yield level for wall, the displacement ductility ratio attained was 2.3/0.5 = 4.6 prior to reaching cycles with substantial strength decay.

7.2.3 Observations Made on Finite Element Analysis Results

Non-linear finite element analysis was conducted to generate analytical predictions of shear wall response for the three shear walls considered in the experimental program. The first step in the analysis was to build shear wall models, and then to validate them against experimental data. The grid weld capacity was introduced by assigning different levels of weld strength to the grids at which point the grids reinforcement would fail in a brittle manner. The transverse grid reinforcement in boundary elements were modelled as smeared steel models for each finite element. Analyses of walls were also conducted for the case of having ductile grids without any weld failure. In this case the grid behavior was modelled to follow the stress-strain relationship of wire as obtained from the coupon tests reported in Chapter 3. The following observations were made on the analytical hysteretic responses generated.

- The VecTor2 finite element software can predict experimental response of shear walls subjected to inelastic deformation reversals fairly accurately. The experimental results agreed well with analytical predictions when the grid strength was between 400 MPa and 500 MPa and governed by weld failure. When the welds were assumed to be stronger than the wires (f_y = 540 MPa; f_u = 650 MPa, and no weld failure) the deformability was slightly overestimated.
- The use of minimum acceptable weld strength of 241 MPa, specified by ASTM-1064, resulted in a very low ductility ratio of 1% in both Shear Walls 2 and 3.
- Shear walls designed to have shear capacity equal to shear force associated with nominal flexural capacity, as in the case of Shear Wall 1, had limited ductility. When the weld failure was prevented and ductile grid behavior was assumed, the wall showed a drift capacity of 1.3%. When weld failure was modelled with 400 MPa to 500 MPa failure stress the drift capacity was limited to 1%.
- Increasing the spacing of grid reinforcement in shear wall boundary elements resulted in reductions in ductility. If the welds did not fail, Shear Walls No 1, 2, and 3 developed drift capacities of 1.3%, 2.3% and 2.8%, respectively.

7.3 Design Recommendations

Design of earthquake resistant flexural walls requires sufficient strength and inelastic deformability (ductility). This section specifically addresses design of WWR grids as transverse reinforcement in shear wall boundary elements for concrete confinement and longitudinal reinforcement buckling restraining elements. More specifically, it addresses additional design considerations that stemmed from the current research project, over and above those required by the relevant sections of ACI 318-14 and CSA A23.3-14. These additional requirements essentially pertain to the grid behavior, the grid weld strength, and the available ductility in grids to be able to fulfill their functions in the inelastic range of shear wall response.

- The material characteristics of WWR grids should be established in a two-step process:
    - When subjected to burst test, if the grids consistently fail through the rupturing of wires, rather than the failure of welds, the stress-strain relationship of steel established through coupon tests of steel wire can be used in design. This behavior establishes equivalency between WWR grids and conventional ties consisting of closed hoops, with or without crossties, and overlapping hoops. Figure 7.1 shows a typical grid failure through the rupturing of wire, rather than the failure of a grid weld illustrated in Figure 7.2. Earlier shipment of WWR grids received at the University of Ottawa for column tests consisted of grids that failed by wire rupturing. Reinforced concrete columns confined by these grids consistently showed ductile behavior, similar to that observed in columns confined by conventional ties (Grira and Saatcioglu 1996, Grira and Saatcioglu, 1997, Saatcioglu and Grira 1999, Saatcioglu and Grira 2011).
    - As a result of burst tests, if the grids show weld failure, as illustrated in Figure. 7.2, then the weld strength shall be investigated. The current project indicates that a close correlation exists between the grid weld strength as established by ASTM-1064 weld tests, WWR grid burst tests conducted on grids embedded in concrete, as well as the observations made on large-scale shear wall tests and finite element analysis of shear walls. It was concluded that the ASTM-1064 weld test would be a reasonably good estimate for grid weld strength in structural members and hence is recommended for use in design. However, lack of ductility in such failure mode

requires further safety considerations. The performance of shear walls, both experimentally and analytically, indicated that the use of ASTM-1064 test data for weld strength provides some degree of conservatism. This is attributed to the redundancy in the system. The ASTM test is a single joint weld test as opposed to the performance of multiple joint grids in structural members, in which case not all the joints fail at the same time. However, it is prudent to introduce a further margin of safety through a material resistance factor, similar to that used for reinforcing steel in the Canadian Standard CSA A23.3. Until further research data becomes available, the use of $\phi_w = 0.85$ is recommended to reduce the grid weld strength established by ASTM-1064 tests. It is worth noting that the walls tested in the experimental program met the transverse steel requirements of current building codes without excess steel. Hence the observed wall ductility without the ductile behavior of grids could not be attributed to excess transverse reinforcement, implying that additional strength can offset lack of grid ductility.

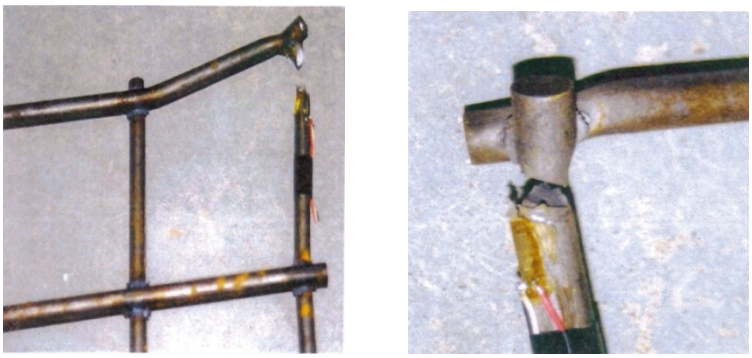

Figure 7.1 Rupturing of wire reinforcement in WWR grids

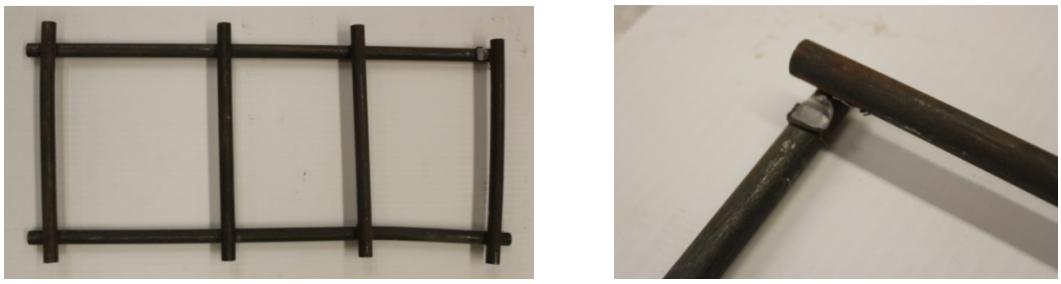

Figure 7.2 Weld failure prior to the yielding of wire reinforcement

- Once the material characteristics are established as described above, the use of existing confinement and buckling restraining reinforcement requirements in existing codes and standards can be followed with transverse steel yield strength defined as $f_{yt} = f_{yw}$ or $f_{yt} = f_w$, depending on whether the grid strength is governed by the yield strength of the wire reinforcement (f_{yw}) or the weld failure strength of the grids (f_w), respectively.
- Shear Wall No.3 tested in the experimental program was designed to have splicing of longitudinal reinforcement as per ACI 318-11 (also applicable to ACI 318-14). Though the shear wall performed in a ductile manner until 2.3% lateral drift without strength decay, corresponding to a displacement ductility ratio of 4.6, and failed during cycles at 2.8% lateral drift, the failure was initiated by the buckling of longitudinal reinforcement in the splice region. While the buckling may be linked to the grid weld failure observed at this stage of deformations, it became clear that the tendency of bar buckling occurred in the splice region. Hence, it is recommended that in earthquake resistant construction, the splicing of longitudinal reinforcement should not all be done at the same location and the recommendations specified in CSA A23.2 should be followed.

7.4 Conclusions

The following conclusions can be drawn from the combined experimental and analytical research conducted as reported in this thesis:

- Reinforced concrete shear walls with WWR grids used as boundary element transverse reinforcement can develop sufficient strength and ductility when designed by current North American Codes and Standards (ACI 318-14 and CSA A23.3-14) provided that the grids have sufficient strength and deformability.
- The WWR grids used in the current investigation have strengths close to the yield strength of wire used to manufacture the grids. However, their joint weld capacity was not sufficiently high to allow the wires to yield. Their use in earthquake resistant construction requires careful assessment of grid material performance.
- WWR grid performance can be assessed through burst tests, as described in the thesis. If the grids fail through yielding and rupturing of wire reinforcement, prior to joint weld failure, this is an indication of their suitability for use as shear wall boundary element

transverse reinforcement with the stress-strain characteristic as obtained from standard wire coupon tests. If the burst tests indicate premature weld failure, then the grid capacity should be established by ASTM-1064 weld tests. The weld strength established by ASTM-1064 tests can be used as design strength, reduced by the proposed material resistance factor $\phi_w = 0.85$ to offset the lack of ductility for increased safety. The flexure-dominant shear walls tested in the current research project (Shear Walls No. 2 and 3), with an ASTM weld capacity varying between 77% and 82% of the wire yield capacity, showed inelastic drift capacities in excess of 2.0%, which are comparable to those observed in equivalent shear walls with conventional ties.

- Shear walls designed based for full ductility, as per ACI 318-14 requirements, may exhibit further increases in wall ductility if the splicing of longitudinal reinforcement is made at different locations along the height of the wall, as required by CSA A23.3-14.
- Maximum elongation of wires used in manufacturing WWR grids fulfils the minimum elongation requirement of 4%.
- Material testing performed on WWR grids embedded in concrete provide a better representation of actual behavior in structural members than the bare grid samples tested.
- The WWR grids used in the material tests developed weld failure prior to reaching the yield strength of wires, including those used in small-scale concrete prisms and columns.
- VecTor2 finite element software provides good estimates of reinforced concrete shear wall behavior in the inelastic range of deformations under reversed cyclic loading.
- Finite element analyses of Shear Walls No. 2 and 3, designed to behave predominantly in the flexure mode, showed very good correlations with experimental data when the WWR grid strength was specified as 90% of the wire yield strength, without any ductility. This observation is in line with the earlier experimental observations that inelastic drift capacities in excess of 2% can be obtained without attaining post-yield ductility in the grids.
- The use of minimum ASTM-1064 strength requirement of 241 MPa was found to result in approximately 1% drift capacity, which was significantly below the value attained during tests of large-scale flexure-dominant walls.
- Increasing grid spacing (reducing percentage of transverse reinforcement while also increasing longitudinal-bar buckling length) by a factor of 2.0 resulted in reductions in

shear wall drift capacities as expected. When grid weld failure strength of 500 MPa was used, the flexure dominant walls experienced a drop of about 20% to 40% in drift capacity with the increase in grid spacing.

- Shear walls with shear strengths equal to shear forces corresponding to nominal flexural capacities develop moderate ductility. Shear Wall No. 1 tested as part of the experimental program indicated that the flexural capacity was attained prior to shear distress with a yield drift capacity 0.36%. Because of the problems encountered during testing of this specimen, inelastic drift capacity could not be observed. However, finite element analysis of the wall with grid weld strength of 500 MPa indicated drift capacity of 1% with a displacement ductility ratio of approximately 3.0.
- The design recommendations developed can be implemented to achieve the intent of current North American Codes and Standards for seismic resisting shear walls.

7.5 Recommendations for Future Research

The current investigation involved tests of WWR grids and large-scale concrete shear walls for earthquake-resistant construction. Valuable observations and design recommendations were made. However, further experimental and analytical research is needed on the topic. Specifically, the following recommendations are made for further research:

- Tests of large-scale reinforced concrete shear wall with a wide range of wall aspect ratios, with boundary elements transversely reinforced with WWR grids having improved inelastic behavior. In these experiments, it is suggested to use:
    - WWR grids with different strength welds, including those that permit the yielding of the grid wires.
    - WWR grids with different patterns and grid cells.
    - WWR grids with different percentages and spacing.
- Analytical research to complement the above recommended shear wall tests, while extending the parameters considered.

References

- Ali Mirza S., MacGregor J. G., "Strength and Ductility of Concrete Slabs Reinforced with Welded Wire Fabric", ACI Journal, September-October 1981, pp. 374-381.

- Antebi J., Utku S, Hansen R. J., "The response of Shear Walls to Dynamic Loads", DASA-1160, Department of Civil Engineering, Massachusetts Institute of Technology, Cambridge, Aug. 1960.

- American Concrete Institute, "ACI 318-71: Building Code Requirements for Structural Concrete", Reported by ACI Committee 318, Detroit, 1971.

- American Concrete Institute, "ACI 318-77: Building Code Requirements for Structural Concrete", Reported by ACI Committee 318, Detroit, 1977.

- American Concrete Institute, "ACI 318-89: Building Code Requirements for Structural Concrete", Reported by ACI Committee 318, Detroit, 1989.

- Barda F., Hanson J. M., and Corley W. G., "Shear Strength of Low-Rise Walls with Boundary Elements", Reinforced Concrete Structures in Seismic Zones, SP-53, American Concrete Institute, Detroit, 1977. Also PCA Research and Development Bulletin RD043.01D.

- Benjamin J.R., Williams H.A., "Investigation of Shear Walls, Part 6 – Continued Experimental ad Mathematical Studies of Reinforced Concrete Walled Bents Under Static Shear Loading", Department of Civil Engineering, Stanford University, Aug. 1953, pp. 59.

- Canadian Standards Association, "CSA A23.3-84: Design of Concrete Structures", 1984, Toronto, Ontario, Canada.

- Canadian Standards Association, “CSA A23.3-94: Design of Concrete Structures”, 1994, Toronto, Ontario, Canada.

- Cardenas A. E. and Magura D., “Strength of High-Rise Shear Walls – Rectangular Cross Sections”, ACI Special Publication 36, 1972, pp. 119-150.

- Cardenas A. E., Hanson J. M., Corley W. G., Hognestad E. H., “Design Provisions for Shear Walls”, Journal of American Concrete Institute, Proceedings Vol. 70, No. 3, March 1973, pages 221-230.

- Cardenas A. E., Russel H.G., Corley W.G., “Strength of Low-Rise Structural Walls”, ACI Special Publication 63, 1980, pp. 221-242.

- Crist R. A., “Shear Behavior of Deep Reinforced Concrete Beams – V.2: Static Tests”, AFWLTR-67-61, The Eric H. Wang Civil Engineering Research Facility, University of New Mexico, Albuquerque, Oct. 1967. Also, Proceedings, RILEM International Symposium on the Effect of Repeated Loading on Materials and Structures (Mexico City, Sept. 1966), Institute de Ingenieria, Mexico City, 1967, V. 4, Theme 4, pp. 31.

- Fiora A. E., Osterle R. G., and Carpenter J. E., “Reversing Load Tests of Five Isolated Structural Walls”, Proceedings of the International Symposium of Earthquake Structural Engineering, University of Missouri – Rolla, August 1976, Vol. 1, pp. 437-453.

- Furlong R.W, Fenves G.L., Kasl E.P., “Welded structural Wire Reinforcement for Columns”, ACI Structural Journal, Sep-Oct. 1991, pp. 585-591.

- Goodsir W.J., “The Design of Coupled Frame-Wall Structures for Seismic Actions”, PhD Thesis, Department of Civil Engineering, University of Canterbury, New Zealand, 1985.

- Goodsir W.J., “The Response of Coupled Shear Walls and Frames”, Master of Engineering Report, University of Canterbury, New Zealand, 1982.

- Goodsir W.J., Paulay T., Carr A.J., “A Study of The Inelastic Seismic Response of Reinforced Concrete Coupled Frame-Shear Wall Structures”, Bulletin of the New Zealand National Society for Earthquake Engineering, 1983, Vol. 16, No. 3, pp. 185-200.

- Grira M., “Innovative Approaches to Column Confinement”, PhD Thesis, Department of Civil Engineering, University of Ottawa, September 1998.

- Grira M., Saatcioglu M., “Concrete Column Confinement with Welded Wire Reinforcement Grids”, Ottawa Carleton Earthquake Engineering Research Center, Report OCEERC 96-05, September 1996.

- Grira, M., and Saatcioglu, M., “Material Tests for Welded Reinforcement Grids,” Ottawa Carleton Earthquake Engineering Research Center, Report OCEERC 97-17, October 1997.

- Lee S.L., Mansur M.A., Tan K.H., Kasiraju K., “Cracking Behavior of One-Way Slab Reinforced with Welded Wire Fabric”, ACI Structural Journal, V. 86, No. 2, Mar-Apr 1989, pp. 208-216.

- Leonhardt F., Walther R., “Deep Beams (Wandartige Traeger)”, Bulletin No. 178, Deutscher Ausschuss fur Stahlbeton, Berlin, 1966, pp. 159.

- Lin C.H., Perng S.M., “Flexural Behavior of Concrete Beams with Welded Wire Fabric as Shear Reinforcement”, ACI Structural Journal, V. 95, No. 5, September-October 1998, pp. 540-546.

- Mansur M.A., Tan K.H., Lee S.L., Kasiraju K., “Crack Width in Concrete Members Reinforced with Welded Wire Fabric”, ACI Structural Journal, V. 88, No. 2, March-April 1991, pp. 147-154.

- Mansur M.A., Lee C.K., Lee S.L., “Deformed Wire Fabric as Shear Reinforcement in Concrete Beams”, ACI Structural Journal, September-October 1987, pp. 392-399.

- Miranda E., Thompson C.L., Bertero V.V., "Cyclic Behavior of Shear Wall Boundary Elements Incorporating Prefabricated Welded Wire Hoops", Research Report, Earthquake Engineering Research Center, College of Engineering, University of California, Berkley, Jan. 1990, pp. 66.

- Muto K., Kokusho S., " Experimental Study on Two-Story Reinforced Concrete Shear Walls", Transactions, Architectural Institute of Japan (Tokyo), No. 47, Sept. 1953, pp. 7.

- Muto K., "Recent Trends in High-Rise Building Design in Japan", Third World Conference on Earthquake Engineering, New Zealand, Proceedings, 1965, Vol. 1, pp. 118-149.

- Ogura K., Kokusho S., and Matsoura N., "Tests to Failure of Two-Story Rigid Frames with Walls, Part 24, Experimental Study No. 6", Report No. 18, Architectural Institute of Japan, Tokyo, Feb. 1952.

- Oesterle R.G., Fiorato A.E., Johal L.S., Carpenter J.E., Russel H.G., Corley W.G., "Earthquake Resistant Structural Walls – Tests of Isolated Walls", Report submitted by Research and Development Construction Technology Laboratories, Portland Cement Association, Report to National Science Foundation (RANN), November 1976.

- Oesterle R.G., Aristizabal-Ochoa J.D., Fiorato A.E., Russell H.G., Corley W.G., "Earthquake Resistant Structural Walls – Tests of Isolated Walls – Phase II, Report submitted by Construction Technology Laboratories, A division of Portland Cement Association, Report to National Science Foundation, Washington, D.C, October 1979.

- Park R., Paulay T., "Reinforced Concrete Structures", Department of Civil Engineering, University of Canterbury, Christchurch, New Zealand, A Wiley-Interscience Publication, 1974.

- Paulay T., "The Coupling of Reinforced Concrete Shear Walls", Proceedings, Fourth World Conference, on Earthquake Engineering, Santiago, Chile, Jan. 1969, V. 1, 11. B2-75 to B2-90.

- Paulay T., “Coupling Beams of Reinforced Concrete Shear Walls”, Proceedings, ASCE, V. 97, ST3, Mar. 1971, pp. 843-862.

- Paulay T., Priestley M. J. N., “Seismic Design of Reinforced Concrete and Masonry Buildings”, A Wiley Interscience Publication, 1992.

- Pincheira J., Rizkalla S.H., Attiogbe E.K., “Performance of Welded Wire Fabric as Shear Reinforcement under Cyclic Loading”, ACI Structural Journal, V. 86, No. 6, November-Decemeber 1989, pp. 728-735.

- Saatcioglu M., Grira M., “Confinement of Reinforced Concrete Columns with Welded Reinforcement Grids”, ACI Structural Journal, Technical Paper 96-S4, V. 96, No. 1, January-February 1999, pp. 29-39.

- Saatcioglu M., Grira M., “High-Strength Concrete (HSC) Columns Confined with Welded Reinforcement Grids,” Ottawa Carleton Earthquake Engineering Research Center, Report OCEERC 11-01, February 2011.

- Standards Association of New Zealand, “New Zealand Standard Code of Practice for the Design of Concrete Structures”, NZS 3101, Parts 1 and 2, 1982, Wellington.

- Standards Association of New Zealand, “New Zealand Standard Code of Practice for the Design of Concrete Structures”, NZS 3101, Parts 1 and 2, 1995, Wellington.

- Thompson C.L., Miranda E., Bertero V.V., “Experimental Studies of the Confinement of Shear Wall Boundary Elements Incorporating Prefabricated Welded Wire Hoops”, Earthquake Engineering Research Center, Report to Sponsor, University of California, September 1989.

- Razvi R. S., “Behavior of Reinforced Concrete Columns Confined with Welded Wire Fabric”, Master of Applied Science Thesis, Department of Civil Engineering, University of Ottawa, January 7, 1988.

- Razvi R. S., Saatcioglu M., “Confinement of Reinforced Concrete Columns with Welded Wire Fabric”, ACI Structural Journal, V. 86, No.5, Technical Paper 86-S60, September-October 1989, pp. 615-623.

- Uniform Building Code (UBC) – 1970, published by International Council of Building Officials, United States of America, 1970.

- Vallenas J.M., Bertero V.V., Popov E. G., “Hysteretic Behavior of Reinforced Concrete Structural Walls”, Report to National Science Foundation, Report conducted at Earthquake Engineering Research Center, College of Engineering, University of California, Berkley, August 1979.

- Williams H. A., Benjamin J. R., “Investigation of Shear Walls, Part 3 – Experimental and Mathematical Studies of the Behavior of Plain and Reinforced Concrete Walled Bents Under Static Shear Loading”, Department of Civil Engineering, Stanford University, July 1953, pp. 142.

Appendix A.1 – Strain Gauge Recordings of Cast-in Concrete WWR Grids – Direct Shear Test

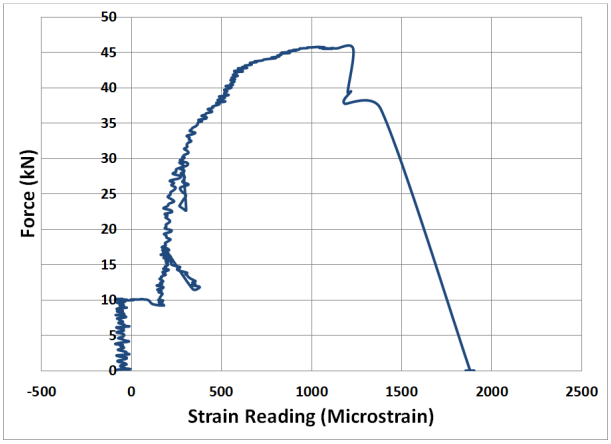

Strain Gauge: SH2-1-1

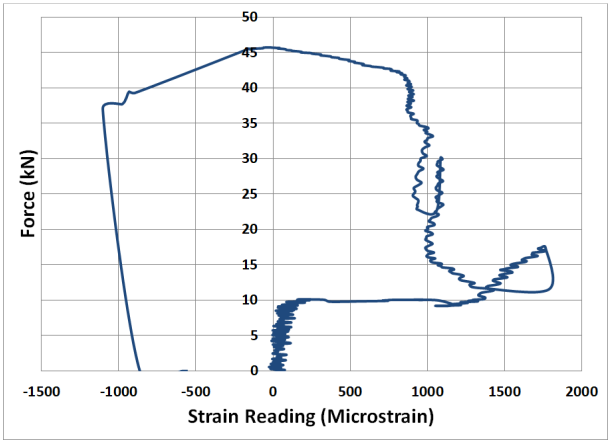

Strain Gauge: SH2-1-2

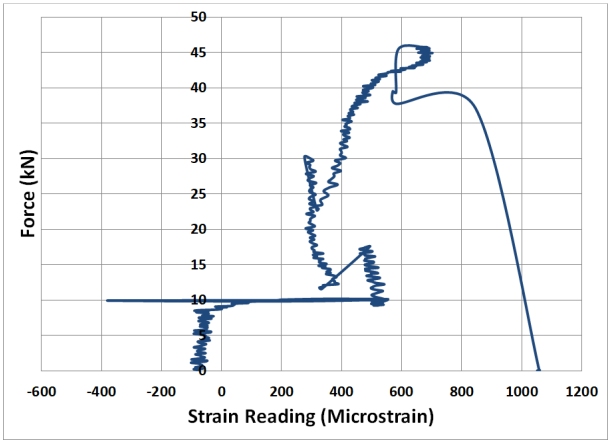

Strain Gauge: SH2-1-3

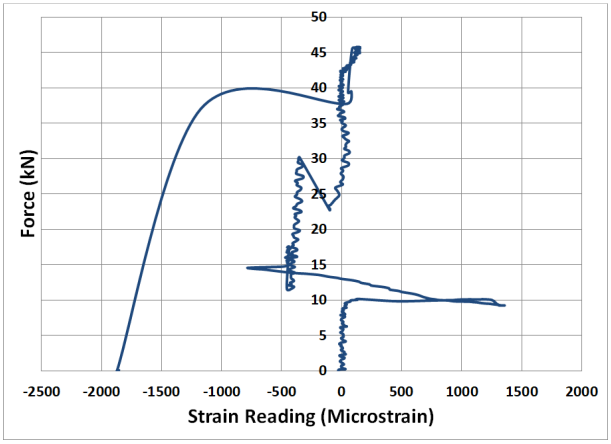

Strain Gauge: SH2-1-4

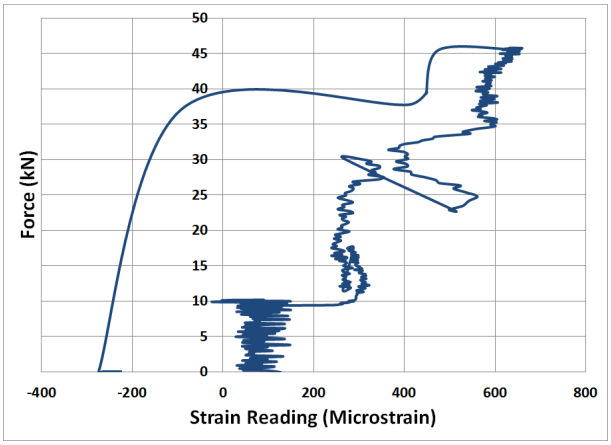

Strain Gauge: SH2-1-5

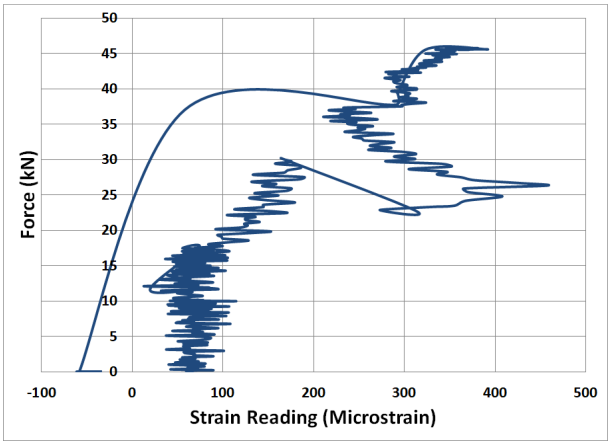

Strain Gauge: SH2-1-6

Figure A1.1 Specimen SH2-1 Strain Gauge Recordings

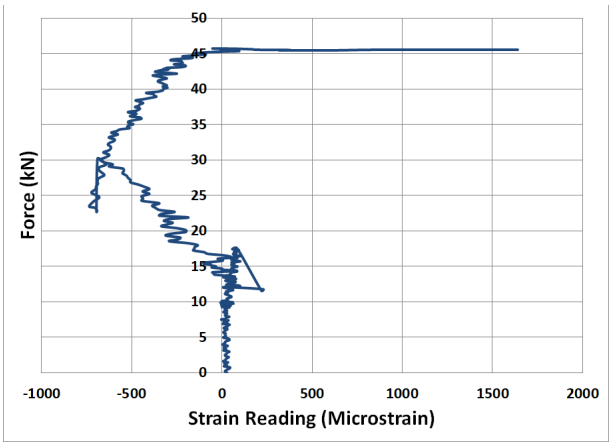

Strain Gauge: SH2-1-7

Figure A1.1 (Cont'd) Specimen SH2-1 Strain Gauge Recordings

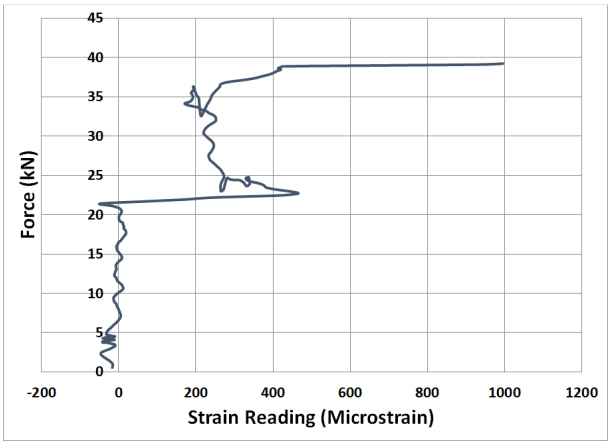

Strain Gauge: SH2-2-2

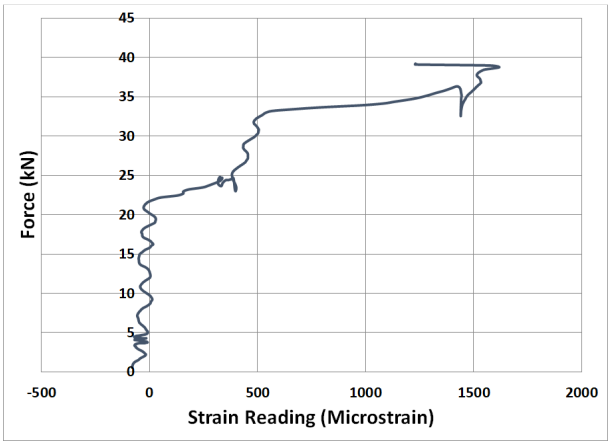

Strain Gauge: SH2-2-3

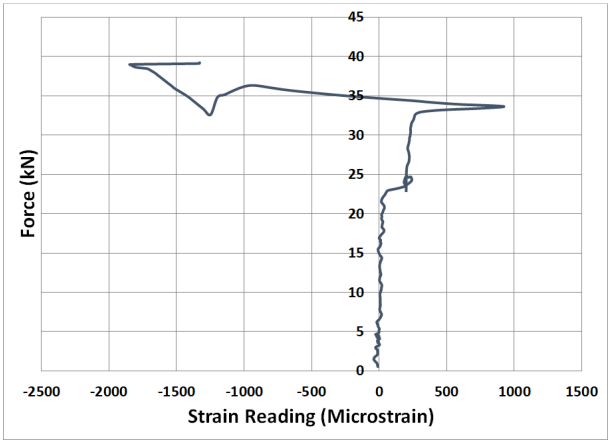

Strain Gauge: SH2-2-4

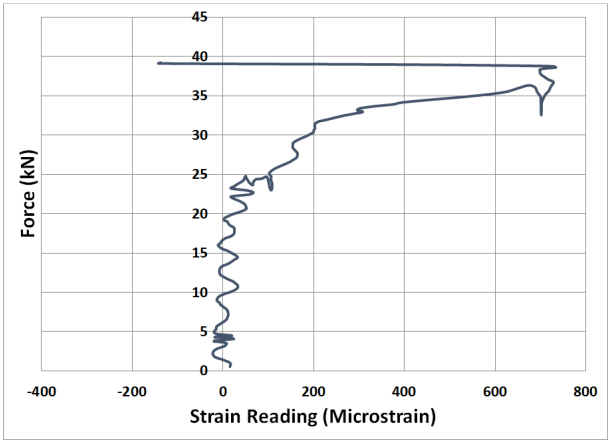

Strain Gauge: SH2-2-5

Figure A1.2 Specimen SH2-2 Strain Gauge Recordings

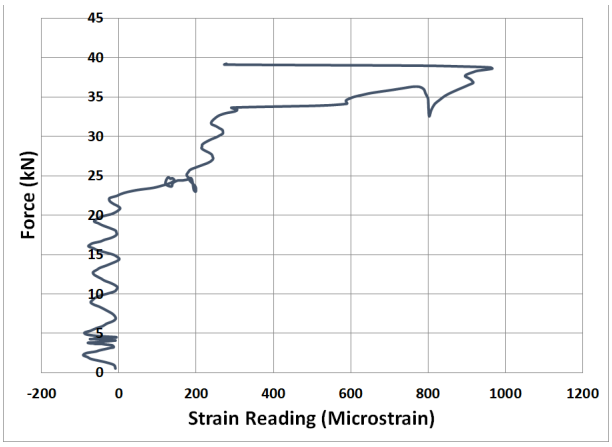

Strain Gauge: SH2-2-6

Figure A1.2 (Cont'd) Specimen SH2-2 Strain Gauge Recordings

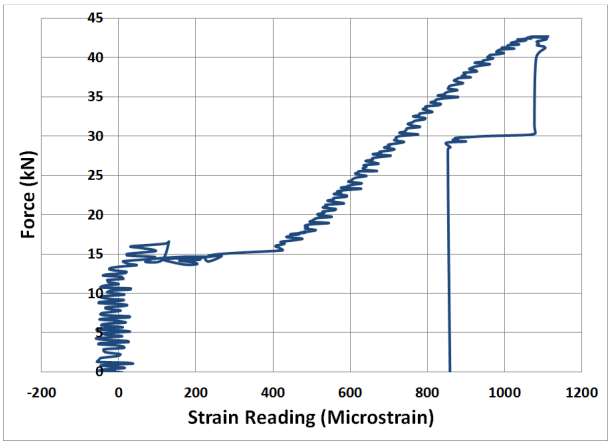

Strain Gauge: SH3-1-1

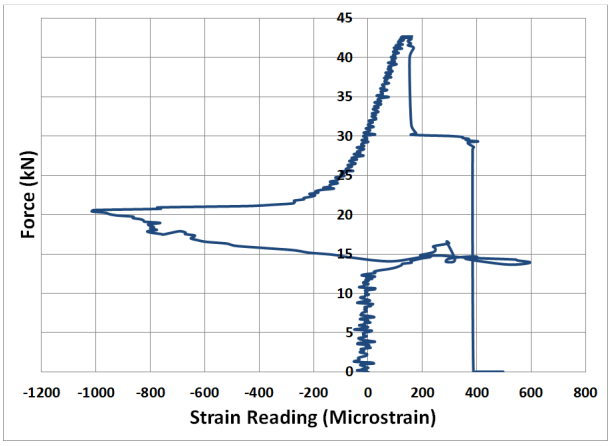

Strain Gauge: SH3-1-3

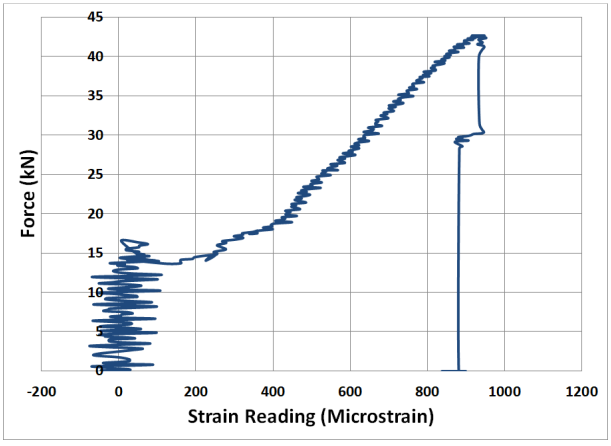

Strain Gauge: SH3-1-4

Figure A1.3 Specimen SH3-1 Strain Gauge Recordings

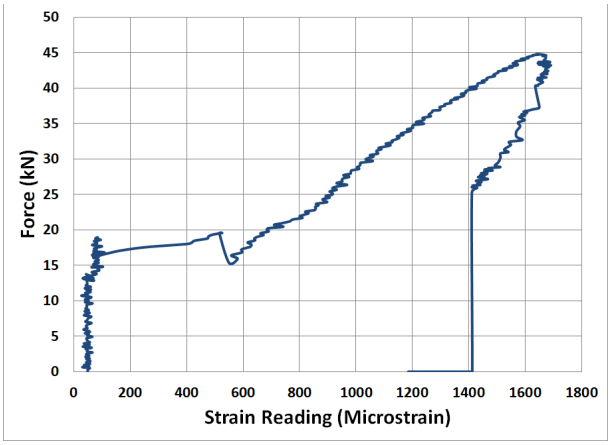

Strain Gauge: SH3-2-1

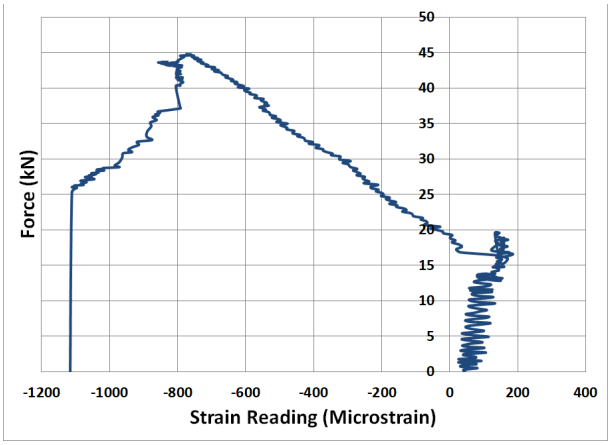

Strain Gauge: SH3-2-2

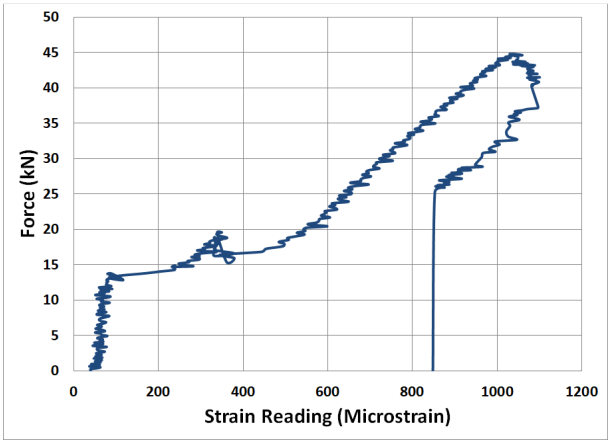

Strain Gauge: SH3-2-4

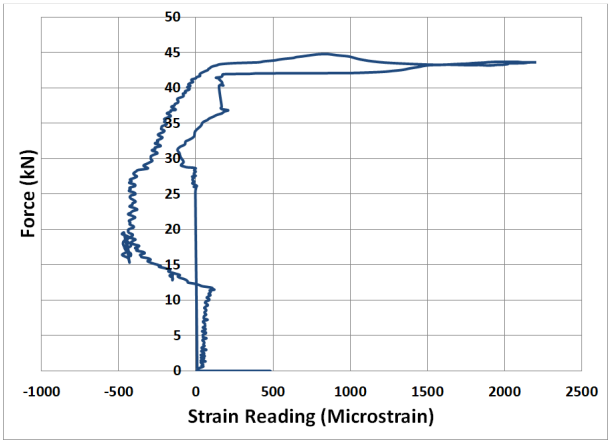

Strain Gauge: SH3-2-6

Figure A1.4 Specimen SH3-2 Strain Gauge Recordings

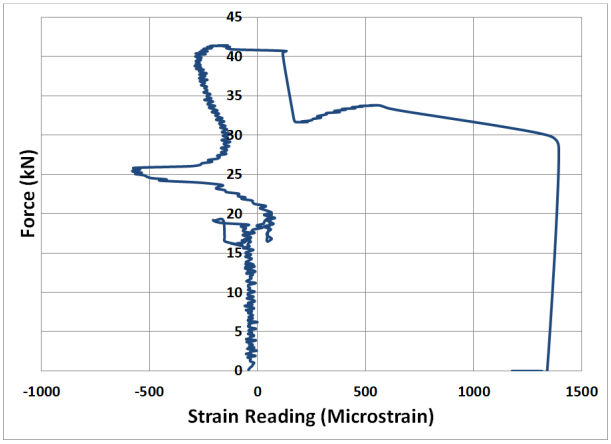

Strain Gauge: SH3-3-1

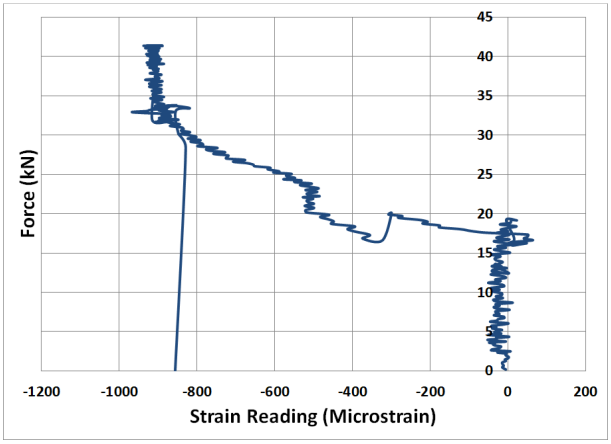

Strain Gauge: SH3-3-2

Figure A1.5 Specimen SH3-3 Strain Gauge Recordings

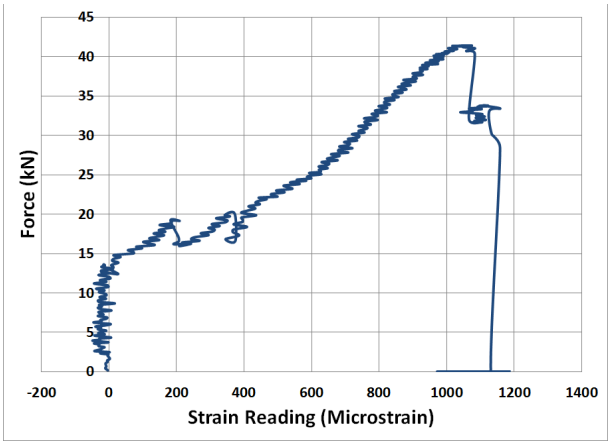

Strain Gauge: SH3-3-3

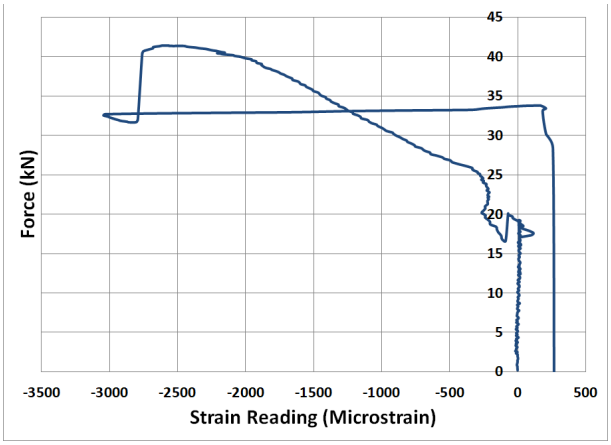

Strain Gauge: SH3-3-7

Figure A1.5 (Cont'd) Specimen SH3-3 Strain Gauge Recordings

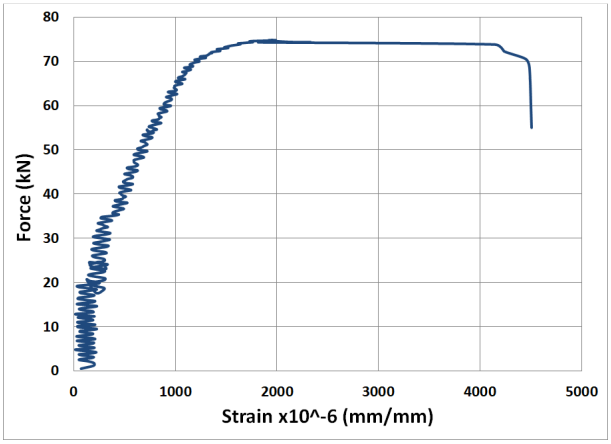

Strain Gauge: SH8-1-1

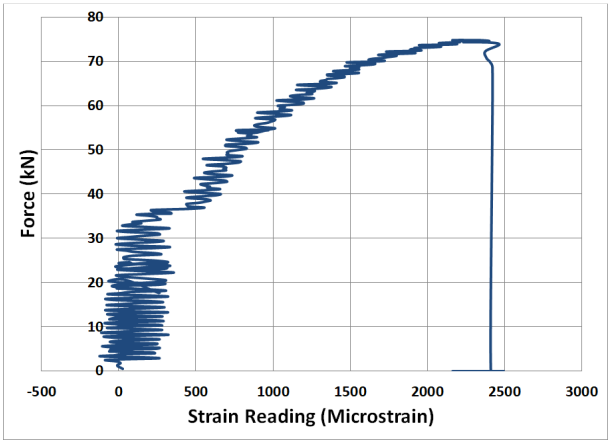

Strain Gauge: SH8-1-2

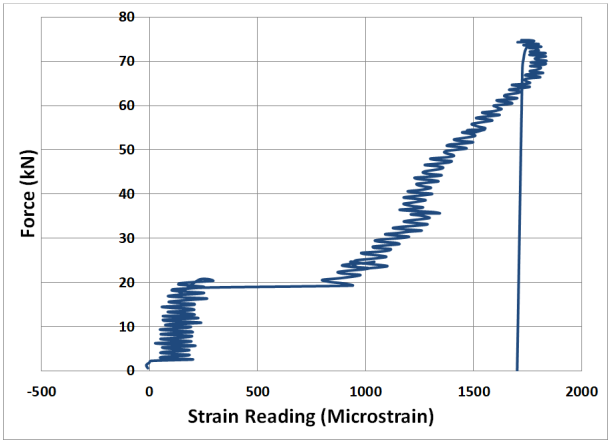

Strain Gauge: SH8-1-3

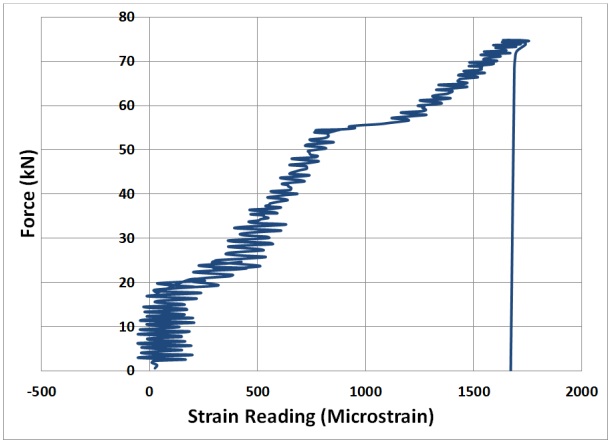

Strain Gauge: SH8-1-4

Figure A1.6 Specimen SH8-1 Strain Gauge Recordings

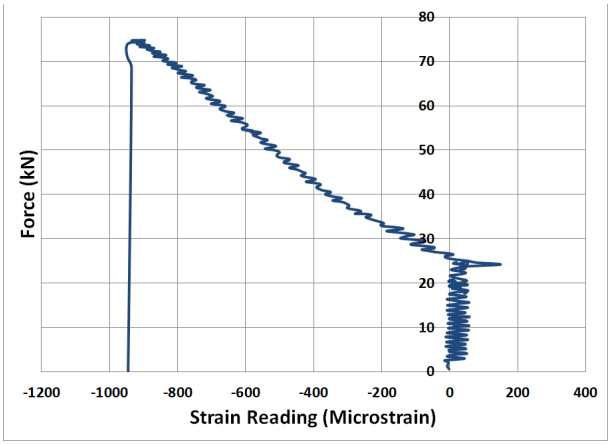

Strain Gauge: SH8-1-6

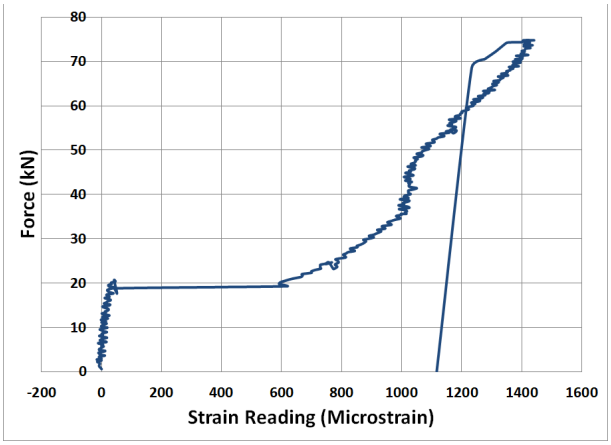

Strain Gauge: SH8-1-8

Figure A1.6 (Cont'd) Specimen SH8-1 Strain Gauge Recordings

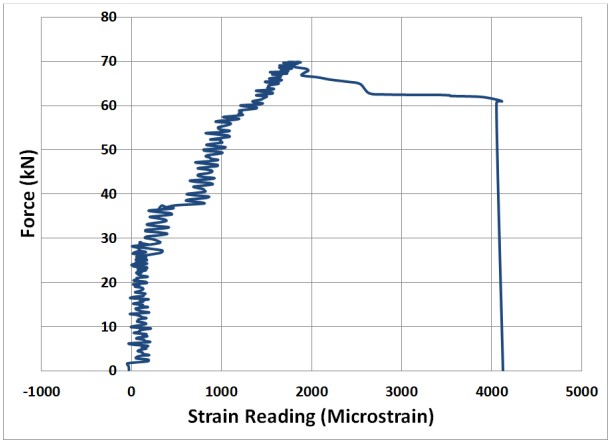

Strain Gauge: SH8-2-2

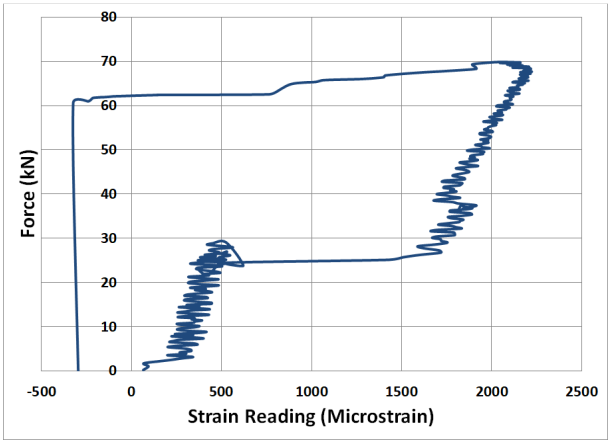

Strain Gauge: SH8-2-3

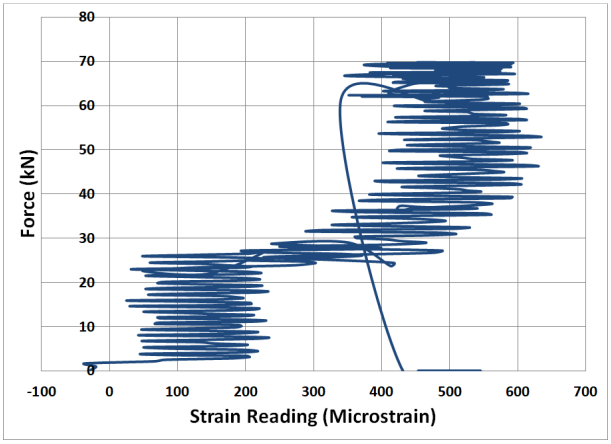

Strain Gauge: SH8-2-4

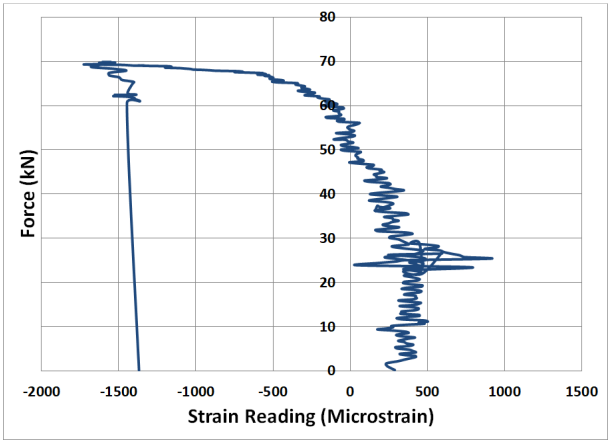

Strain Gauge: SH8-2-5

Figure A1.7 Specimen SH8-2 Strain Gauge Recordings

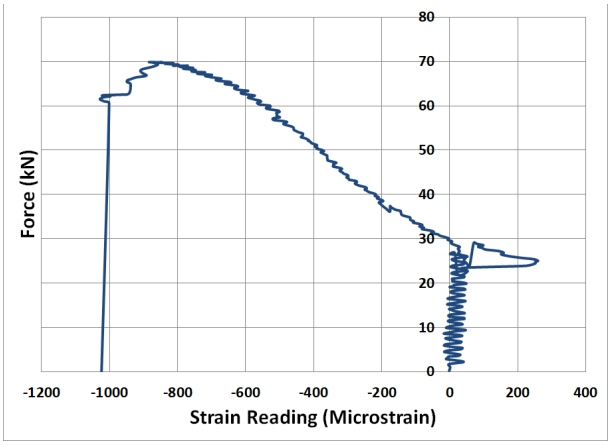

Strain Gauge: SH8-2-6

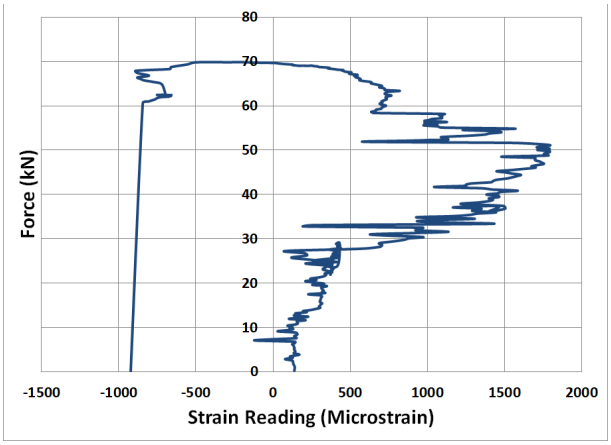

Strain Gauge: SH8-2-7

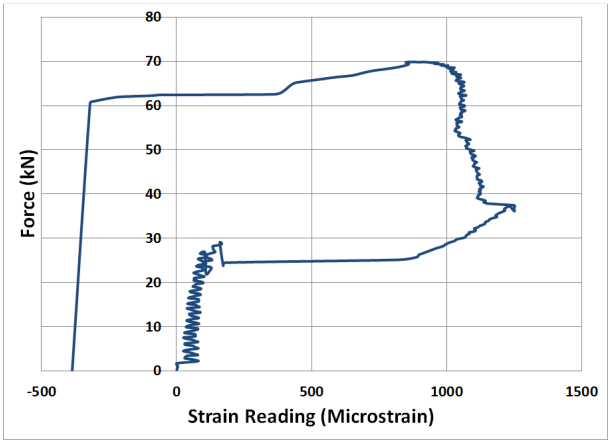

Strain Gauge: SH8-2-8

Figure A1.7 (Cont'd) Specimen SH8-2 Strain Gauge Recordings

Appendix A.2 – Strain Gauge Recordings of Cast-in Concrete WWR Grids – Burst Test

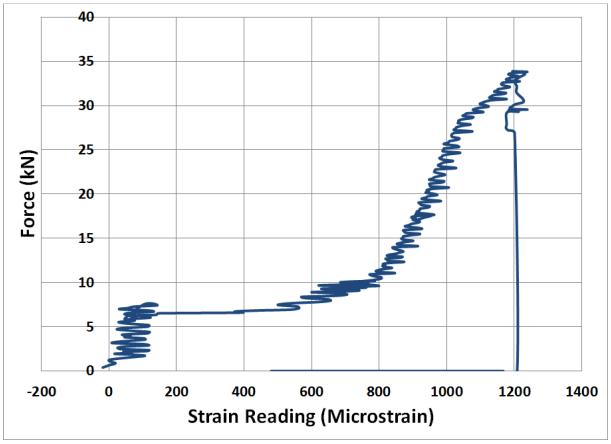

Strain Gauge: B2-1-1

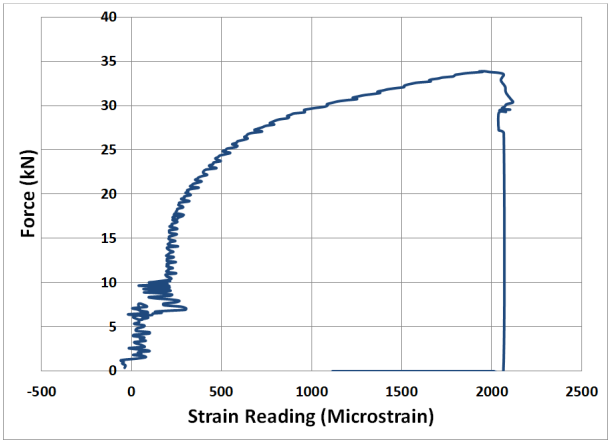

Strain Gauge: B2-1-2

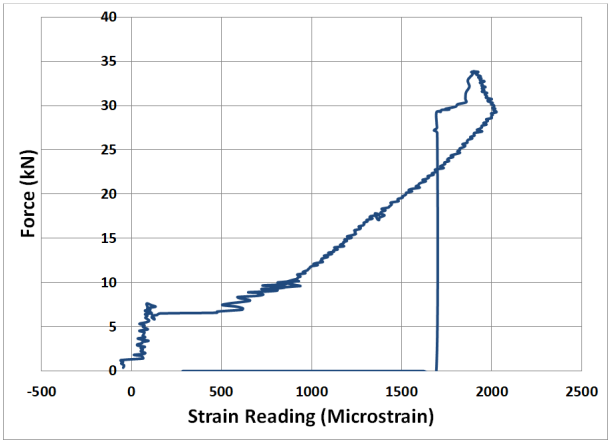

Strain Gauge: B2-1-3

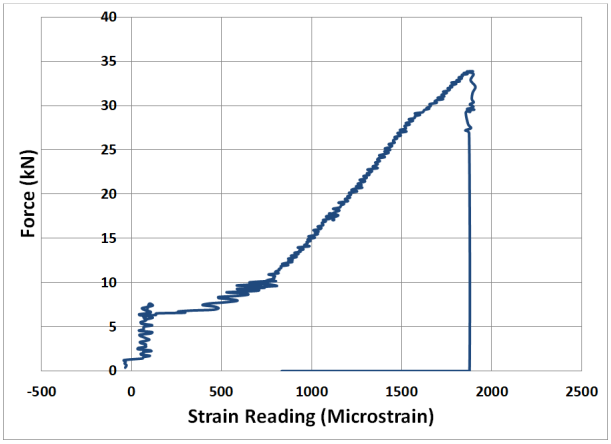

Strain Gauge: B2-1-4

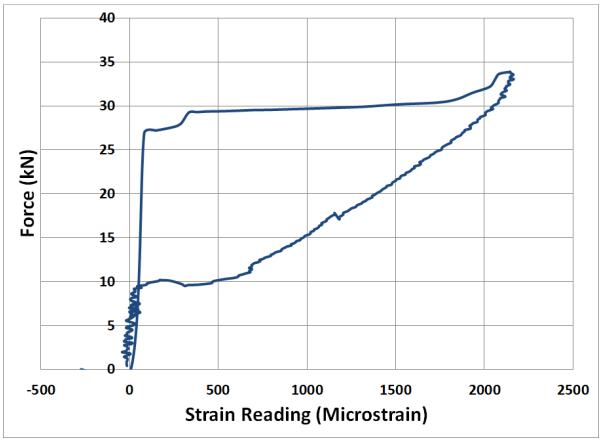

Strain Gauge: B2-1-6

Figure A2.1 Specimen B2-1 Strain Gauge Recordings

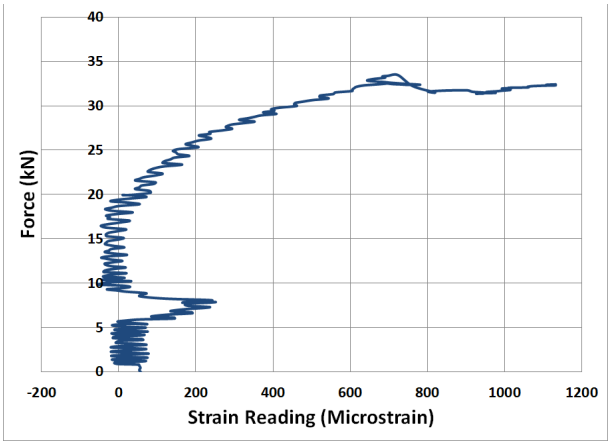

Strain Gauge: B2-2-2

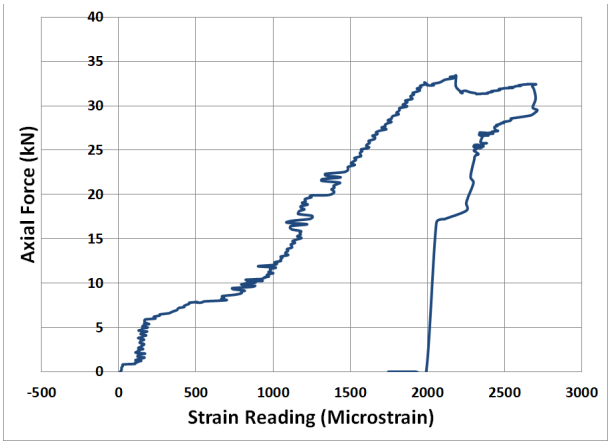

Strain Gauge: B2-2-4

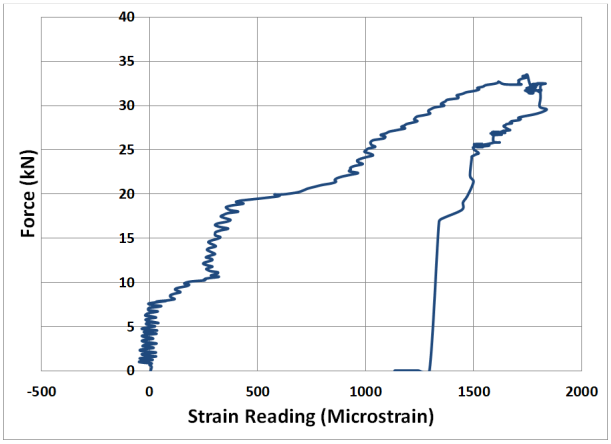

Strain Gauge: B2-2-5

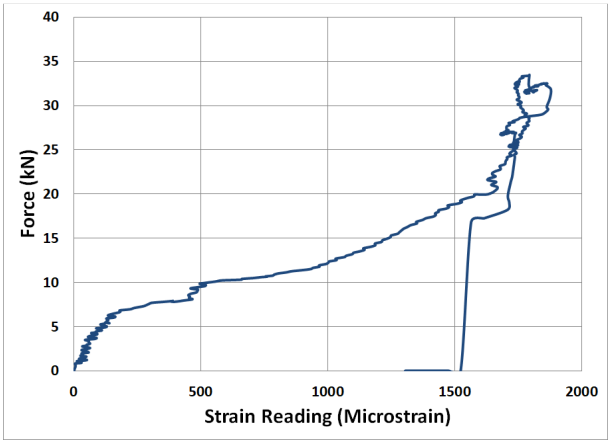

Strain Gauge: B2-2-6

Figure A2.2 Specimen B2-2 Strain Gauge Recordings

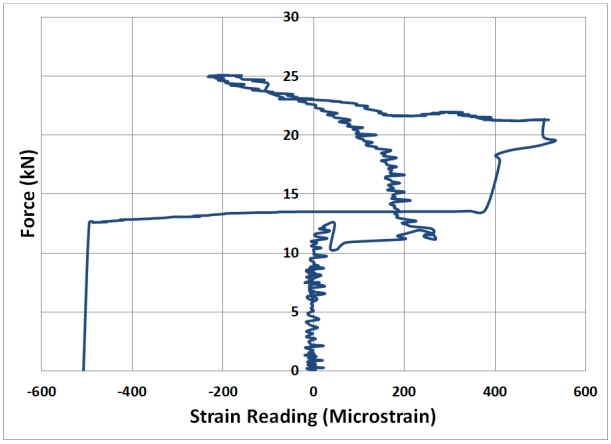

Strain Gauge: B3-1-1

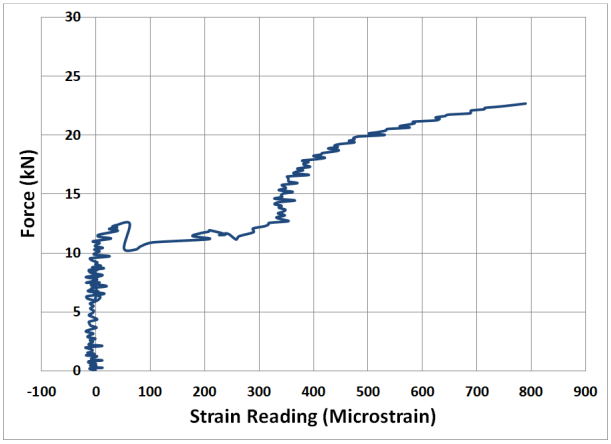

Strain Gauge: B3-1-2

Figure A2.3 Specimen B3-1 Strain Gauge Recordings

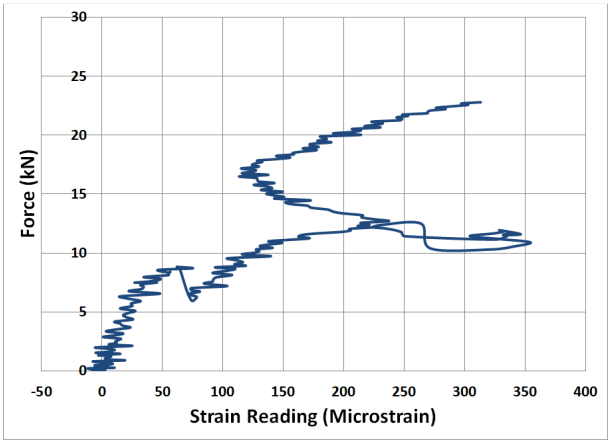

Strain Gauge: B3-1-3

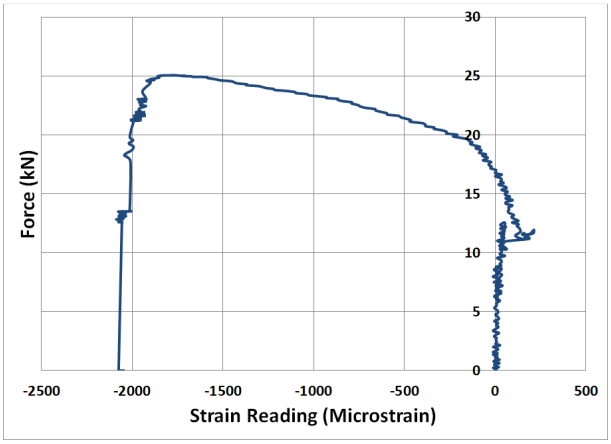

Strain Gauge: B3-1-4

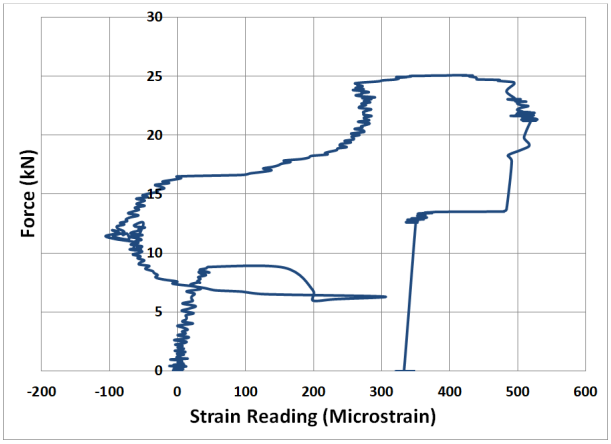

Strain Gauge: B3-1-6

Figure A2.3 (Cont'd) Specimen B3-1 Strain Gauge Recordings

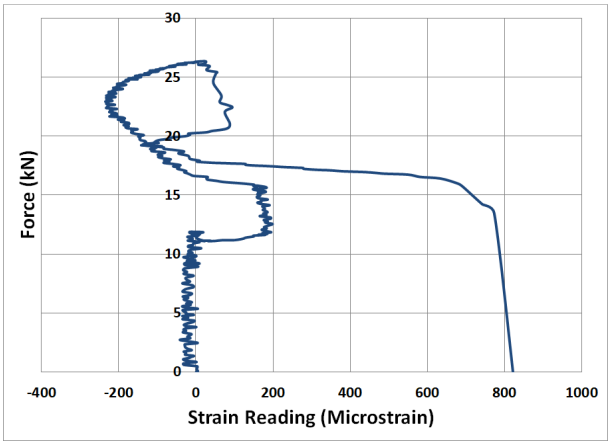

Strain Gauge: B3-2-2

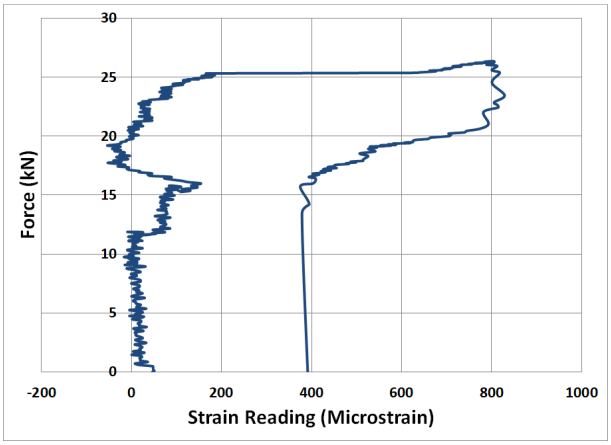

Strain Gauge: B3-2-3

Figure A2.4 Specimen B3-2 Strain Gauge Recordings

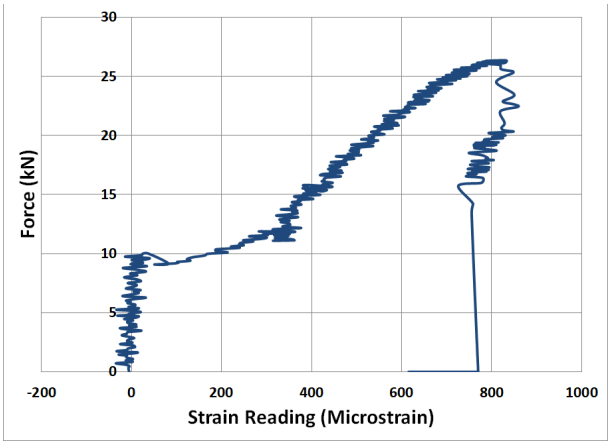

Strain Gauge: B3-2-4

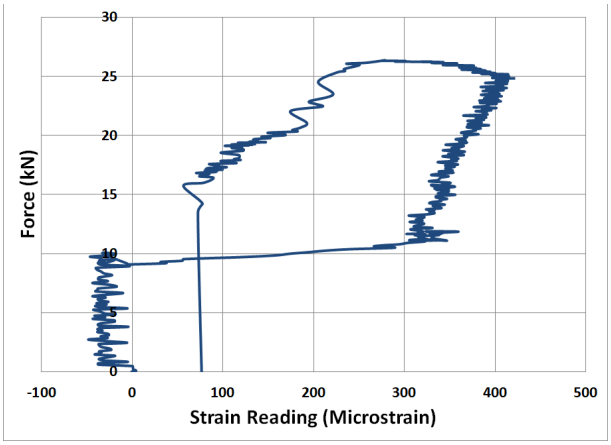

Strain Gauge: B3-2-5

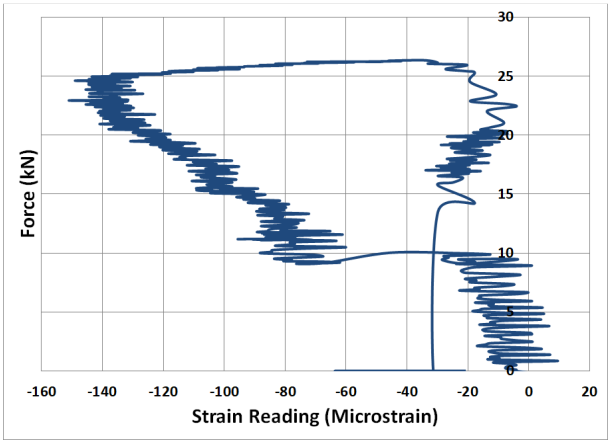

Strain Gauge: B3-2-6

Figure A2.4 (Cont'd) Specimen B3-2 Strain Gauge Recordings

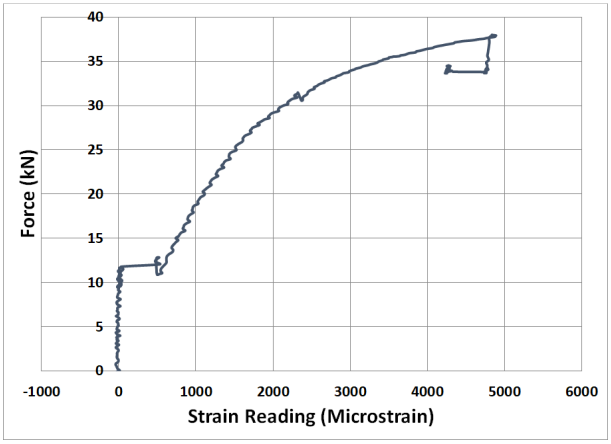

Strain Gauge: B8-1-1

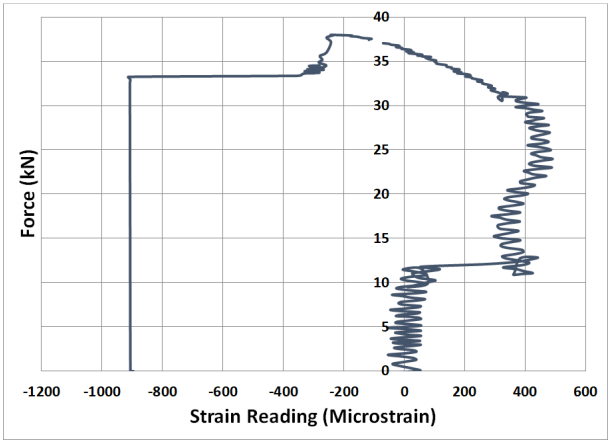

Strain Gauge: B8-1-2

Figure A2.5 Specimen B8-1 Strain Gauge Recordings

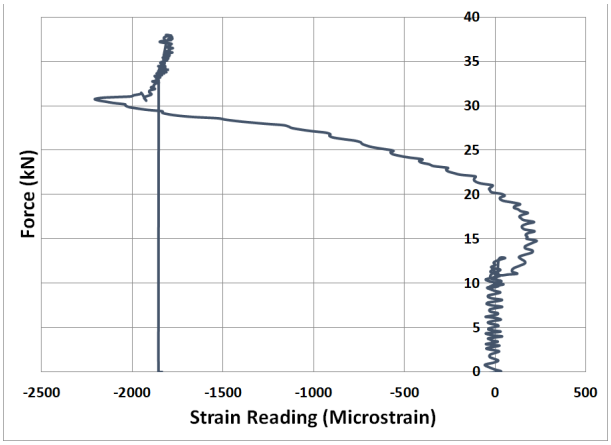

Strain Gauge: B8-1-3

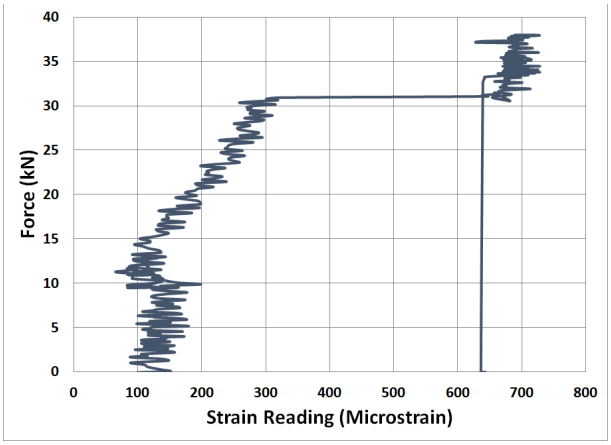

Strain Gauge: B8-1-4

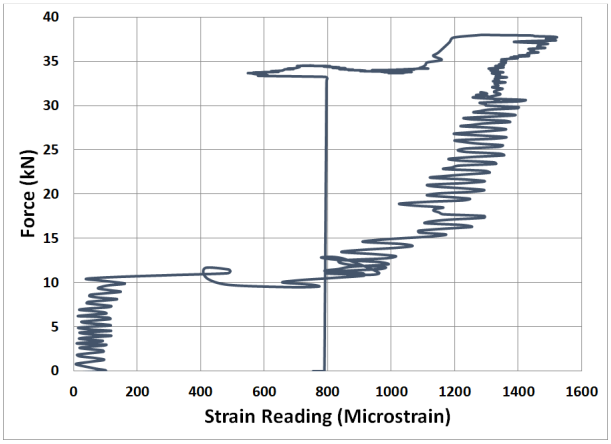

Strain Gauge: B8-1-5

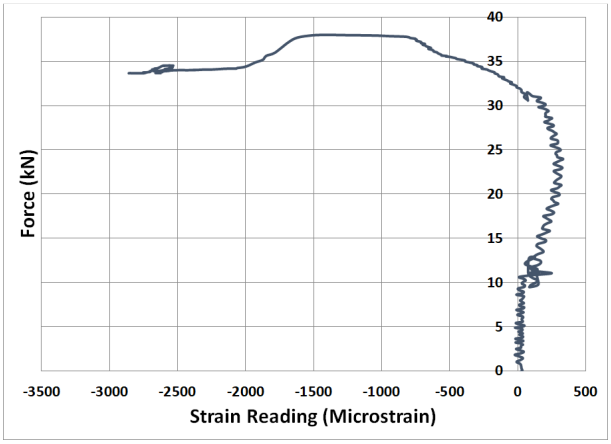

Strain Gauge: B8-1-6

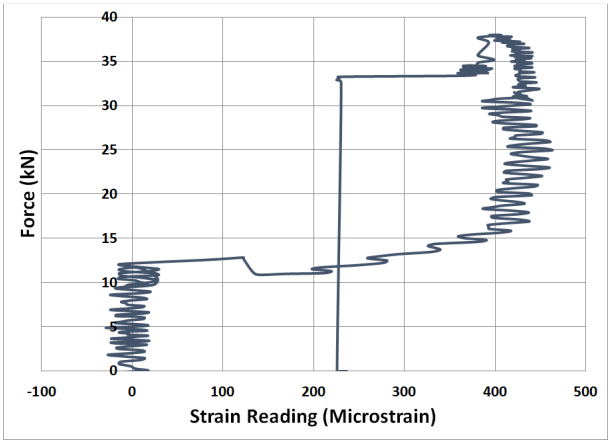

Strain Gauge: B8-1-8

Figure A2.5 (Cont'd) Specimen B8-1 Strain Gauge Recordings

Appendix A.3 – Strain Recordings of Concentrically Loaded Small-Scale Columns

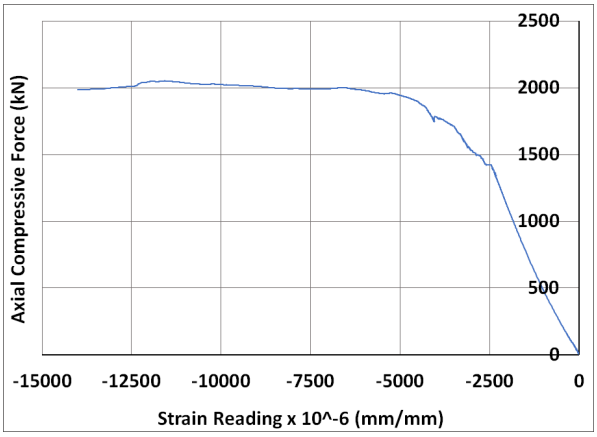

Strain Gauge: SG-LONG-1

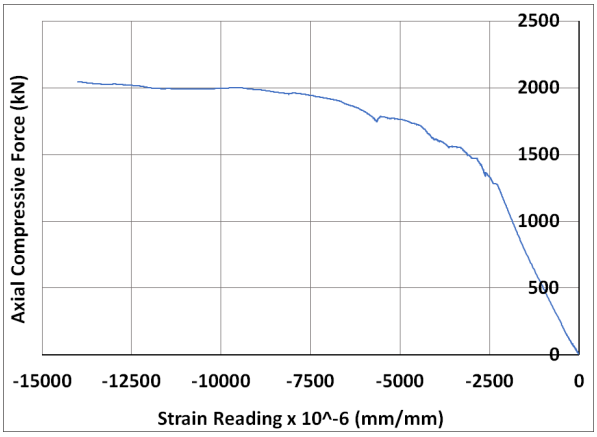

Strain Gauge: SG-LONG-2

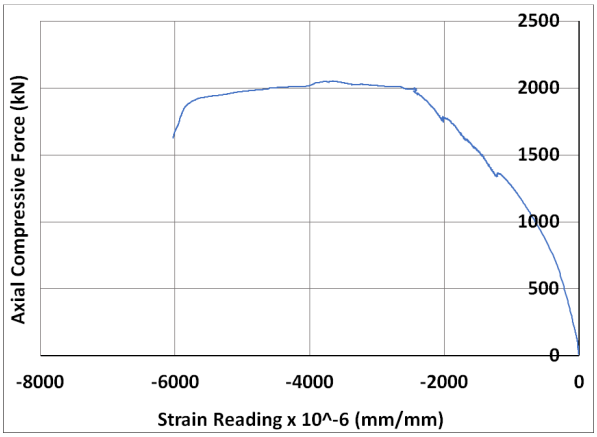

Strain Gauge: SG-LONG-3

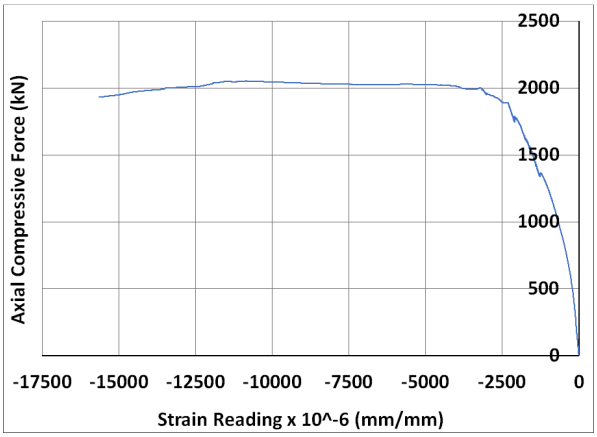

Strain Gauge: SG-LONG-4

Figure A3.1 Specimen SC-0-35 – Longitudinal Bars Strain Recordings

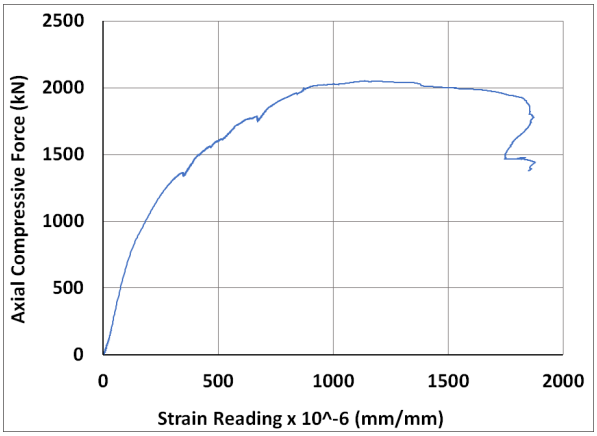

Strain Gauge: SG-G1-1

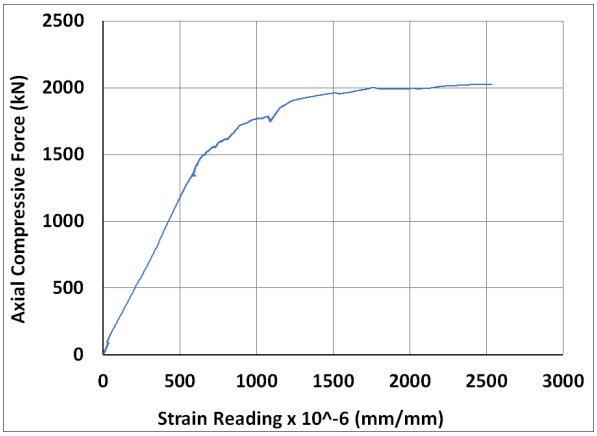

Strain Gauge: SG-G1-2

Figure A3.2 Specimen SC-0-35 – WWR Grids Strain Gauge Recordings

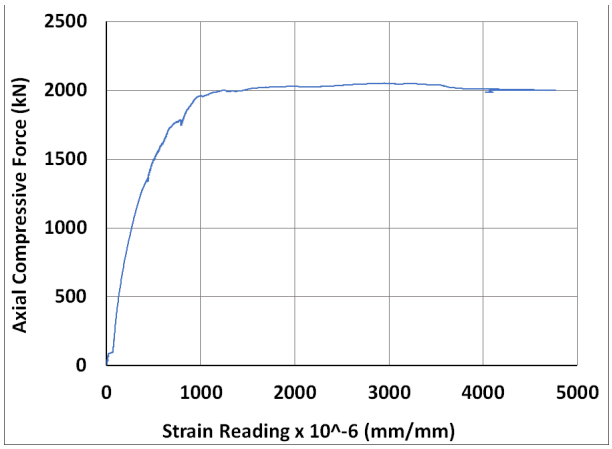

Strain Gauge: SG-G1-3

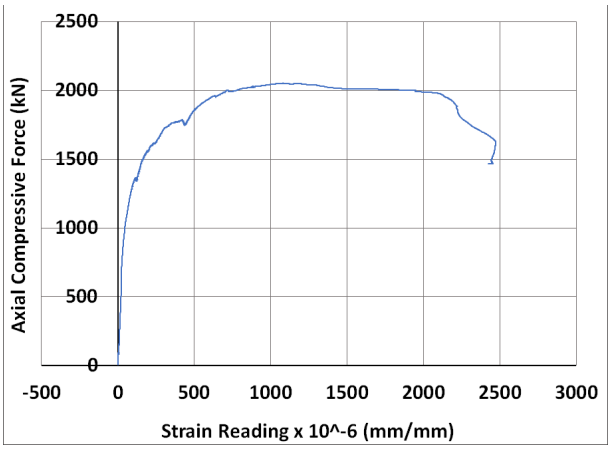

Strain Gauge: SG-G1-4

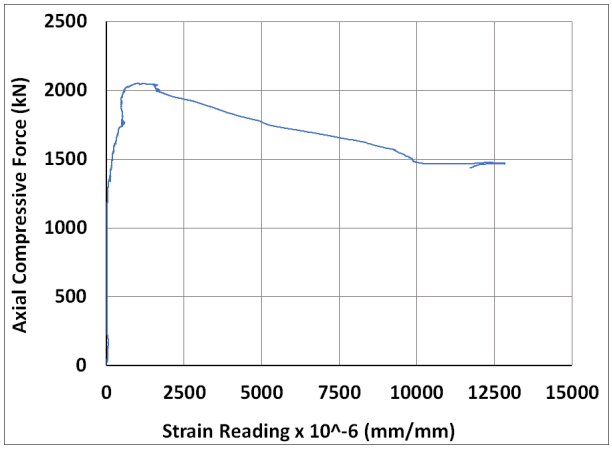

Strain Gauge: SG-G2-1

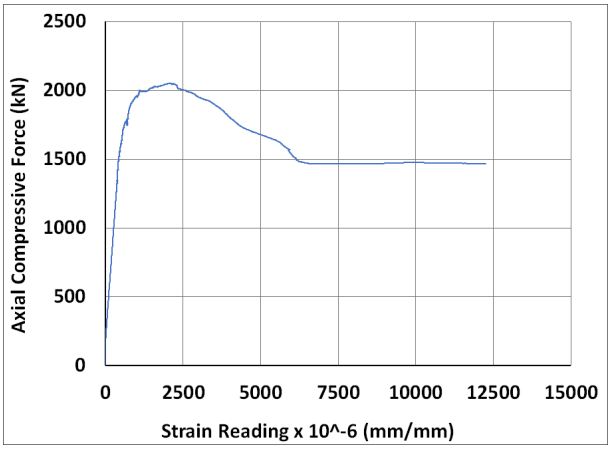

Strain Gauge: SG-G2-2

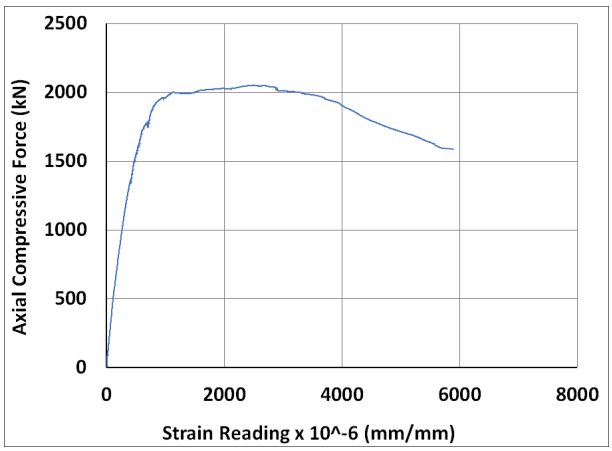

Strain Gauge: SG-G2-3

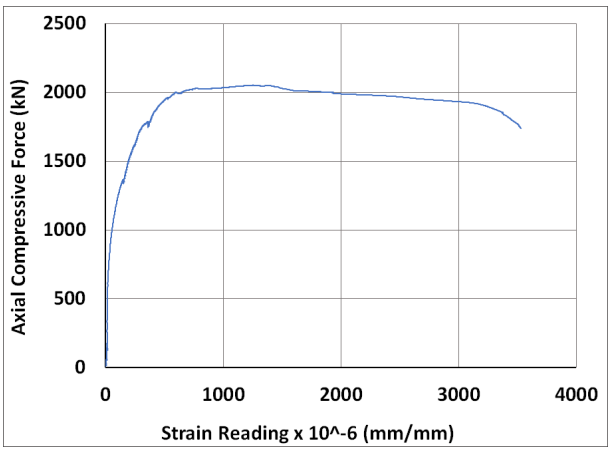

Strain Gauge: SG-G2-4

Figure A3.2 (Cont'd) Specimen SC-0-35 – WWR Grids Strain Gauge Recordings

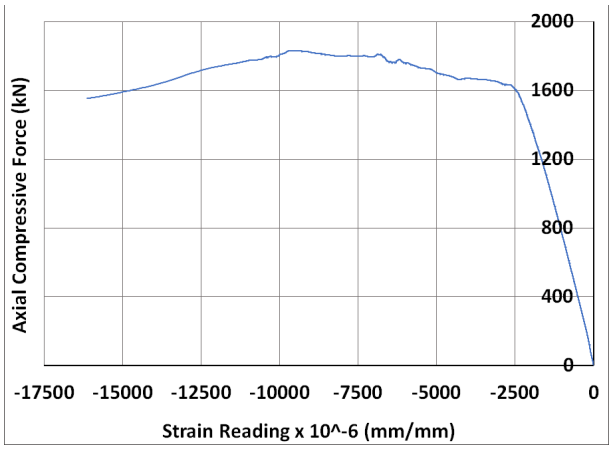

Strain Gauge: SG-LONG-1

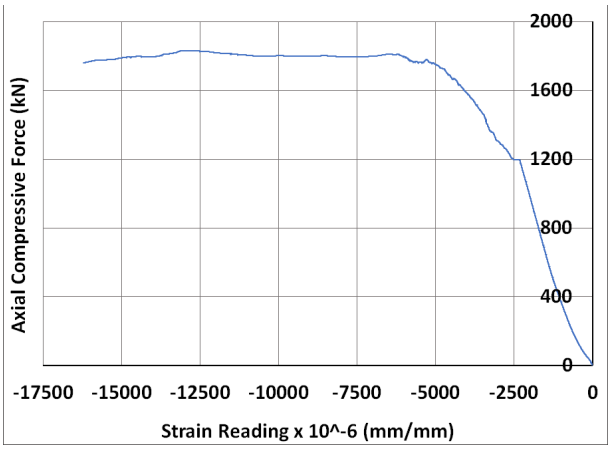

Strain Gauge: SG-LONG-2

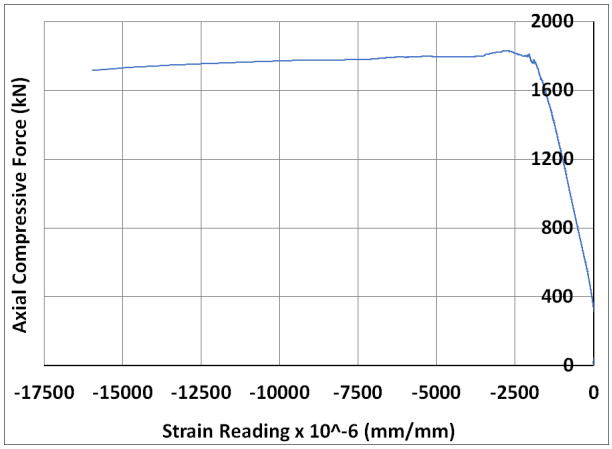

Strain Gauge: SG-LONG-3

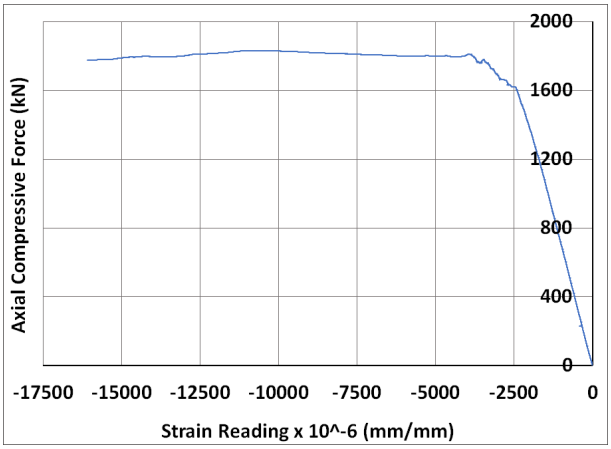

Strain Gauge: SG-LONG-4

Figure A3.3 Specimen SC-0-70 – Longitudinal Bars Strain Recordings

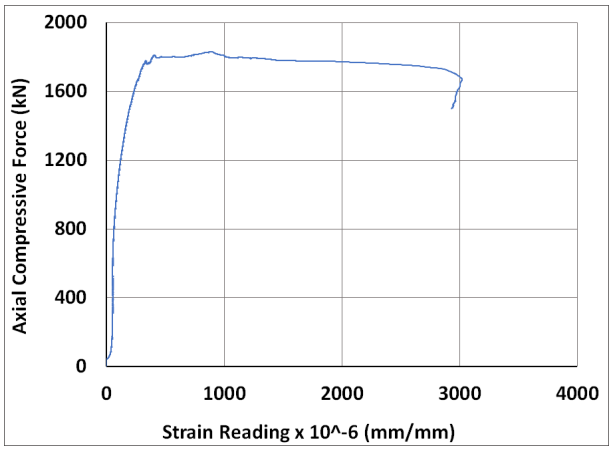

Strain Gauge: SG-G1-1

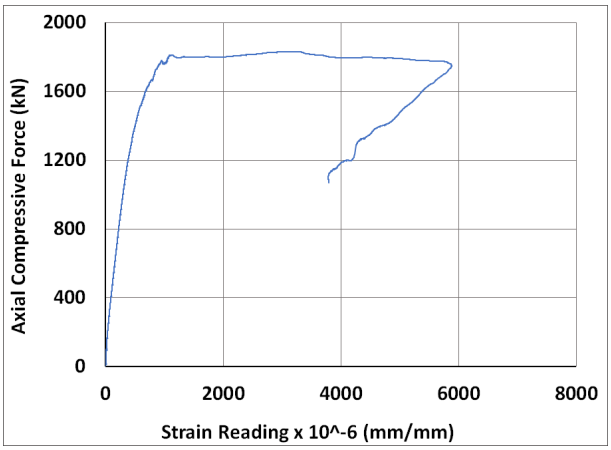

Strain Gauge: SG-G1-2

Figure A3.4 Specimen SC-0-70 – WWR Grids Strain Gauge Recordings

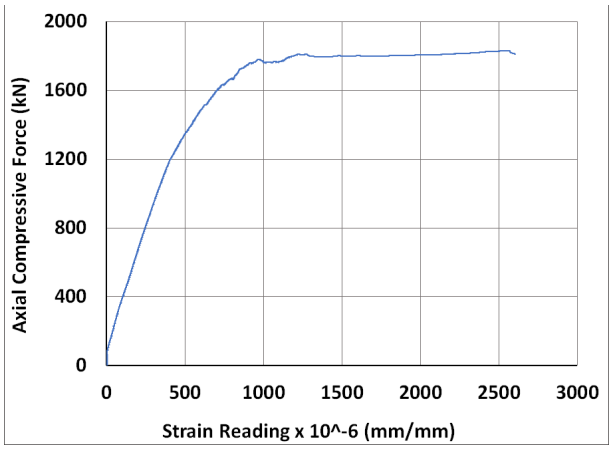

Strain Gauge: SG-G1-3

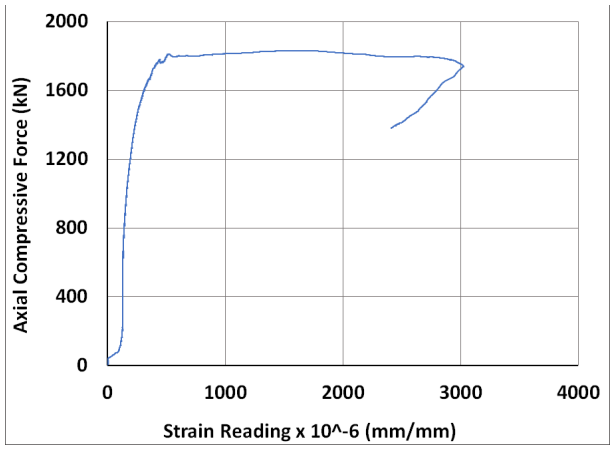

Strain Gauge: SG-G1-4

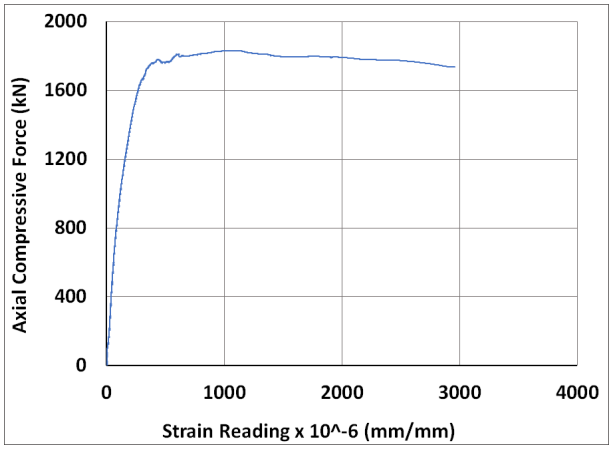

Strain Gauge: SG-G2-1

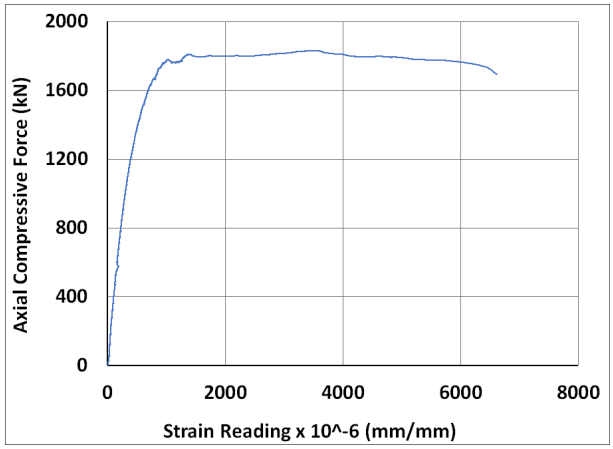

Strain Gauge: SG-G2-2

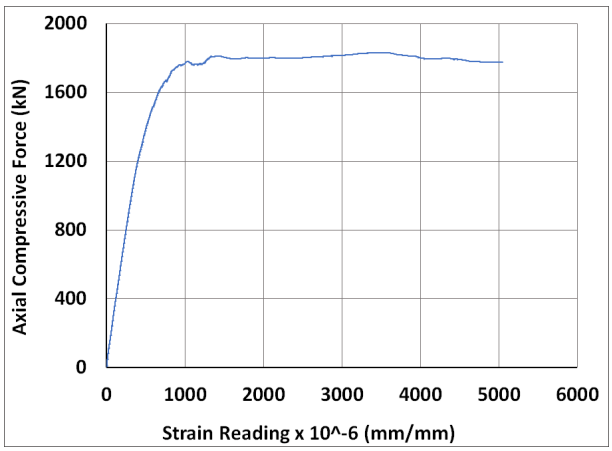

Strain Gauge: SG-G2-3

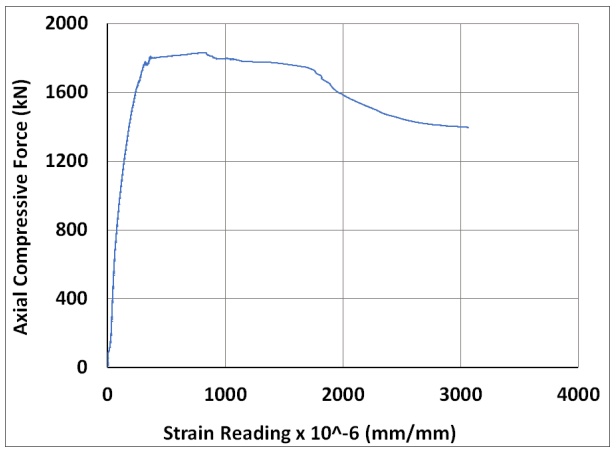

Strain Gauge: SG-G2-4

Figure A3.4 (Cont'd) Specimen SC-0-70 – WWR Grids Strain Gauge Recordings

Appendix A.4 – Strain Recordings of Eccentrically Loaded Small-Scale Columns

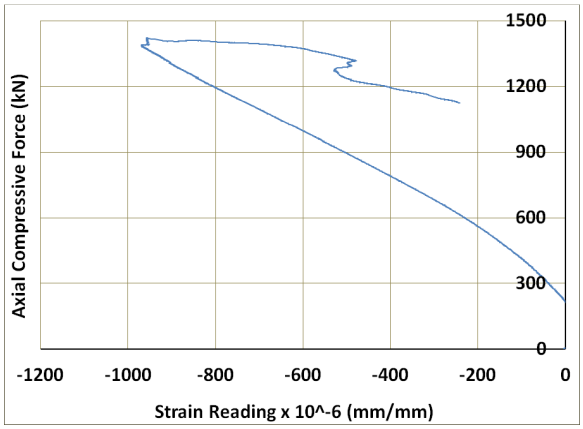

Strain Gauge: SG-LONG-1

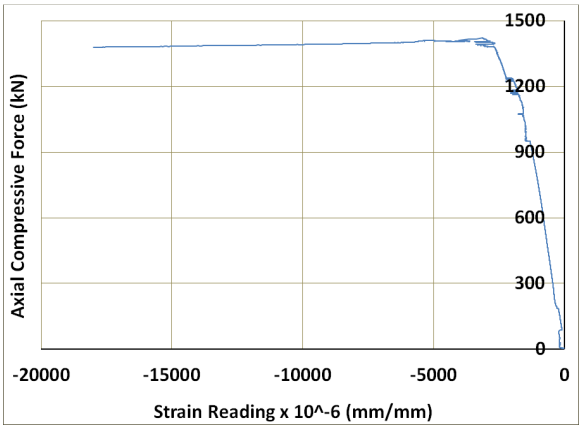

Strain Gauge: SG-LONG-2

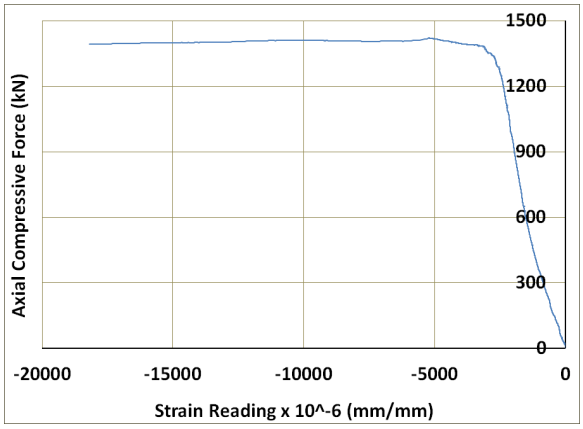

Strain Gauge: SG-LONG-3

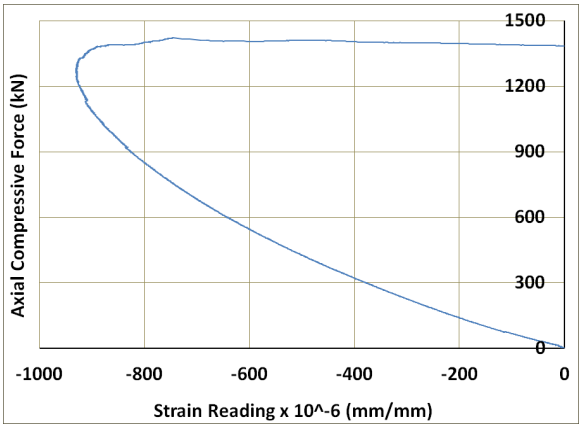

Strain Gauge: SG-LONG-4

Figure A4.1 Specimen SC-9-35 – Longitudinal Bars Strain Recordings

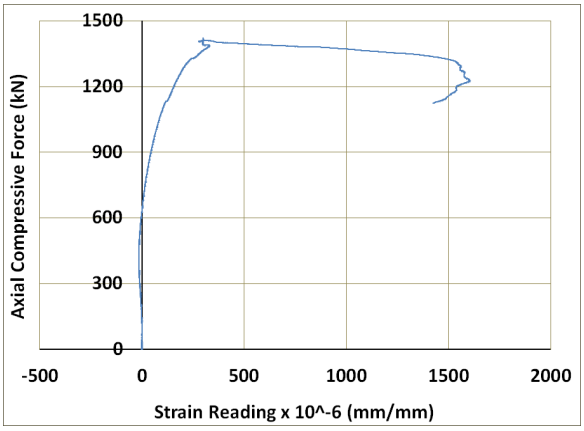

Strain Gauge: SG-G1-1

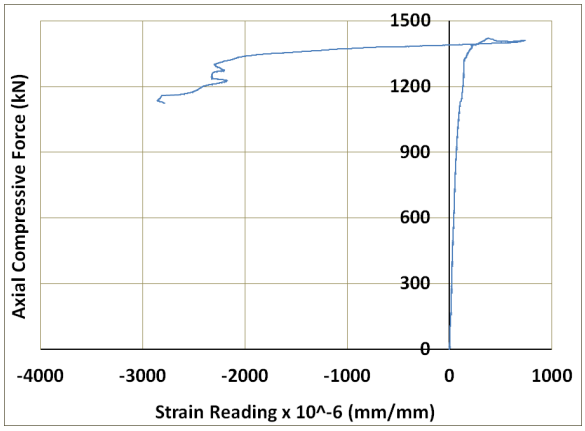

Strain Gauge: SG-G1-2

Figure A4.2 Specimen SC-9-35 – WWR Grids Strain Gauge Recordings

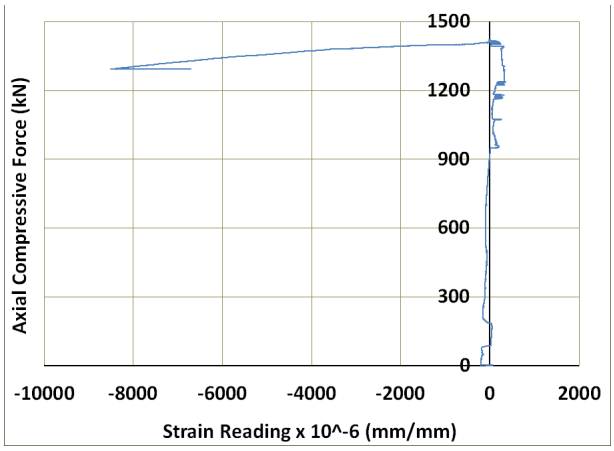

Strain Gauge: SG-G1-4

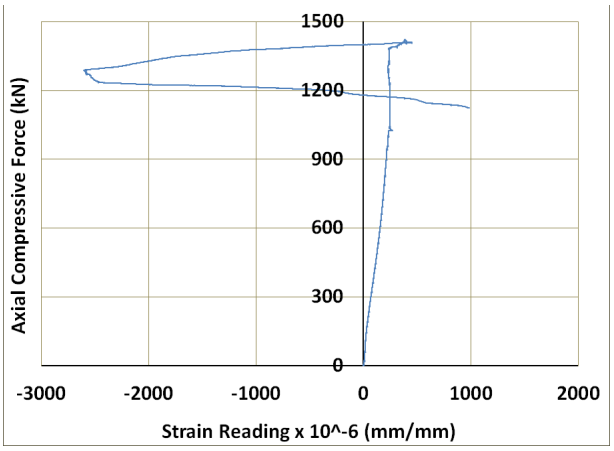

Strain Gauge: SG-G1-5

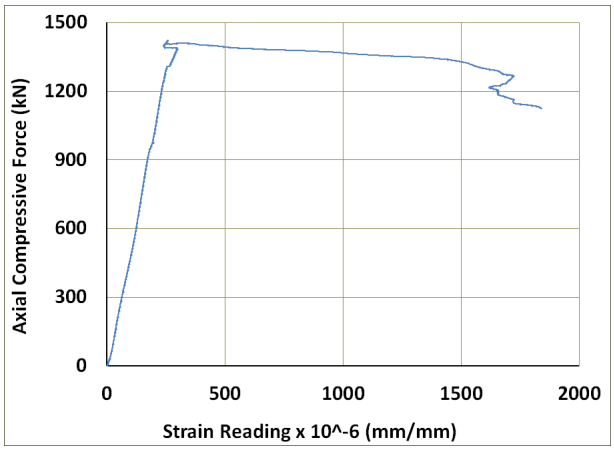

Strain Gauge: SG-G1-6

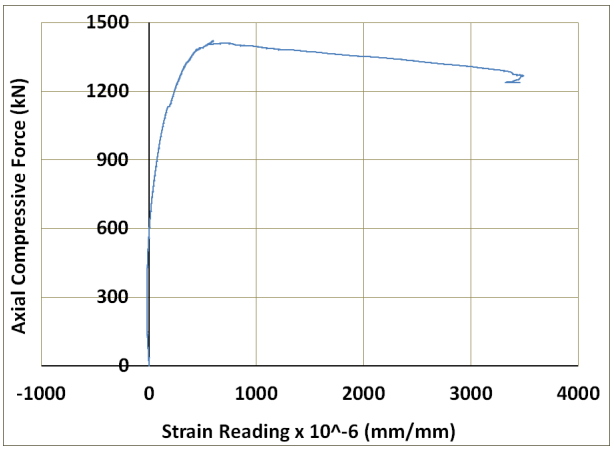

Strain Gauge: SG-G2-1

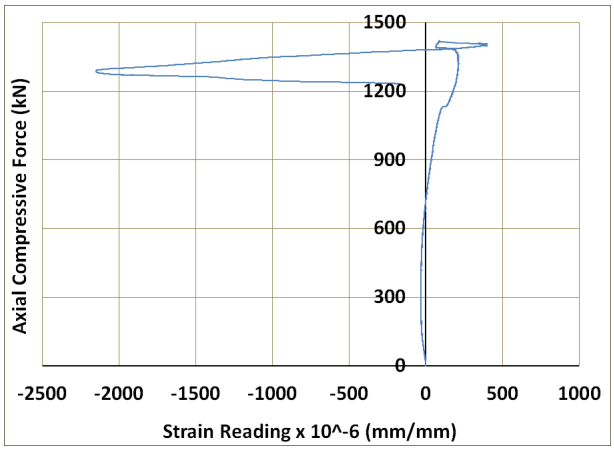

Strain Gauge: SG-G2-2

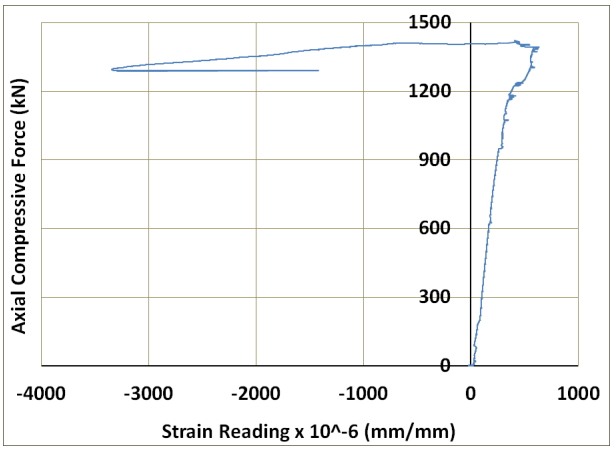

Strain Gauge: SG-G2-3

Figure A4.2 (Cont'd) Specimen SC-9-35 – WWR Grids Strain Gauge Recordings

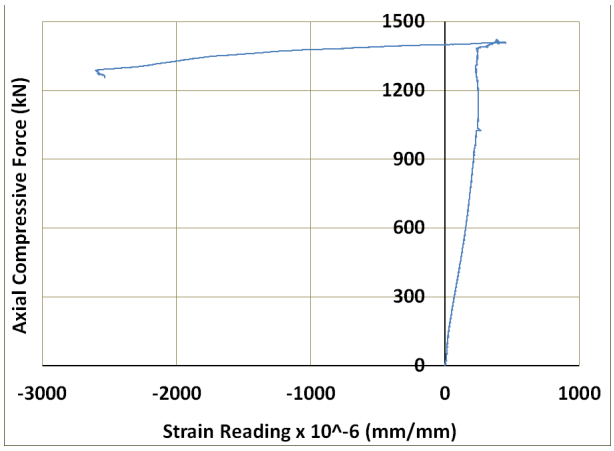

Strain Gauge: SG-G2-5

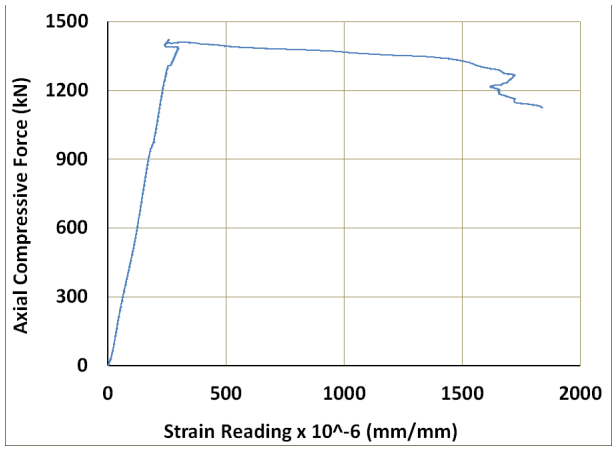

Strain Gauge: SG-G2-6

Figure A4.2 (Cont'd) Specimen SC-9-35 – WWR Grids Strain Gauge Recordings

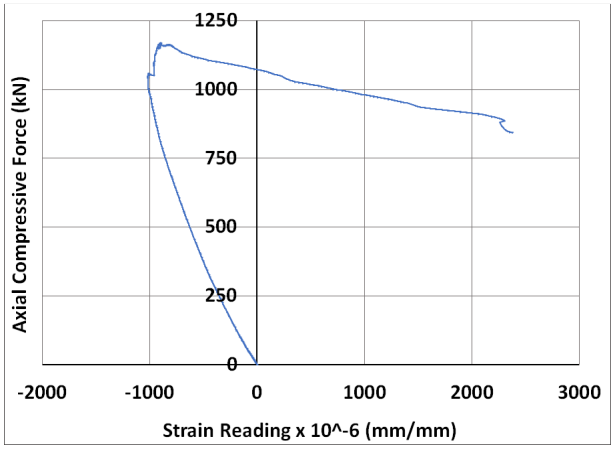

Strain Gauge: SG-LONG-1

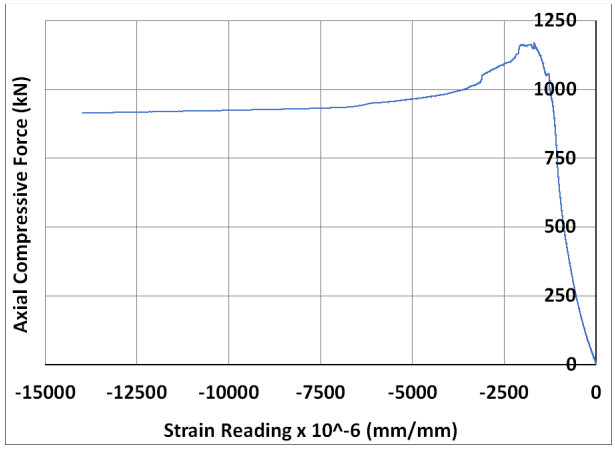

Strain Gauge: SG-LONG-2

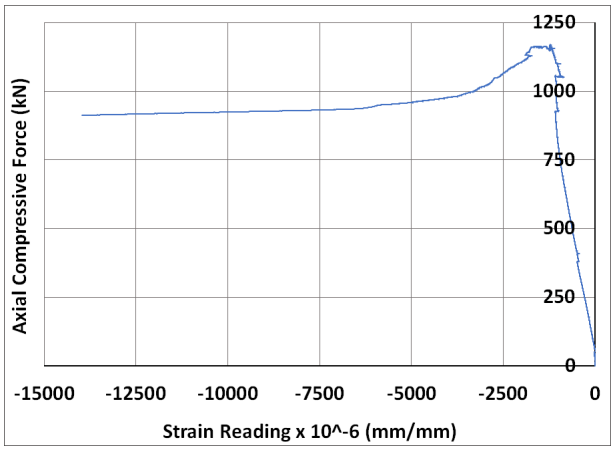

Strain Gauge: SG-LONG-3

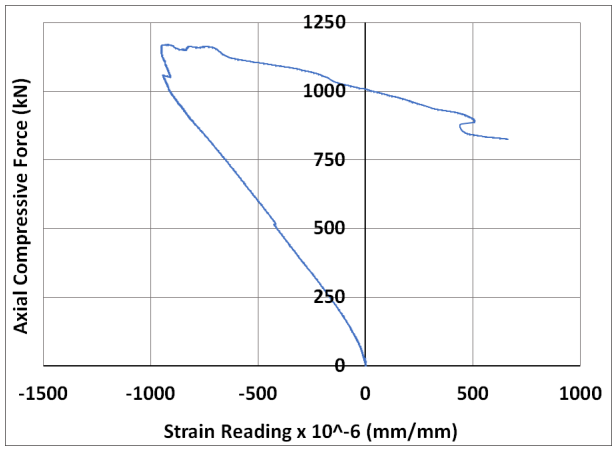

Strain Gauge: SG-LONG-4

Figure A4.3 Specimen SC-9-70 – Longitudinal Bars Strain Recordings

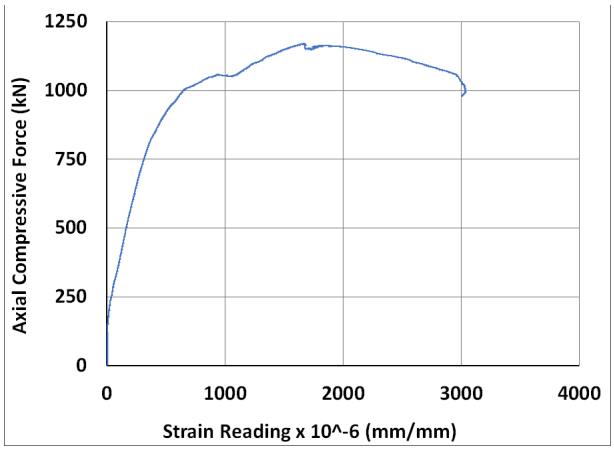

Strain Gauge: SG-G1-1

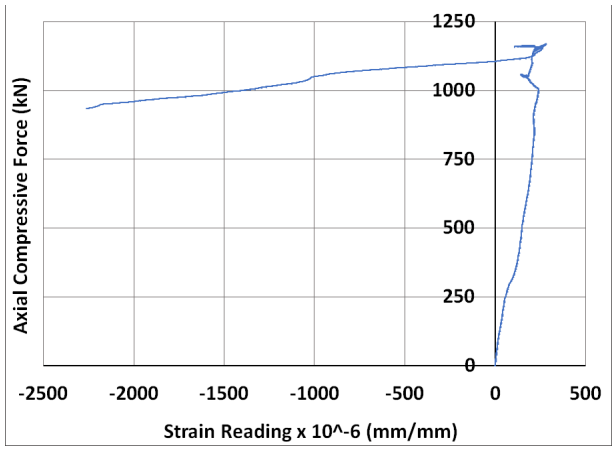

Strain Gauge: SG-G1-2

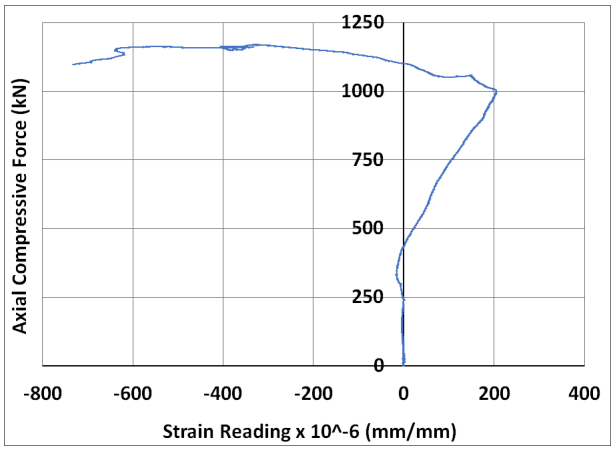

Strain Gauge: SG-G1-3

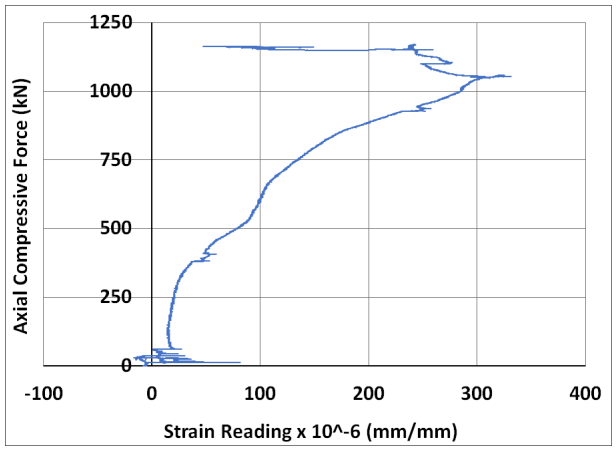

Strain Gauge: SG-G1-4

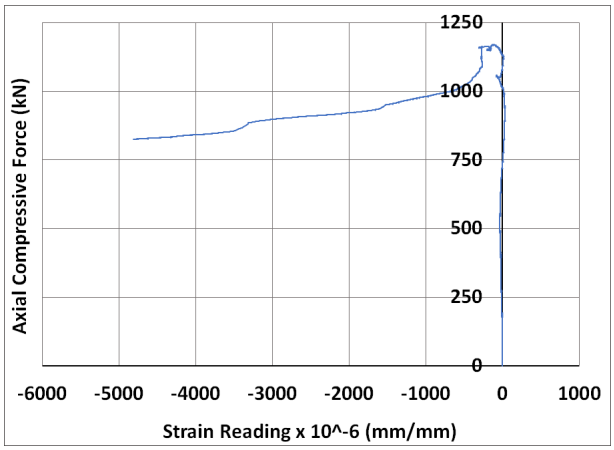

Strain Gauge: SG-G1-5

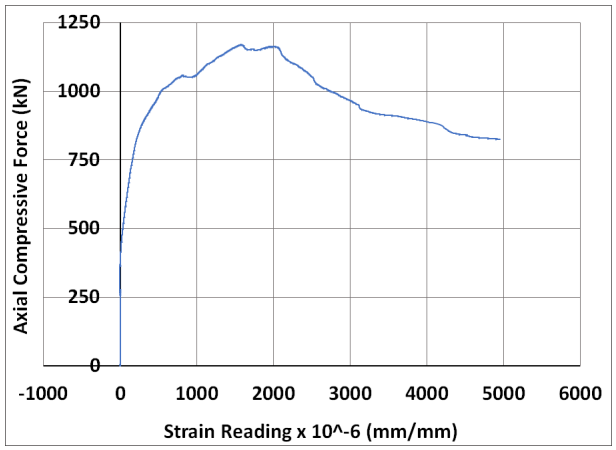

Strain Gauge: SG-G1-6

Figure A4.4 Specimen SC-9-70 – WWR Grids Strain Gauge Recordings

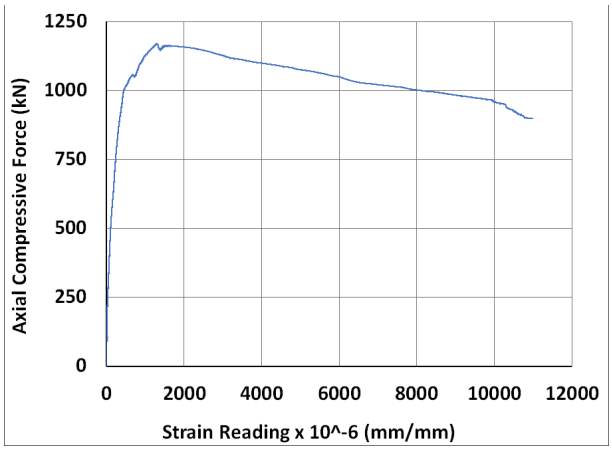

Strain Gauge: SG-G2-1

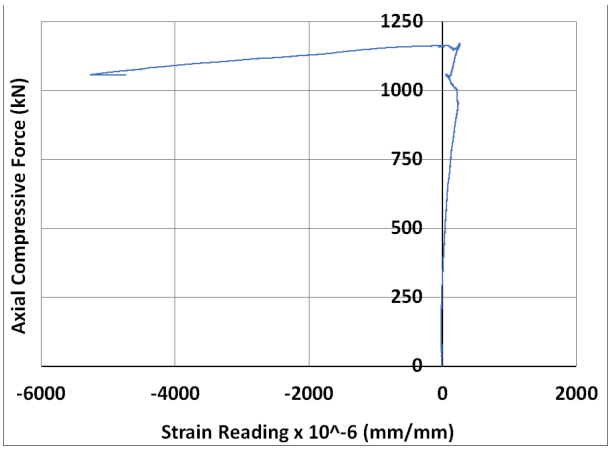

Strain Gauge: SG-G2-2

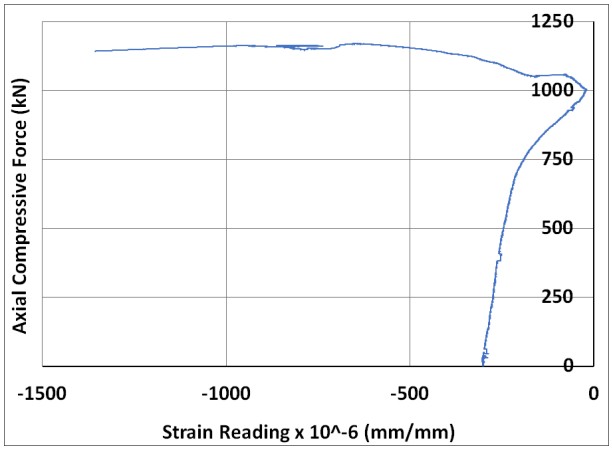

Strain Gauge: SG-G2-3

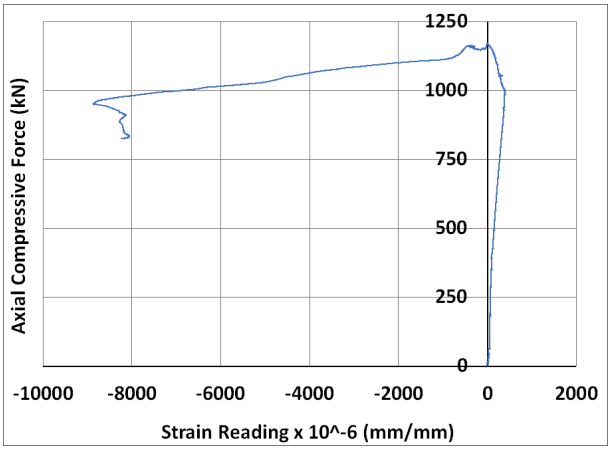

Strain Gauge: SG-G2-4

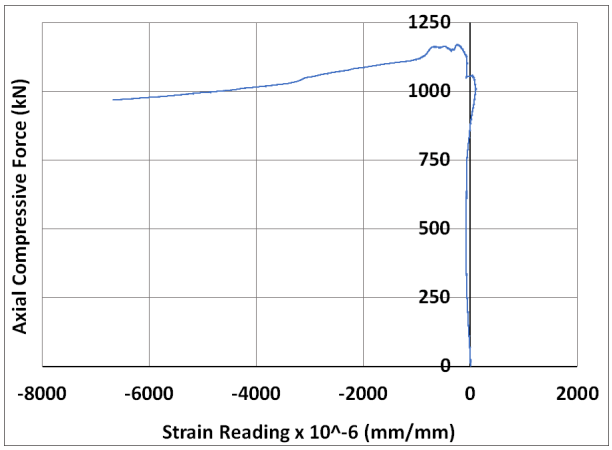

Strain Gauge: SG-G2-5

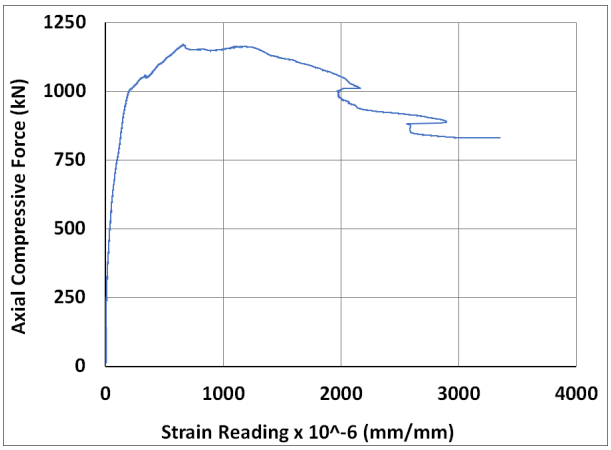

Strain Gauge: SG-G2-6

Figure A4.4 (Cont'd) Specimen SC-9-70 – WWR Grids Strain Gauge Recordings

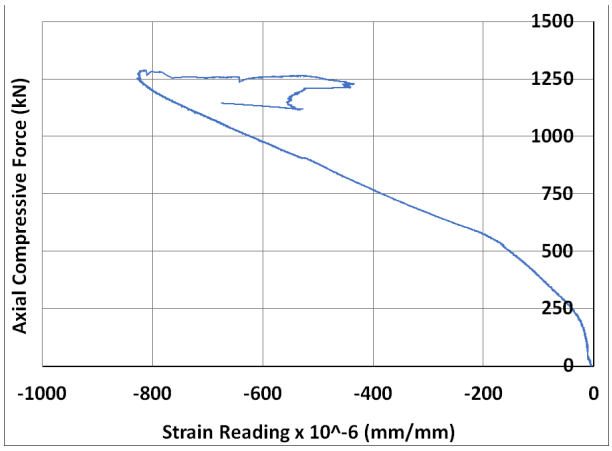

Strain Gauge: SG-LONG-1

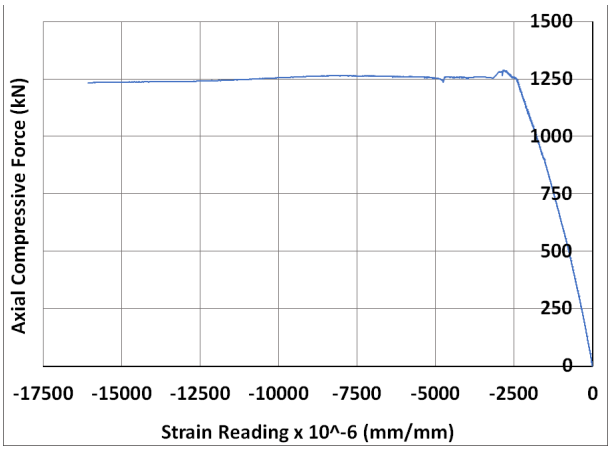

Strain Gauge: SG-LONG-2

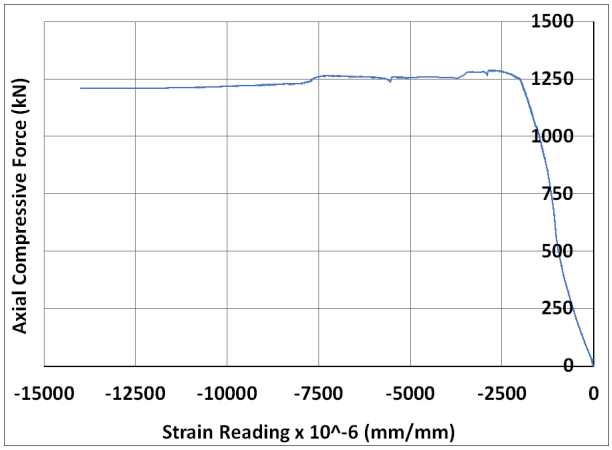

Strain Gauge: SG-LONG-3

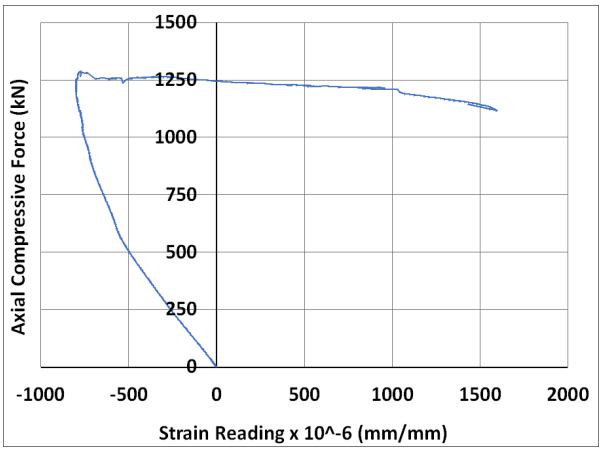

Strain Gauge: SG-LONG-4

Figure A4.5 Specimen SC-18-35 – Longitudinal Bars Strain Recordings

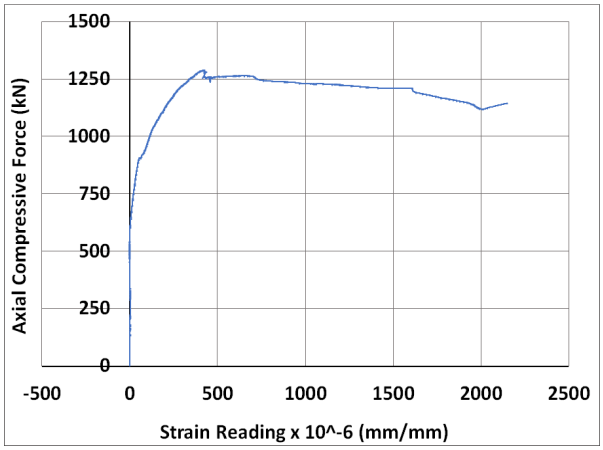

Strain Gauge: SG-G1-1

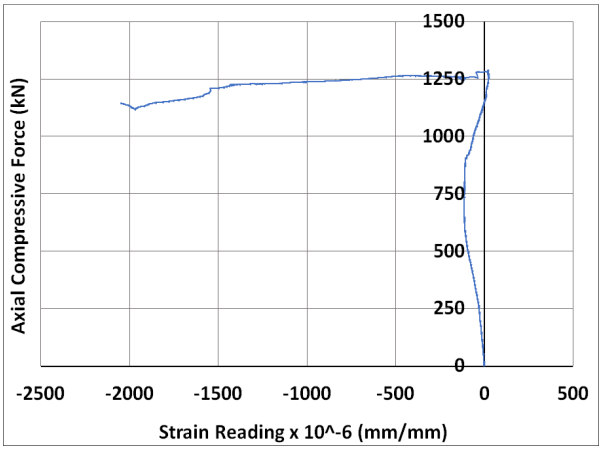

Strain Gauge: SG-G1-2

Figure A4.6 Specimen SC-18-35 – WWR Grids Strain Gauge Recordings

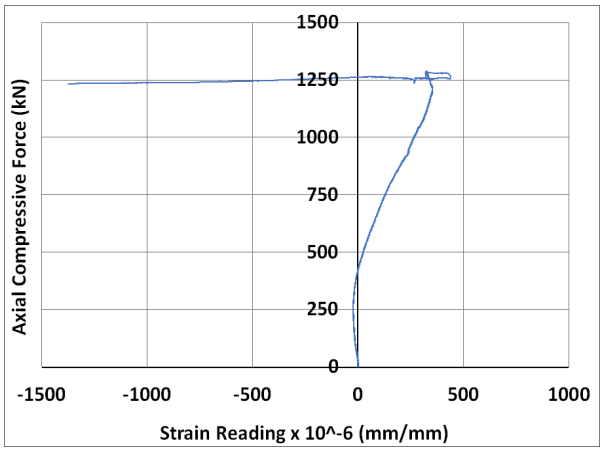

Strain Gauge: SG-G1-3

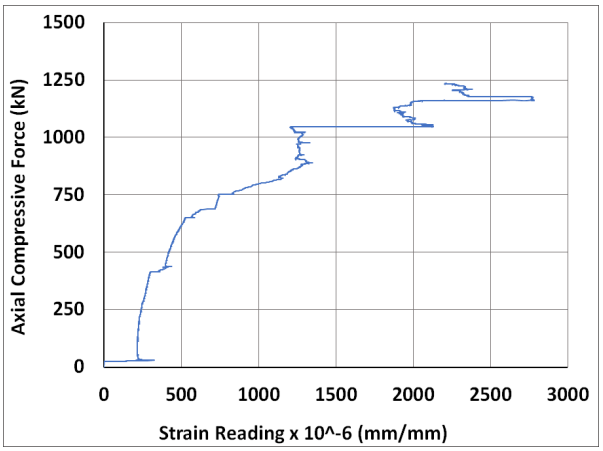

Strain Gauge: SG-G1-4

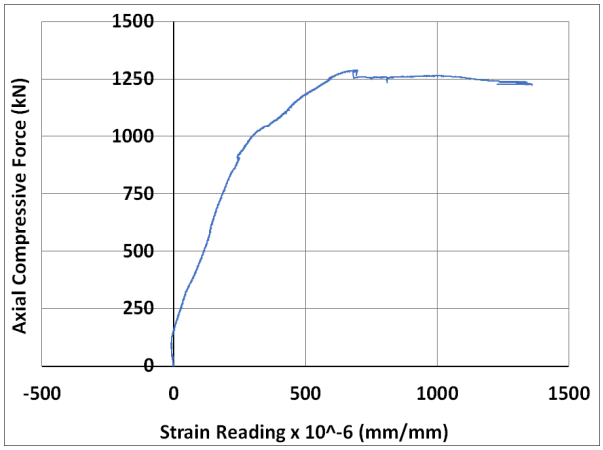

Strain Gauge: SG-G1-6

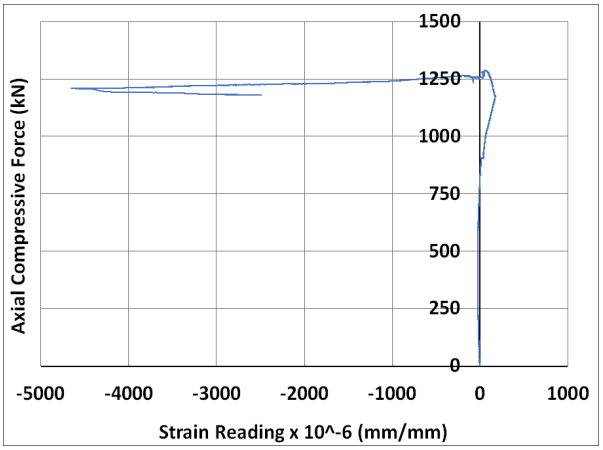

Strain Gauge: SG-G2-2

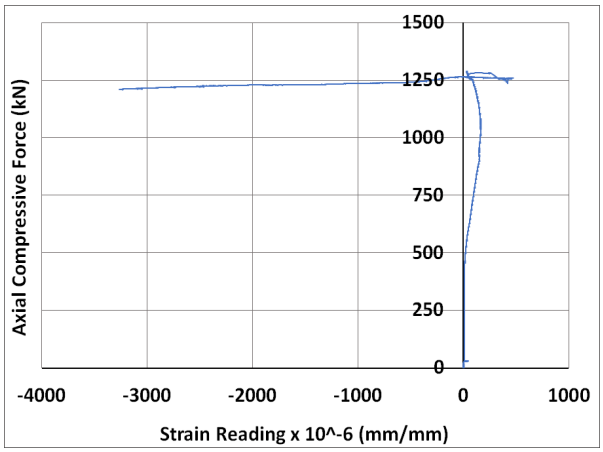

Strain Gauge: SG-G2-3

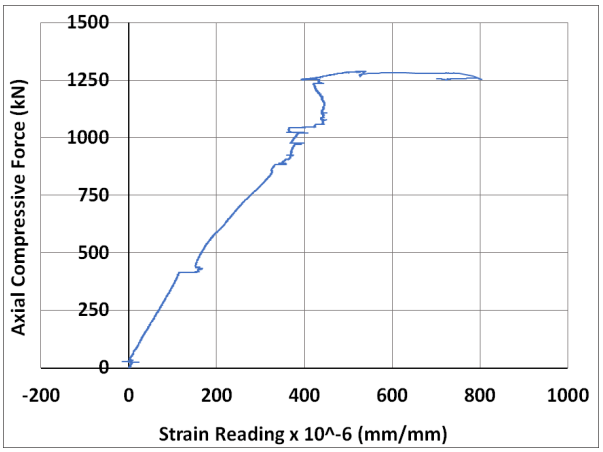

Strain Gauge: SG-G2-4

Figure A4.6 (Cont'd) Specimen SC-18-35 – WWR Grids Strain Gauge Recordings

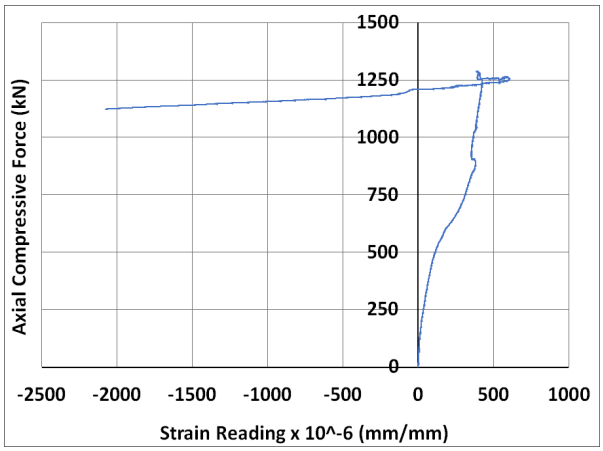

Strain Gauge: SG-G2-5

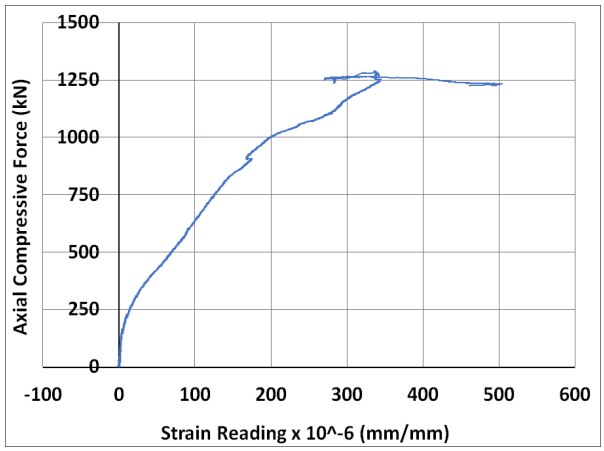

Strain Gauge: SG-G2-6

Figure A4.6 (Cont'd) Specimen SC-18-35 – WWR Grids Strain Gauge Recordings

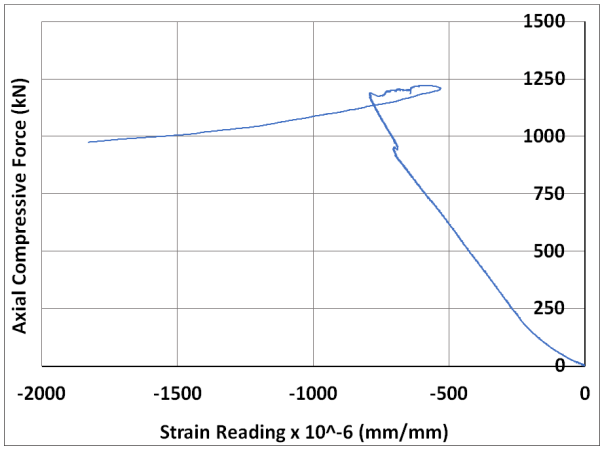

Strain Gauge: SG-LONG-1

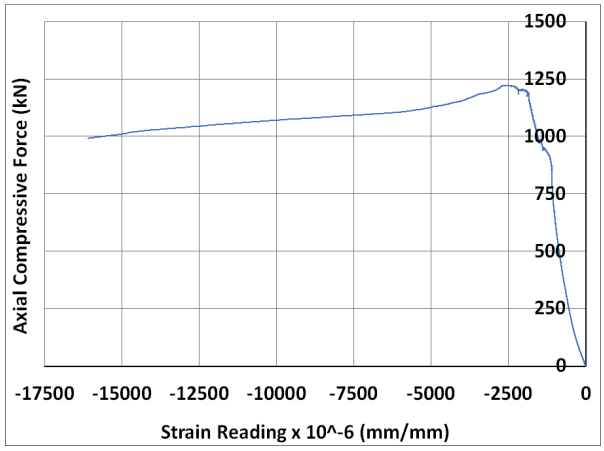

Strain Gauge: SG-LONG-2

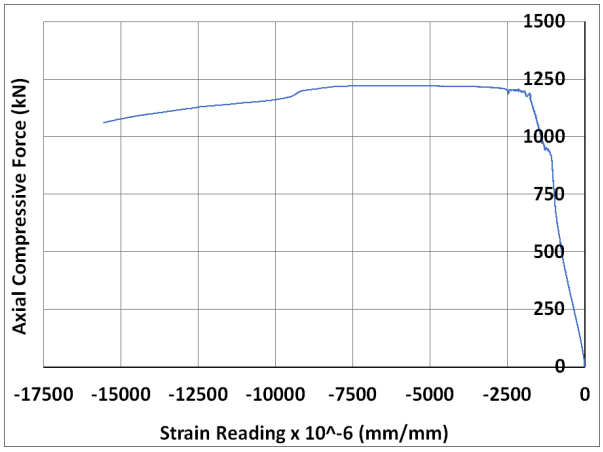

Strain Gauge: SG-LONG-3

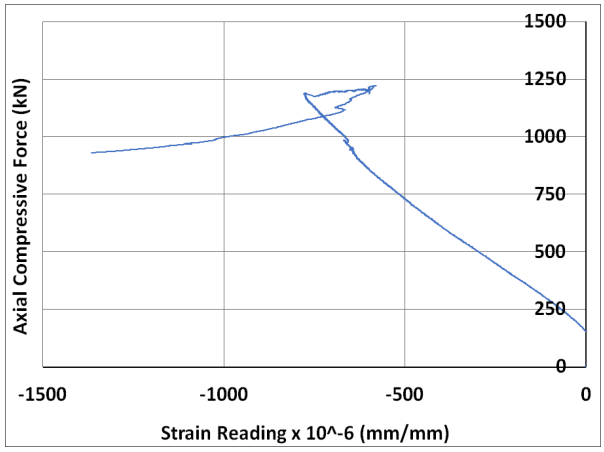

Strain Gauge: SG-LONG-4

Figure A4.7 Specimen SC-18-70 – Longitudinal Bars Strain Recordings

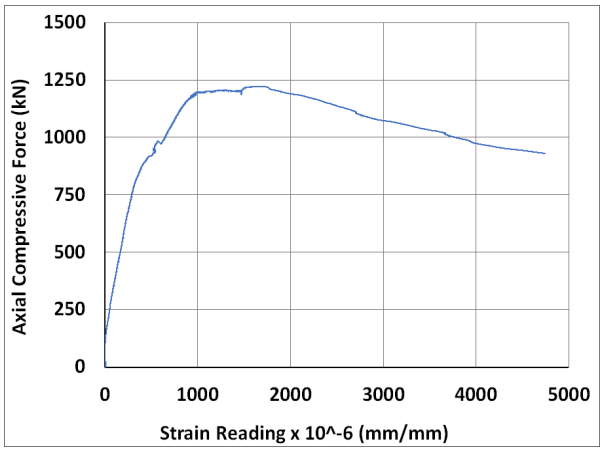

Strain Gauge: SG-G1-1

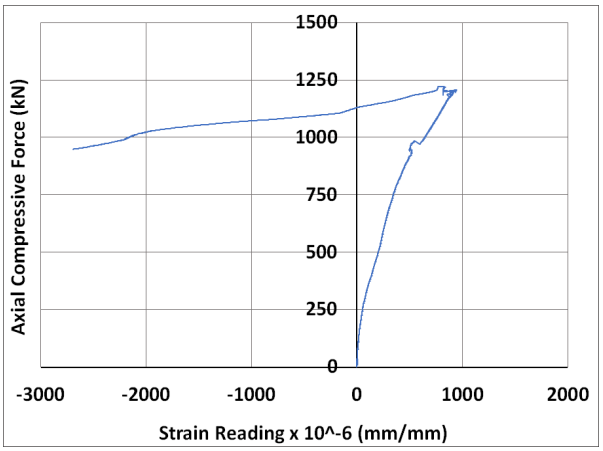

Strain Gauge: SG-G1-2

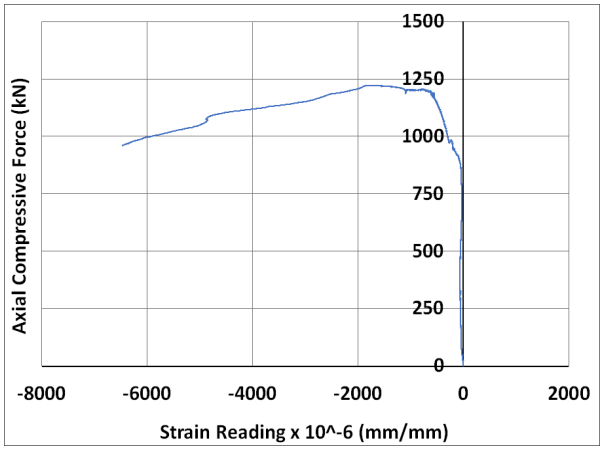

Strain Gauge: SG-G1-3

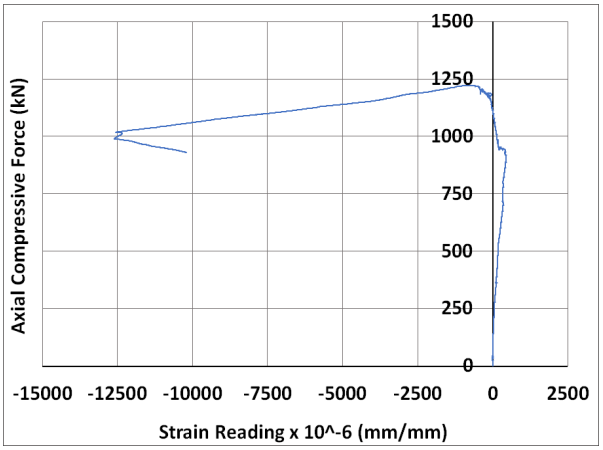

Strain Gauge: SG-G1-4

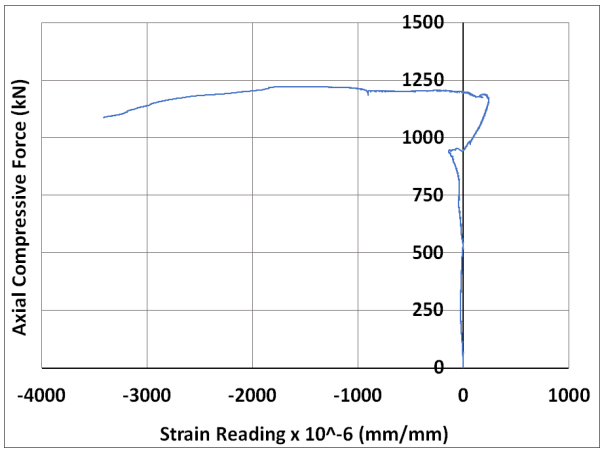

Strain Gauge: SG-G1-5

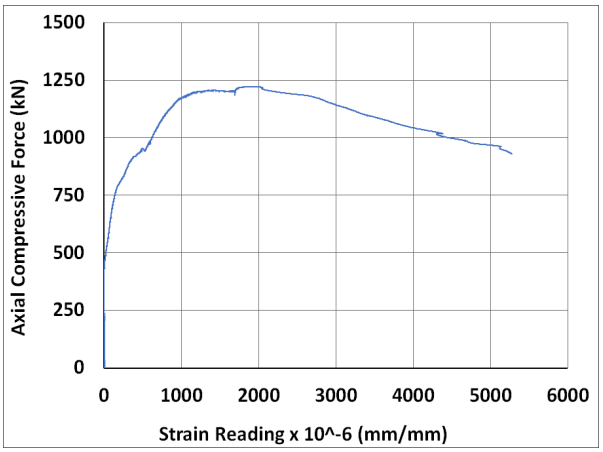

Strain Gauge: SG-G1-6

Figure A4.8 Specimen SC-18-70 – WWR Grids Strain Gauge Recordings

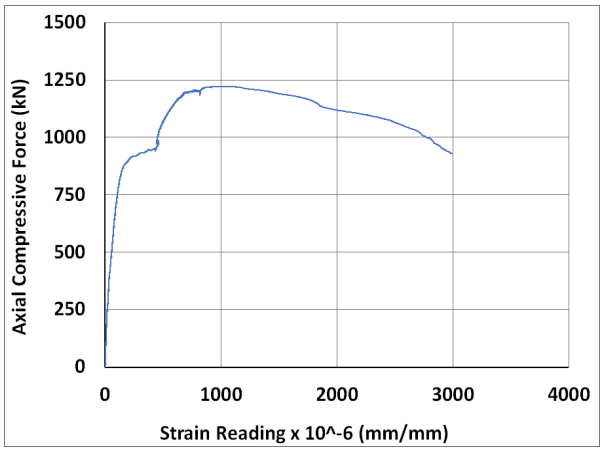

Strain Gauge: SG-G2-1

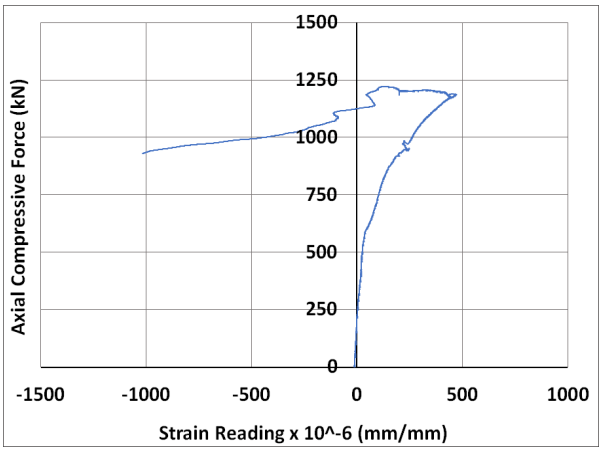

Strain Gauge: SG-G2-2

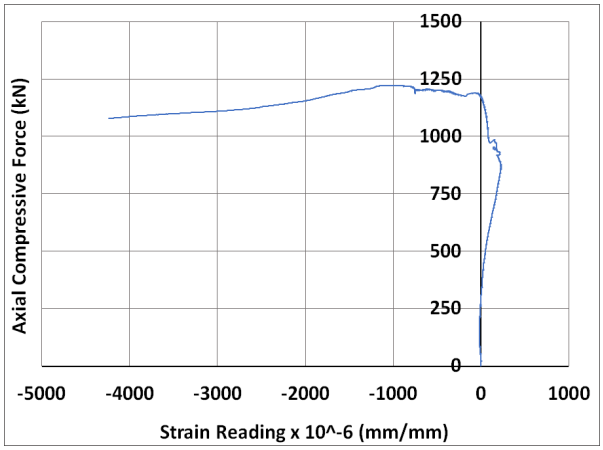

Strain Gauge: SG-G2-3

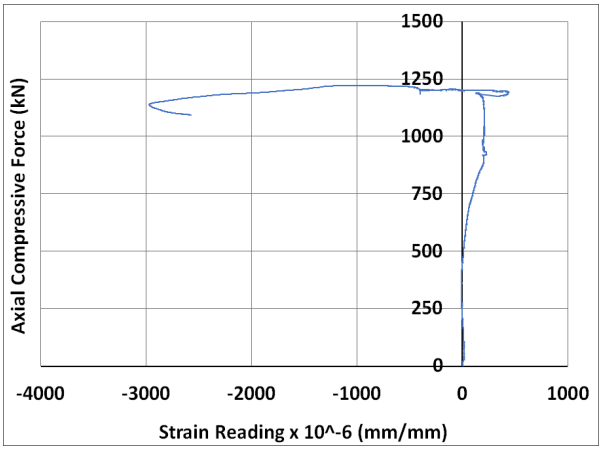

Strain Gauge: SG-G2-4

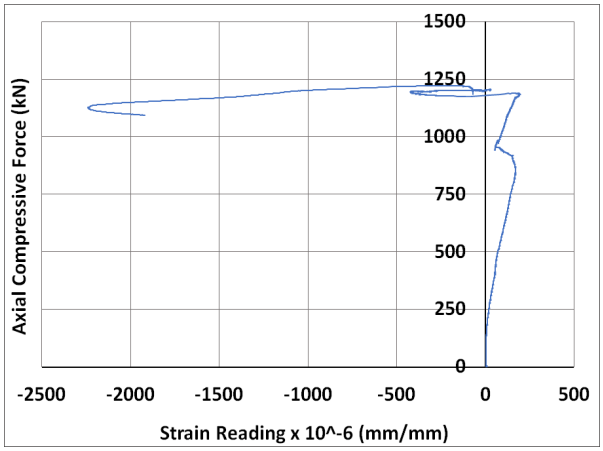

Strain Gauge: SG-G2-5

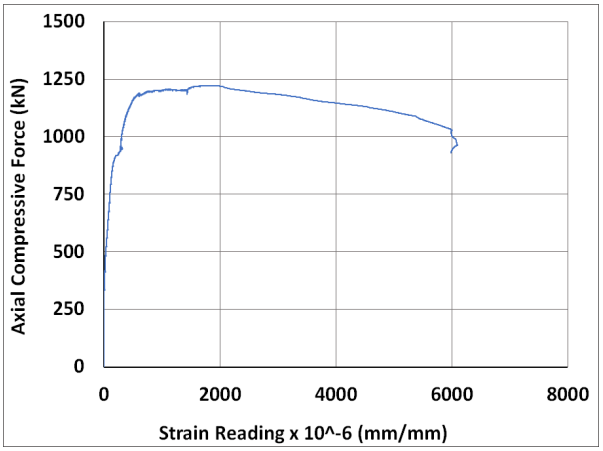

Strain Gauge: SG-G2-6

Figure A4.8 (Cont'd) Specimen SC-18-70 – WWR Grids Strain Gauge Recordings

Appendix B.1 – Shear Wall No. 1 Strain Gauge Recordings

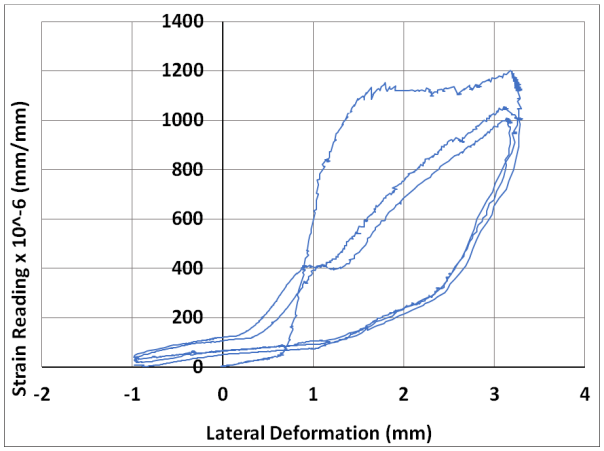

Strain Gauge: Dowel W-1

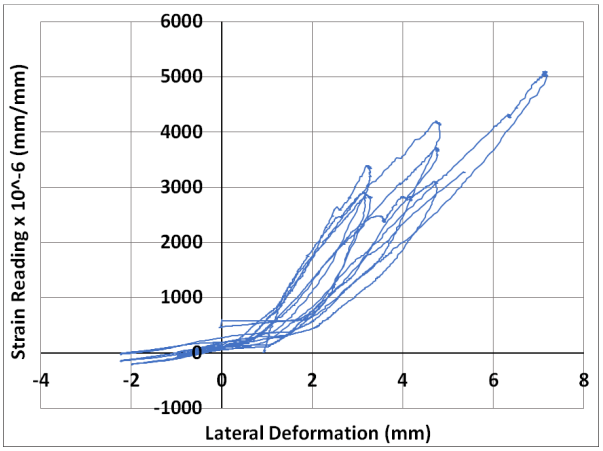

Strain Gauge: Dowel E-1

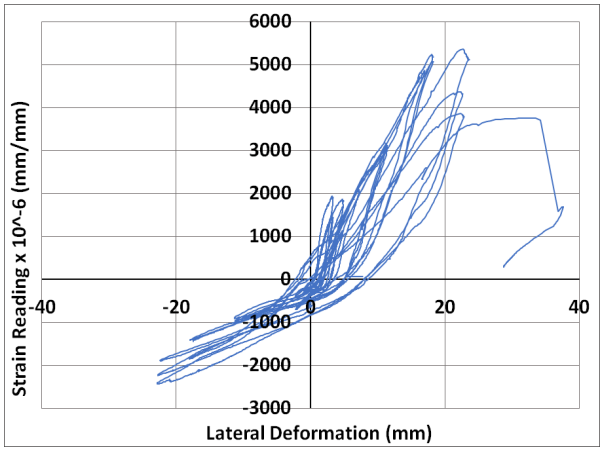

Strain Gauge: Dowel E-2

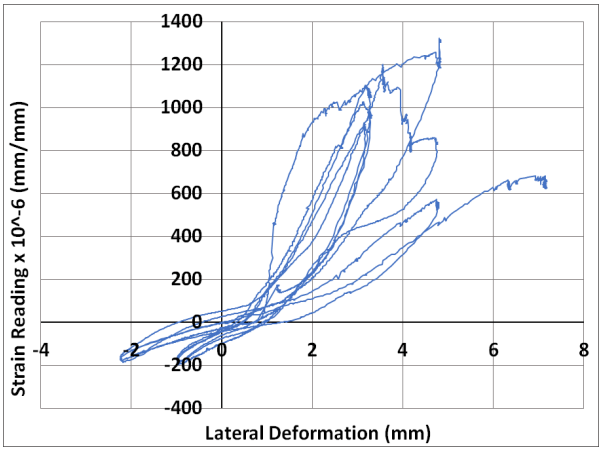

Strain Gauge: Long W-1

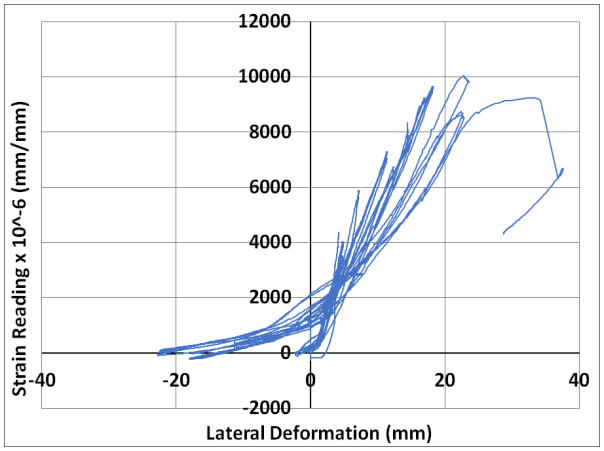

Strain Gauge: Long W-2

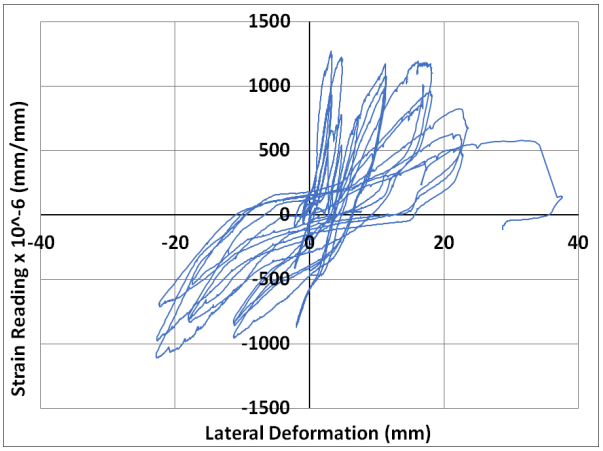

Strain Gauge: Long E-1

Figure B1.1 Shear Wall No. 1 – Strain Gauge Recordings of Longitudinal Bars and Dowels

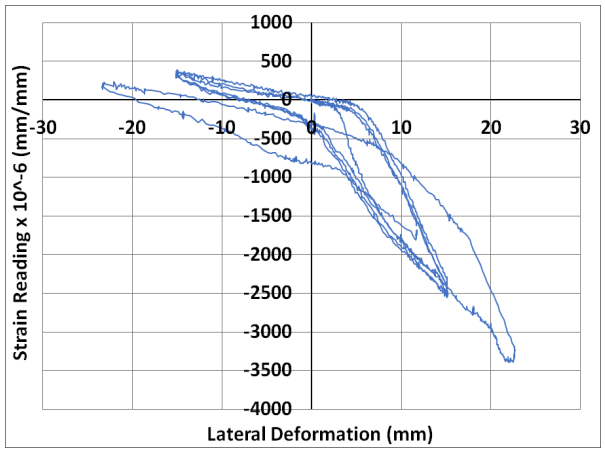

Strain Gauge: Long E-2

Figure B1.1 (Cont'd) Shear Wall No. 1- Strain Gauge Recordings of Longitudinal Bars and Dowels

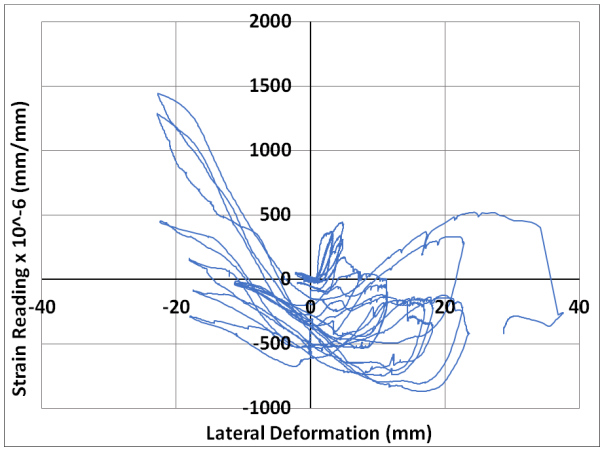

Strain Gauge: WWR W1-6

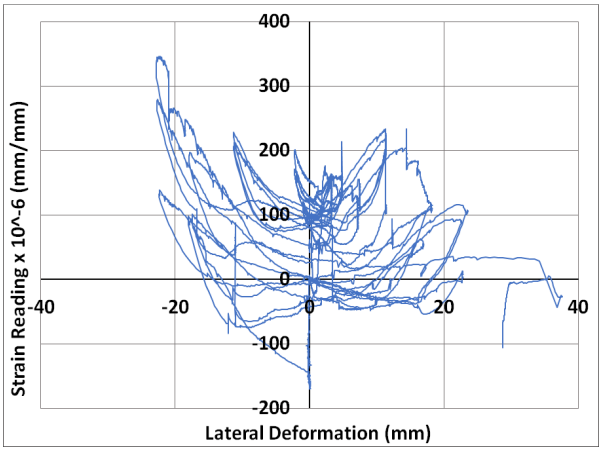

Strain Gauge: WWR W2-1

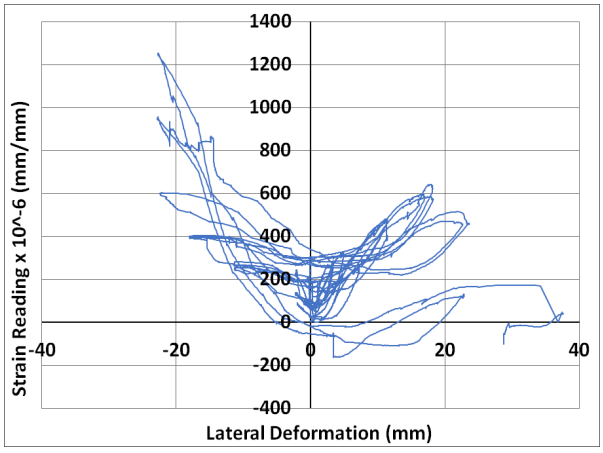

Strain Gauge: WWR W2-5

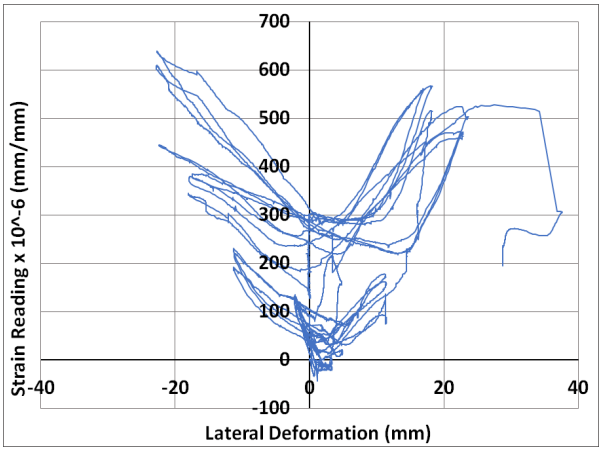

Strain Gauge: WWR W3-2

Figure B1.2 Shear Wall No. 1 – Strain Gauge Recordings of WWR Grids

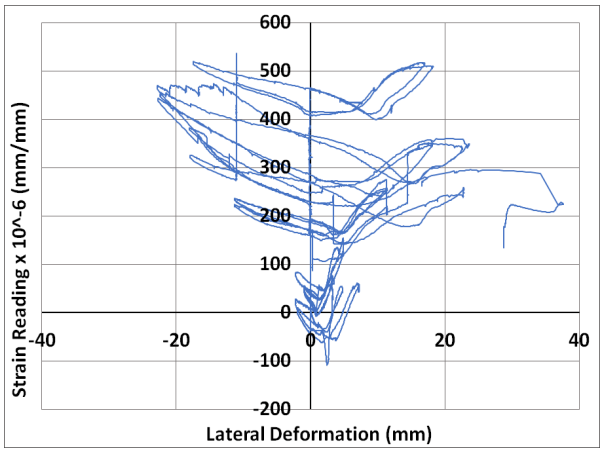

Strain Gauge: WWR W3-7

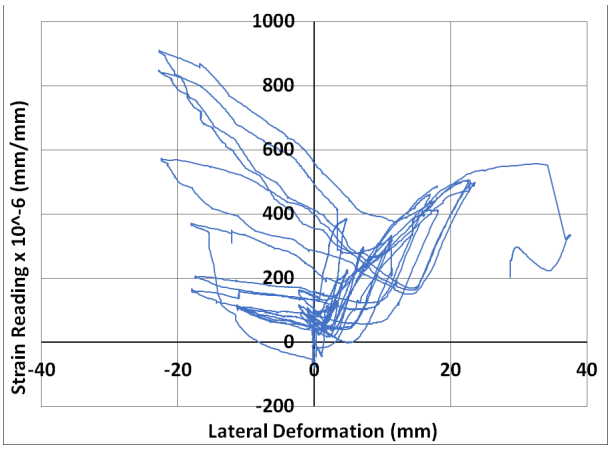

Strain Gauge: WWR W4-6

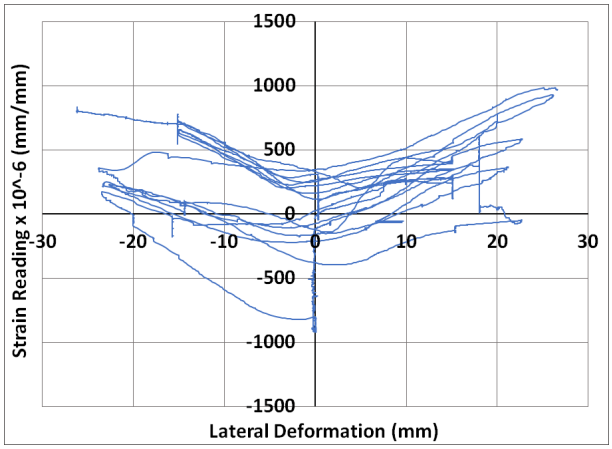

Strain Gauge: WWR E1-1

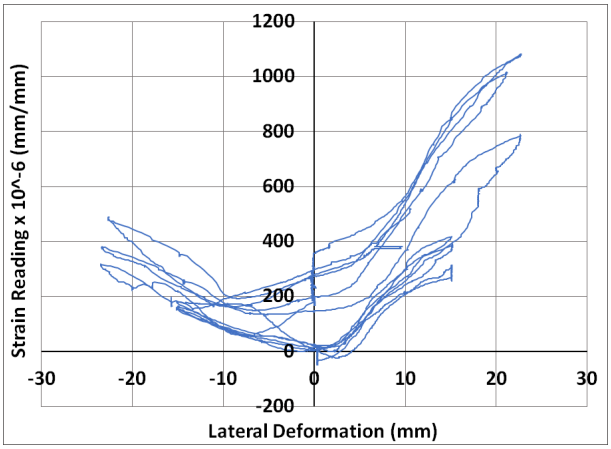

Strain Gauge: WWR E2-3

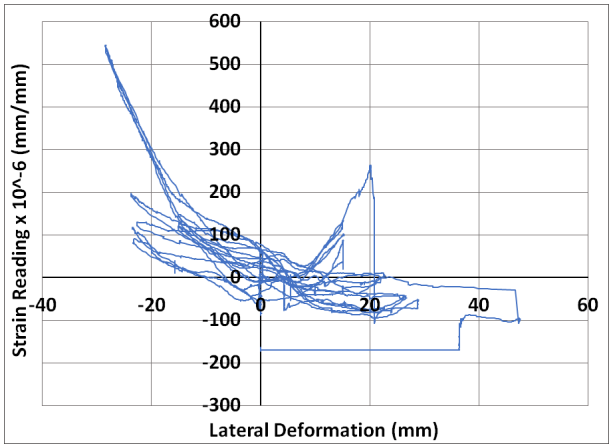

Strain Gauge: WWR E2-4

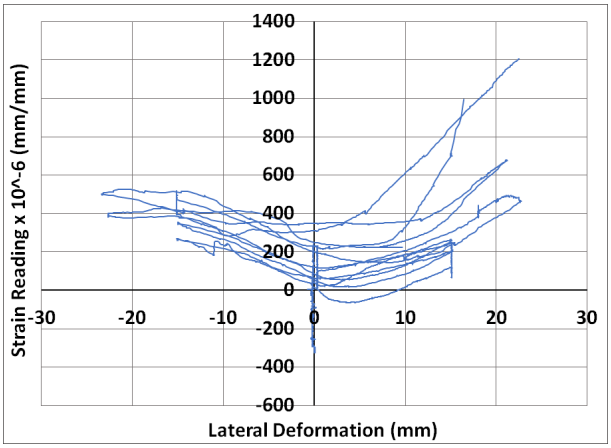

Strain Gauge: WWR E3-3

Figure B1.2 (Cont'd) Shear Wall No. 1 – Strain Gauge Recordings of WWR Grids

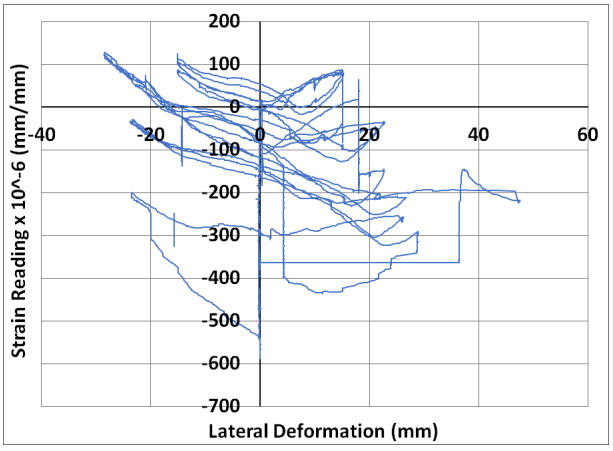

Strain Gauge: WWR E4-7

Figure B1.2 (Cont'd) Shear Wall No. 1 – Strain Gauge Recordings of WWR Grids

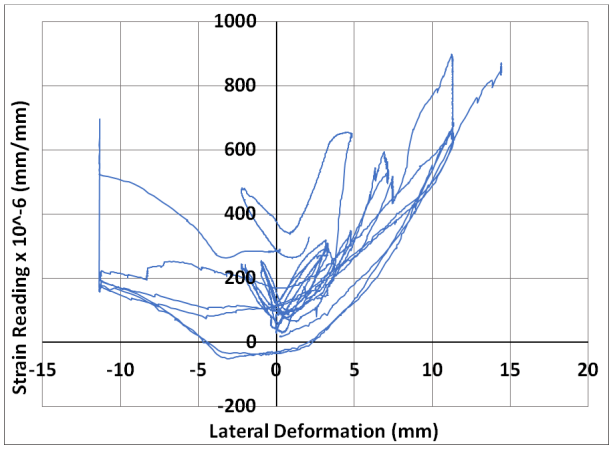

Strain Gauge: Web W-1

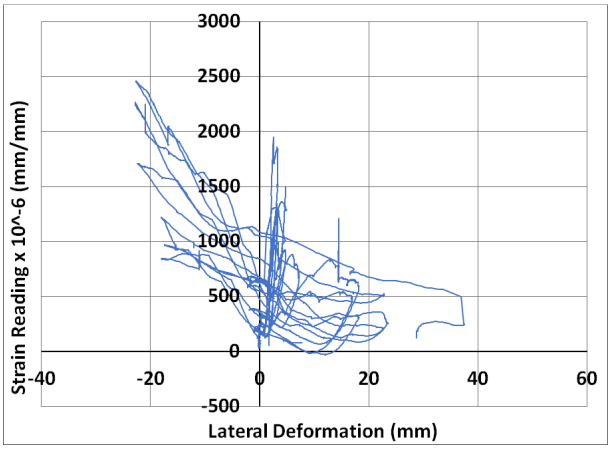

Strain Gauge: Web E-1

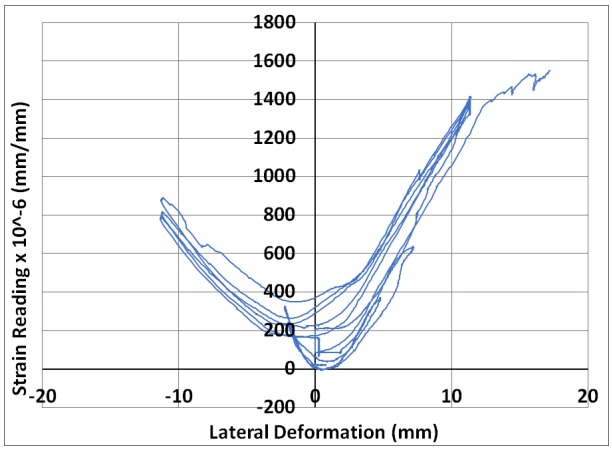

Strain Gauge: Web W-2

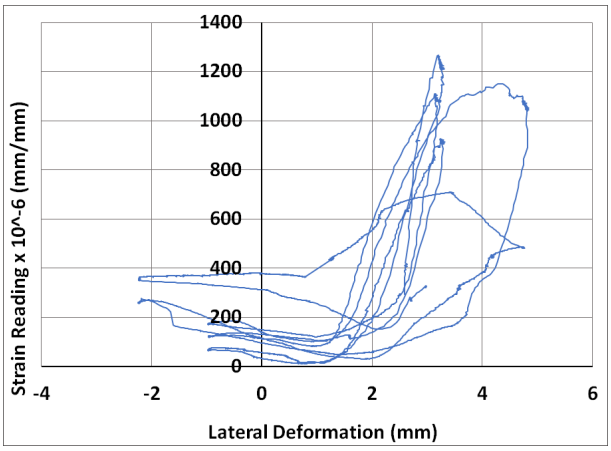

Strain Gauge: Web E-2

Figure B1.3 Shear Wall No. 1 – Strain Gauge Recordings of WWR Grids

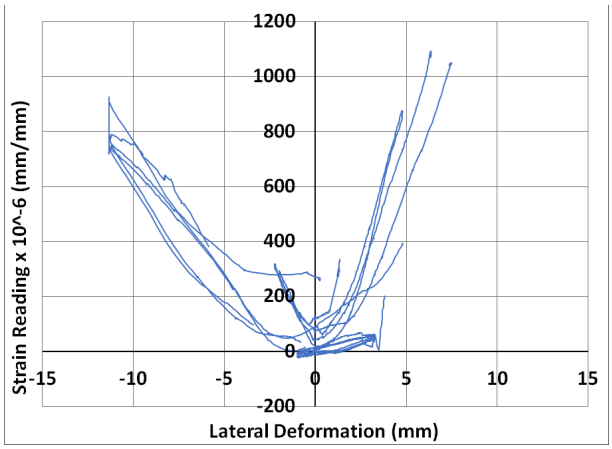

Strain Gauge: Web W-3

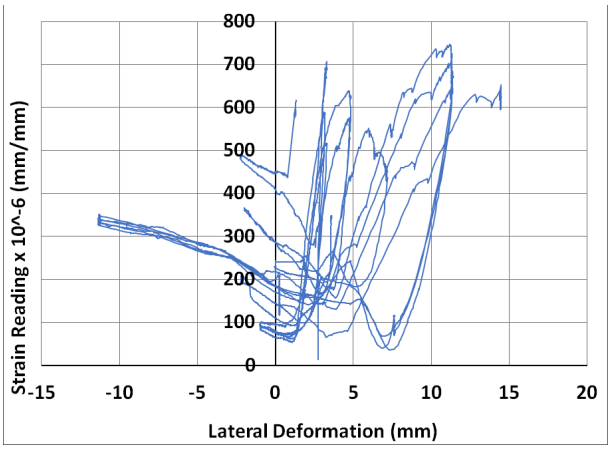

Strain Gauge: Web E-3

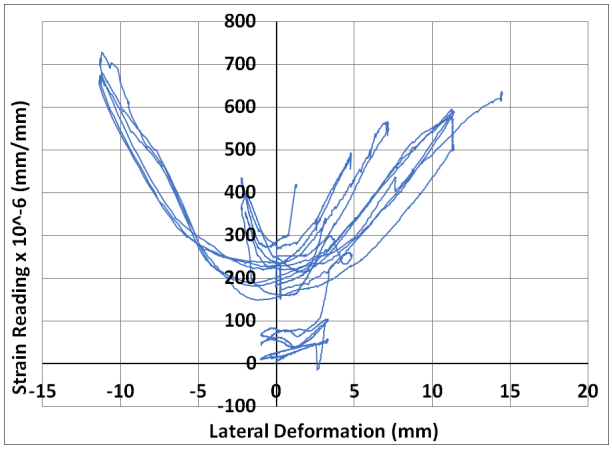

Strain Gauge: Web W-4

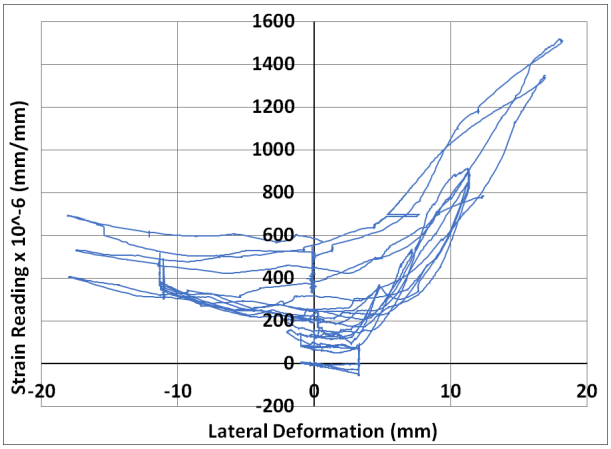

Strain Gauge: Web E-4

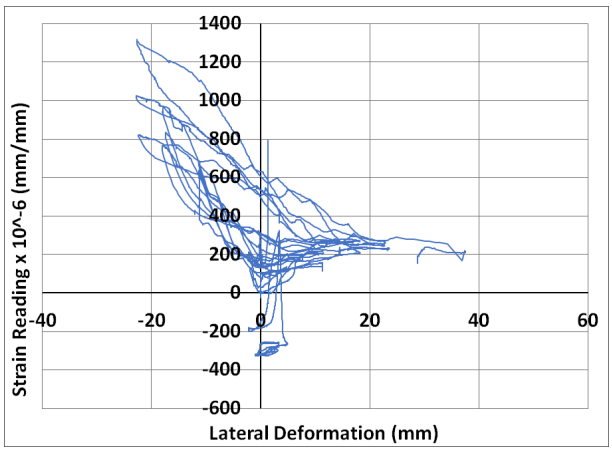

Strain Gauge: Web W-5

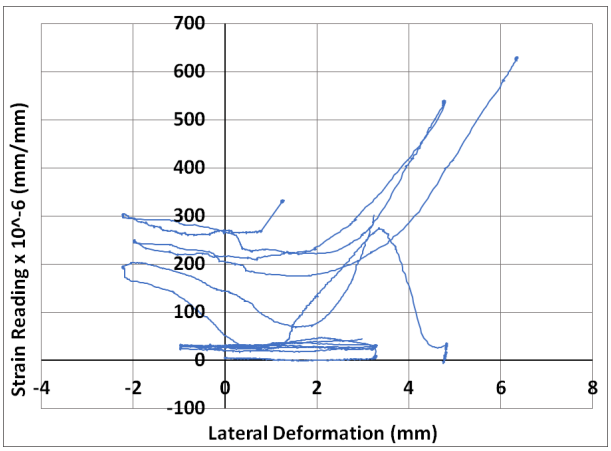

Strain Gauge: Web E-5

Figure B1.3 (Cont'd) Shear Wall No. 1 – Strain Gauge Recordings of WWR Grids

Appendix B.2 – Shear Wall No. 2 Strain Gauge Recordings

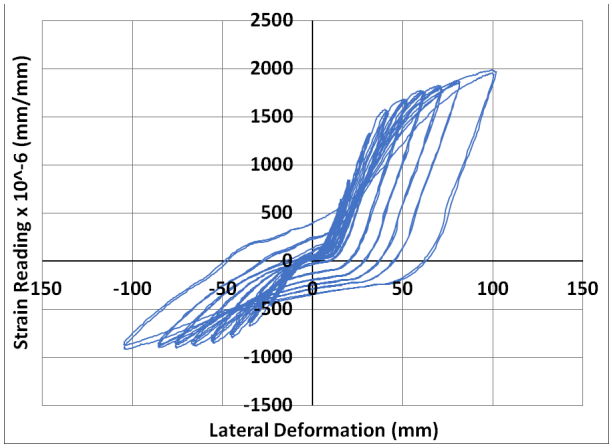

Strain Gauge: Dowel W-1

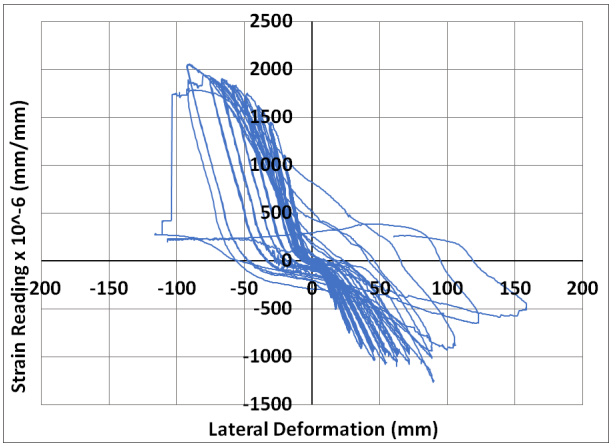

Strain Gauge: Dowel E-1

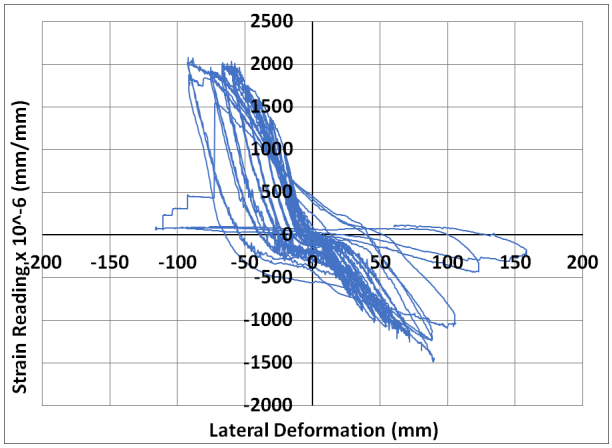

Strain Gauge: Dowel E-2

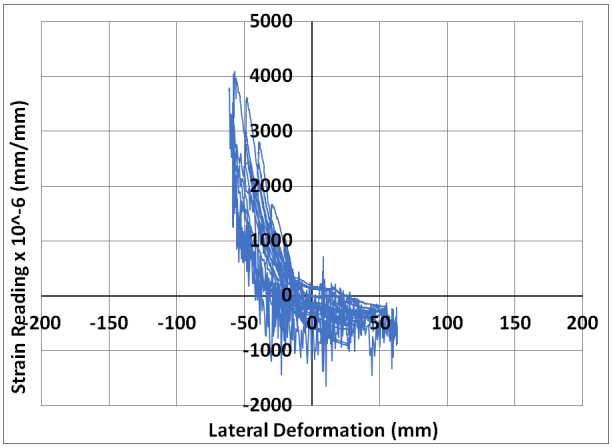

Strain Gauge: Dowel E-3

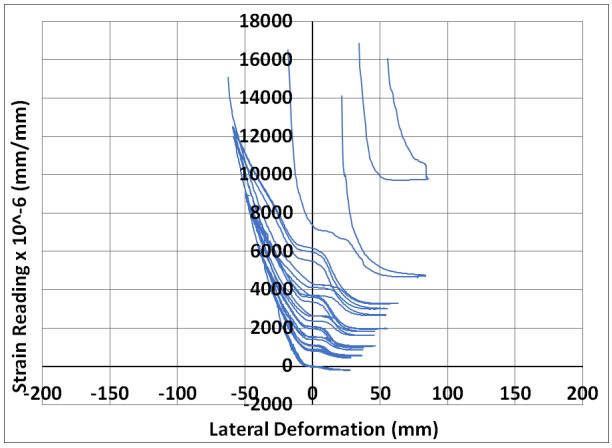

Strain Gauge: Dowel E-4

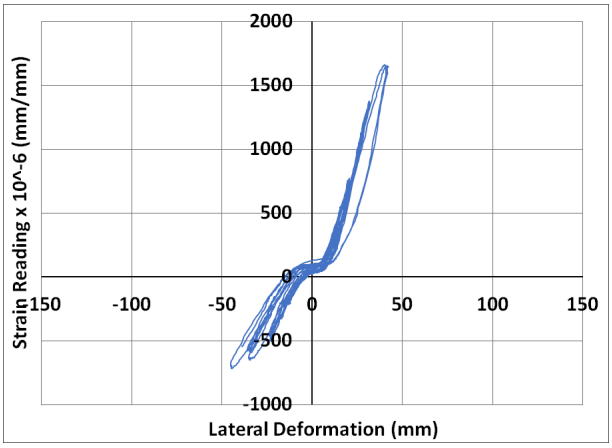

Strain Gauge: Long W-1

Figure B2.1 Shear Wall No. 2 - Strain Gauge Recordings of Longitudinal Bars and Dowels

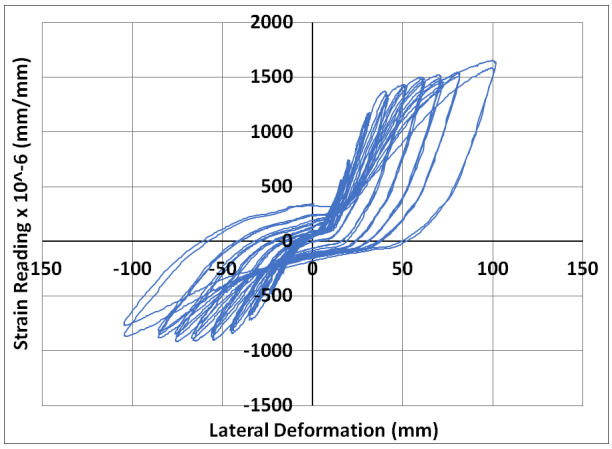

Strain Gauge: Long W-2

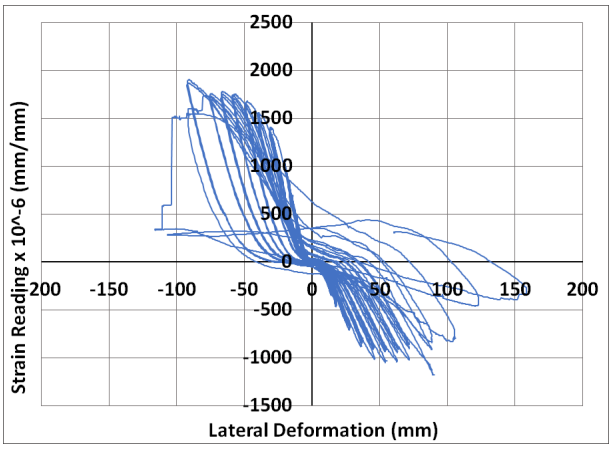

Strain Gauge: Long E-1

Figure B2.1 (Cont'd) Shear Wall No. 2 - Strain Gauge Recordings of Longitudinal Bars and Dowels

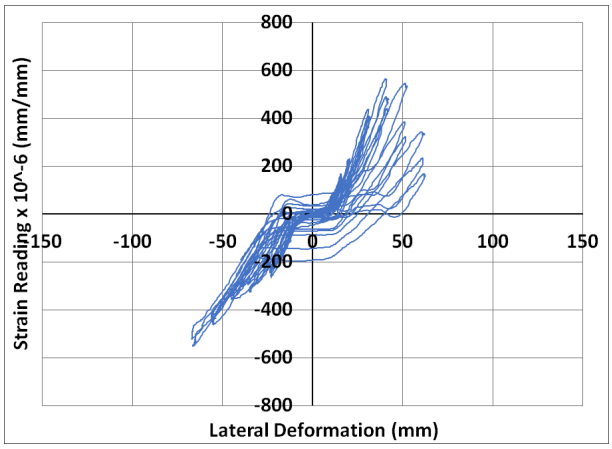

Strain Gauge: W-1b

Figure B2.2 Shear Wall No. 2 - Strain Gauge Recordings of WWR W-1 Grid

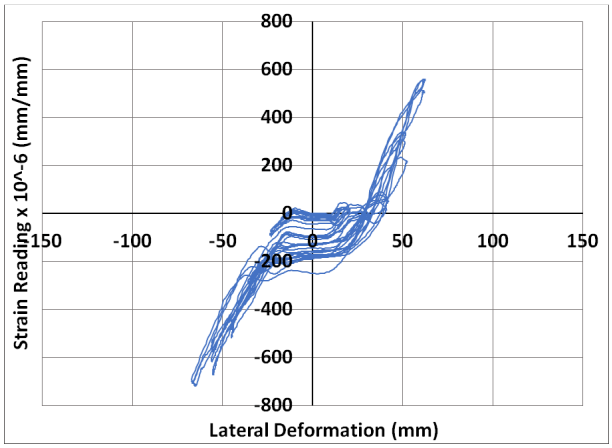

Strain Gauge: W-2a

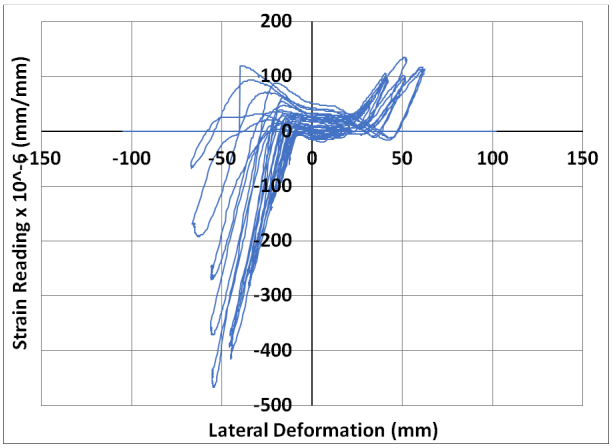

Strain Gauge: W-2b

Figure B2.3 Shear Wall No. 2 - Strain Gauge Recordings of WWR W-2 Grid

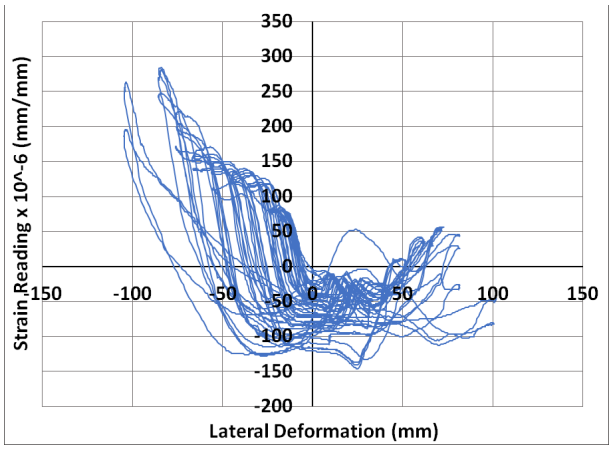

Strain Gauge: W-2c

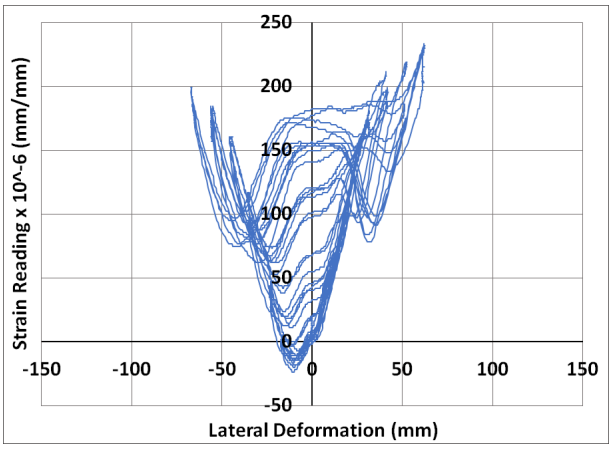

Strain Gauge: W-2d

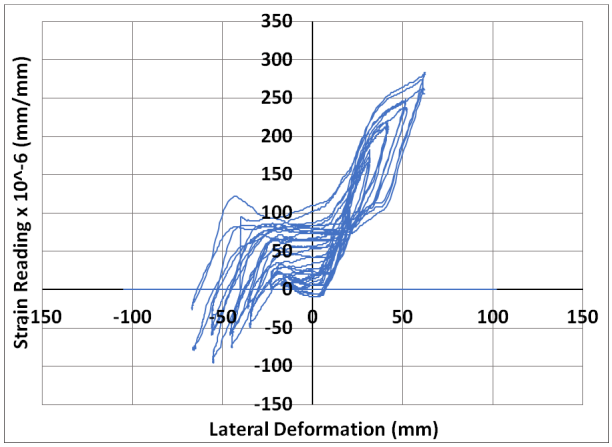

Strain Gauge: W-2e

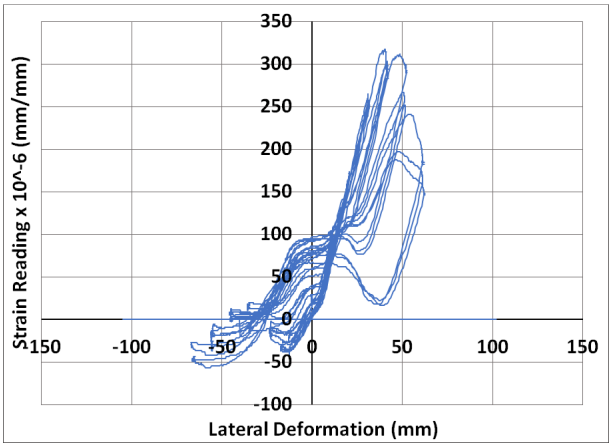

Strain Gauge: W-2h

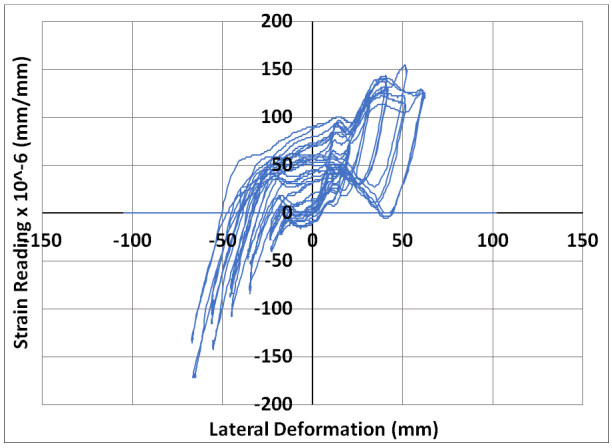

Strain Gauge: W-2i

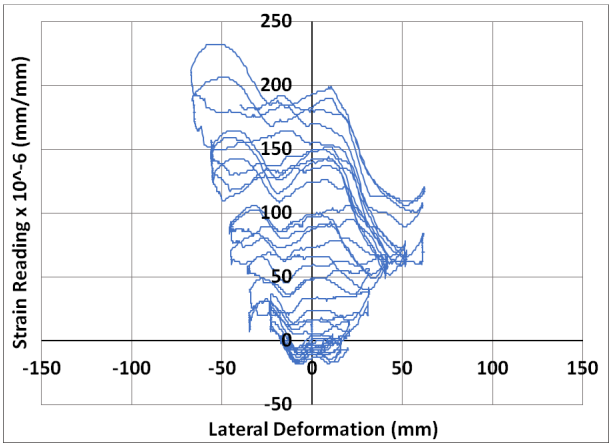

Strain Gauge: W-2n

Figure B2.3 (Cont'd) Shear Wall No. 2 - Strain Gauge Recordings of WWR W-2 Grid

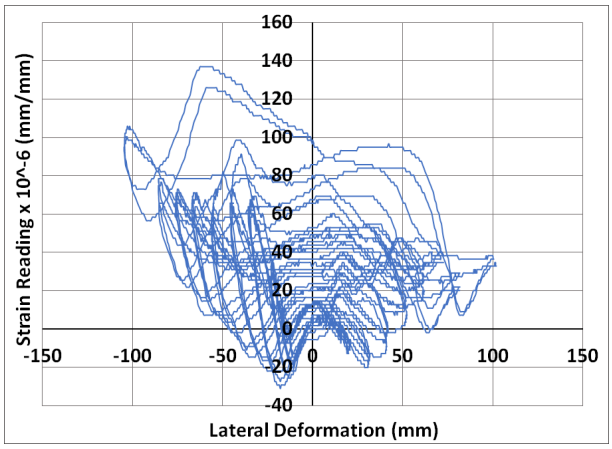

Strain Gauge: W-3a

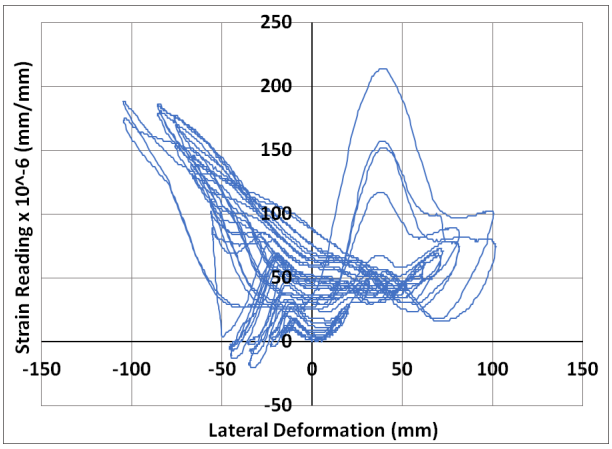

Strain Gauge: W-3b

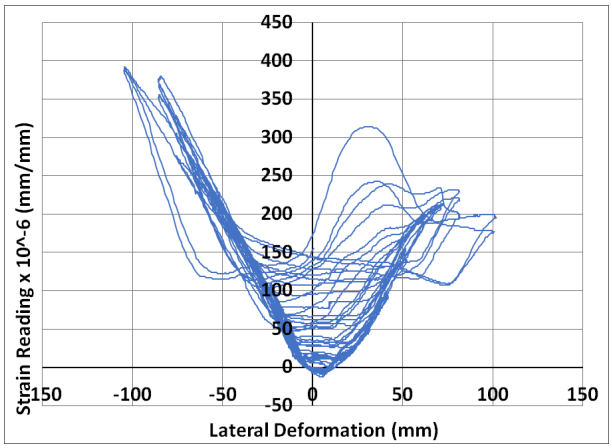

Strain Gauge: W-3c

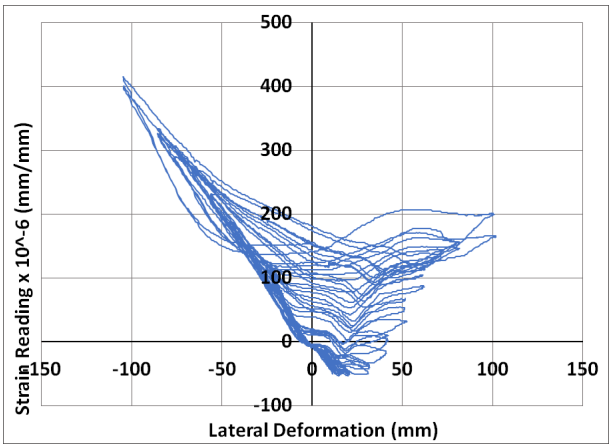

Strain Gauge: W-3d

Figure B2.4 Shear Wall No. 2 - Strain Gauge Recordings of WWR W-3 Grid

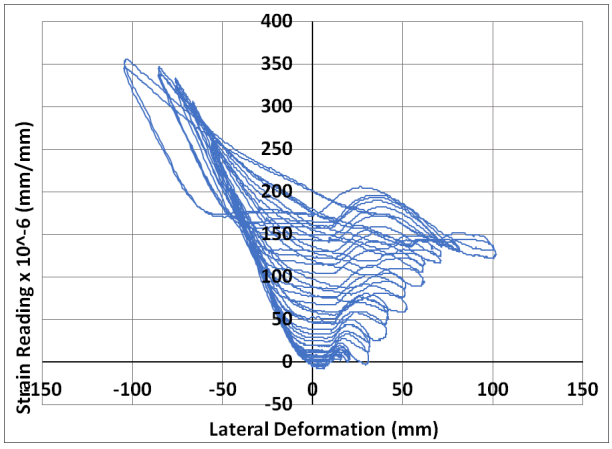

Strain Gauge: W-4b

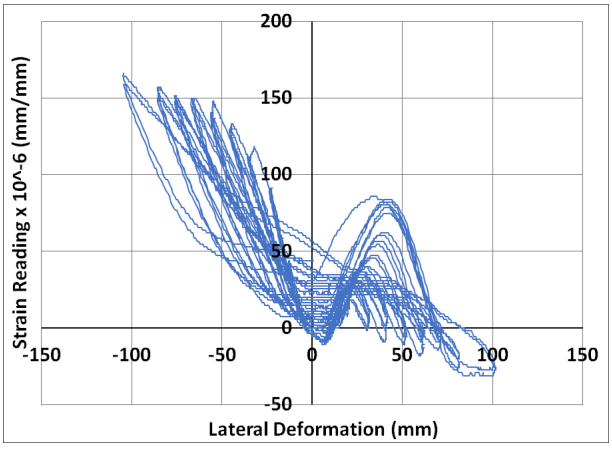

Strain Gauge: W-4c

Figure B2.5 Shear Wall No. 2 - Strain Gauge Recordings of WWR W-4 Grid

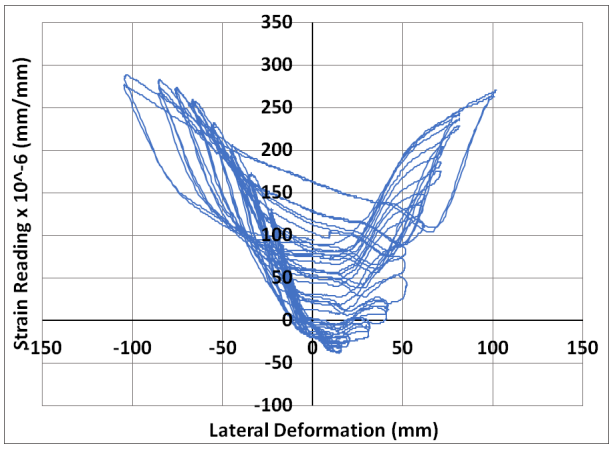

Strain Gauge: W-5a

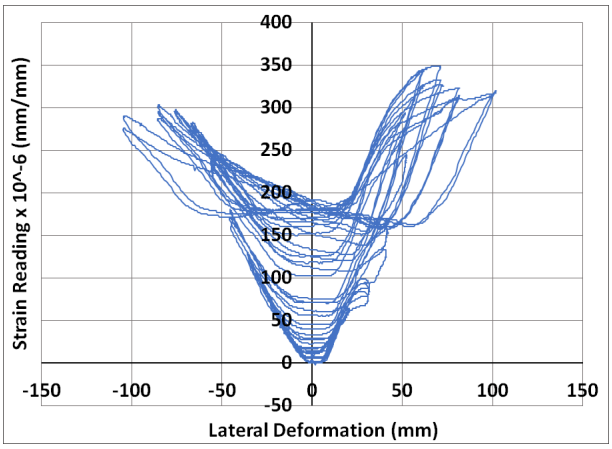

Strain Gauge: W-5b

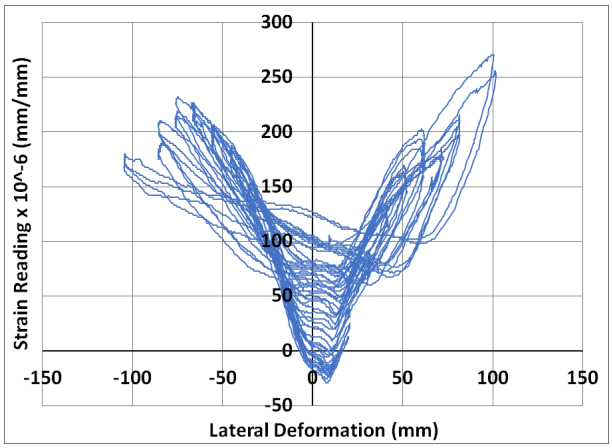

Strain Gauge: W-5c

Figure B2.6 Shear Wall No. 2 - Strain Gauge Recordings of WWR W-5 Grid

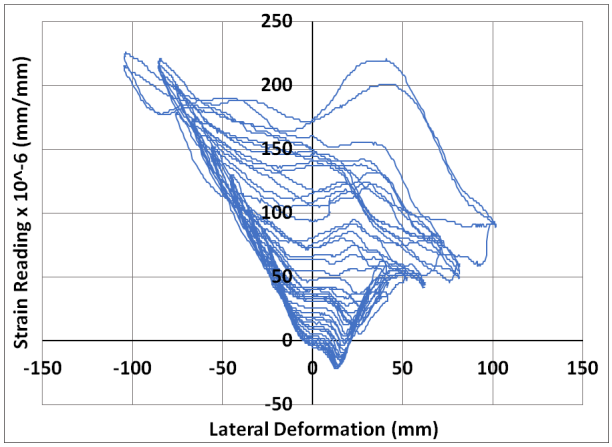

Strain Gauge: W-6a

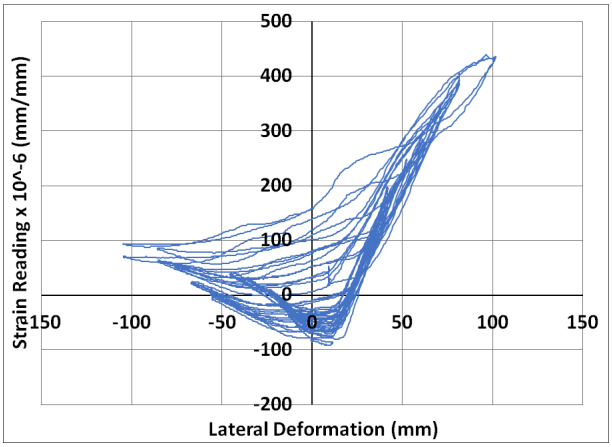

Strain Gauge: W-6c

Figure B2.7 Shear Wall No. 2 - Strain Gauge Recordings of WWR W-6 Grid

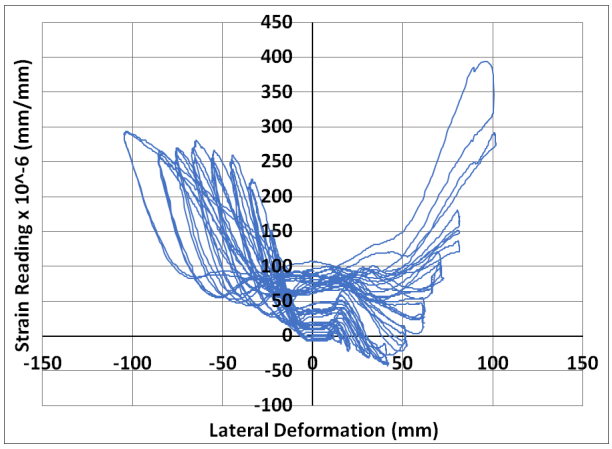

Strain Gauge: W-7a

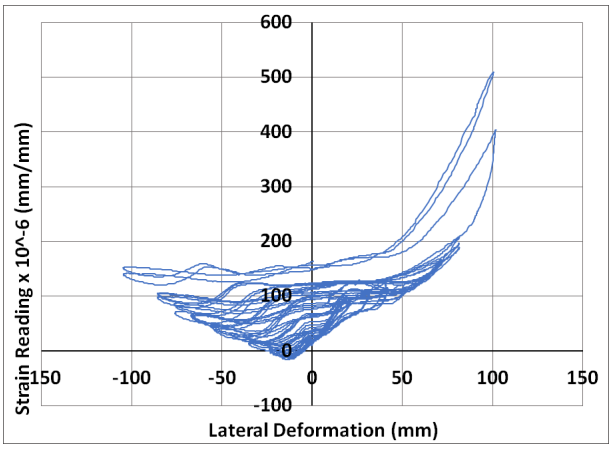

Strain Gauge: W-7b

Figure B2.8 Shear Wall No. 2 - Strain Gauge Recordings of WWR W-7 Grid

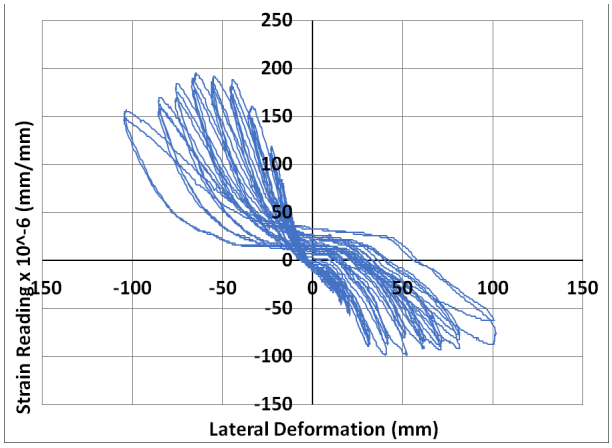

Strain Gauge: W-8a

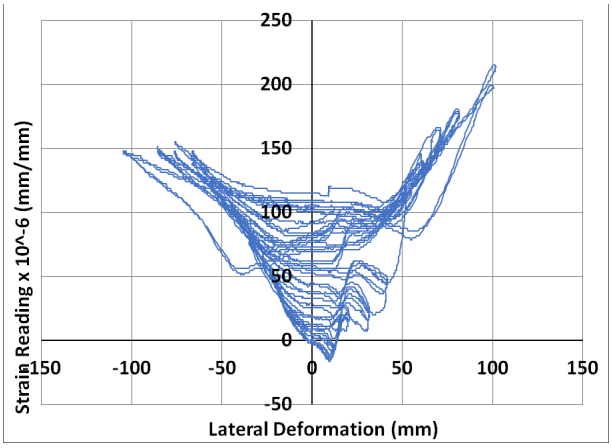

Strain Gauge: W-8b

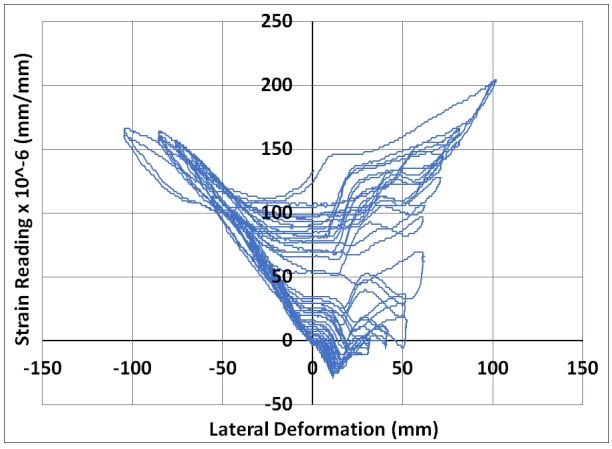

Strain Gauge: W-8c

Figure B2.9 Shear Wall No. 2 - Strain Gauge Recordings of WWR W-8 Grid

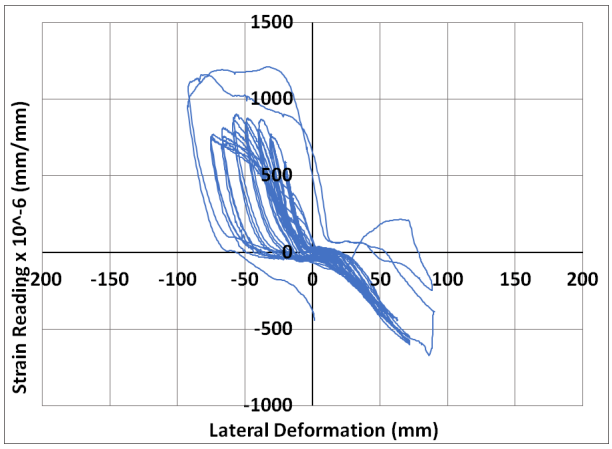

Strain Gauge: E-1b

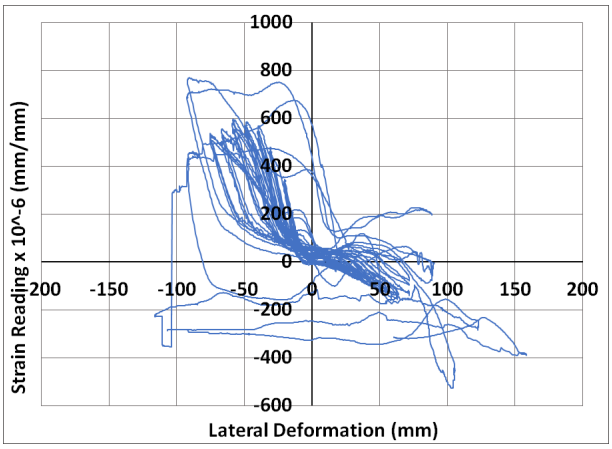

Strain Gauge: E-1c

Figure B2.10 Shear Wall No. 2 - Strain Gauge Recordings of WWR E-1 Grid

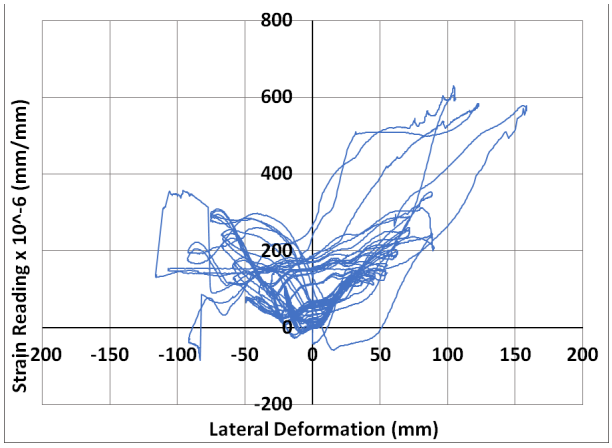

Strain Gauge: E-2b

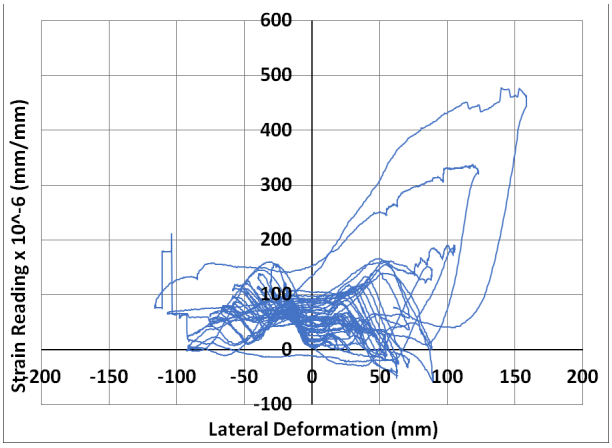

Strain Gauge: E-2c

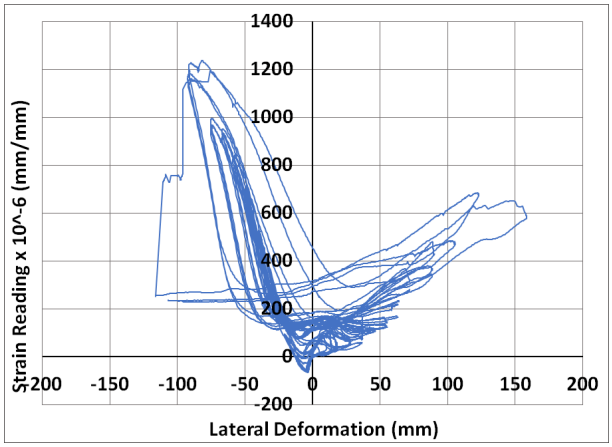

Strain Gauge: E-2d

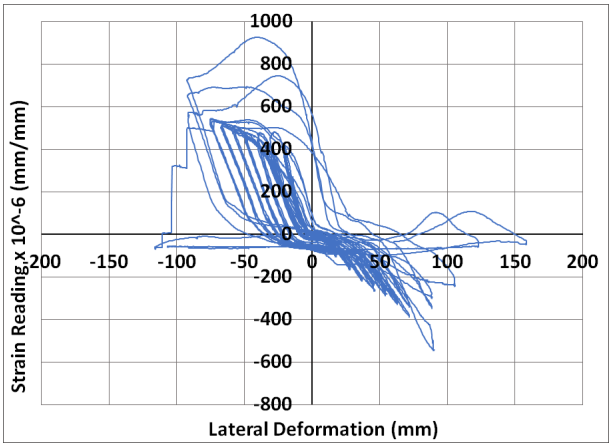

Strain Gauge: E-2e

Figure B2.11 Shear Wall No. 2 - Strain Gauge Recordings of WWR E-2 Grid

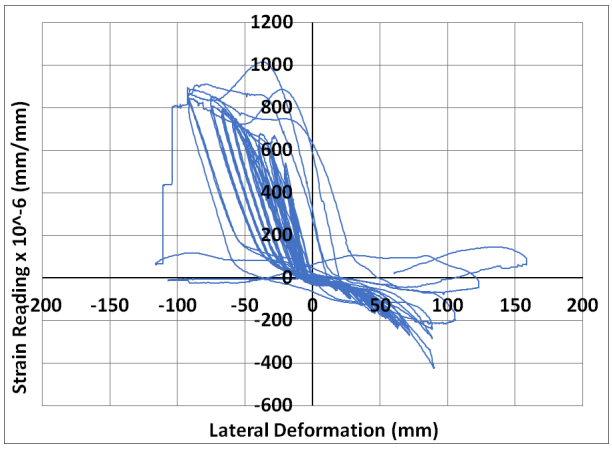

Strain Gauge: E-2i

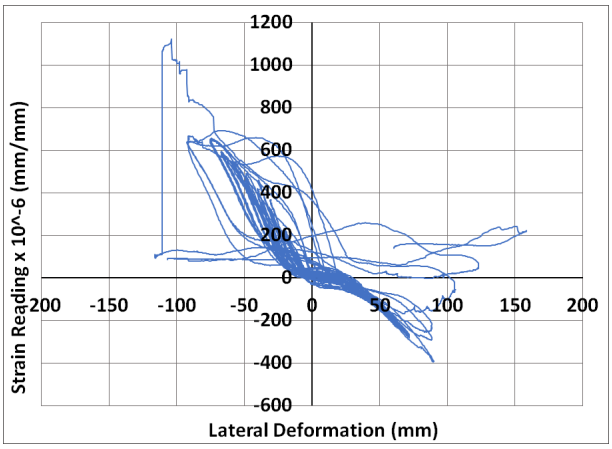

Strain Gauge: E-2k

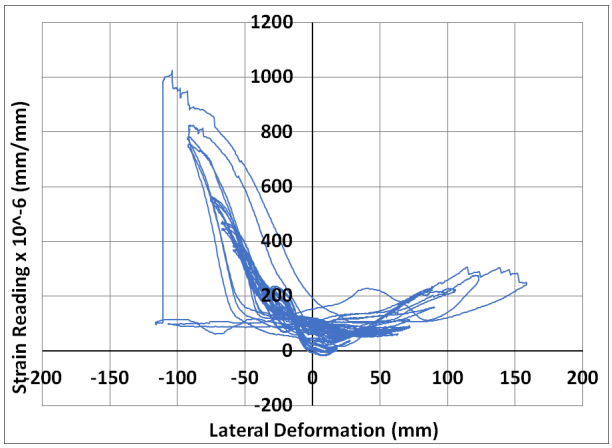

Strain Gauge: E-2n

Figure B2.11 (Cont'd) Shear Wall No. 2 - Strain Gauge Recordings of WWR E-2 Grid

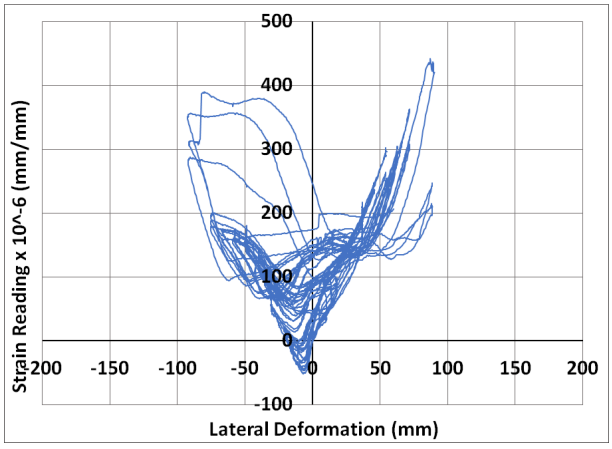

Strain Gauge: E-3a

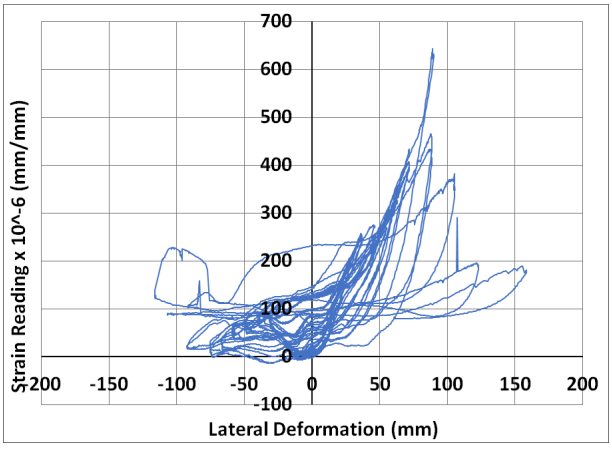

Strain Gauge: E-3b

Figure B2.12 Shear Wall No. 2 - Strain Gauge Recordings of WWR E-3 Grid

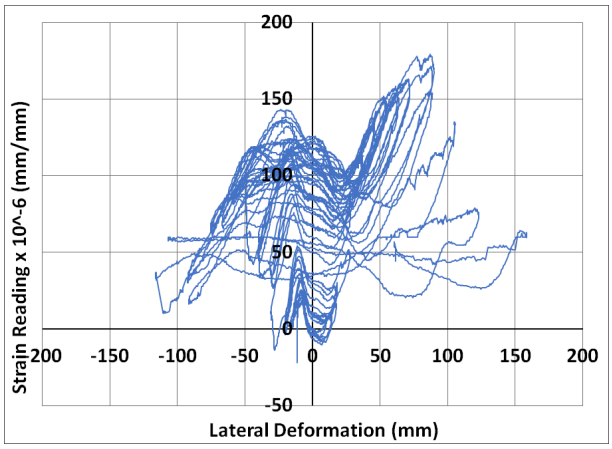

Strain Gauge: E-3c

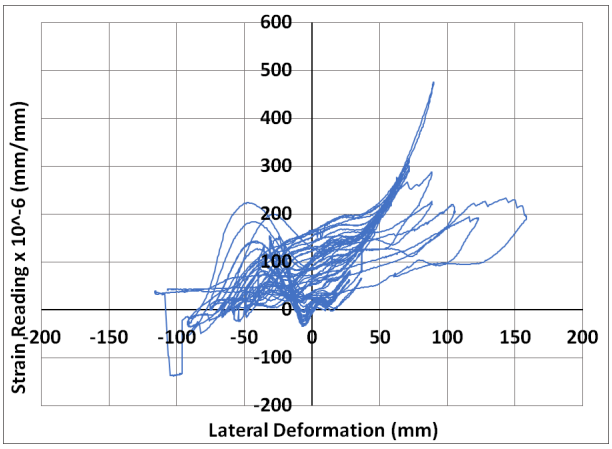

Strain Gauge: E-3d

Figure B2.12 (Cont'd) Shear Wall No. 2 - Strain Gauge Recordings of WWR E-3 Grid

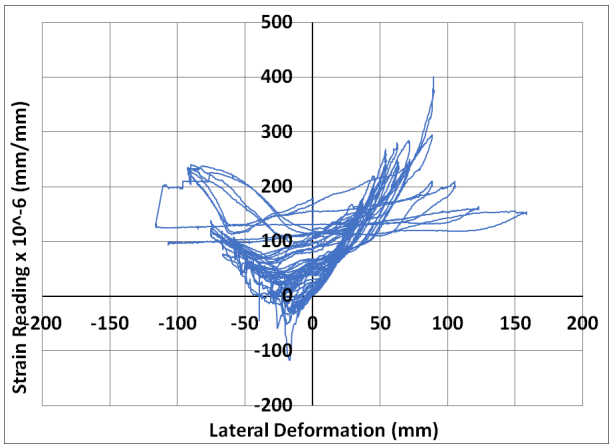

Strain Gauge: E-4a

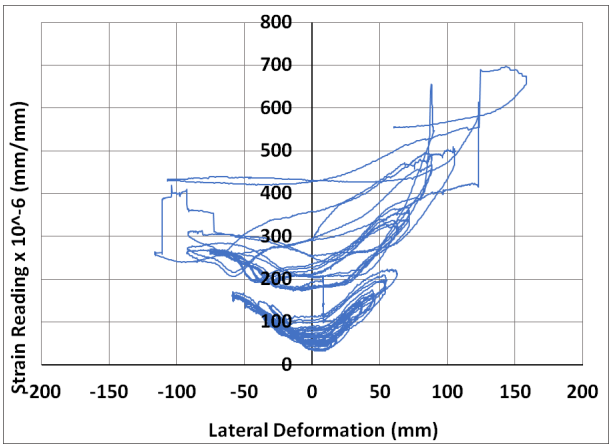

Strain Gauge: E-4b

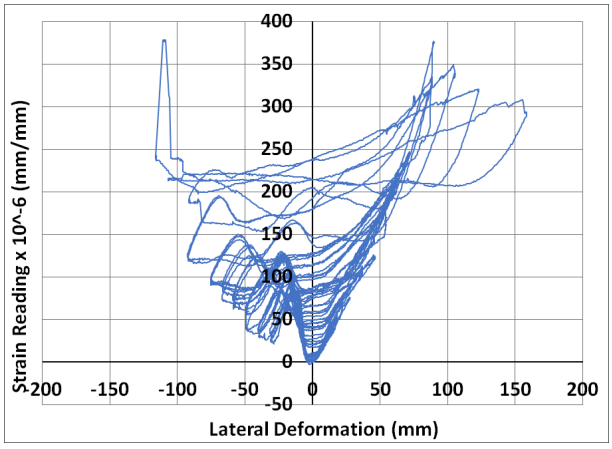

Strain Gauge: E-4c

Figure B2.13 Shear Wall No. 2 - Strain Gauge Recordings of WWR E-4 Grid

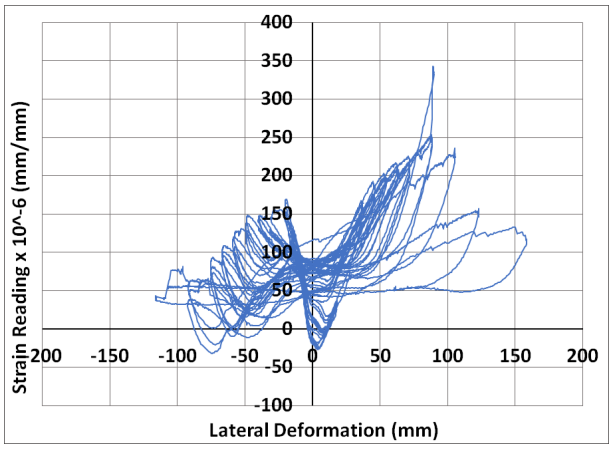

Strain Gauge: E-5b

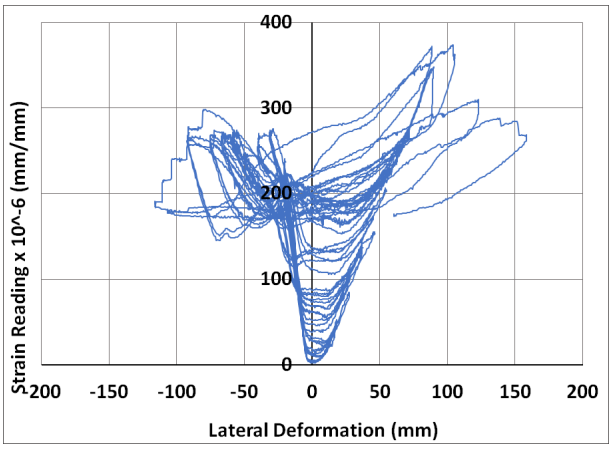

Strain Gauge: E-5c

Figure B2.14 Shear Wall No. 2 - Strain Gauge Recordings of WWR E-5 Grid

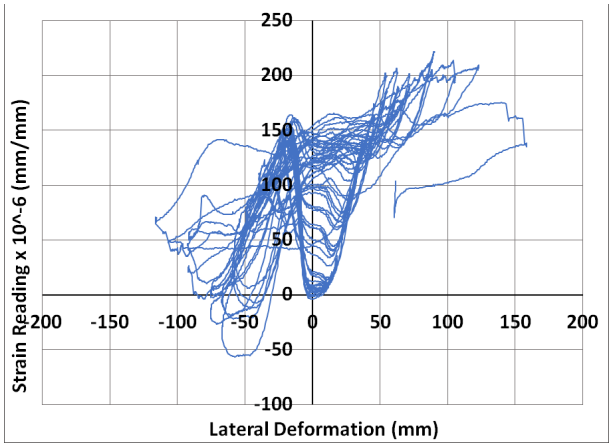

Strain Gauge: E-6c

Figure B2.15 Shear Wall No.2 - Strain Gauge Recordings of WWR E-6 Grid

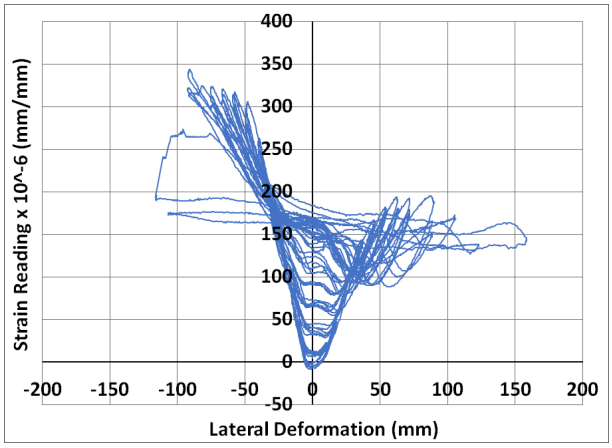

Strain Gauge: E-7a

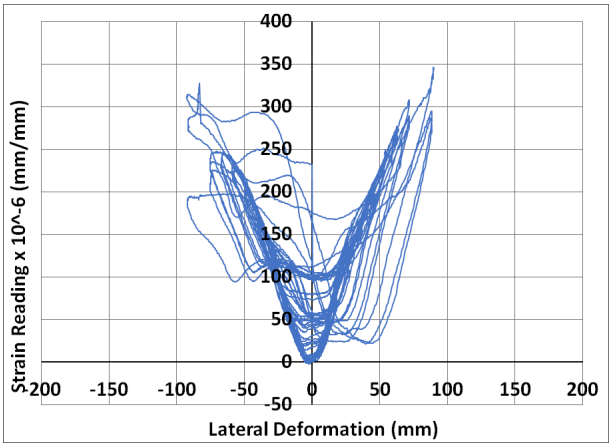

Strain Gauge: E-7b

Figure B2.16 Shear Wall No. 2 - Strain Gauge Recordings of WWR E-7 Grid

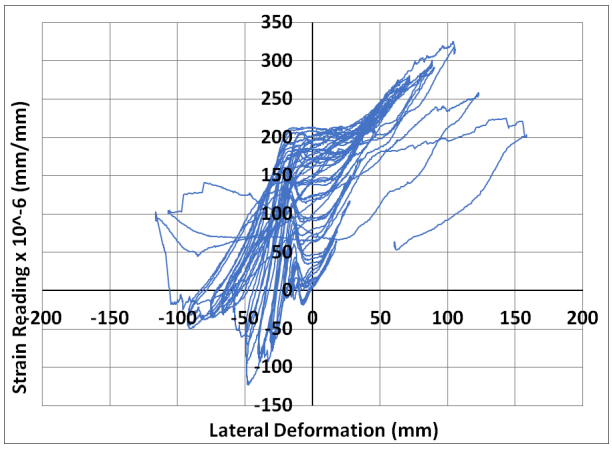

Strain Gauge: E-7c

Figure B2.16 (Cont'd) Shear Wall No. 2 - Strain Gauge Recordings of WWR E-7 Grid

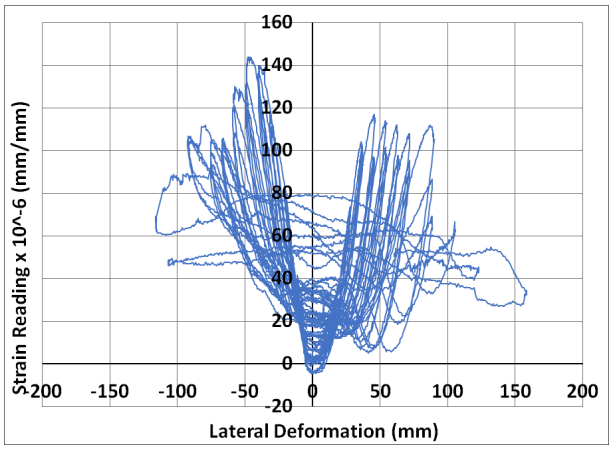

Strain Gauge: E-8a

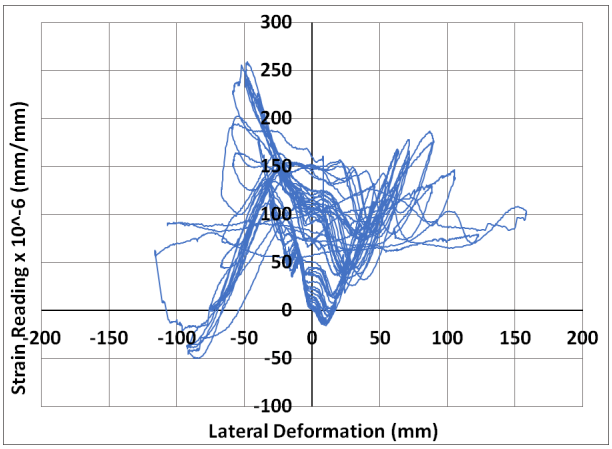

Strain Gauge: E-8b

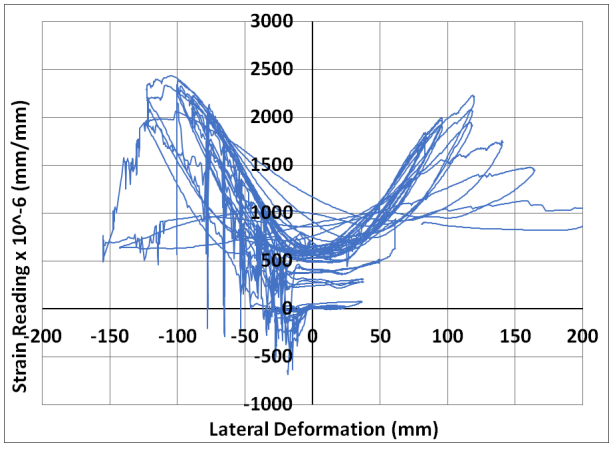

Strain Gauge: E-8c

Figure B2.17 Shear Wall No. 2 - Strain Gauge Recordings of WWR E-8 Grid

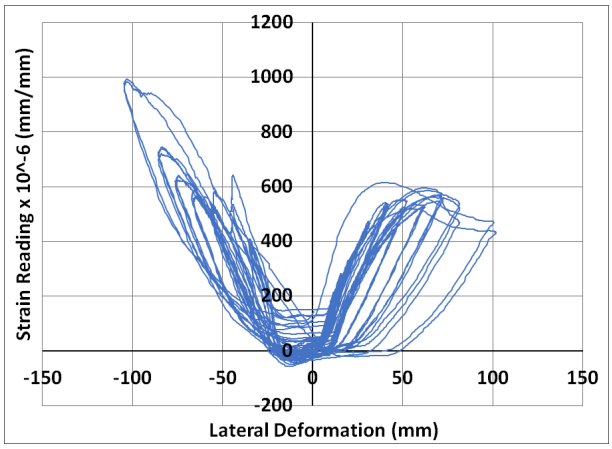

Strain Gauge: Web W-1

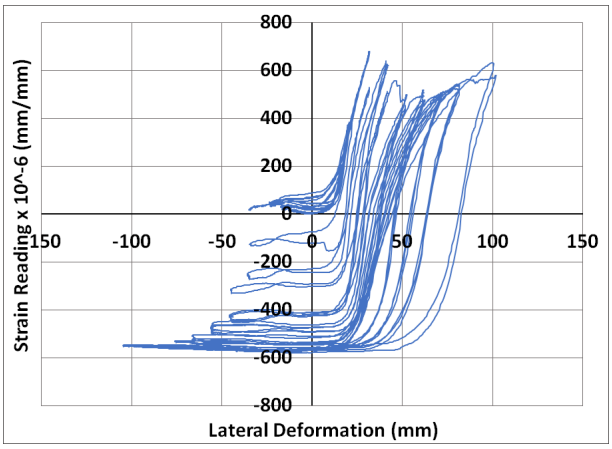

Strain Gauge: Web W-3

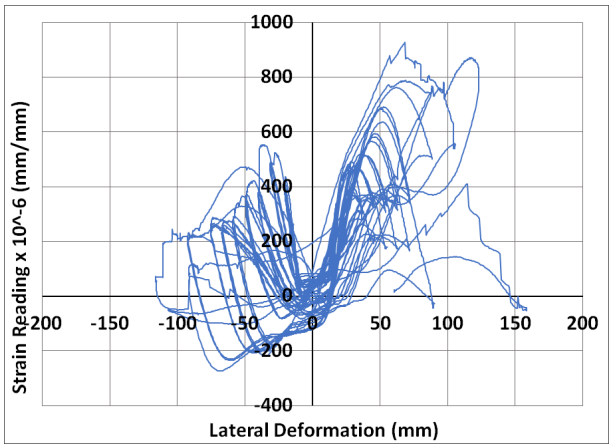

Strain Gauge: Web E-1

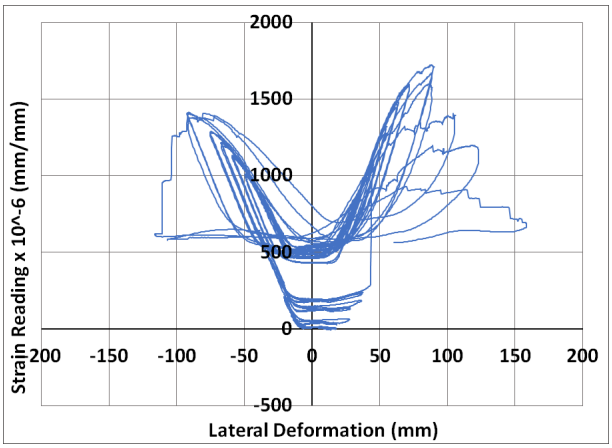

Strain Gauge: Web E-2

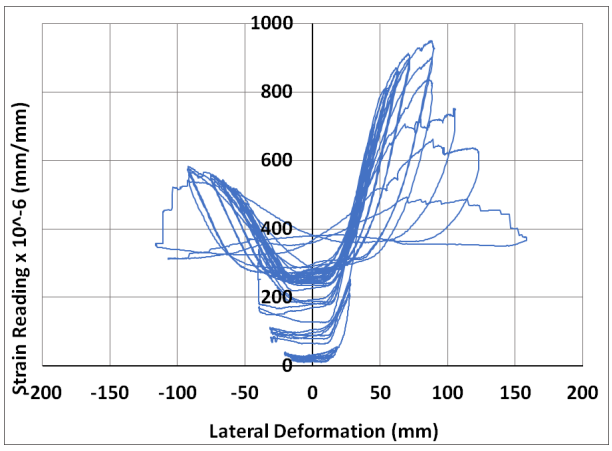

Strain Gauge: Web E-4

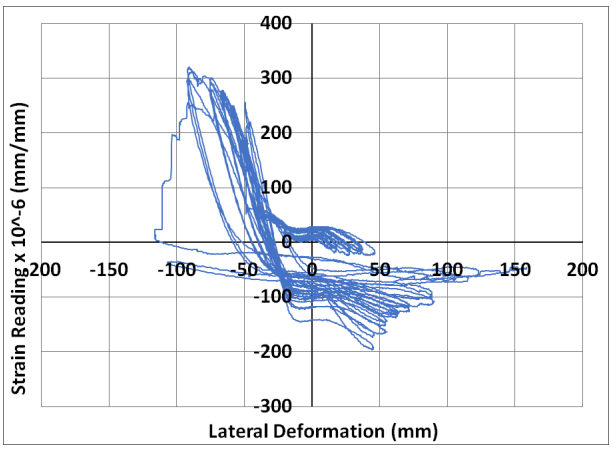

Strain Gauge: Web E-5

Figure B2.18 Shear Wall No. 2 - Strain Gauge Recordings of Web Reinforcement

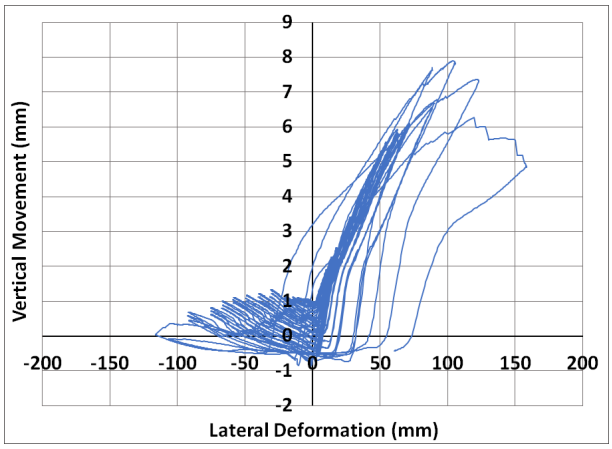

LVDT: FND-1 (WEST)

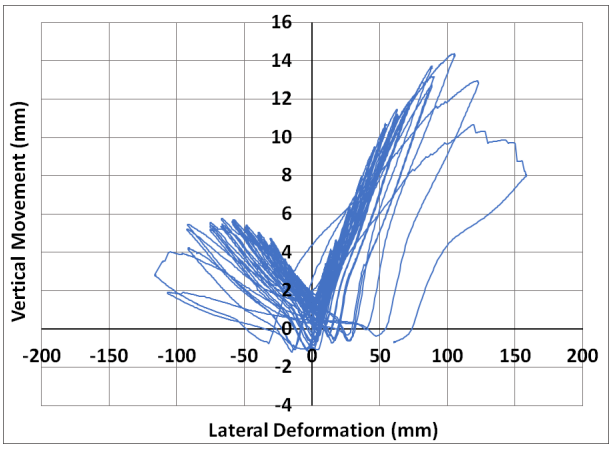

LVDT: FND-2

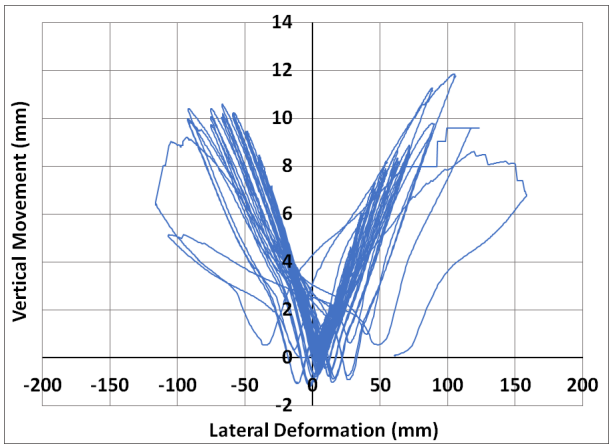

LVDT: FND-3

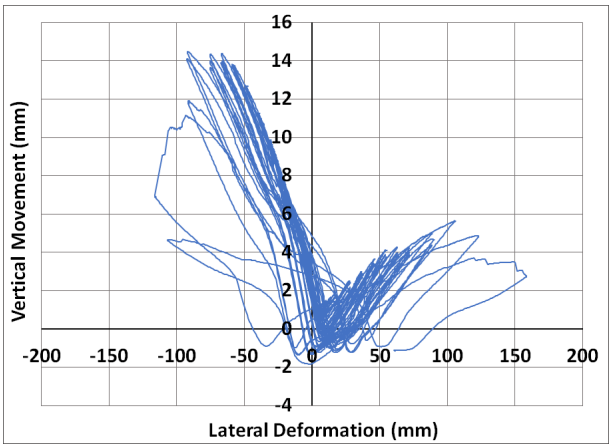

LVDT: FND-4

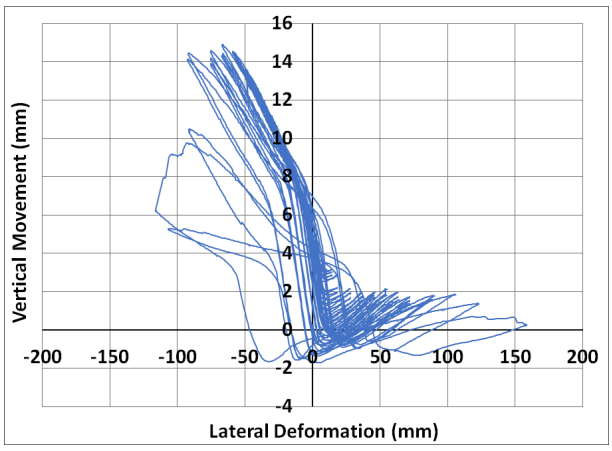

LVDT: FND-5 (WEST)

Figure B2.18 Shear Wall No. 2 – Foundation Vertical Movements vs. Wall Lateral Deformations

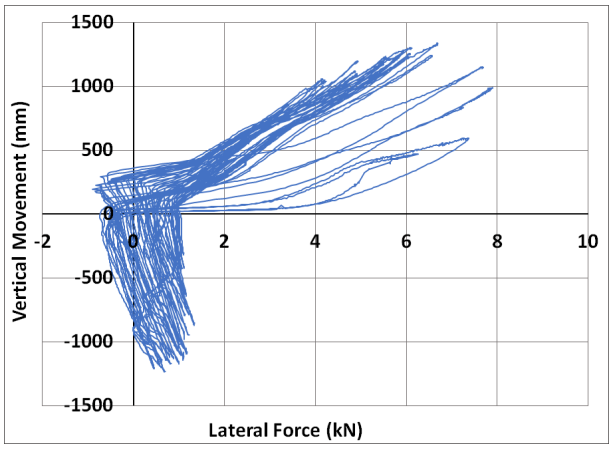

LVDT: FND-1 (WEST)

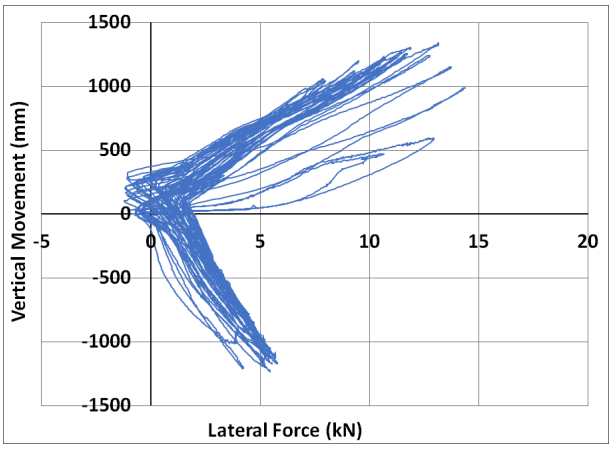

LVDT: FND-2

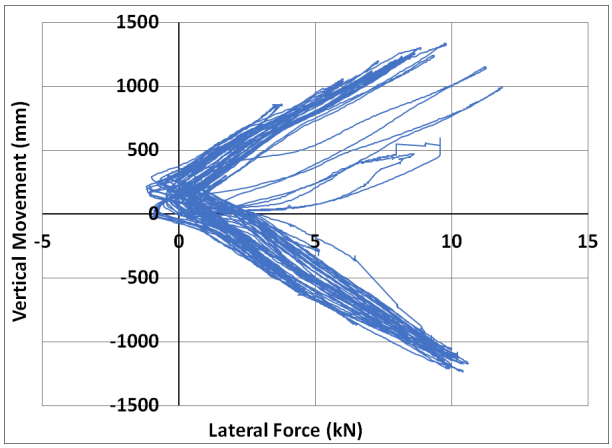

LVDT: FND-3

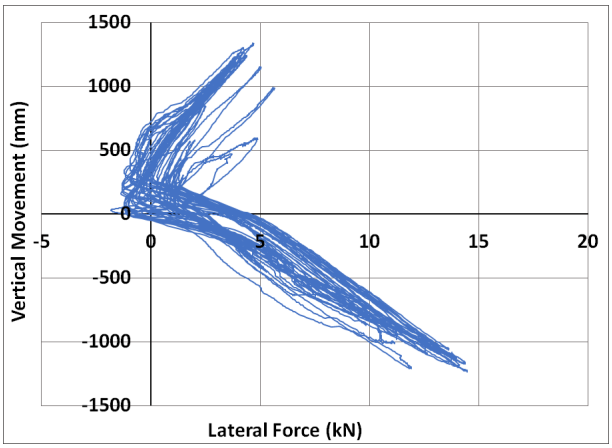

LVDT: FND-4

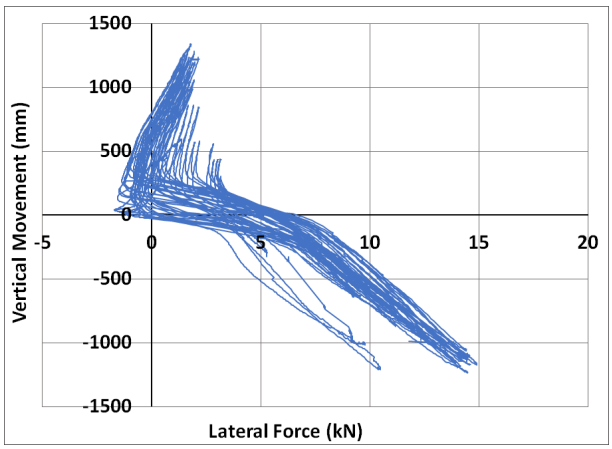

LVDT: FND-5 (WEST)

Figure B2.19 Shear Wall No. 2 – Foundation Vertical Movements vs. Lateral Load

Appendix B.3 – Shear Wall No. 3 Strain Gauge Recordings

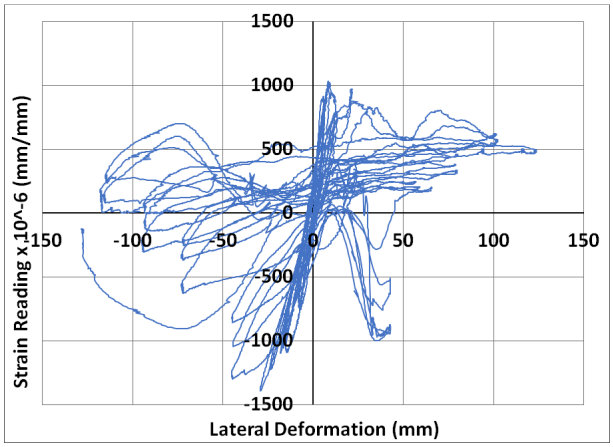

Strain Gauge: Dowel W-1

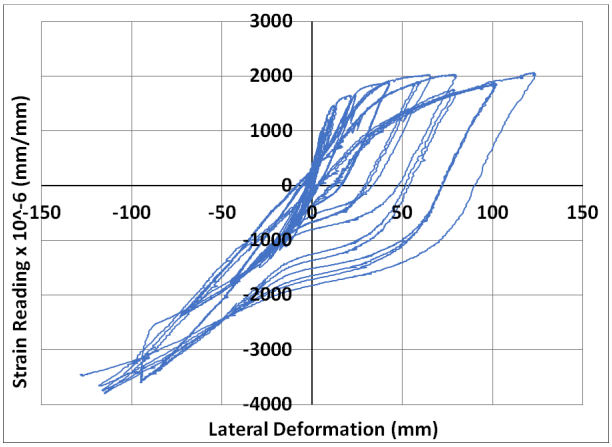

Strain Gauge: Dowel W-2

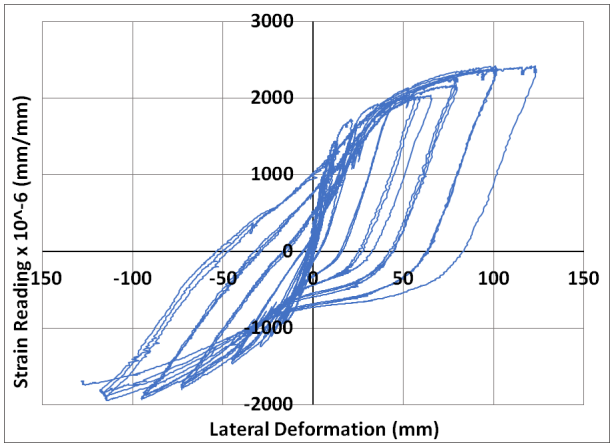

Strain Gauge: Dowel W-3

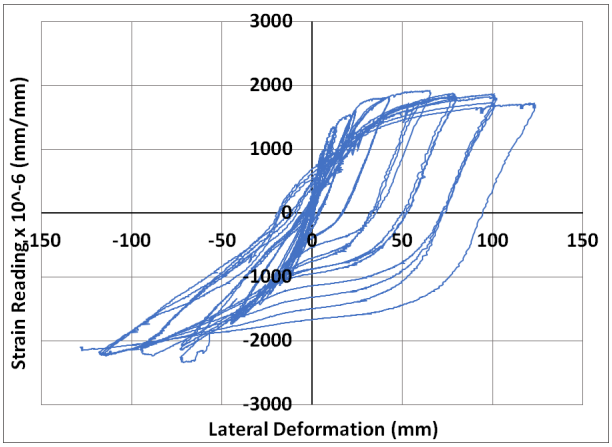

Strain Gauge: Long W-1

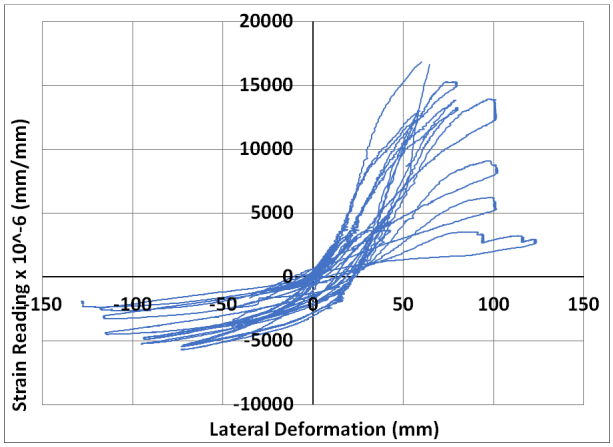

Strain Gauge: Long W-2

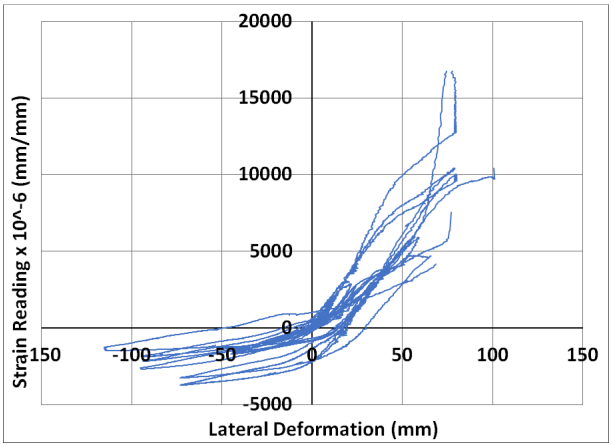

Strain Gauge: Long W-3

Figure B3.1 Shear Wall No.3 - Strain Gauge Recordings of Longitudinal Bars and Dowels

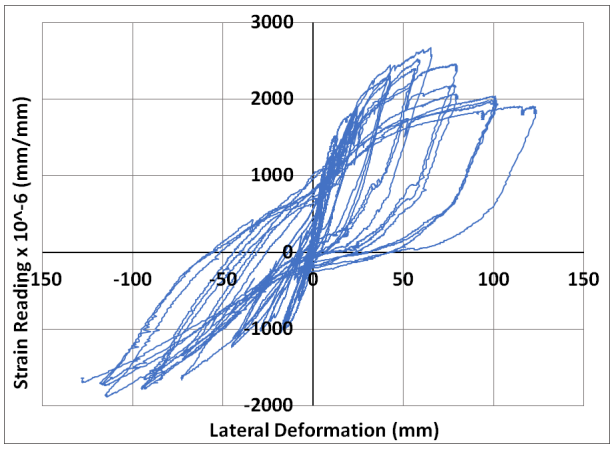

Strain Gauge: Long W-4

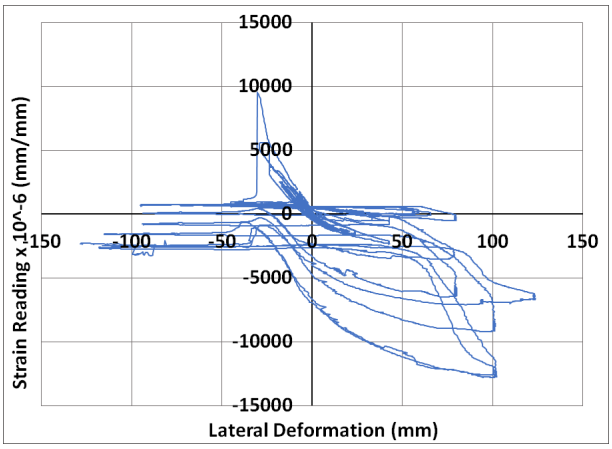

Strain Gauge: Dowel E-1

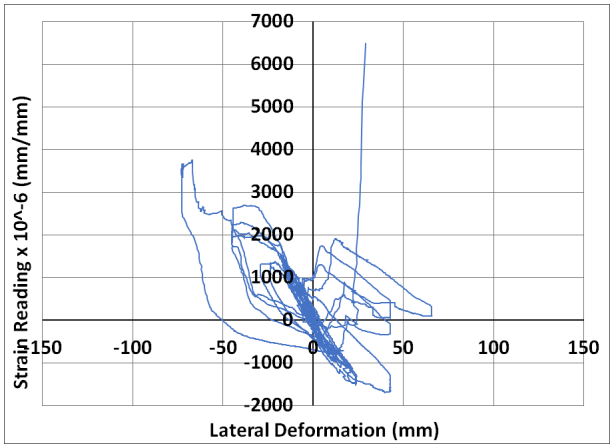

Strain Gauge: Dowel E-2

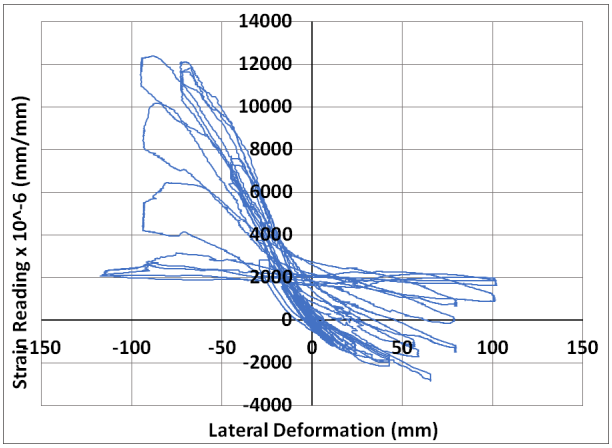

Strain Gauge: Dowel E-3

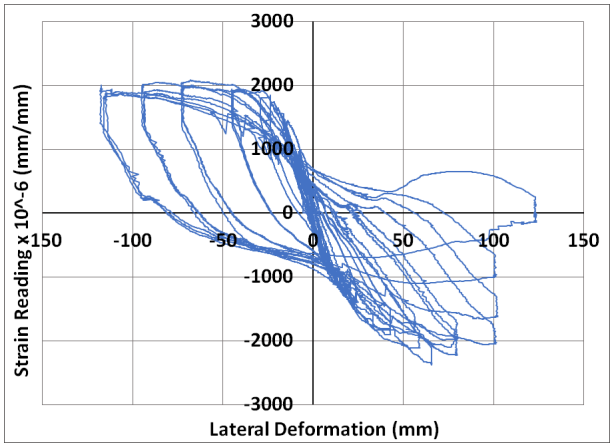

Strain Gauge: Dowel E-4

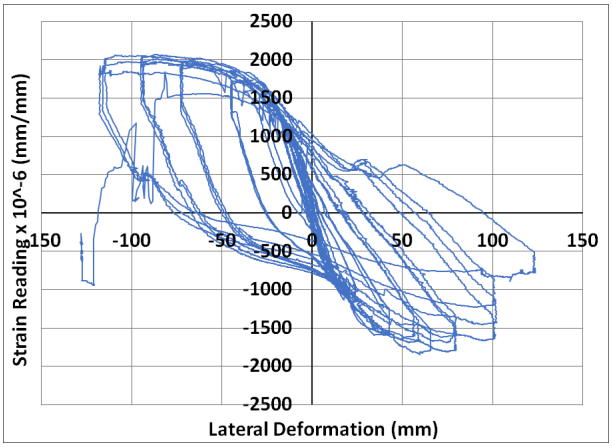

Strain Gauge: Long E-1

Figure B3.1 (Cont'd) Shear Wall No.3 - Strain Gauge Recordings of Longitudinal Bars and Dowels

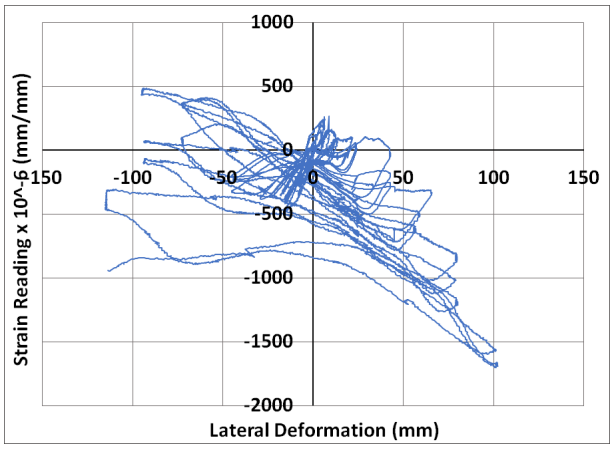

Strain Gauge WWR W-1a

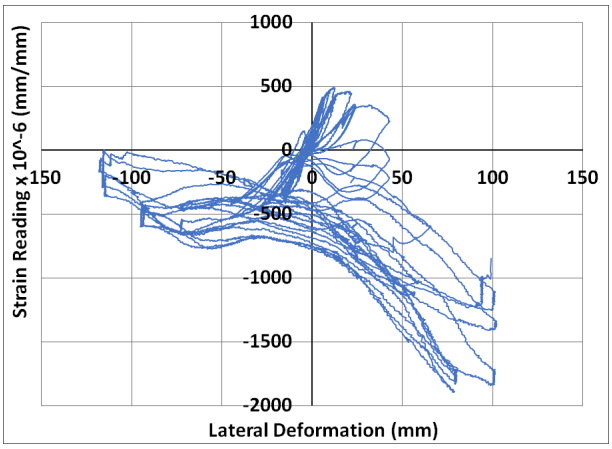

Strain Gauge WWR W-1b

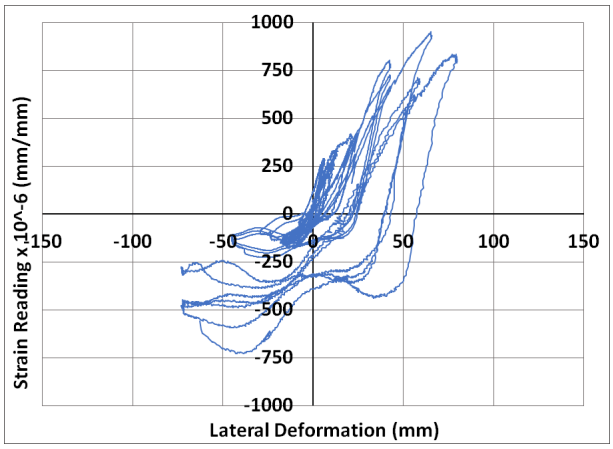

Strain Gauge WWR W-1d

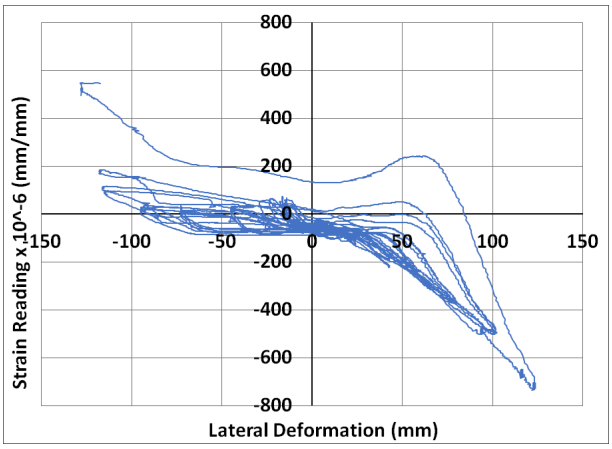

Strain Gauge WWR W-1e

Figure B3.2 Shear Wall No.3 - Strain Gauge Recordings of WWR W-1 Grid

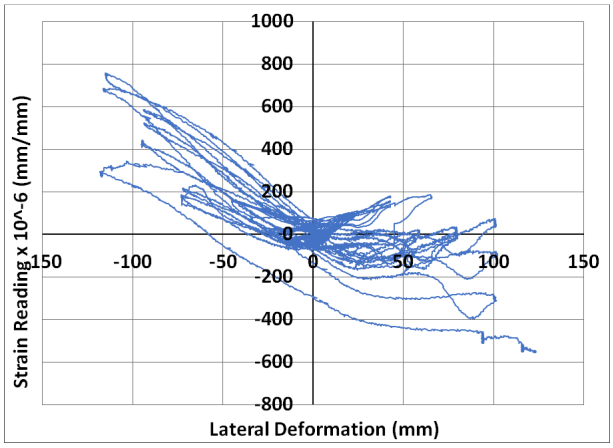

Strain Gauge WWR W-2a

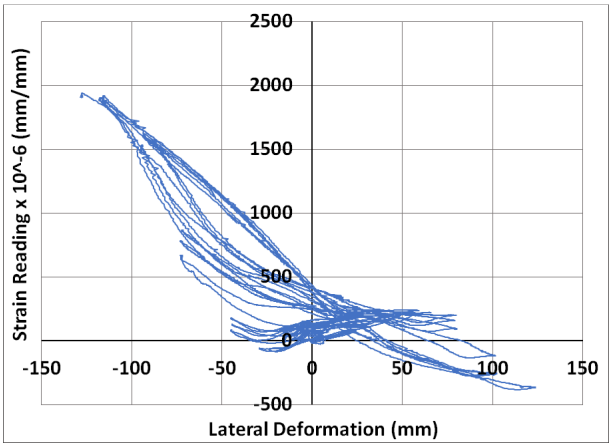

Strain Gauge WWR W-2b

Figure B3.3 Shear Wall No.3 - Strain Gauge Recordings of WWR W-2 Grid

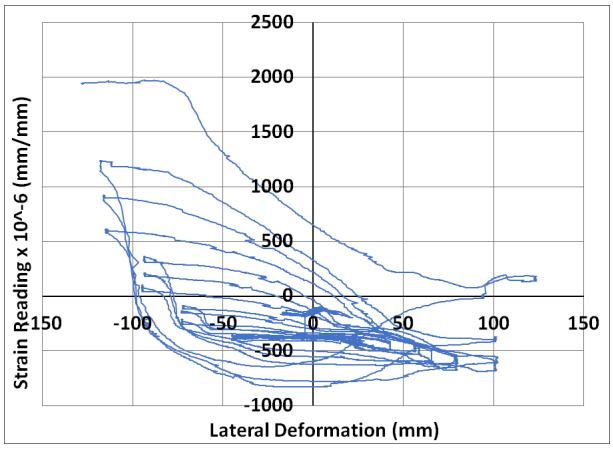

Strain Gauge WWR W-2c

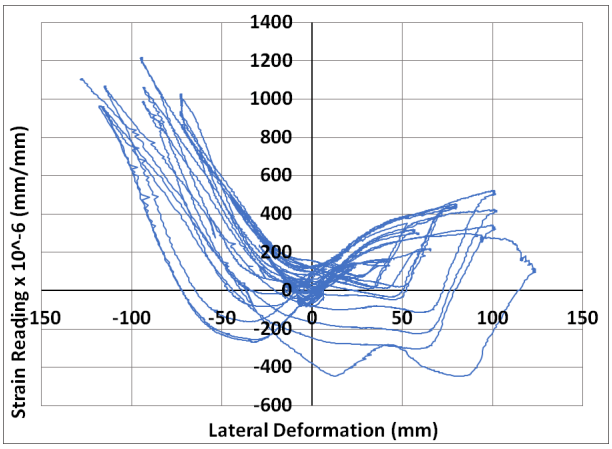

Strain Gauge WWR W-2d

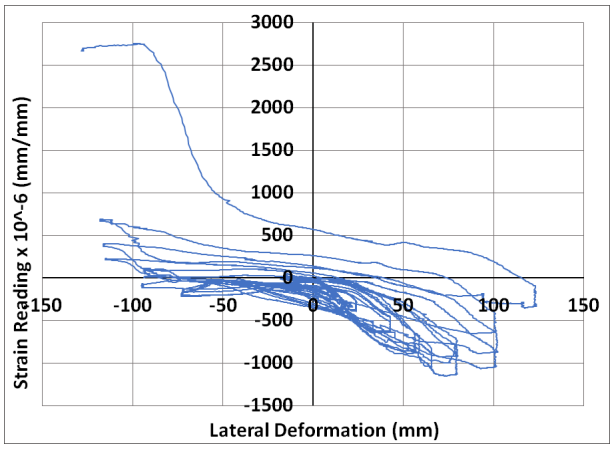

Strain Gauge WWR W-2e

Figure B3.3 (Cont'd) Shear Wall No.3 - Strain Gauge Recordings of WWR W-2 Grid

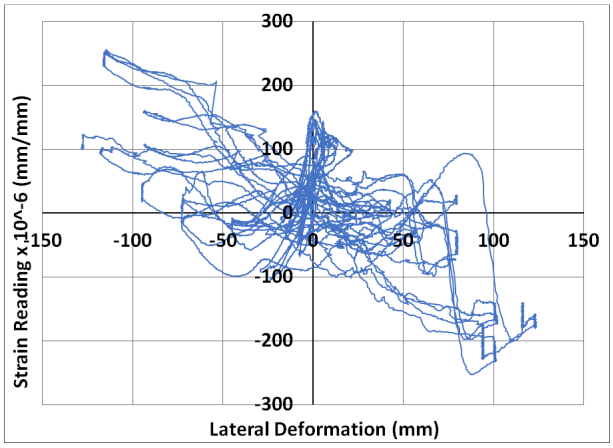

Strain Gauge WWR W-3a

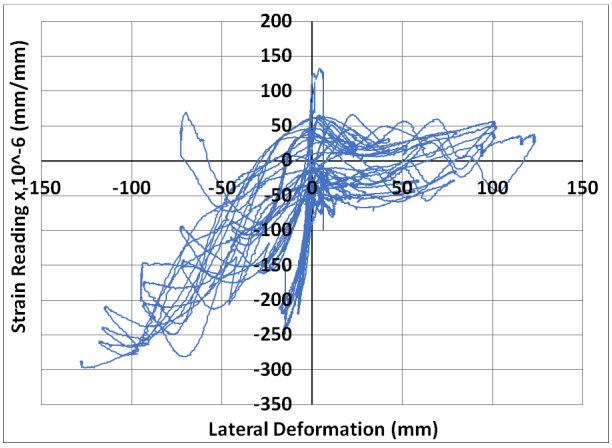

Strain Gauge WWR W-3b

Figure B3.4 Shear Wall No.3 - Strain Gauge Recordings of WWR W-3 Grid

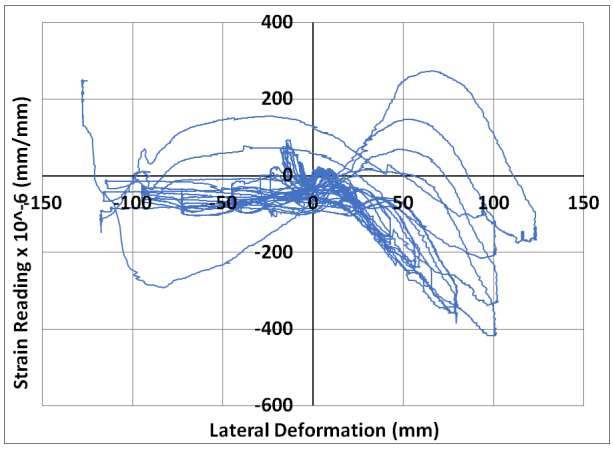

Strain Gauge WWR W-3c

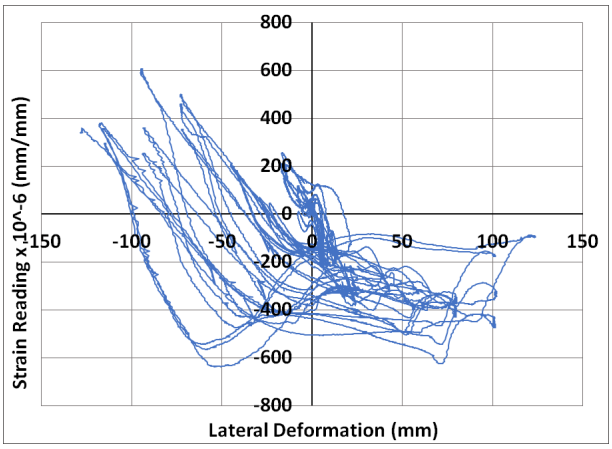

Strain Gauge WWR W-3d

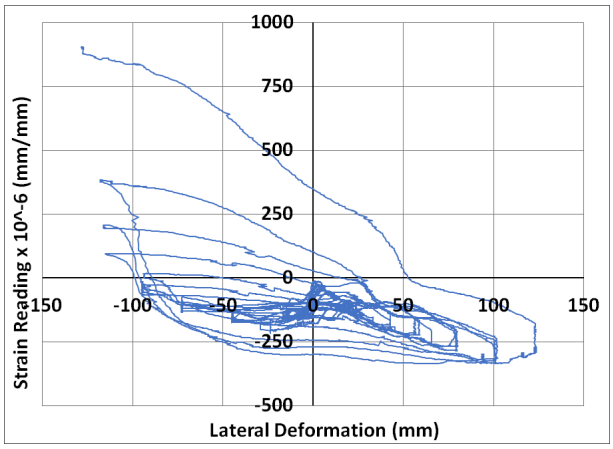

Strain Gauge WWR W-3e

Figure B3.4 (Cont'd) Shear Wall No.3 - Strain Gauge Recordings of WWR W-3 Grid

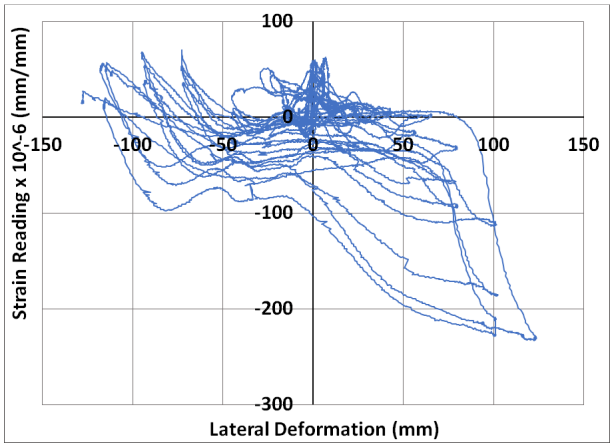

Strain Gauge WWR W-4a

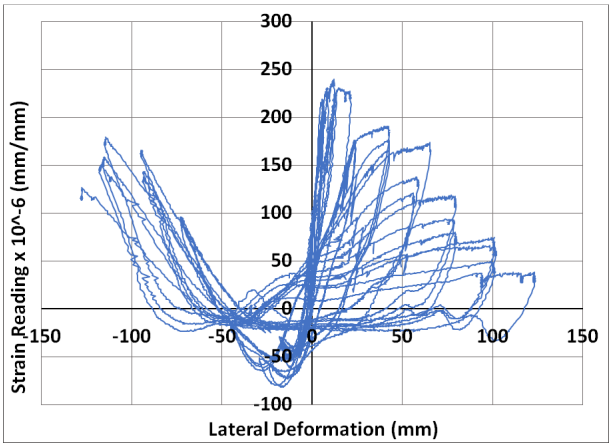

Strain Gauge WWR W-4b

Figure B3.5 Shear Wall No.3 - Strain Gauge Recordings of WWR W-4 Grid

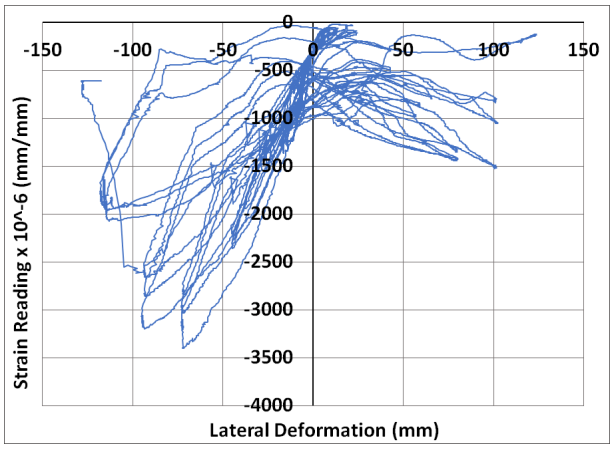

Strain Gauge WWR W-4e

Figure B3.5 (Cont'd) Shear Wall No.3 - Strain Gauge Recordings of WWR W-4 Grid

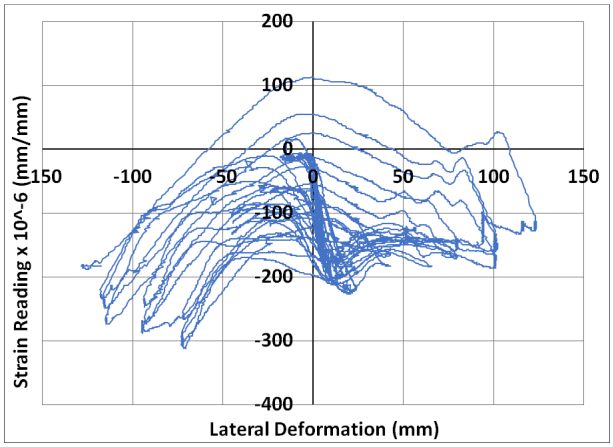

Strain Gauge WWR W-5a

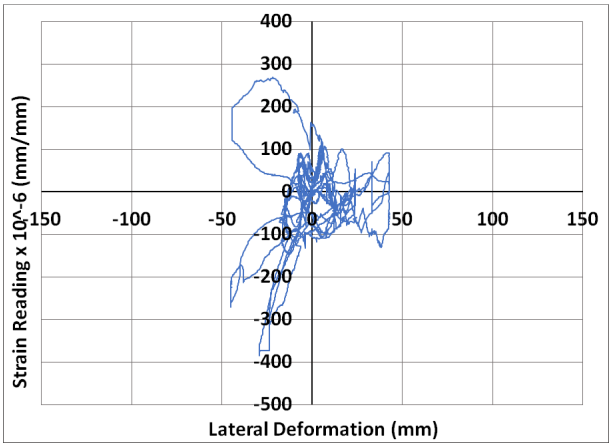

Strain Gauge WWR W-5b

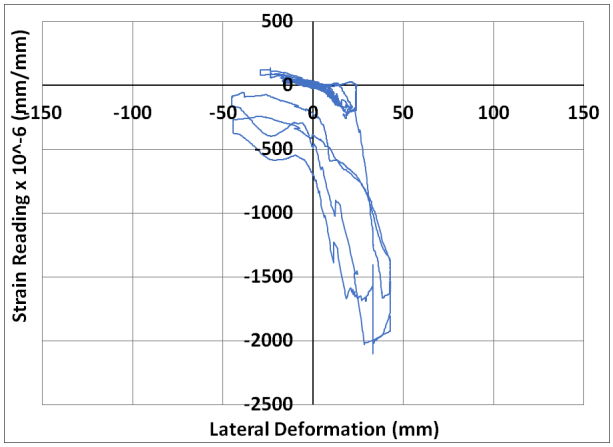

Strain Gauge WWR W-5d

Figure B3.6 Shear Wall No.3 - Strain Gauge Recordings of WWR W-5 Grid

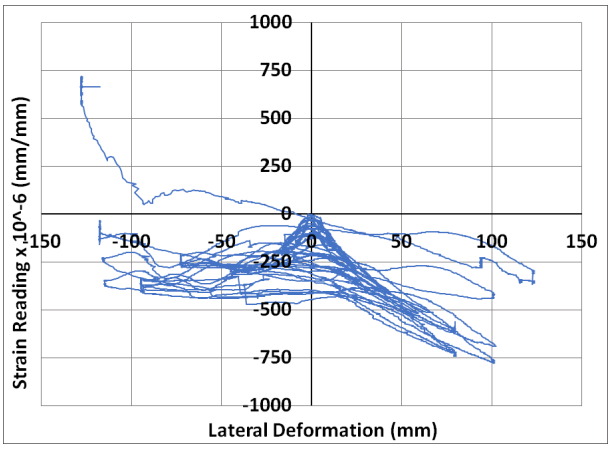

Strain Gauge WWR E-1a

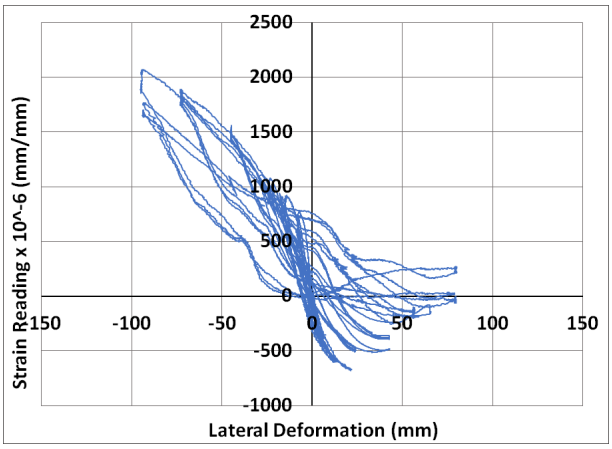

Strain Gauge WWR E-1b

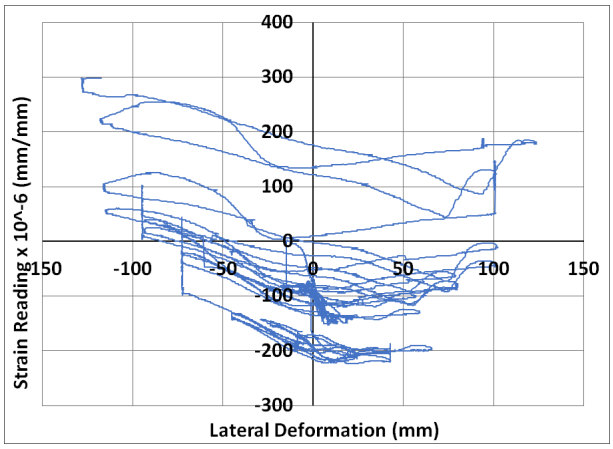

Strain Gauge WWR E-1d

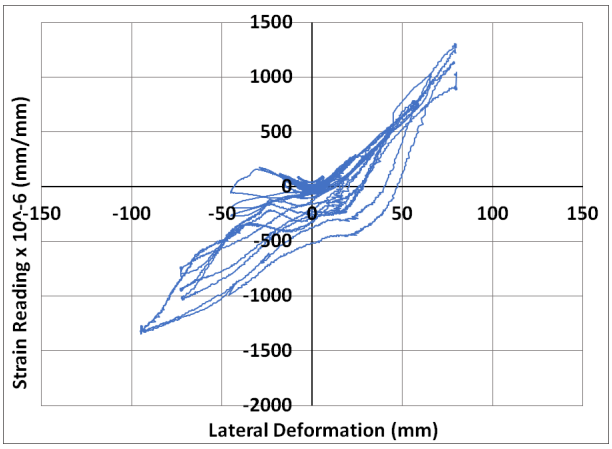

Strain Gauge WWR E-1e

Figure B3.7 Shear Wall No.3 - Strain Gauge Recordings of WWR E-1 Grid

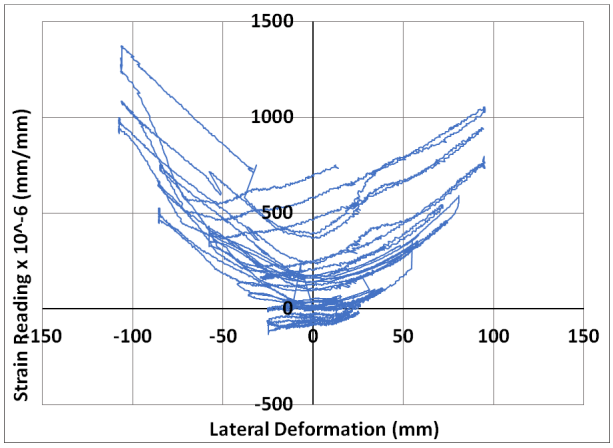

Strain Gauge WWR E-2c

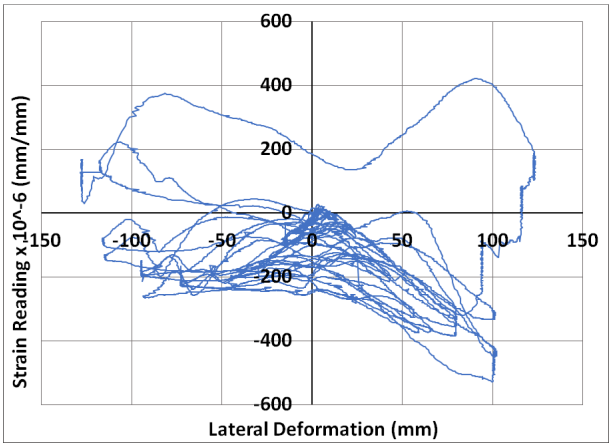

Strain Gauge WWR E-2d

Figure B3.8 Shear Wall No.3 - Strain Gauge Recordings of WWR E-2 Grid

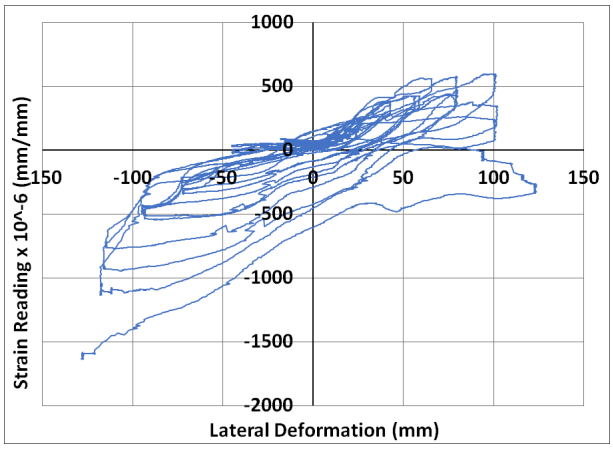

Strain Gauge WWR E-2e

Figure B3.8 (Cont'd) Shear Wall No.3 - Strain Gauge Recordings of WWR E-2 Grid

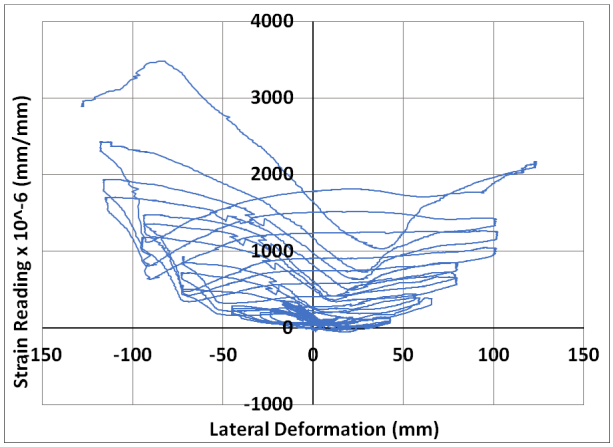

Strain Gauge WWR E-3a

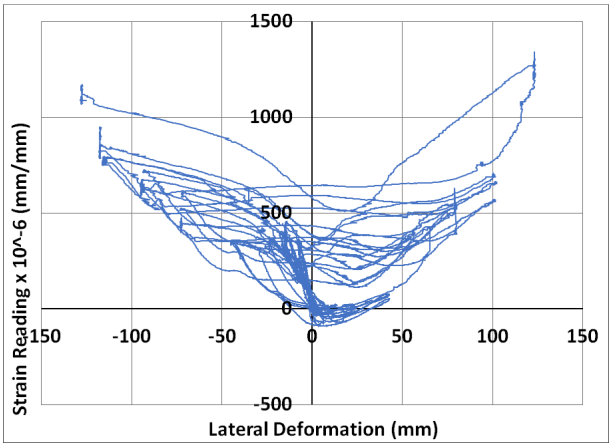

Strain Gauge WWR E-3b

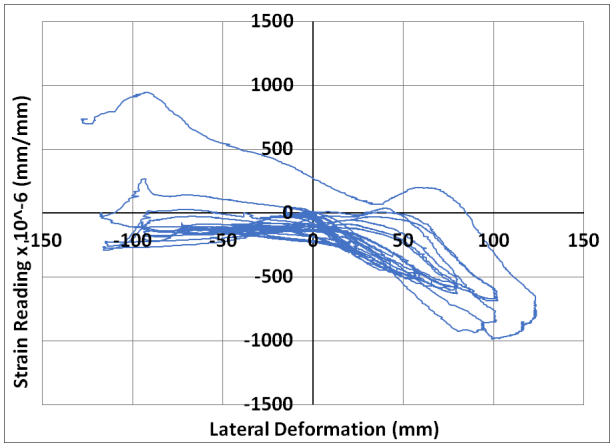

Strain Gauge WWR E-3d

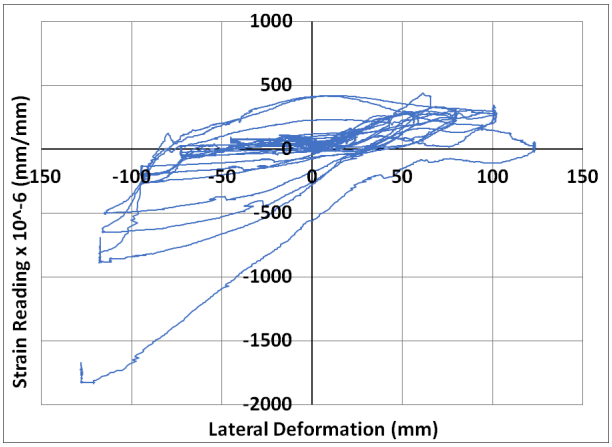

Strain Gauge WWR E-3e

Figure B3.9 Shear Wall No.3 - Strain Gauge Recordings of WWR E-3 Grid

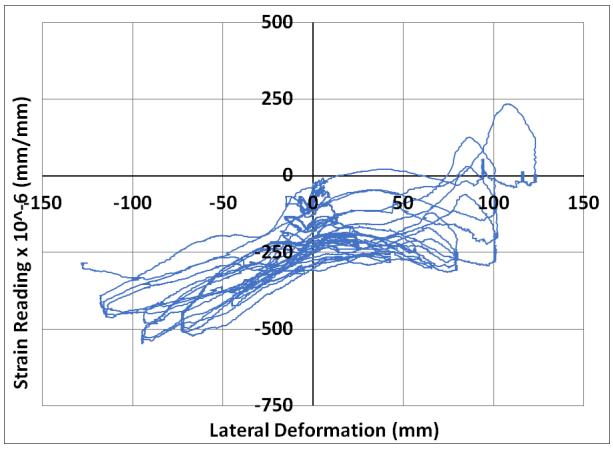

Strain Gauge WWR E-4a

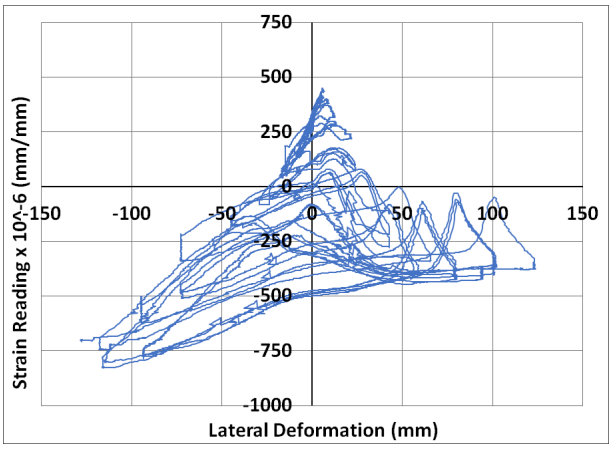

Strain Gauge WWR E-4b

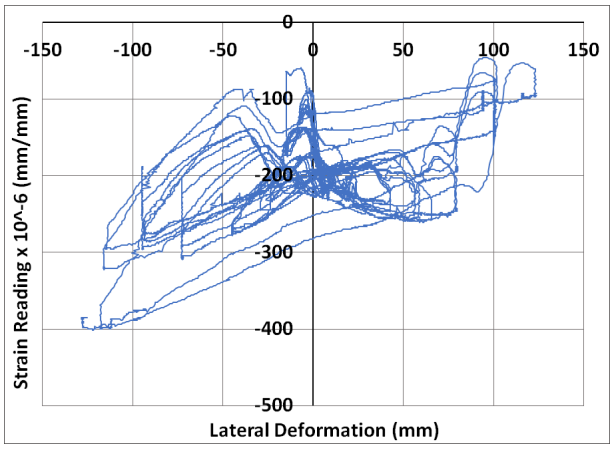

Strain Gauge WWR E-4c

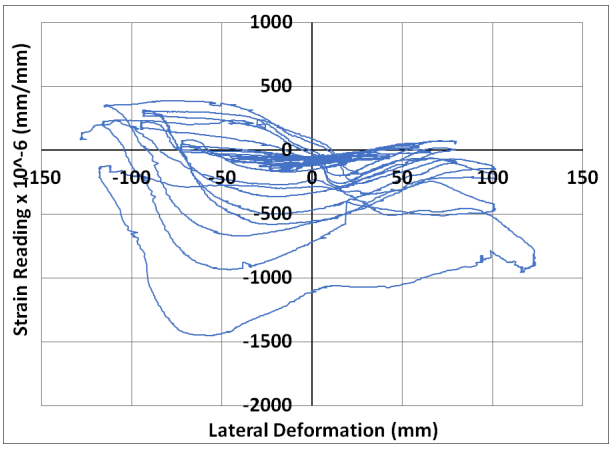

Strain Gauge WWR E-4d

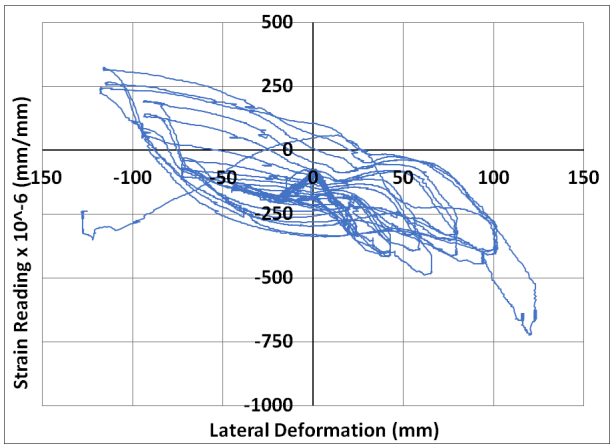

Strain Gauge WWR E-4e

Figure B3.10 Shear Wall No.3 - Strain Gauge Recordings of WWR E-4 Grid

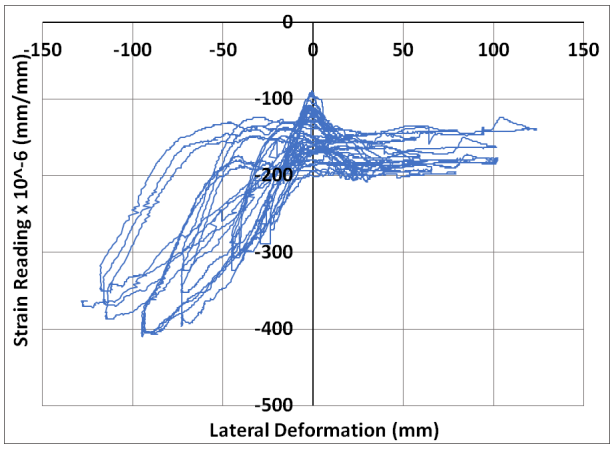

Strain Gauge WWR E-5a

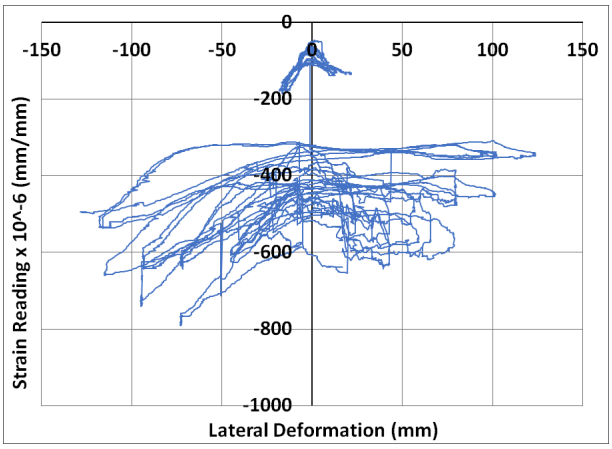

Strain Gauge WWR E-5c

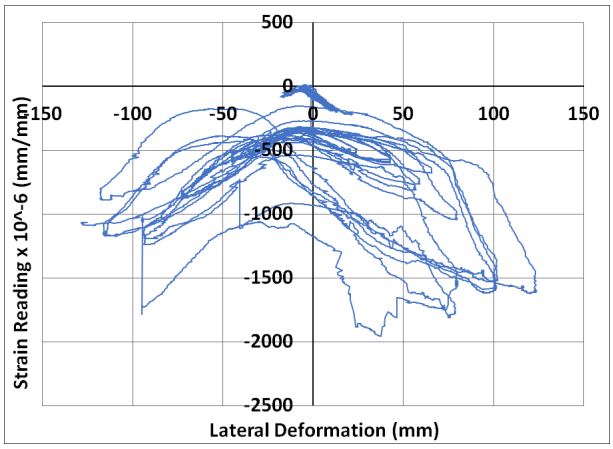

Strain Gauge WWR E-5e

Figure B3.11 Shear Wall No.3 - Strain Gauge Recordings of WWR E-5 Grid

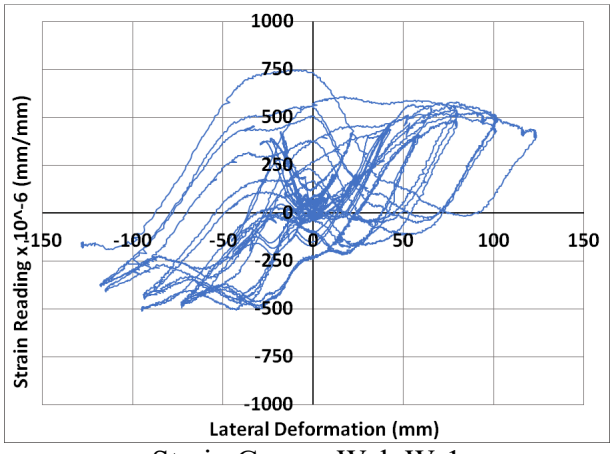

Strain Gauge: Web W-1

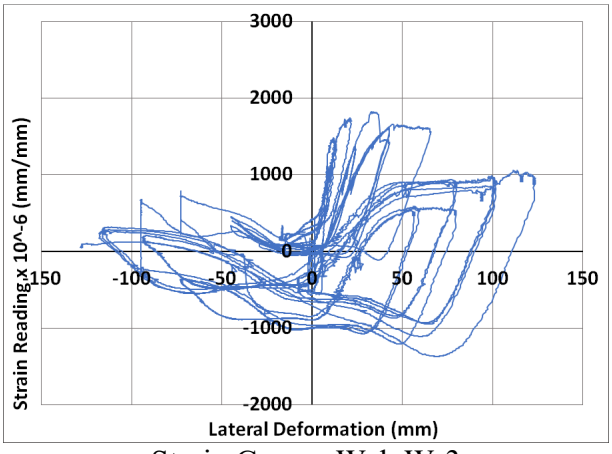

Strain Gauge: Web W-3

Figure B3.12 Shear Wall No.3 - Strain Gauge Recordings of Web Horizontal Reinforcement

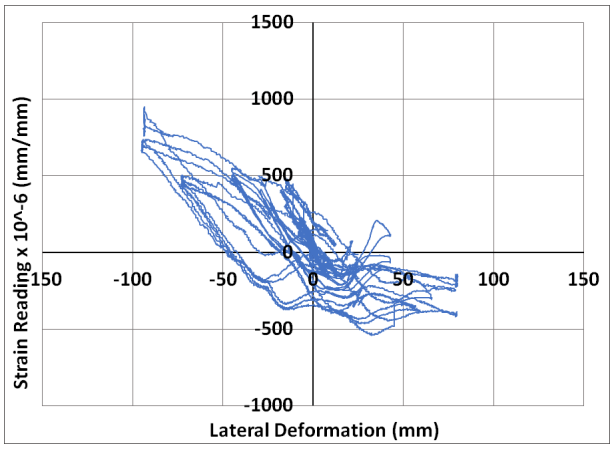

Strain Gauge: Web E-1

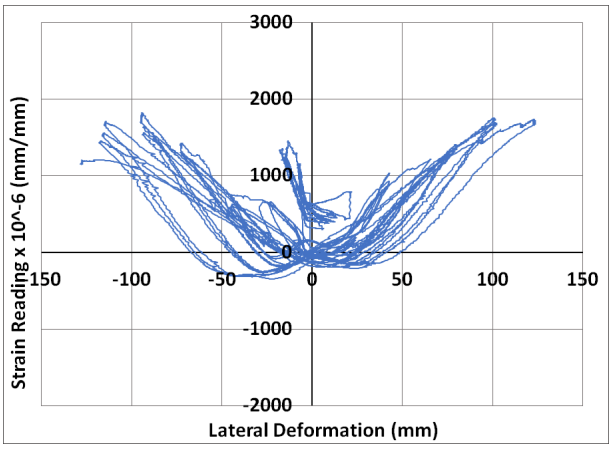

Strain Gauge: Web E-2

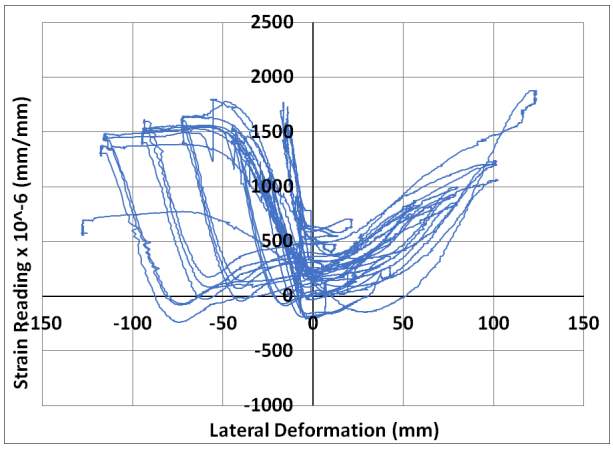

Strain Gauge: Web E-3

Figure B3.12 (Cont'd) Shear Wall No.3 - Strain Gauge Recordings of Web Horizontal Reinforcement

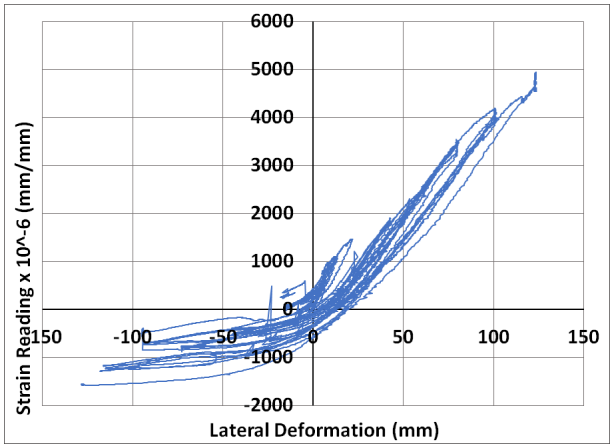

Strain Gauge Tendon No. 1

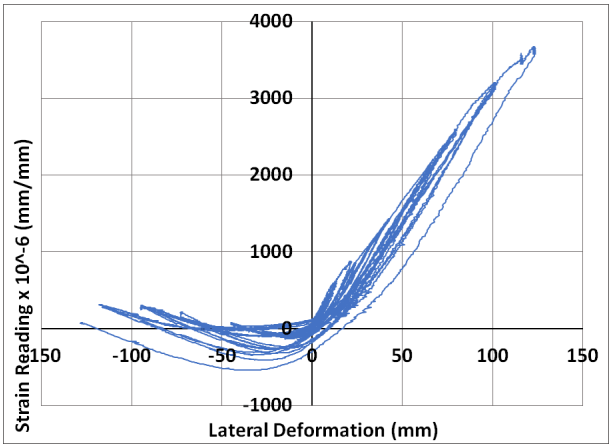

Strain Gauge Tendon No. 2

Figure B3.13 Shear Wall No.3 - Strain Gauge Recordings of Prestressing Tendons

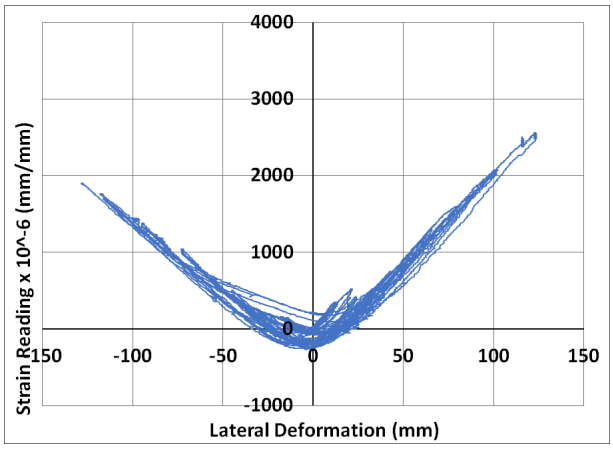

Strain Gauge Tendon No. 3

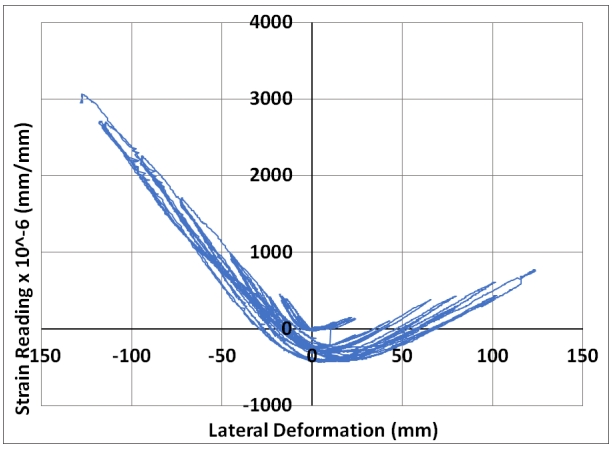

Strain Gauge Tendon No. 4

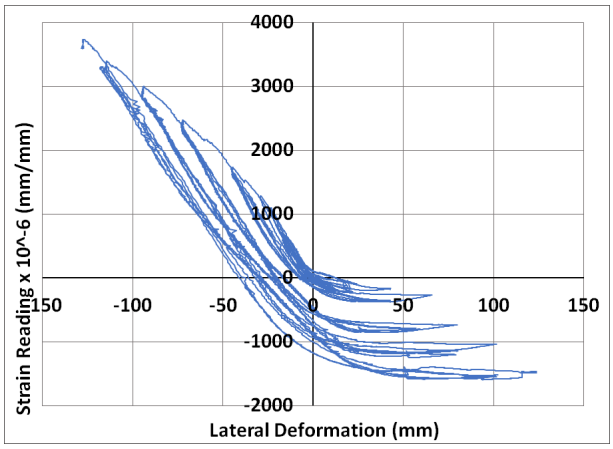

Strain Gauge Tendon No. 5

Figure B3.13 (Cont'd) Shear Wall No.3 - Strain Gauge Recordings of Prestressing Tendons